Molecular mechanisms of Endothelial-Mesenchymal Transition in coronary artery stenosis and cardiac fibrosis

Vanchin, Byambasuren

Molecular mechanisms of Endothelial-Mesenchymal Transition in coronary artery stenosis and cardiac fibrosis

Byambasuren Vanchin

2018

The research described in this thesis was performed at the Cardiovascular Regenerative Medicine laboratory at the Department of Pathology and Medical Biology in University Medical Center Groningen. The work was funded by Mongolian State Training Fund and Groningen University Institute for Drug Exploration (GUIDE), Graduate School of Medical Sciences.

The author gratefully acknowledges the financial support for printing of this thesis by: The Graduate School of Medical Sciences and Centre for East Asian Studies Groningen (CEASG).

ISBN: 978-94-034-0756-2 (printer version)
ISBN: 978-94-034-0755-5 (digital version)

Front cover design: Viktoriia Starokozhko & Byambasuren Vanchin
Layout design: Byambasuren Vanchin
Printed by: Gildeprint, Enschede, The Netherlands

university of groningen

Molecular mechanisms of Endothelial-Mesenchymal Transition in coronary artery stenosis and cardiac fibrosis

PhD thesis

to obtain the degree of PhD at the
University of Groningen
on the authority of the
Rector Magnificus Prof. E. Sterken
and in accordance with
the decision by the College of Deans.

This thesis will be defended in public on
Tuesday 26 June 2018 at 09.00 hours

by

Byambasuren Vanchin

born on 13 December 1986
in Ulaanbaatar, Mongolia

Supervisor
Prof. M.C. Harmsen

Co-supervisor
Dr. G. Krenning

Assessment Committee
Prof. J.L. Hillebrands
Prof. M.J.T.H. Goumans
Prof. E.M. Zeisberg

Paranymphs

Maroesjka Spiekman
Marloes Sol

CONTENTS

CHAPTER 1

Introduction

GLOBAL BURDEN OF CARDIOVASCULAR DISEASE

Cardiovascular diseases (CVD) are the leading cause of mortality worldwide. In 2015, an estimated 17.7 million people died from CVD, representing 31% of all mortalities worldwide. The majority of cardiovascular deaths can be attributed to coronary heart disease and cerebrovascular diseases, representing 42 and 38% of CVD-related deaths, respectively (1) wherein arteriosclerosis is the main underlying pathology.

From epidemiological studies, systemic risk factors for the development of atherosclerosis are identified, including behavioral risk factors such as an unhealthy *Western* diet, physical inactivity, smoking and the excessive use of alcohol. These behavioral risk factors can culminate in intermediate risk factors such as hyperglycemia, hyperlipidemia, obesity and hypertension (2). The non-modifiable risk factors for arteriosclerosis development are aging, gender and genetic susceptibility (1, 3). Although the whole vasculature is exposed to the above mentioned systemic risk factors, atherosclerosis is a focal disease that primarily develops at the site of vascular branches and the inner curvatures of large vessels (4), implying that focal risk factors are involved in the pathogenesis of atherosclerosis (5).

Atherosclerotic plaques are lesions in the arteries characterized by excessive accumulation of oxidized low-density lipoprotein cholesterol in the vessel wall (6, 7), inflammatory cell infiltration (8), smooth muscle cell proliferation, extracellular matrix accumulation and intimal thickening (9). It is commonly accepted that endothelial dysfunction is the initiating event in atherosclerosis development (10, 11), however, the underlying molecular mechanisms that cause endothelial dysfunction in the so-called atheroprone areas remain elusive. The current dogma revolves around biomechanical forces (figure 1) – fluid shear stress (12) and cyclic strain (13) – that have distinct patterns in areas that are atherosclerosis-prone and areas that are resistant to atherosclerosis development (the so-called atheroprotected areas).

Fluid shear stress, the frictional force per unit area generated by the blood flow, plays a crucial role in endothelial homeostasis and disease (14, 15). Areas exposed to laminar flow are protected from the atherosclerosis. In contrast, disturbed flow can induce endothelial cell activation, oxidative stress and the expression of leukocyte adhesion molecules that might induce an inflammatory reaction in the vessel wall (extensively reviewed (16, 17)) Indeed, in animal models wherein disturbed flow is induced by the constriction of an otherwise healthy vessel, atherosclerotic lesions develop in the absence of systemic atherosclerosis risk factors (18, 19).

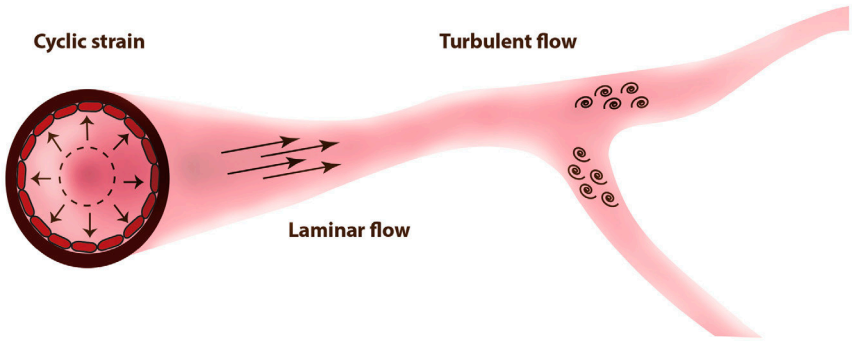

Figure 1. Blood vessels are constantly exposed to biomechanical forces, namely shear stress and cyclic strain. *Cyclic strain is the circumferential stretch of the vessel. Shear stress is the frictional force per unit area and its magnitude is measured by dyne/cm^2. Depending on the direction of the flow, shear stress can be further classified into laminar shear stress (unidirectional) and oscillatory shear stress (disturbed). High laminar shear stress is atheroprotective flow, whereas low oscillatory shear stress is considered as atheroprone flow, present at sites where atherosclerotic lesions preferentially develop.*

ENDOTHELIAL CELLS IN VASCULAR HOMEOSTASIS AND THE DEVELOPMENT OF CVD

The blood vessels serve as the conduits of circulation, transporting nutrients and oxygen and removing catabolites and carbon dioxide from the tissues. Besides the lymph system, there are 3 major type of blood vessels that differ in morphology and function, namely arteries, veins and capillaries. The arteries carry blood from the heart, then capillaries enable the exchange of gas, nutrients, and catabolites in the tissues, whereas veins transport the blood back to the heart. From the aorta to the smallest capillaries and back through the venous system, the endothelium covers the entire vasculature and is over 100.000 km in length, weighs about 1 kg and represents approximately 1% of the body mass (20).

The endothelium is the most inner luminal cell layer of all blood vessels. In a landmark experiment, Furchgott demonstrated that the endothelial layer is not just a simple barrier between the blood and the surrounding tissues, but the endothelium has number of crucial functions in vascular homeostasis. The removal of the endothelium from isolated aortas precluded acetylcholine-induced vasorelaxation (21). These data exemplify that the endothelium is not solely a static barrier, but also a key player in vasomotor function. Since, many studies have reported on other pivotal functions of the endothelium in safeguarding vascular homeostasis, such as the semi-permeable regulation of oxygen and nutrient exchange from the blood to the underlying tissues, leukocyte recruitment, platelet adhesion/activation, blood clotting and angiogenesis (22, 23).

Various stimuli, such as oxidative stress and oscillatory shear stress can disrupt endothelial homeostasis, which results in endothelial dysfunction. Endothelial dysfunction is a comprehensive concept referring to the reduction of the endothelium-

derived relaxing factors (EDRFs) - in particular nitric oxide(NO) - while, the endothelial-derived contracting factors (EDCFs) are increased.

Endothelial dysfunction not only impairs vasodilation, but also comprises pro-thrombotic, proliferative and pro-inflammatory phenotypes (Figure 2). As a result, the dysfunctional endothelium facilitates other pathophysiological pathways that might induce atherosclerosis (24, 25).

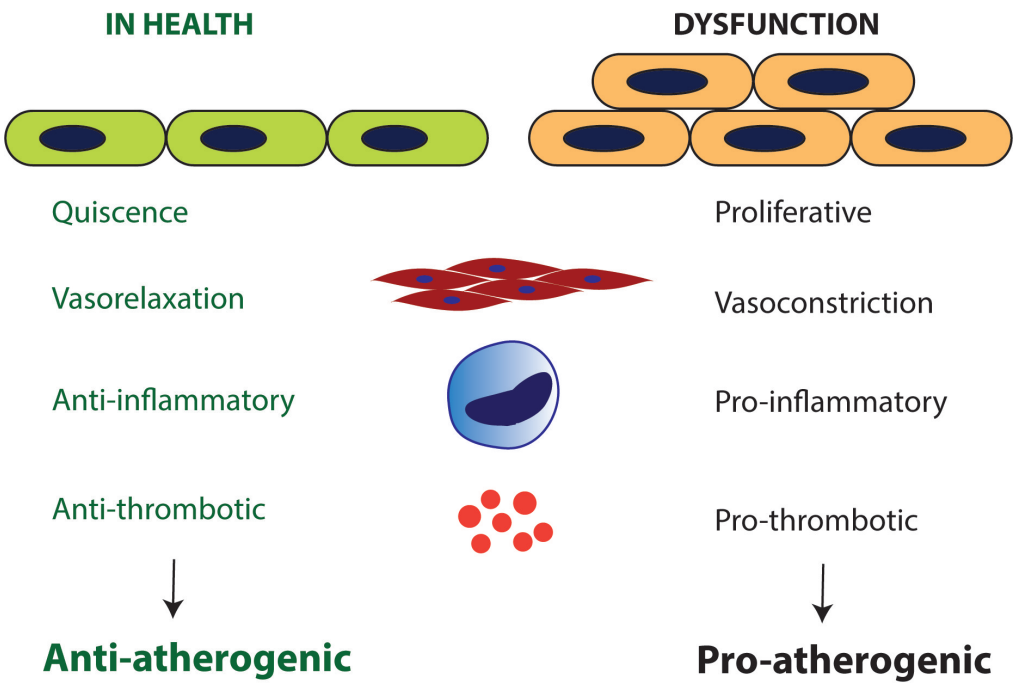

Figure 2. Endothelial cells in health and disease. *The healthy quiescent endothelium has anti-atherogenic capacities. Dysfunctional endothelial cells lose their protective capacities and acquire pro-atherogenic functions such as proliferation, vasoconstriction, inflammatory activation, and pro-thrombotic activity which contribute to atherogenesis.*

EPIGENETIC REGULATION OF ENDOTHELIAL GENE EXPRESSION

As phenotypic heterogeneity is the consequence of differential gene and protein expression patterns, the molecular mechanisms that affect endothelial gene and protein expression are extensively investigated in the context of atherosclerosis(26, 27). Although we have an increasing understanding about the endothelial behavior during atherosclerosis development, the contribution of endothelial biomechanical and epigenetic signaling during atherosclerosis development is still elusive.

Berger et al defined epigenetics as "the stable and heritable changes in genome function resulting from changes in the chromatin without alterations in the underlying DNA sequence"(28). As a blueprint of the human body, the DNA needs to be accessible to transcription factors in a spatiotemporal accurate manner in order to regulate gene expression. Each cell contains approximately 2 meters of DNA, which is folded into a nucleus of less than 10μm in diameter. To ensure this compaction, the DNA is wrapped around an octamer of core histone proteins (H2A, H2B, H3, H4 - two times each) which forms the nucleosomes (Figure 3). The nucleosomes are further compacted by the exterior histone H1 into 10nm fibers and complexed into 30nm fibers by scaffolding proteins forming the chromatin (29).

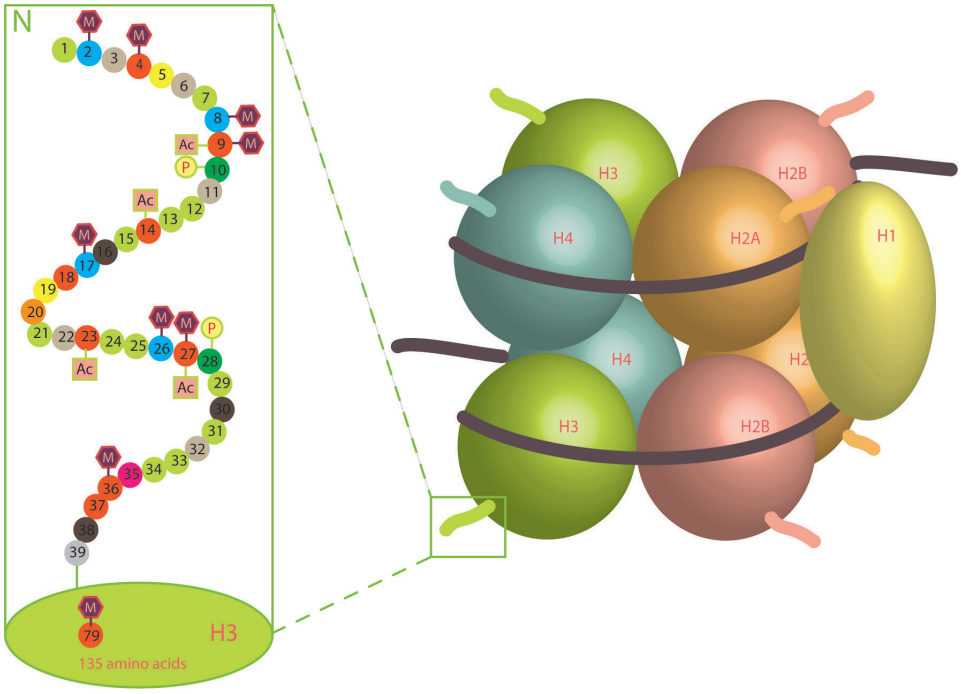

Figure 3. The nucleosome is a subunit of chromatin. *Each nucleosome consists of an octamer of histone proteins (Two copies of H2A, H2B, H3 and H4) and approximately 147bp of DNA that wraps around the histone octamer in 1,7 helical turns. Histone tails protrude from each core histone protein. Histone 1 binds to the histone/DNA complex and bridges neighboring nucleosomes.*

This high-order folding or 3D arrangement of the nucleosomes has distinct chromatin states in the genome; euchromatin is the state wherein a portion of the DNA is loosely wrapped and more accessible to the transcriptional machinery. In contrast, heterochromatin is densely packed and less accessible state (Figure 4). This higher-order folding is not merely in place to compact the DNA, but is also pivotal in the regulation of gene expression (30). Despite having the identical genomic information, a single fertilized egg can give rise over 200 types of morphologically and functionally distinct cell types. These structural and functional diversities are the consequence of differential gene expression profiles. Epigenetic regulation poses a layer of transcriptional regulation that culminates in phenotypic diversities between cells (31).

DNA methylation is a process where the addition of methyl group on a cytosine nucleotide forms 5-methylcytosine. DNA methylation mostly occurs on CpG islands, which are DNA sequences enriched in cytosine nucleotide followed by a guanine nucleotide coupled via phosphate bonds. CpG islands are mostly found in gene promoter areas (32). In mammals, de novo DNA methylation is performed by the methyltransferases DNMT3a and DNMT3b (33), whereas DNMT1 recognizes hemi-methylated DNA and copies the methylation to the secondary locus thereby allowing the daughter cells keep the same DNA methylation pattern.

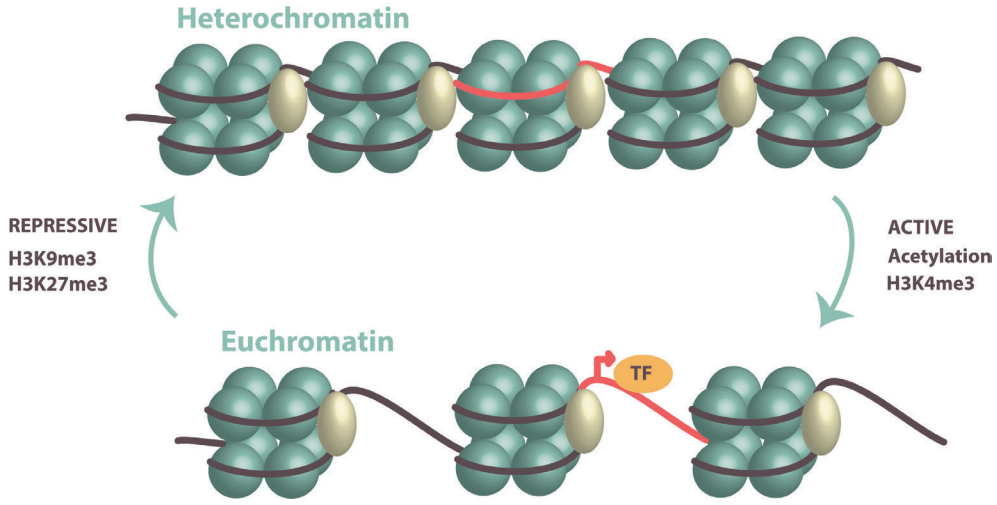

Figure 4. Heterochromatin versus Euchromatin. *Heterochromatin is densely packed chromatin wherein the DNA is inaccessible for the transcriptional machinery. Repressive histone modifications (e.g. H3K27Me3) and DNA methylation induce heterochromatin formation. Euchromatin is loosely packed chromatin wherein the DNA is accessible to the transcriptional machinery. Acetylation of histone tail residues changes the charge of the histone core proteins which results in electrostatic repulsion and the opening of the chromatin.*

Histone modifications: Each core histone molecules has N-terminal tail (29) which protrudes out of the histone protein and can undergo a number of modifications (Figure 3). Histone modifications include methylation, acetylation, ubiquitination, phosphorylation, sumoylation, ribosolyation and others. The orchestrated arrangement of the histone modifications is regulated by epigenetic enzymes. Depending on the histone modification produced, epigenetic enzymes are divided into epigenetic writers, readers and erasers. Lysine acetylation on histone tails in general results in chromatin opening and thus enhanced gene expression, whereas the tri-methylation of lysine 9 and 27 on histone 3 (H3K9me3 and H3K27me3, respectively) culminate in chromatin closure and gene silencing.

Polycomb Repressive Complex mediated gene silencing: The Polycomb repressive complex is an evolutionary preserved transcriptional silencing system that plays a crucial role in stem cell identity and differentiation (34). Two multiprotein Polycomb complexes are identified; Polycomb Repressive Complex 2 (PRC 2) consists of Enhancer of Zeste Homologue 2 (EZH2) or its homologue (EZH1), Embryonic Ectoderm Development (EED), Suppressor of Zeste 12 (SUZ12) and Retinoblastoma binding protein 48 (RbAP48).

Among these proteins, EZH2 and its homologue EZH1 has SET domain holding methyltransferase activity, which enables the writing of the tri-methylation on the 27th lysine residue on the tail of Histone 3 (H3k27me3). H3K27me3 acts as docking site for the Polycomb Repressive Complex 1 (PRC1), which writes a mono-ubiquitination on the 119th lysine residue on the tail of Histone 2A (H2AK119ub1) (35, 36). PRC1 precludes the activation of the RNA polymerase II complex thereby silencing gene expression(37).

Post-transcriptional silencing - microRNAs: MicroRNAs are around 23 nucleotides in length, non-protein coding RNAs. They induce posttranscriptional repression by pairing to the transcripts of the protein coding genes (mRNAs). The microRNA precursors are transcribed from the DNA by the RNA polymerase II as longer transcript, the pri-microRNA. The precursor miRNAs undergoes a series of alterations to finally form the mature microRNA that is loaded into the RNA induced silencing complex (RISC). The RISC complex can bind to the 3' UTR of a target mRNA, causing cleavage, destabilization or inhibition of mRNA translation. A single microRNA can target multiple mRNAs simultaneously, if their 3' UTR sequence match with the seed sequence of the microRNA (38, 39).

PHENOTYPE SWITCHING OF ENDOTHELIAL CELLS: A DRIVING FORCE FOR DEVELOPING CARDIOVASCULAR DISEASE?

As mentioned above, the healthy endothelium is quiescent and performs valuable functions for vascular homeostasis, such as the regulation of vascular permeability and the prevention of vasospasms, inflammation, thrombosis and platelet activation. In this thesis, we investigated the influence of a specific epigenetic modification (i.e. H3K27Me3) on the development of endothelial dysfunction and Endothelial-Mesenchymal Transition (EndMT).

Endothelial-mesenchymal transition (EndMT) is a specific subtype of endothelial dysfunction wherein endothelial cells lose their endothelial specific markers and morphology while acquiring a mesenchymal phenotype. The loss of endothelial specific markers, such as VE-cadherin, CD31, Tie1/2 and VEGFRII and the concurrent gain in expression of mesenchymal marker proteins αSMA, SM22α, calponin, PAI and vimentin is prominent during EndMT. Functionally, endothelial cells acquire contractile behavior while their angiogenic and anti-thrombogenic capacities are constrained. Moreover, extracellular matrix (ECM) production by endothelial cells is increased during EndMT, culminating in the adaptation of a pro-atherogenic endothelial phenotype (16).

EndMT was first described during the formation of the cardiac cushions and valves during cardiac development (40). In the adult, EndMT contributes to the development of various chronic diseases such as cancer (41), fibrosis (42) (43) (44) (45), cerebral cavernous malformations (46), and endocardial fibroelastosis (47). Recent studies show that EndMT also contributes to atherosclerosis (48, 49) and neointima formation (50, 51).

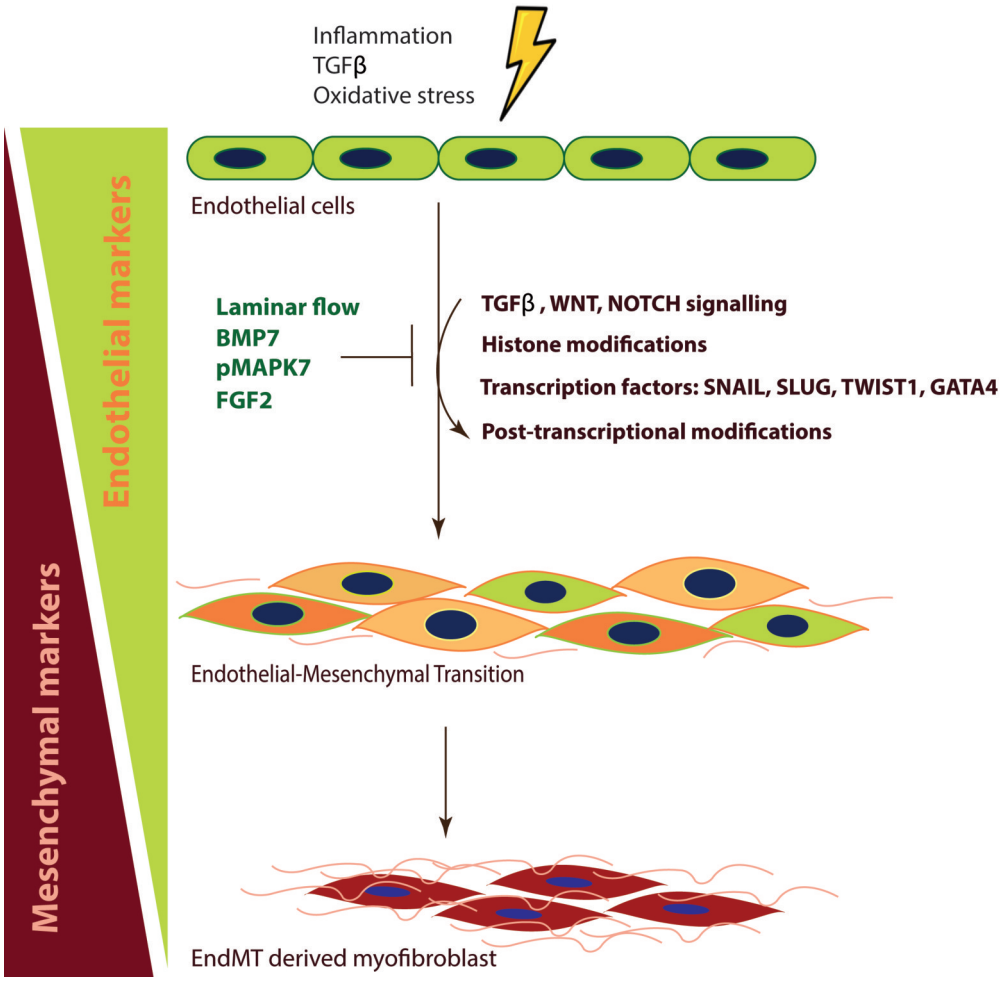

Figure 5. Endothelial-Mesenchymal transition (EndMT). *The healthy quiescent endothelium is a main mediator of vascular homeostasis. During EndMT, the expression of endothelial cell-specific markers such as VE-cadherin and CD31 is reduced whereas mesenchymal cell-specific markers such as aSMA and Calponin is induced. TGFβ, inflammation and oxidative stress induce EndMT, conversely BMP7, laminar flow-mediated pMAPK7 activity and FGF2 inhibit EndMT. The TGFβ, WNT, NOTCH signaling, histone modifications, transcription factors and post-transcriptional modifications modulate EndMT.*

Postnatal EndMT is predominantly induced in a TGFβ- or inflammation and oxidative stress-driven manner (Figure 5). ***TGFβ-driven EndMT*** is extensively investigated in the context of fibrotic diseases. Canonical TGF-β signaling activates its downstream intermediates SMAD2/3, thereby inducing mesenchymal transcription factors and gene expression. Non-canonical TGF-β signaling can activate downstream molecules such as ERK1/2 and p38 MAPK, which activate the transcription factor SNAIL, the classical transcription factor for the induction of EndMT(16).

On the other hand, inflammation-driven EndMT is initiated by the signaling actions of inflammatory cytokines such as TNFα and IL1β or reactive oxygen species (ROS). This inflammation driven pathway might blend into the TGF-β-driven pathway, since inflammatory-activated endothelial cells induce the endogenous expression of TGF-β (16). Interestingly, the inflammatory cytokine IL1β and TGFβ can synergistically induce EndMT in viitro (52). These data indicate that these two distinct pathways are somehow interwined and synergize each other at the certain points (5).

Potent TGF-β antagonists such as BMP7 (53) and FGF2 (54) inhibit EndMT. Also high laminar shear stress inhibits EndMT via the activation of MAPK7 signaling (50). Systemic administration bone morphogenic protein 7 (BMP7) significantly inhibites EndMT and the progression of fibrosis in the heart and kidney(42), and the endothelial cell-specific ablation of FGFRI culminates in the activation of TGFβ signaling and the development of EndMT in vitro and in vivo(55).

AIM OF THIS THESIS

Significant advancements have been made in the development of new treatments of cardiovascular diseases, yet CVD are still the leading cause of mortality worldwide. Although the endothelium and atherosclerosis are extensively studied and Endothelial-mesenchymal transition is established as a key component of atherosclerosis, the relative contribution, specific form of-, and functional contribution of endothelial-mesenchymal transition is elusive. **The aim of this thesis is to elucidate the molecular and epigenetic mechanisms of how uniform laminar shear stress might modulate endothelial homeostasis and how these mechanisms are disrupted during intimal hyperplasia and cardiac fibrosis.**

OUTLINE OF THIS THESIS

A general introduction to the topics under investigation is presented here (**Chapter 1)**. The altered function of the endothelium is an important component of atherosclerosis yet no current anti-atherosclerosis therapies are specifically focused on the amelioration of endothelial dysfunction. Hence, in **Chapter 2,** we review the current atherosclerosis treatments and investigate how some epigenetic enzymes might be beneficial to normalize endothelial function in disturbed flow areas to preclude atherosclerosis development and its progression

In healthy blood vessels, the vascular lumen is lined with a quiescent endothelium. In contrast, during vascular pathologies such as atherosclerosis, the endothelium has a fibro-proliferative phenotype, characterized by intimal hyperplasia and mesenchymal phenotype. Uniform laminar flow activates MAPK7 signaling thereby inhibiting Endothelial-Mesenchymal transition. However, how this protective mechanism is overruled in the atheroprone regions is unknown. In **Chapter 3**, we investigate the mechanism by which TGFβ reduces the expression and activity of MAPK7 signaling during intimal hyperplasia with a focus on TGFb-sensitive microRNAs that might target the MAPK7 signaling cascade.

Next, we investigate how endothelial quiescence is governed by fluid shear stress and how the histone methyltransferase EZH2, as a pivotal epigenetic mediator, regulates endothelial quiescence. In **Chapter 4**, we investigate how high laminar shear stress and EZH2 modulate the gene expression profile in endothelial cells by using an RNA sequencing approach. We focus on genes that regulate the cell cycle in endothelial cells and investigate how these are regulated by fluid shear stress and EZH2. Surprisingly, we uncovered that the epigenetic enzyme EZH2 crosstalk's with MAPK7 signaling in a reciprocal fashion. This finding intrigued us to investigate the crosstalk between these two molecules in **Chapter 5**. Also, we questioned whether this reciprocity is in imbalance during coronary artery stenosis.

EndMT plays a pivotal role in the development of cardiac fibrosis. Zeisberg et al found that around 30% of myofibroblasts in cardiac fibrosis are derived from the endothelium (42). Meanwhile, Galectin 3 was identified as a key initiator of cardiac fibrosis, and plasma Galectin 3 levels associate with the increased risk of heart failure and mortality (56). However, the molecular mechanism of Galectin 3-induced cardiac fibrosis is elusive. In **Chapter 6** we assessed if Galectin 3-induced cardiac fibrosis might originate from EndMT. In **Chapter 7**, we summarize our main findings of this thesis, describing the complex and multilayered regulation of endothelial-mesenchymal transition by epigenetic and post-transcriptional silencing mechanisms (i.e. EZH2 and microRNAs) and how these are influenced by fluid shear stress. Moreover, we describe how these mechanisms are in imbalance during the development of intimal hyperplasia and cardiac fibrosis. In **Chapter 8**, we propose future perspectives resulting from our findings.

REFERENCES

1. WHO. Fact sheet: Cardiovascular diseases: World Health Organization; 2017 [Available from: http://www.who.int/mediacentre/factsheets/fs317/en/.
2. Canto JG, Iskandrian AE. Major risk factors for cardiovascular disease: debunking the only 50% myth. Jama. 2003;290(7):947-9.
3. Black HR. Cardiovascular risk factors. Yale university school of medicine heart book. 1992:23-35.
4. Texon M. The hemodynamic concept of atherosclerosis. Bulletin of the New York Academy of Medicine. 1960;36(4):263.
5. Souihol CE, Harmsen MC, Evans PC, Krenning G. Endothelial-Mesenchymal Transition in Atherosclerosis. Cardiovascular research. 2018.
6. Holvoet P, Vanhaecke J, Janssens S, Van de Werf F, Collen D. Oxidized LDL and malondialdehyde-modified LDL in patients with acute coronary syndromes and stable coronary artery disease. Circulation. 1998;98(15):1487-94.
7. Watson AD, Leitinger N, Navab M, Faull KF, Hörkkö S, Witztum JL, et al. Structural identification by mass spectrometry of oxidized phospholipids in minimally oxidized low density lipoprotein that induce monocyte/endothelial interactions and evidence for their presence in vivo. Journal of Biological Chemistry. 1997;272(21):13597-607.
8. Libby P, Ridker PM, Maseri A. Inflammation and atherosclerosis. Circulation. 2002;105(9):1135-43.
9. Nakashima Y, Wight TN, Sueishi K. Early atherosclerosis in humans: role of diffuse intimal thickening and extracellular matrix proteoglycans. Cardiovascular research. 2008;79(1):14-23.
10. Davignon J, Ganz P. Role of endothelial dysfunction in atherosclerosis. Circulation. 2004;109(23 suppl 1):III-27-III-32.
11. Gimbrone MA, Topper JN, Nagel T, Anderson KR, GARCIA-CARDEÑA G. Endothelial dysfunction, hemodynamic forces, and atherogenesis. Annals of the New York Academy of Sciences. 2000;902(1):230-40.
12. Dewey C, Bussolari S, Gimbrone M, Davies PF. The dynamic response of vascular endothelial cells to fluid shear stress. Journal of biomechanical engineering. 1981;103(3):177-85.
13. Iba T, Sumpio BE. Morphological response of human endothelial cells subjected to cyclic strain in vitro. Microvascular research. 1991;42(3):245-54.
14. Davies PF. Hemodynamic shear stress and the endothelium in cardiovascular pathophysiology. Nature clinical practice Cardiovascular medicine. 2009;6(1):16.
15. Conway DE, Schwartz MA. Flow-dependent cellular mechanotransduction in atherosclerosis. J Cell Sci. 2013;126(22):5101-9.
16. Krenning G, Barauna VG, Krieger JE, Harmsen MC, Moonen J-RA. Endothelial plasticity: shifting phenotypes through force feedback. Stem cells international. 2016;2016.
17. Kwak BR, Bäck M, Bochaton-Piallat M-L, Caligiuri G, Daemen MJ, Davies PF, et al. Biomechanical factors in atherosclerosis: mechanisms and clinical implications. European heart journal. 2014;35(43):3013-20.
18. Nam D, Ni C-W, Rezvan A, Suo J, Budzyn K, Llanos A, et al. Partial carotid ligation is a model of acutely induced disturbed flow, leading to rapid endothelial dysfunction and atherosclerosis. American Journal of Physiology-Heart and Circulatory Physiology. 2009;297(4):H1535-H43.
19. Winkel LC, Hoogendoorn A, Xing R, Wentzel JJ, Van der Heiden K. Animal models of surgically manipulated flow velocities to study shear stress-induced atherosclerosis. Atherosclerosis. 2015;241(1):100-10.
20. De Caterina R, Massaro M, Libby P. Endothelial functions and dysfunctions. Endothelial dysfunctions in vascular disease. 2007:1-25.

21. Furchgott RF, Zawadzki JV. The obligatory role of endothelial cells in the relaxation of arterial smooth muscle by acetylcholine. Nature. 1980;288(5789):373-6.
22. Vita JA. Endothelial function. Circulation. 2011;124(25):e906-e12.
23. Sena CM, Pereira AM, Seiça R. Endothelial dysfunction—a major mediator of diabetic vascular disease. Biochimica et Biophysica Acta (BBA)-Molecular Basis of Disease. 2013;1832(12):2216-31.
24. Bonetti PO, Lerman LO, Lerman A. Endothelial dysfunction: a marker of atherosclerotic risk. Arteriosclerosis, thrombosis, and vascular biology. 2003;23(2):168-75.
25. Vanhoutte P, Shimokawa H, Feletou M, Tang E. Endothelial dysfunction and vascular disease–a 30th anniversary update. Acta Physiologica. 2017;219(1):22-96.
26. Passerini AG, Polacek DC, Shi C, Francesco NM, Manduchi E, Grant GR, et al. Coexisting proinflammatory and antioxidative endothelial transcription profiles in a disturbed flow region of the adult porcine aorta. Proceedings of the National Academy of Sciences of the United States of America. 2004;101(8):2482-7.
27. Brooks AR, Lelkes PI, Rubanyi GM. Gene expression profiling of human aortic endothelial cells exposed to disturbed flow and steady laminar flow. Physiological genomics. 2002;9(1):27-41.
28. Berger SL, Kouzarides T, Shiekhattar R, Shilatifard A. An operational definition of epigenetics. Genes & development. 2009;23(7):781-3.
29. Luger K, Mader AW, Richmond RK, Sargent DF, Richmond TJ. Crystal structure of the nucleosome core particle at 2.8 angstrom resolution. Nature. 1997;389(6648):251.
30. Margueron R, Reinberg D. Chromatin structure and the inheritance of epigenetic information. Nature Reviews Genetics. 2010;11(4):285-96.
31. Reik W. Stability and flexibility of epigenetic gene regulation in mammalian development. Nature. 2007;447(7143):425-32.
32. Bird AP. CpG-rich islands and the function of DNA methylation. Nature. 1986;321(6067):209-13.
33. Okano M, Bell DW, Haber DA, Li E. DNA methyltransferases Dnmt3a and Dnmt3b are essential for de novo methylation and mammalian development. Cell. 1999;99(3):247-57.
34. Aloia L, Di Stefano B, Di Croce L. Polycomb complexes in stem cells and embryonic development. Development. 2013;140(12):2525-34.
35. Di Croce L, Helin K. Transcriptional regulation by Polycomb group proteins. Nature structural & molecular biology. 2013;20(10):1147-55.
36. Simon JA, Kingston RE. Mechanisms of polycomb gene silencing: knowns and unknowns. Nature reviews Molecular cell biology. 2009;10(10):697-708.
37. Lehmann L, Ferrari R, Vashisht AA, Wohlschlegel JA, Kurdistani SK, Carey M. Polycomb repressive complex 1 (PRC1) disassembles RNA polymerase II preinitiation complexes. Journal of Biological Chemistry. 2012;287(43):35784-94.
38. Bartel DP. MicroRNAs: target recognition and regulatory functions. cell. 2009;136(2):215-33.
39. Fabian MR, Sonenberg N, Filipowicz W. Regulation of mRNA translation and stability by microRNAs. Annual review of biochemistry. 2010;79:351-79.
40. Markwald RR, Fitzharris TP, Manasek FJ. Structural development of endocardial cushions. Developmental Dynamics. 1977;148(1):85-119.
41. Zeisberg EM, Potenta S, Xie L, Zeisberg M, Kalluri R. Discovery of endothelial to mesenchymal transition as a source for carcinoma-associated fibroblasts. Cancer research. 2007;67(21):10123-8.
42. Zeisberg EM, Tarnavski O, Zeisberg M, Dorfman AL, McMullen JR, Gustafsson E, et al. Endothelial-to-mesenchymal transition contributes to cardiac fibrosis. Nature medicine. 2007;13(8):952.

43. Zeisberg EM, Potenta SE, Sugimoto H, Zeisberg M, Kalluri R. Fibroblasts in kidney fibrosis emerge via endothelial-to-mesenchymal transition. Journal of the American Society of Nephrology. 2008;19(12):2282-7.
44. Kato H, Fu YY, Zhu J, Wang L, Aafaqi S, Rahkonen O, et al. Pulmonary vein stenosis and the pathophysiology of "upstream" pulmonary veins. The Journal of thoracic and cardiovascular surgery. 2014;148(1):245-53.
45. Rieder F, Kessler SP, West GA, Bhilocha S, De La Motte C, Sadler TM, et al. Inflammation-induced endothelial-to-mesenchymal transition: a novel mechanism of intestinal fibrosis. The American journal of pathology. 2011;179(5):2660-73.
46. Maddaluno L, Rudini N, Cuttano R, Bravi L, Giampietro C, Corada M, et al. EndMT contributes to the onset and progression of cerebral cavernous malformations. Nature. 2013;498(7455):492.
47. Xu X, Friehs I, Hu TZ, Melnychenko I, Tampe B, Alnour F, et al. Endocardial Fibroelastosis Is Caused by Aberrant Endothelial to Mesenchymal TransitionNovelty and Significance. Circulation research. 2015;116(5):857-66.
48. Evrard SM, Lecce L, Michelis KC, Nomura-Kitabayashi A, Pandey G, Purushothaman K-R, et al. Endothelial to mesenchymal transition is common in atherosclerotic lesions and is associated with plaque instability. Nature communications. 2016;7.
49. Chen P-Y, Qin L, Baeyens N, Li G, Afolabi T, Budatha M, et al. Endothelial-to-mesenchymal transition drives atherosclerosis progression. The Journal of clinical investigation. 2015;125(12):4514.
50. Moonen J-RA, Lee ES, Schmidt M, Maleszewska M, Koerts JA, Brouwer LA, et al. Endothelial-to-mesenchymal transition contributes to fibro-proliferative vascular disease and is modulated by fluid shear stress. Cardiovascular research. 2015;108(3):377-86.
51. Cooley BC, Nevado J, Mellad J, Yang D, Hilaire CS, Negro A, et al. TGF-β signaling mediates endothelial-to-mesenchymal transition (EndMT) during vein graft remodeling. Science translational medicine. 2014;6(227):227ra34-ra34.
52. Maleszewska M, Moonen J-RA, Huijkman N, van de Sluis B, Krenning G, Harmsen MC. IL-1β and TGFβ2 synergistically induce endothelial to mesenchymal transition in an NFκB-dependent manner. Immunobiology. 2013;218(4):443-54.
53. Zeisberg M, Hanai J-i, Sugimoto H, Mammoto T, Charytan D, Strutz F, et al. BMP-7 counteracts TGF-β1–induced epithelial-to-mesenchymal transition and reverses chronic renal injury. Nature medicine. 2003;9(7):964-8.
54. Correia AC, Moonen J-RA, Brinker MG, Krenning G. FGF2 inhibits endothelial–mesenchymal transition through microRNA-20a-mediated repression of canonical TGF-β signaling. J Cell Sci. 2016;129(3):569-79.
55. Chen P-Y, Qin L, Tellides G, Simons M. Fibroblast growth factor receptor 1 is a key inhibitor of TGFb signaling in the endothelium. 2014.
56. Ho JE, Liu C, Lyass A, Courchesne P, Pencina MJ, Vasan RS, et al. Galectin-3, a marker of cardiac fibrosis, predicts incident heart failure in the community. Journal of the American College of Cardiology. 2012;60(14):1249-56.

Chapter 2

Pleiotropic treatment of pro-atherogenic endothelium: are SIRT1 and EZH2 promising candidates?

Byambasuren Vanchin[1], Marianne G Rots[2], Guido Krenning[1]

[1]Cardiovascular Regenerative Medicine Group, Department of Pathology and Medical Biology, University Medical Center Groningen, Hanzeplein 1, 9713GZ, Groningen, The Netherlands
[2]Epigenetic Editing Research Group, Department of Pathology and Medical Biology, University Medical Center Groningen, Hanzeplein 1, 9713GZ, Groningen, The Netherlands

Submitted

ABSTRACT

Cardiovascular diseases are the leading cause of mortality worldwide and account for almost 17.7 million deaths worldwide annually. Atherosclerosis is one of the main underlying pathologies of coronary artery and cerebrovascular diseases. Current atherosclerosis care is well developed at the emergency room or in the operation theatre by performing percutaneous intervention and vascular grafting per occasion when local atherosclerosis plaque cause infarction or severe ischemia. Moreover, preventative and follow-up therapies of atherosclerosis are predominantly limited by the reduction of cholesterol levels and inhibiting platelet aggregation.

It is well established that endothelial dysfunction is the major initiating event in atherogenesis and continues throughout atherosclerosis progression, yet no endothelial cell-specific therapies are available for the treatment of atherosclerosis. In this perspective, we review the contribution of the endothelium to atherogenesis and postulate that the dysregulation of epigenetic enzymes aggravate endothelial dysfunction in a pleiotropic fashion. We propose that targeted delivery of a SIRT1 activator or an EZH2 inhibitor to the pro-atherogenic endothelium might reduce the atherosclerosis development and prevent from the life-threatening complications.

I. THE ATHEROSCLEROTIC ENDOTHELIUM

The endothelium forms the innermost layer of all blood vessels and is a major regulator of vascular homeostasis. The endothelium plays a critical role in the regulation of vascular permeability, leukocyte trafficking, vascular tone, inflammation, thrombogenesis, fibrinolysis and angiogenesis. The healthy quiescent endothelium mediates vascular homeostasis by the inhibition of unwarranted inflammation, blood clotting and vasoconstriction and the maintenance of the vascular barrier, whereas endothelial dysfunction refers to a proinflammatory, prothrombotic and vasoconstrictive state of the endothelium wherein vascular permeability if often increased. Endothelial dysfunction is the initial stage of atherosclerosis (1). Dysfunctional endothelial cells facilitate lipid accumulation in the vessel wall, leukocyte extravasation, the secretion of pro-inflammatory cytokines, vasoconstriction, thrombogenesis and the accumulation of fibrous elements in the vessel wall, which form the basic elements of atherogenesis (2, 3).

Even before the first anatomical evidence of atherosclerotic plaque formation, endothelial dysfunction is appeared in hypercholesteremic children (Familial hypercholesterolemia) and young adult smokers (4). Moreover, the contribution of the endothelium to the pathogenesis of atherosclerosis has been established in a clinical long-term follow-up study, which compared non-obstructive coronary artery disease patients in which endothelial function was severely impaired to patients with only mild or moderate endothelial dysfunction. This study revealed that the group of patients with severe endothelial dysfunction has a higher incidence of cardiac events compared to the patients with mild and moderate endothelial dysfunction, implying the importance of endothelial dysfunction in the progression of atherosclerosis to cardiovascular events (5).

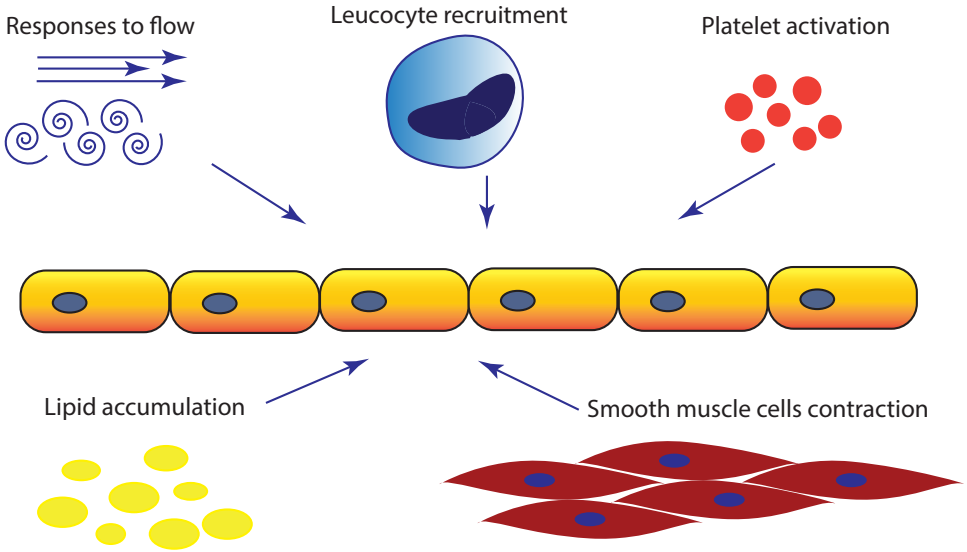

Figure 1. Endothelial cells are a pivotal mediator of atherogenic pathways. *Located on luminal side of the blood vessels, endothelial cells regulate smooth muscle cell contraction and platelet activation. Forming a barrier between the blood and the underlying tissue, the endothelium plays a crucial role in the selective recruitment of leukocytes and the lipid accumulation in the vessel wall.*

The classical risk factors for the development of atherosclerosis, such as physical inactivity, obesity, diabetes, hypertension, smoking, dyslipidemia and aging (6) act at the systemic level, yet atherosclerotic lesions preferentially develop in areas where endothelial cells are exposed by low oscillatory flow, suggesting that focal risk factors for the development of atherosclerosis exist (7-9). The vascular areas at risk, the so-called atheroprone regions, are commonly found at the outer wall of vascular bifurcations and the inner wall of vascular curvatures. Interestingly, the induction of blood flow disturbances in animals by for instance arteriovenous fistula (10), aortic ligation/constriction model (11) and partial carotid ligation (12) induces intimal hyperplasia and the development of a neointima even in absence of systemic atherosclerosis risk factors. A distinct gene expression profile is observed in endothelial cells exposed to high laminar shear stress vs low oscillatory shear stress in the human and porcine aorta (13, 14).

Endothelial cells in atheroprone areas produce less nitric oxide (NO) compared to endothelial cells at atheroprotected sites (15, 16). Furthermore, atheroprone, or low oscillatory shear stress induces a proinflammatory phenotype in endothelial cells (17). Inflammation is crucial in atherosclerosis development, progression and plaque stability (extensively reviewed (18, 19)). The inflammatory reaction at the atheroprone site increases the endothelial permeability to circulating lipids and initiates leukocyte recruitment, wherein the expression of leukocyte adhesion molecules by endothelial cells crucially regulates inflammatory cell influx into the forming atherosclerotic plaque (20). Attracted by monocyte chemotactic protein-1, monocytes transmigrate through the vessel wall, differentiate into macrophages and start to take up oxidized LDL (ox-LDL) and other cholesterol esters using their scavenger receptors, thereby differentiating in foam cells (21, 22). The foam cells which release more chemokines, cytokines and reactive oxygen species aggravating disease progression (23). Besides this fatty streak formation and inflammation, a hallmark of the initial stages of atherosclerosis is intimal hyperplasia or neointimal formation. Medial smooth muscle cells, adventitial fibroblasts and circulating fibrocytes are all implicated as origin of neointimal cells, however, an increasing body of evidence suggest that upon TGFβ and inflammatory activation, endothelial cells might acquire a mesenchymal-like or fibroproliferative phenotype and migrate into the neointima (24, 25). Endothelial lineage-tracing studies indicate that luminal endothelial cells undergo a process called Endothelial-Mesenchymal Transition (EndMT) and form myofibroblast-like cells that accumulate in the neointima and fibrous cap of atherosclerotic lesions (26, 27). EndMT is a cellular transdifferentiation process wherein endothelial cells lose the expression of endothelial cell-specific markers while the expression of mesenchymal cell markers is induced. Moreover, at the functional level, endothelial cells lose the ability to produce NO, loosen their endothelial cell-cell junctions, transit from a quiescent to a (hyper)proliferative state, acquire migratory and contractile properties and start to produce extracellular matrix components, culminating in enhanced leukocyte diapedesis, intimal lipid accumulation, intimal accumulation of fibroproliferative cells and the accumulation of fibrotic elements(28, 29). Also ageing is the major non-modifiable risk factor for the development of atherosclerosis. Cellular senescence is the phenomenon by which cells cease to divide in response to telomere shortening ageing or biochemical damages (e.g. ROS accumulation and DNA damage)(30).

Senescent endothelial cells adopt pro-inflammatory, pro-thrombotic phenotype and lose their cell-cell junction and regenerative capacity(31). Senescent endothelial cells are found in the atherosclerotic lesion (32), which indicates that endothelial senescence might contribute to the development and aggravation of atherosclerotic lesions.

From the above, we can conclude that endothelial dysfunction (i.e. endothelial oxidative stress, mesenchymal transition and senescence) plays a pivotal role in atherogenesis and therefore postulate that the endothelium might serve as an efficacious therapeutic target cell for anti-atherogenic therapies. In this perspective, we discuss the potential to ameliorate atherogenesis via the restoration of endothelial homeostasis using epigenetic drugs.

II. CURRENT ATHEROSCLEROSIS TREATMENTS

Current medical treatments to prevent atherosclerosis development, progression and plaque rupture encompass lipid lowering and the prevention of blood clotting (Figure 2) and emerging anti-inflammatory therapies are currently under clinical investigations to increase the efficacy of anti-atherosclerosis treatment. Below, we discuss the currently available therapeutic agents and their rationale as an anti-atherogenic agent.

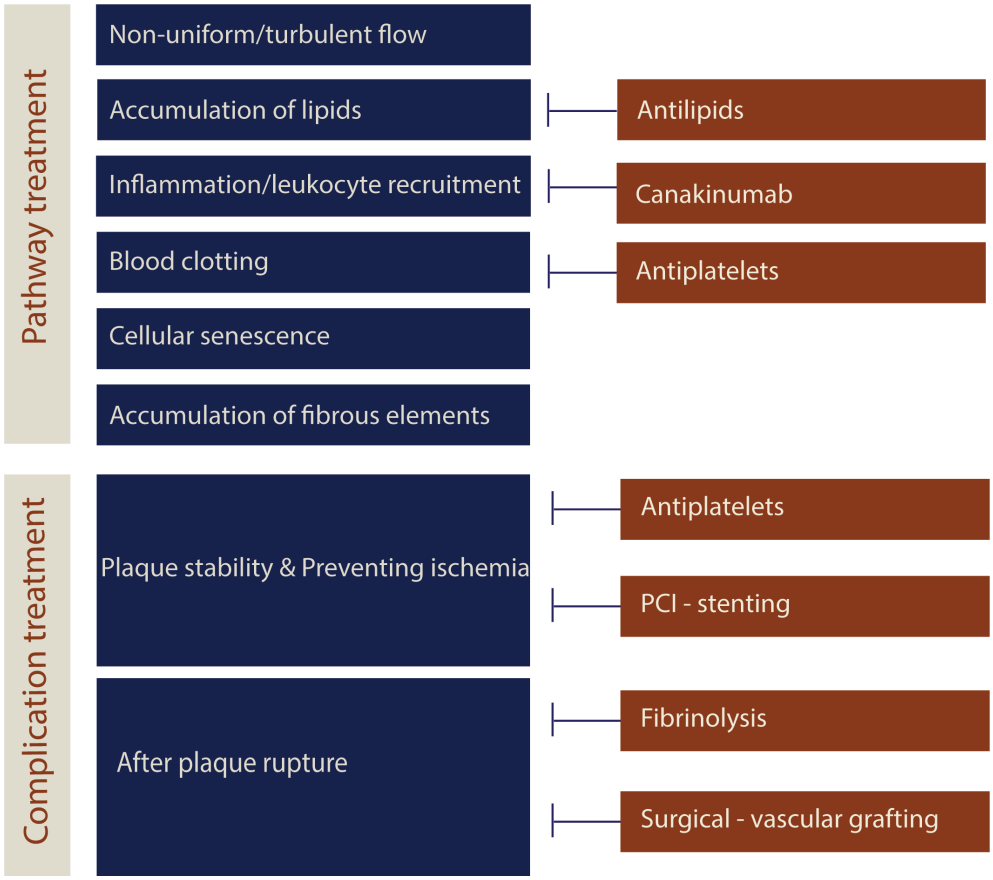

Figure 2. Current anti-atherosclerosis therapies. *Established atherogenic pathways are depicted in blue bars and if treatments are currently available to counteract these pathways, it is depicted in the according brown bars. Current anti-atherogenic therapies successfully preclude dyslipidemia, platelet aggregation and systemic inflammation, however the fundamental problem "endothelial dysfunction" is not sufficiently addressed therapeutically.*

ATHEROSCLEROSIS PATHOGENESIS THERAPIES

II.1 HYPERCHOLESTEROLEMIA:

The principal current pharmaceutical intervention for the treatment of atherosclerosis aims to reduce the lipid risk. As evidenced by epidemiological cohort studies as well as the clinical trials and meta-analysis, increasing levels of low density lipoproteins-C (LDL-C) associate strongly to the development of atherosclerosis and other cardiovascular diseases (extensively condensed in (33)). Extensive basic and clinical research has supported the dyslipidemia hypothesis and several groups of lipid lowering medications are currently available in the clinical practice.

Statins: Although a reduction in dietary cholesterol intake is able to reduce the serum cholesterol level, over two-thirds of serum cholesterol is synthesized in the liver. Statins, also known as HMG-CoA reductase inhibitors, act by reducing the liver's production of cholesterol via the inhibition of the conversion of HMG CoA to mevalonic acid (34). Besides reducing serum LDL-C levels, statins offer anti-inflammatory (35) effects and increase endothelial NO production primarily through the activation of the endothelial nitric oxide synthase (eNOS) (36), which might alleviate endothelial oxidative stress. These pleiotropic effects might explain why statins outperform other lipid lowering drugs and statins are considered as the first-choice medicament to reduce lipid risk in the secondary prevention of multiple CVD. The reduction of LDL cholesterol by 1.0 mmol/L with statins reduces the risk of a major vascular events (myocardial infarction or coronary death, stroke, coronary revascularization) by 25%, regardless of the baseline LDL cholesterol level (37). According to the European Society for Cardiology (ESC) clinical guideline for dyslipidemias (ESC), statin treatment is recommended when patients have a LDL-C level greater than 3.0 mmol/L or have a (very) high 10-year risk to develop a fatal cardiovascular event (38).

PCSK9 inhibitors (Evolocumab, Bococizumab and Alirocumab): Although statins are the most-effective therapy available now for lowering LDL-C level, in part of the treatment population, the desired LDL-C level can't be reached with the maximal tolerated dose of statin therapy. Proprotein convertase subtilisin/kexin type 9 (PCSK9) is an enzyme which regulates the degradation of LDL-receptors (LDLR) in the liver. Monoclonal antibodies against PCSK9 reduce the degradation of LDL receptors and increase the clearance of the LDL-C (39). On the other hand, atorvastation treatment reciprocally increased PCSK9 protein levels in serum by 34% compared to the placebo controlled group (40). This data suggested that PCSK9 inhibition in combination with statin treatment can further decrease LDL-C levels. Phase III clinical trial results proved that combination of statin and PCSK9 inhibitors can further decrease the LDL-C level and combination therapies are recommended if necessary (38, 41).

Cholesterol absorption inhibitors (Ezetimibe): Ezetimibe reduces the absorption of cholesterol from the intestine via a mechanism involving the Niemann-Pick C1-like 1 (NPC1L1) protein on the gastrointestinal epithelial cells (42). Ezetimibe itself can decrease LDL-C around 15-22% and in combination with statin treatment and additional 15-20% LDL-C lowering observed (38).

LDL-C reduction through the above-mentioned medications is one of the most efficient secondary prevention to decrease both relative and absolute risk. In certain extend, several clinical trial results indicated these beneficial effect is achieved not only through the lipid lowering, but also reducing the inflammation, implying that anti-inflammatory medications are important part of atherosclerosis treatment (43).

II.2 ANTI-INFLAMMATORY AGENTS

Inflammation plays critical role in the development and progression of atherosclerosis (18, 19) and the discovery of drugable targets that reduce inflammation in atherosclerosis has been a topic of intense research in cardiovascular medicine for several decades. Inflammation regulatory pathways such as interleukin-1(IL-1), tumor necrosis factor α (TNF α), interleukin-6 (IL-6) are extensively targeted by selective inhibitors and monoclonal antibodies and some medicaments are in Phase III clinical trials. Also vascular targeted antioxidants, selective phospholipase A2 (PLA2) inhibitors, adhesion molecule inhibitors, serpines/sirtuins, FLAP inhibitors, 5-LO inhibitors, CCL2-CCR2 inhibitors and other molecules underwent extensive experimental and clinical research (extensively reviewed (44, 45)) Recently, promising results were reported by the CANTOS trial using monoclonal antibody named canakinumab.

Canakinumab: Canakinumab is a monoclonal antibody against Interleukin 1β (IL1β) and an approved drug for treating cryopyrin-associated periodic syndrome (CAPS) (46). IL1β is released from macrophages and one of the main mediators of innate immunity. In Canakinumab-treated patients, markers of inflammation such as Interleukin 6 (IL-6) and high sensitivity CRP (hs-CRP) were decreased without changes in their lipid profile (47) resulting in an reduced cardiovascular event risk score. A randomized double blinded clinical trial result indicated that canakinumab significantly lowers the occurrence of cardiovascular events and cardiovascular deaths compared to the placebo control group. However, an increasing incidence of fatal infections, sepsis and mild thrombocytopenia was associated with Canakinumab treatment (48).

II.3 ANTI-THROMBOTIC AGENTS

Arterial thrombosis is commonly initiated by the rupture of an atherosclerotic plaque which triggers platelet aggregation and thrombus formation (49). This process is called atherothrombosis and is the main cause of mortality in atherosclerosis. Hence, inhibiting platelet aggregation (anti-aggregants) and inhibiting blood coagulation (anti-coagulants) are pivotal parts of anti-atherosclerosis treatment, especially in the late stages. The damaged endothelium recruit platelets and enables primary and secondary hemostasis. In contrast, the quiescent healthy endothelium prevents these thrombogenic processes via prostaglandin I2 activation (50) and NO induction (51).

Thromboxane A2 inhibitor (Aspirin): Low dose aspirin (acetylsalycilic acid) inhibits platelet cyclooxygenase which is vital enzyme for thromboxane A2 generation. Thromboxane A2 triggers platelet aggregation and adhesion. The long-term usage of antiplatelet therapies shown to reduce vascular events around 25% among patients who have already experienced occlusive vascular diseases (52). In primary prevention trials, aspirin usage reduced the frequency of cardiovascular events over 12% in patients that have a myocardial infarction in their history (53).

$P2Y_{12}$ inhibitors (Clopidegril, Ticagrelor, Prasugrel, Cangrelor): Inhibiting the $P2Y_{12}$ receptor blocks the binding of extracellular adenosine diphosphate (ADP) to its receptor, which prevents thrombocyte aggregation. The $P2Y_{12}$ inhibitor (clopidegril) combined with aspirin reduced serious vascular events by 20% in myocardial infarction patients with ST-segment elevation. (54). Clopidegril is prodrug which is metabolized and converted into its active form by Cytochrome P 450 enzyme (CYP). Patients who have different isoforms of the CYP enzyme respond different to clopidegril treatment (49). Prasugrel, another P2Y12 inhibitor, acts faster and was shown to reduce recurrent vascular events and stent complications compared to clopidegril after angioplasty and PCI (55).

GPIIb/IIIa inhibitors (Tirofiban, Eptifibatide, Abciximb): GPIIb/IIIa inhibitors(GPIs) are potent and rapid acting antiplatelet drugs. The GPIs target the $\alpha_{IIb}\beta_3$ integrin on the platelet membrane, thereby inhibiting platelet aggregation (56). Meta-analysis indicted that 30-day death or myocardial infarction was moderately decreased after using these medications compared to the placebo group, the effect was highly pronounced in patients undergoing PCI (57).

PAR-1 inhibitors (Voraxapar): The novel class of antiplatelets drugs are developed to inhibit protease activated receptors (PAR-1) which mediates thrombin-induced platelet activation. Interestingly, the PAR-1 receptors are not only present at the platelets but also at endothelial cells, smooth muscle cells and fibroblasts (58). A phase III clinical trial indicates that Voraxapar addition to the standard treatment can decrease the risk of cardiovascular death and ischemic events, but moderate and severe bleedings occur more often (59).

From the above, it becomes evident that among the core atherogenic pathways, only lipid accumulation, inflammation and platelet aggregation are addressed by currently available therapeutic agents and therapeutic agent in development. As emphasized above, the endothelium plays a pivotal role in all atherogenic pathways, yet no endothelial-targeted therapy is available. In the next section, we elaborate on how endothelial-specific epigenetic molecules might offer a potential therapeutic benefit for patients suffering from atherosclerosis.

III. ENDOTHELIAL SPECIFIC PRO-ATHEROGENIC TREATMENT

Endothelial cells play a crucial role in the development and progression of atherosclerosis. Stimulated by uniform laminar flow, the endothelial cells acquire healthy quiescent phenotype that precludes atherosclerosis pathways (24). In contrast, disturbed flow alters the endothelial phenotype, which enables atherosclerosis pathways. This phenotypic shift might be the consequence of differential gene expression regulated by epigenetic modifications. An important feature of the epigenetics is the reversibility.

Following the fact that epigenetic molecules are well established as mediators of health and disease, epigenetic enzymes or their activator/inhibitors can be exploited as therapeutic target (60, 61).

III.1. EPIGENETIC MOLECULES ARE PROMISING CANDIDATES TO TREAT THE PRO-ATHEROGENIC ENDOTHELIUM

Epigenetics refers to heritable yet stable changes in genome function resulting from changes in the chromatin without alterations in the underlying DNA sequence. In other words "changing the cells' phenotype without changing genotype"(62). Epigenetic modifications can explain how one fertilized egg gives rise to more than 200 different cell types that compose the human body (63). Moreover, epigenetics explain novel mechanisms for complex and chronic diseases such as diabetes (64), cancer (65, 66) and cardiovascular diseases (67). Epigenetic traits consist of several interconnected parameters, i.e. histone modifications and DNA methylation (68).

On average, a human cell has a 2-metre long DNA molecule. Cell size and timely transcriptional activity requires organized folding of the DNA. In the nucleus, the DNA strand is 1.7 times coiled around an octamer of core histone proteins, forming the nucleosomes. (H2A, H2B, H3 and H4, 2 copies of each) (69). Core histone proteins contain a globular domain and an amino terminal tail which can undergo post-transcriptional modifications such as acetylation, methylation (lysines/arginines), phosphorylation, sumoylation, ubiquitylation, ADP ribosylation, deamination, proline isomerization and other modifications (70). Many of these modifications are known to play functional roles in gene expression. The functional role of lysine acetylation and methylation of histone core proteins on transcriptional level are well studied. For instance, histone acetylation is associated with transcriptional activation by amongst others neutralizing the basic charges of lysine residues (71), whereas the consequence of histone methylation depend on the specific lysine or arginine residue that is methylated. Methylation of H3K27 and H3K9 correlate with the transcriptional repression, but methylation of H3K4 and H3K36 correlates transcriptional activation (72). Thus, histone modifications affect gene expression via altering chromatin structure and accessibility.

DNA methylation refers to the addition of a methyl group (-CH3) on 5th carbon atom of cytosine of the DNA. When DNA methylation occurs at gene promoter areas rich in cytosine and guanidine residues (so-called CpG islands) linked to the transcriptional repression (73). However, 5 methylcytosine (5mC) also found in gene body (transcribable region) and related to the supportive function in transcription (74, 75). The contribution of epigenetic mechanisms to atherosclerosis development is under extensive research. Here, we focus on the contribution of epigenetic modifications in the early stages of atherosclerosis and question if reversing those changes may have anti-atherosclerosis capacity.

One of the main epigenetic features found in early atherogenesis is DNA hypomethylation. CpG islands in newly forming atherosclerosis lesions are mostly hypomethylated compared to non-atherogenic vessel areas. However, several hypermethylated genes also be identified (76). By using high performance liquid chromatography analysis, the 5mC content was 3.2%±0.2 in healthy arteries and declined to 2.9%±0.1 in advanced atherosclerosis lesions (77).

The finding was supported by the study results implicating that 84% of differentially methylated promoter sites were hypomethylated (de-methylated) in femoral artery atherectomy samples compared to the non-sclerosed mammary artery samples (78). These studies indicate that DNA hypomethylation is dominantly occurring during atherosclerosis.

Human carotid artery atherosclerosis samples showed increased acetylation (active mark) of H3K9 and H3K27 in endothelial cells in early stage of atherosclerosis and this increment was consistently kept high in advanced atherosclerotic plaques. Quantitative PCR result revealed that the expression of histone acetyltransferase *GCN5L* is elevated in advanced atherosclerotic plaques compared to control. Also, H3K4 methylation (active mark) was increased in endothelial cells in early stage maintained high during the advanced atherosclerosis (79).This finding matches with the previous finding from Wierda et al (80), who showed increased H3K4 methylation and expression of the H3K4 writer MLL2/4 in endothelial cells in atherosclerotic lesions compared to non-atherogenic sites. The methylation level of H3K27 (repressive mark) is higher in early stages of atherosclerosis and normalizes during the advanced atherosclerotic plaques in endothelial cells (79). It is interesting phenomenon that concurrent increment of H3k27 methylation, H3k27 acetylation and H3k4 methylation was observed in early stage of atherosclerosis, which may imply the presence of "bivalent domains" (81) that might contribute to endothelial dysfunction and atherosclerosis. However, it is still elusive whether these opposing modifications are occurring at the same gene locus or reflect epigenetic regulation across different loci.

The above-mentioned data indicate that during atherosclerosis, the epigenome of the endothelial cells changes, and it raises the question if we can we ameliorate atherosclerosis progression via reversal of these modifications? Here we demonstrate the beneficial effects of epigenetic therapies by exemplifying two histone modifying enzymes as molecules for targeting the pro-atherogenic endothelium and promote endothelial homeostasis.

EZH2- ENHANCER OF ZESTE HOMOLOGUE 2

Rationale: Methylation of H3K27 is increased during the early stage of atherosclerosis in endothelial cells. Thereby, decreasing Ezh2 might be beneficial to ameliorate pro-atherogenic endothelium via reducing the methylation of H3K27.

Enhancer of zeste homologue 2 (Ezh2) is the catalytic subunit of Polycomb Repressive Complex 2 (PRC 2). In mammals, Polycomb Repressive Complex 2 core subunits are EED, SUZ12 and EZH2/EZH1. EZH2 and its close homologue EZH1 have SET domain which encompasses its histone methyltransferase activity. EZH2 trimethylates lysine 27 on N terminal tail of histone 3 protein. H3K27me3 act as docking site for chromobox-domain (CBX) of Polycomb Repressive Complex 1. H3K27me3 is a repressive chromatin mark that leads to the formation of condensed chromatin and transcriptional silencing of the target gene.(82) The rationale of targeting EZH2 in the endothelium to ameliorate atherogenesis is summarized in Table 1. Shear stress regulates the protein expression of histone methyltransferase EZH2. Under atheroprotective -laminar flow, EZH2 protein expression is low, thereby inducing a quiescent phenotype in endothelial cells (83). Elevated serum homocysteine is one of the independent risk factors of the atherosclerosis and has adverse effects on endothelial cells.

Interestingly, homocysteine enhanced fat accumulation and increased EZH2 and H3K27me3 levels are found in atherosclerosis-prone APOE-/- mice (84). The metabolic conversion of homocysteine Hcy-thiolactone induces the expression of EZH2 in a dose-dependent manner in endothelial cells (85). Moreover, LDL-C can reduce the expression of KLF2 – a well-established antiatherogenic transcription factor - which can be precluded by inhibiting EZH2 (86). These findings indicate that the elevated expression levels of EZH2 during atherogenesis is detrimental for endothelial homeostasis and might aggravate atherogenesis. One of the main representatives of the statin therapies, *i.e.* simvastatin decreased the transcriptional and translational levels of EZH2 in colorectal cancer cells. This finding suggest that some beneficial effects of statin outside the lipid-lowering effects might be achieved through the reduction of EZH2 in endothelial cells (87).

Besides the endothelium, elevated expression of EZH2 in marcophages enhances foam cell formation via *ABCA1* gene promoter DNA methylation(88) and EZH2 affects DNA methylation in polycomb target gene areas via modulating DNMTs (89). Based on the above, EZH2 inhibition might be beneficial to endothelial homeostasis and may ameliorate atherosclerosis progression.

SIRT1- NAD+ DEPENDENT DEACETYLASE GROUP III

Rationale: Acetylation of H3K9 and H3K27 is increased during the early and advanced stages of atherosclerosis in endothelial cells. Thereby increasing histone deacetylase SIRT1 might be beneficial via reversing the acetylation of H3K9 and H3K27.

Sirtuin 1, the mammalian ortholog of yeast Sir2, is a nicotinamide adenine dinucleotide (NAD) dependent deacetylase. SIRT1 removes acetyl group from histone tails and non-histone proteins. Higher expression levels of SIRT1 positively correlate with lifespan in yeast, flies and mice.(90) SIRT1 activation protects cardiomyocytes from endoplasmic reticulum(ER) stress-induced apoptosis by attenuating PERK/eIF2α pathway activation. The rationale of using SIRT1 to ameliorate atherogenesis is exemplified in *Table 1*.

SIRT1 is also a shear stress responsive protein. Atheroprotective - uniform laminar flow induces SIRT1 protein expression, while static or oscillatory shear stress inhibits SIRT1 expression(91). As mentioned above, inflammation plays a key role in endothelial dysfunction and atherogenesis. NF-κB is the core transcription factor of inflammation and inflammation mediated responses. SIRT1 can de-acetylate and deactivate NF-κB, thereby inhibiting inflammation(92). Also endothelial senescence contributes to the atherosclerosis development and SIRT1 induction was shown to prevent from H_20_2-induced endothelial senescence(93). Moreover, SIRT1 elevates NO production in endothelial cells. Albeit that the SIRT1-dependent favorable effects on the endothelium are pleiotropic, in synergy these effects enable endothelial homeostasis and might offer therapeutic benefit in atherosclerosis.

Several clinical trials have demonstrated and the SIRT1 activator SRT2014 can decrease serum LDL levels (94) via decreasing the PCSK9 secretion of from hepatic cells (95). Interestingly, SIRT1 modulates DNA methylation and the target genes overlap with the Polycomb group proteins (96), implying an interconnection between these two epigenetic enzymes.

Functions	EZH2- histone methyltransferase (writer)	SIRT1- NAD dependent histone deacetylase (eraser)
Non-uniform/turbulent flow	Laminar flow decreases Ezh2 and upregulation of Ezh2 post-transcriptionally inhibit MAPK7 activity Static condition upregulates Ezh2 (83)	Laminar flow increases SIRT1 and its activity Static/oscillatory shear stress inhibits SIRT1 level (91)
Lipid accumulation	Homocystein induced atherosclerosis via upregulating EZH2 and H3K27me3 in APOE-/- mice(84) Homocystein metabolite HCy-thiolactone(1000uM) stimulation induce EZH2 gene expression 5.36 fold in endothelial cells (85)	SIRT1 activator SRT3025 reduces serum LDL-C via reducing hepatic PCSK9 secretion (95)
Inflammation / leukocyte recruitment	Overexpression of EZH2 induces lipid accumulation in macrophages by methylating ABCA1 gene promoter thereby accelerate atherosclerosis progression in apoE-/- mice (88)	Hyperglycemia induced endothelial dysfunction is prevented via SIRT1 dependent P66shC downregulation (97) SIRT1 deacetylase NFκB thereby prevent chronic inflammation (92)
Blood clotting	EZH2 knockdown prevents LDL induced downregulation of thrombomodulin (TM) thereby prevents from the unnecessary platelet aggregation (86)	
Endothelial senescence		H202 induced endothelial senescence rescued by the SIRT1 (93) SIRT1 downregulates PAI thereby prevents replicative senescence (98)
Accumulation of fibrous element (EndMT)	Ezh2 regulates sm22a/TAGLN expression (99)	SIRT1 modulates EMT in cancer (100)
NO production	EZH2 knockdown prevents LDL induced downregulation of the NO decline through the KLF2 promoter methylation (86)	SIRT1 induce NO production via increasing eNOS production (101) Vitamin D rescues endothelial cells from oxidative stress mek/erk- SIRT1 cascade(102) SIRT1 promotes mitochondrial biogenesis via activation of PGC1α
DNA methylation	Ezh2 directly controls DNA methylation (89)	SIRT1 affects DNA methylation of polycomb group target genes (96)

Table 1. *EZH2 and SIRT1 role in endothelial homeostasis and contribution to the development of atherosclerosis*

III.2. AVAILABILITY OF THE EPIGENETIC ENZYME MEDICAMENTS

The current therapeutic strategies and possibilities of using epigenetic molecules for the treatment of cancer and other diseases have been reviewed previously (103, 104) and several studies are already using EZH2 and SIRT1 as epigenetic targets in clinical trials.(see table 2)

The possibility of using histone methyltransferases and demethylases(105) especially EZH2 inhibitors (106) in cancer therapy have been reviewed previously. EZH2 inhibitors are being tested in Phase I/II clinical trials in cancer field, but they are not yet used in trials for atherosclerosis. (Table 2). Compared to the EZH2, SIRT1 activators are well known in field of the cardiovascular medicine. Several SIRT1 activators are recognized and being tested and cardiovascular outcomes were measured (Table 2). Resveratol, a well-known activator of SIRT1 was used in cancer, neurological disorder, cardiovascular diseases, diabetes and other diseases clinical trials (extensively reviewed in (107)).

Drug name	*Mechanism of action*	*Phase*	*Indication*	*Clinical trial #*
Tazemetostat	EZH2 inhibitor	II	INI1-negative tumors	NCT02601950
GSK2816126	EZH2 inhibitor	I	Diffuse B cell Lymphoma, other Non- Hodgkin Lymphoma, solid tumors and multiple myeloma	NCT02082977
SRT2104	SIRT1 activator	I	60-80 years old males	NCT00964340
SRT2104	SIRT1 activator	II	Otherwise healthy smokers	NCT01031108

Table 2. EZH2 inhibitors and SIRT1 activators in clinical trials. *Showing early phase clinical trials using above mentioned epigenetic enzymes – implying these therapeutic molecules are already available and tolerated to use in human.*

From above mentioned results we can see that EZH2 inhibition (open chromatin) and SIRT1 induction (closed chromatin) can be beneficial in providing endothelial homeostasis thereby slowing down atherosclerosis progression. Moreover, small molecules that inhibit EZH2 or activate SIRT1 are available in clinical trials which warrants the adaptation of cardiovascular endpoints in these trials. Moreover, given the current safety record of these experimental medicines, the clinical testing in the context of atherosclerosis could be performed in the near future.

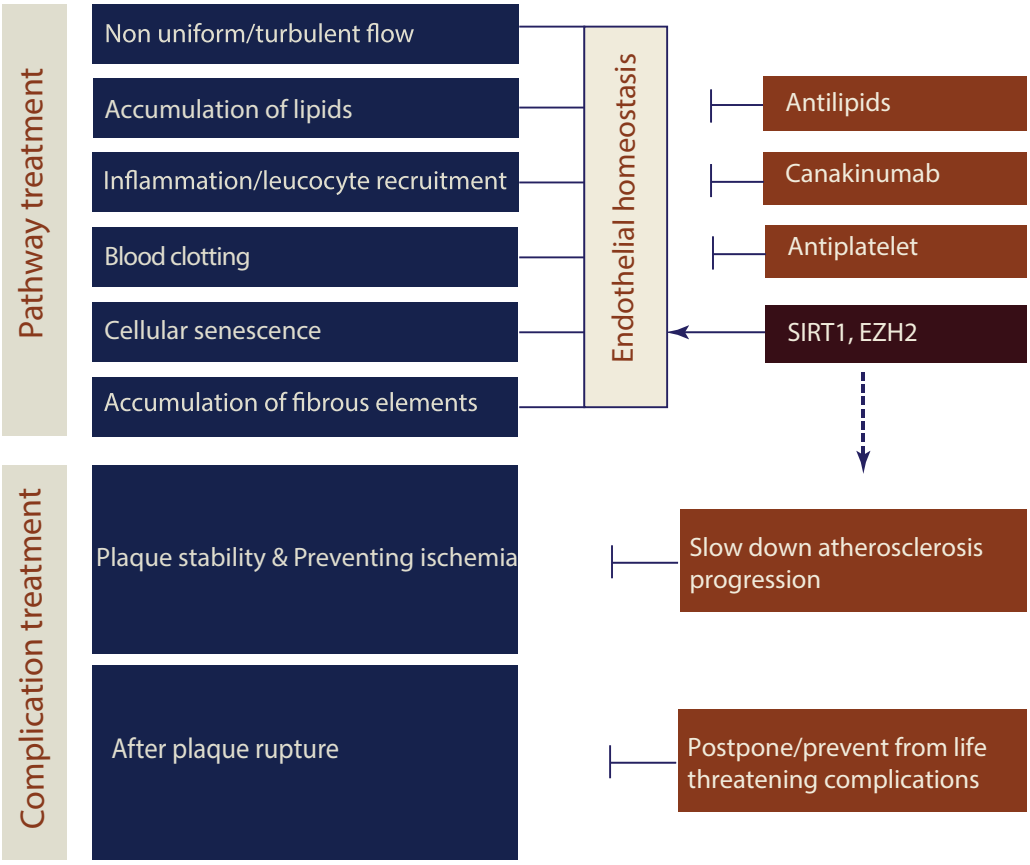

Figure 3. SIRT1 activator and EZH2 inhibitor based treatment of atherosclerotic endothelium. *We explained how epigenetic molecules can be promising candidates to treatment pro-atherogenic endothelium using two pre-examplary molecules namely SIRT1 and EZH2. Together with the current medications, our proposed pro-atherogenic endothelium treatment may slow down the atherosclerosis progression and prevent from the life-threatening complications.*

Although the chromatin modeling consequence of these two enzymes is controversial, the effect is target gene dependent. Epigenetic modifications can be reversed and "Epigenetic editing" is an emerging research field in medicine (extensively reviewed (108, 109)). Epigenetic repression and epigenetic activation are successfully accomplished by using Zinc Finger Proteins (ZFP), Transcription- Activator-Like Effectors (TALEs) arrays or Clustered Regulatory Interspaced Short Palindromic Repeats (CRISPR). Moreover, the newly edited modifications are shown sustainability through the cell division (110).

III.3. TARGETED APPROACH TO ENDOTHELIAL CELLS IN ATHEROPRONE AREAS

Since atherosclerosis lesions develop exclusively at vascular branches and curvatures, the ideal treatment would be to target the affected endothelial cells at these atheroprone areas only. Moreover, lineage committed cell have a distinct epigenome landscape including DNA methylation and histone modifications, (111, 112) which might make the systemic application of epigenetic drugs harmful to non-target cells in the human body. Promising liposome-based drug delivery approaches are available that might be suitable to deliver therapeutic agents to the pre-atherogenic activated endothelium exclusively (113). For instance, SAINT-O-Somes directed to microvascular endothelial cells expressing VCAM-1 (114) successfully inhibited inflammatory genes in microvascular endothelial cells without toxic effects liver and kidney (115). Also, E-selectin targeted immunoliposomes successfully abrogated ANCA-induced glomerulonephritis via targeted delivery of siRNA against NF-kB in glomerular endothelial cells (116). Some studies used specific peptides for the targeted treatment approach. For example, the ICAM-targeted CLIRRTSIC peptide was successful in targeting endothelial cells in disturbed flow exposed areas in vivo (117). Outcome of endothelial cells-specific SIRT1 overexpression was tested in ApoE-/- mice; this study revealed an enhancement of the endothelium-dependent vasodilation and less atherosclerosis lesion development (118).

CONCLUSION

Endothelial dysfunction is a critical component of the development of the atherosclerosis. Current atherosclerosis treatment encompasses lipid lowering, inhibiting platelet aggregation and anti-inflammatory drugs, however there is no treatment available that targets pathway “endothelial dysfunction”. In this review, we proposed the targeting of two epigenetic pathways (i.e. SIRT1 and EZH2) to ameliorate atherogenesis and exemplify a number of established medicaments that would allow for rapid clinical valorization. Moreover, we set forth a future strategy that utilizes a cell-targeted strategy using drug carriers that might further enhance endothelial homeostasis and ameliorate atherosclerosis development.

REFERENCES

1. Davignon J, Ganz P. Role of endothelial dysfunction in atherosclerosis. Circulation. 2004;109(23 suppl 1):III-27-III-32.
2. Gimbrone MA. Vascular endothelium: an integrator of pathophysiologic stimuli in atherosclerosis. The American journal of cardiology. 1995;75(6):67B-70B.
3. Lusis AJ. Atherosclerosis. Nature. 2000;407(6801):233-41.
4. Celermajer DS, Sorensen KE, Gooch V, Spiegelhalter D, Miller O, Sullivan I, et al. Non-invasive detection of endothelial dysfunction in children and adults at risk of atherosclerosis. The lancet. 1992;340(8828):1111-5.
5. Al Suwaidi J, Hamasaki S, Higano ST, Nishimura RA, Holmes DR, Lerman A. Long-term follow-up of patients with mild coronary artery disease and endothelial dysfunction. Circulation. 2000;101(9):948-54.
6. Canto JG, Iskandrian AE. Major risk factors for cardiovascular disease: debunking the only 50% myth. Jama. 2003;290(7):947-9.
7. TEXON M. A hemodynamic concept of atherosclerosis, with particular reference to coronary occlusion. AMA archives of internal medicine. 1957;99(3):418-27.
8. Caro C, Fitz-Gerald J, Schroter R. Arterial wall shear and distribution of early atheroma in man. Nature. 1969;223(5211):1159-61.
9. Conway DE, Schwartz MA. Flow-dependent cellular mechanotransduction in atherosclerosis. J Cell Sci. 2013;126(22):5101-9.
10. Castier Y, Lehoux S, Hu Y, Fonteinos G, Tedgui A, Xu Q. Characterization of neointima lesions associated with arteriovenous fistulas in a mouse model. Kidney international. 2006;70(2):315-20.
11. Hollander W, Madoff I, Paddock J, Kirkpatrick B. Aggravation of atherosclerosis by hypertension in a subhuman primate model with coarctation of the aorta. Circulation research. 1976;38(6):63-72.
12. Nam D, Ni C-W, Rezvan A, Suo J, Budzyn K, Llanos A, et al. Partial carotid ligation is a model of acutely induced disturbed flow, leading to rapid endothelial dysfunction and atherosclerosis. American Journal of Physiology-Heart and Circulatory Physiology. 2009;297(4):H1535-H43.
13. Brooks AR, Lelkes PI, Rubanyi GM. Gene expression profiling of human aortic endothelial cells exposed to disturbed flow and steady laminar flow. Physiological genomics. 2002;9(1):27-41.
14. Passerini AG, Polacek DC, Shi C, Francesco NM, Manduchi E, Grant GR, et al. Coexisting proinflammatory and antioxidative endothelial transcription profiles in a disturbed flow region of the adult porcine aorta. Proceedings of the National Academy of Sciences of the United States of America. 2004;101(8):2482-7.
15. Dimmeler S, Fleming I, Fisslthaler B, Hermann C, Busse R, Zeiher AM. Activation of nitric oxide synthase in endothelial cells by Akt-dependent phosphorylation. Nature. 1999;399(6736):601-5.
16. Corson MA, James NL, Latta SE, Nerem RM, Berk BC, Harrison DG. Phosphorylation of endothelial nitric oxide synthase in response to fluid shear stress. Circulation research. 1996;79(5):984-91.
17. Green JP, Souilhol C, Xanthis I, Martinez-Campesino L, Bowden NP, Evans PC, et al. Atheroprone flow activates inflammation via endothelial ATP-dependent P2X7-p38 signalling. Cardiovascular research. 2017.
18. Libby P, Ridker PM, Maseri A. Inflammation and atherosclerosis. Circulation. 2002;105(9):1135-43.
19. Libby P, Ridker PM, Hansson GK, on Atherothrombosis LTN. Inflammation in atherosclerosis: from pathophysiology to practice. Journal of the American College of Cardiology. 2009;54(23):2129-38.
20. Cybulsky MI, Iiyama K, Li H, Zhu S, Chen M, Iiyama M, et al. A major role for VCAM-1, but not ICAM-1, in early atherosclerosis. Journal of Clinical Investigation. 2001;107(10):1255.

21. Greaves DR, Gordon S. Thematic review series: the immune system and atherogenesis. Recent insights into the biology of macrophage scavenger receptors. Journal of lipid research. 2005;46(1):11-20.
22. Westhorpe CL, Dufour EM, Maisa A, Jaworowski A, Crowe SM, Muller WA. Endothelial cell activation promotes foam cell formation by monocytes following transendothelial migration in an in vitro model. Experimental and molecular pathology. 2012;93(2):220-6.
23. Moore KJ, Sheedy FJ, Fisher EA. Macrophages in atherosclerosis: a dynamic balance. Nature Reviews Immunology. 2013;13(10):709-21.
24. Krenning G, Barauna VG, Krieger JE, Harmsen MC, Moonen J-RA. Endothelial plasticity: shifting phenotypes through force feedback. Stem cells international. 2016;2016.
25. Souihol CE, Harmsen MC, Evans PC, Krenning G. Endothelial-Mesenchymal Transition in Atherosclerosis. Cardiovascular research. 2018.
26. Chen P-Y, Qin L, Baeyens N, Li G, Afolabi T, Budatha M, et al. Endothelial-to-mesenchymal transition drives atherosclerosis progression. The Journal of clinical investigation. 2015;125(12):4514.
27. Evrard SM, Lecce L, Michelis KC, Nomura-Kitabayashi A, Pandey G, Purushothaman K-R, et al. Endothelial to mesenchymal transition is common in atherosclerotic lesions and is associated with plaque instability. Nature communications. 2016;7.
28. Moonen JR, Lee ES, Schmidt M, Maleszewska M, Koerts JA, Brouwer LA, et al. Endothelial-to-mesenchymal transition contributes to fibro-proliferative vascular disease and is modulated by fluid shear stress. Cardiovasc Res. 2015;108(3):377-86. doi: 10.1093/cvr/cvv175. Epub 2015 Jun 17.
29. Mahmoud M, Kim HR, Xing R, Hsiao S, Mammmoto A, Chen J, et al. TWIST1 integrates endothelial responses to flow in vascular dysfunction and atherosclerosis. Circulation research. 2016:CIRCRESAHA. 116.308870.
30. Campisi J, di Fagagna FdA. Cellular senescence: when bad things happen to good cells. Nature reviews Molecular cell biology. 2007;8(9):729.
31. Erusalimsky JD. Vascular endothelial senescence: from mechanisms to pathophysiology. Journal of Applied Physiology. 2009;106(1):326-32.
32. Minamino T, Miyauchi H, Yoshida T, Ishida Y, Yoshida H, Komuro I. Endothelial cell senescence in human atherosclerosis. Circulation. 2002;105(13):1541-4.
33. Ference BA, Ginsberg HN, Graham I, Ray KK, Packard CJ, Bruckert E, et al. Low-density lipoproteins cause atherosclerotic cardiovascular disease. 1. Evidence from genetic, epidemiologic, and clinical studies. A consensus statement from the European Atherosclerosis Society Consensus Panel. European heart journal. 2017;38(32):2459-72.
34. Liao JK, Laufs U. Pleiotropic effects of statins. Annu Rev Pharmacol Toxicol. 2005;45:89-118.
35. Istvan ES, Deisenhofer J. Structural mechanism for statin inhibition of HMG-CoA reductase. Science. 2001;292(5519):1160-4.
36. Ridker PM, Rifai N, Clearfield M, Downs JR, Weis SE, Miles JS, et al. Measurement of C-reactive protein for the targeting of statin therapy in the primary prevention of acute coronary events. New England Journal of Medicine. 2001;344(26):1959-65.
37. Laufs U, La Fata V, Plutzky J, Liao JK. Upregulation of endothelial nitric oxide synthase by HMG CoA reductase inhibitors. Circulation. 1998;97(12):1129-35.
38. Catapano AL, Graham I, De Backer G, Wiklund O, Chapman MJ, Drexel H, et al. 2016 ESC/EAS Guidelines for the Management of Dyslipidaemias. European heart journal. 2016;37(39):2999-3058.
39. Dadu RT, Ballantyne CM. Lipid lowering with PCSK9 inhibitors. Nature Reviews Cardiology. 2014;11(10):563-75.
40. Careskey HE, Davis RA, Alborn WE, Troutt JS, Cao G, Konrad RJ. Atorvastatin increases human serum levels of proprotein convertase subtilisin/kexin type 9. Journal of lipid research. 2008;49(2):394-8.

41. Robinson JG, Farnier M, Krempf M, Bergeron J, Luc G, Averna M, et al. Efficacy and safety of alirocumab in reducing lipids and cardiovascular events. New England Journal of Medicine. 2015;372(16):1489-99.
42. Garcia-Calvo M, Lisnock J, Bull HG, Hawes BE, Burnett DA, Braun MP, et al. The target of ezetimibe is Niemann-Pick C1-Like 1 (NPC1L1). Proceedings of the National Academy of Sciences of the United States of America. 2005;102(23):8132-7.
43. Ridker PM. Residual inflammatory risk: addressing the obverse side of the atherosclerosis prevention coin. European heart journal. 2016;37(22):1720-2.
44. Ridker PM, Lüscher TF. Anti-inflammatory therapies for cardiovascular disease. European heart journal. 2014;35(27):1782-91.
45. Charo IF, Taub R. Anti-inflammatory therapeutics for the treatment of atherosclerosis. Nature reviews Drug discovery. 2011;10(5):365.
46. Lachmann HJ, Kone-Paut I, Kuemmerle-Deschner JB, Leslie KS, Hachulla E, Quartier P, et al. Use of canakinumab in the cryopyrin-associated periodic syndrome. New England Journal of Medicine. 2009;360(23):2416-25.
47. Ridker PM, Howard CP, Walter V, Everett B, Libby P, Hensen J, et al. Effects of interleukin-1β inhibition with canakinumab on hemoglobin A1c, lipids, C-reactive protein, interleukin-6, and fibrinogen: a phase IIb randomized placebo controlled trial. Circulation. 2012:CIRCULATIONAHA. 112.122556.
48. Ridker PM, Everett BM, Thuren T, MacFadyen JG, Chang WH, Ballantyne C, et al. Antiinflammatory therapy with canakinumab for atherosclerotic disease. 2017.
49. Meadows TA, Bhatt DL. Clinical aspects of platelet inhibitors and thrombus formation. Circulation research. 2007;100(9):1261-75.
50. Weksler BB, Marcus AJ, Jaffe EA. Synthesis of prostaglandin I2 (prostacyclin) by cultured human and bovine endothelial cells. Proceedings of the National Academy of Sciences. 1977;74(9):3922-6.
51. Loscalzo J. Nitric oxide insufficiency, platelet activation, and arterial thrombosis. Circulation research. 2001;88(8):756-62.
52. Trialists'Collaboration A. Collaborative meta-analysis of randomised trials of antiplatelet therapy for prevention of death, myocardial infarction, and stroke in high risk patients. Bmj. 2002;324(7329):71-86.
53. Baigent C, Blackwell L, Collins R, Emberson J, Godwin J, Peto R, et al. Aspirin in the primary and secondary prevention of vascular disease: collaborative meta-analysis of individual participant data from randomised trials. Elsevier; 2009.
54. Sabatine MS, Cannon CP, Gibson CM, López-Sendón JL, Montalescot G, Theroux P, et al. Addition of clopidogrel to aspirin and fibrinolytic therapy for myocardial infarction with ST-segment elevation. New England Journal of Medicine. 2005;352(12):1179-89.
55. Wiviott SD, Braunwald E, McCabe CH, Montalescot G, Ruzyllo W, Gottlieb S, et al. Prasugrel versus clopidogrel in patients with acute coronary syndromes. New England Journal of Medicine. 2007;357(20):2001-15.
56. Topol EJ, Byzova TV, Plow EF. Platelet GPIIb-IIIa blockers. The Lancet. 1999;353(9148):227-31.
57. Roffi M, Chew D, Mukherjee D, Bhatt D, White J, Moliterno D, et al. Platelet glycoprotein IIb/IIIa inhibition in acute coronary syndromes. Gradient of benefit related to the revascularization strategy. European Heart Journal. 2002;23(18):1441-8.
58. Coughlin SR. Thrombin signalling and protease-activated receptors. Nature. 2000;407(6801):258-64.
59. Morrow DA, Braunwald E, Bonaca MP, Ameriso SF, Dalby AJ, Fish MP, et al. Vorapaxar in the secondary prevention of atherothrombotic events. New England Journal of Medicine. 2012;366(15):1404-13.
60. Egger G, Liang G, Aparicio A, Jones PA. Epigenetics in human disease and prospects for epigenetic therapy. Nature. 2004;429(6990):457-63.

61. Altucci L, Rots MG. Epigenetic drugs: from chemistry via biology to medicine and back. BioMed Central; 2016.
62. Berger SL, Kouzarides T, Shiekhattar R, Shilatifard A. An operational definition of epigenetics. Genes & development. 2009;23(7):781-3.
63. Reik W. Stability and flexibility of epigenetic gene regulation in mammalian development. Nature. 2007;447(7143):425-32.
64. Villeneuve LM, Reddy MA, Natarajan R. Epigenetics: deciphering its role in diabetes and its chronic complications. Clinical and Experimental Pharmacology and Physiology. 2011;38(7):451-9.
65. Sharma S, Kelly TK, Jones PA. Epigenetics in cancer. Carcinogenesis. 2010;31(1):27-36.
66. Esteller M. Epigenetics in cancer. New England Journal of Medicine. 2008;358(11):1148-59.
67. Ordovás JM, Smith CE. Epigenetics and cardiovascular disease. Nature Reviews Cardiology. 2010;7(9):510.
68. Allis CD, Jenuwein T. The molecular hallmarks of epigenetic control. Nature Reviews Genetics. 2016;17(8):487.
69. Luger K, Mader AW, Richmond RK, Sargent DF, Richmond TJ. Crystal structure of the nucleosome core particle at 2.8 angstrom resolution. Nature. 1997;389(6648):251.
70. Kouzarides T. Chromatin modifications and their function. Cell. 2007;128(4):693-705.
71. Shahbazian MD, Grunstein M. Functions of site-specific histone acetylation and deacetylation. Annu Rev Biochem. 2007;76:75-100.
72. Strahl BD, Allis CD. The language of covalent histone modifications. Nature. 2000;403(6765):41.
73. Bird AP. CpG-rich islands and the function of DNA methylation. Nature. 1986;321(6067):209-13.
74. Hellman A, Chess A. Gene body-specific methylation on the active X chromosome. science. 2007;315(5815):1141-3.
75. Aran D, Toperoff G, Rosenberg M, Hellman A. Replication timing-related and gene body-specific methylation of active human genes. Human molecular genetics. 2010;20(4):670-80.
76. Lund G, Andersson L, Lauria M, Lindholm M, Fraga MF, Villar-Garea A, et al. DNA methylation polymorphisms precede any histological sign of atherosclerosis in mice lacking apolipoprotein E. Journal of Biological Chemistry. 2004;279(28):29147-54.
77. Hiltunen MO, Turunen MP, Häkkinen TP, Rutanen J, Hedman M, Mäkinen K, et al. DNA hypomethylation and methyltransferase expression in atherosclerotic lesions. Vascular medicine. 2002;7(1):5-11.
78. Aavik E, Lumivuori H, Leppänen O, Wirth T, Häkkinen S-K, Bräsen J-H, et al. Global DNA methylation analysis of human atherosclerotic plaques reveals extensive genomic hypomethylation and reactivation at imprinted locus 14q32 involving induction of a miRNA cluster. European heart journal. 2014;36(16):993-1000.
79. Greißel A, Culmes M, Burgkart R, Zimmermann A, Eckstein H-H, Zernecke A, et al. Histone acetylation and methylation significantly change with severity of atherosclerosis in human carotid plaques. Cardiovascular Pathology. 2016;25(2):79-86.
80. Wierda RJ, Rietveld IM, van Eggermond MC, Belien JA, van Zwet EW, Lindeman JH, et al. Global histone H3 lysine 27 triple methylation levels are reduced in vessels with advanced atherosclerotic plaques. Life sciences. 2015;129:3-9.
81. Bernstein BE, Mikkelsen TS, Xie X, Kamal M, Huebert DJ, Cuff J, et al. A bivalent chromatin structure marks key developmental genes in embryonic stem cells. Cell. 2006;125(2):315-26.
82. Di Croce L, Helin K. Transcriptional regulation by Polycomb group proteins. Nature structural & molecular biology. 2013;20(10):1147-55.
83. Maleszewska M, Vanchin B, Harmsen MC, Krenning G. The decrease in histone methyltransferase EZH2 in response to fluid shear stress alters endothelial gene expression and promotes quiescence. Angiogenesis. 2016;19(1):9-24.

84. Xiaoling Y, Li Z, ShuQiang L, Shengchao M, Anning Y, Ning D, et al. Hyperhomocysteinemia in ApoE-/-mice leads to overexpression of enhancer of Zeste Homolog 2 via miR-92a regulation. PloS one. 2016;11(12):e0167744.
85. Gurda D, Handschuh L, Kotkowiak W, Jakubowski H. Homocysteine thiolactone and N-homocysteinylated protein induce pro-atherogenic changes in gene expression in human vascular endothelial cells. Amino Acids. 2015;47(7):1319-39.
86. Kumar A, Kumar S, Vikram A, Hoffman TA, Naqvi A, Lewarchik CM, et al. Histone and DNA Methylation–Mediated Epigenetic Downregulation of Endothelial Kruppel-Like Factor 2 by Low-Density Lipoprotein CholesterolSignificance. Arteriosclerosis, thrombosis, and vascular biology. 2013;33(8):1936-42.
87. Ishikawa S, Hayashi H, Kinoshita K, Abe M, Kuroki H, Tokunaga R, et al. Statins inhibit tumor progression via an enhancer of zeste homolog 2-mediated epigenetic alteration in colorectal cancer. International journal of cancer. 2014;135(11):2528-36.
88. Lv Y-C, Tang Y-Y, Zhang P, Wan W, Yao F, He P-P, et al. Histone methyltransferase enhancer of zeste homolog 2-mediated ABCA1 promoter DNA methylation contributes to the progression of atherosclerosis. PloS one. 2016;11(6):e0157265.
89. Viré E, Brenner C, Deplus R, Blanchon L, Fraga M, Didelot C, et al. The Polycomb group protein EZH2 directly controls DNA methylation. Nature. 2006;439(7078):871.
90. Imai S-I, Armstrong CM, Kaeberlein M, Guarente L. Transcriptional silencing and longevity protein Sir2 is an NAD-dependent histone deacetylase. Nature. 2000;403(6771):795-800.
91. Chen Z, Peng IC, Cui X, Li YS, Chien S, Shyy JY. Shear stress, SIRT1, and vascular homeostasis. Proc Natl Acad Sci U S A. 2010;107(22):10268-73. doi: 10.1073/pnas.1003833107. Epub 2010 May 17.
92. Kauppinen A, Suuronen T, Ojala J, Kaarniranta K, Salminen A. Antagonistic crosstalk between NF-κB and SIRT1 in the regulation of inflammation and metabolic disorders. Cellular signalling. 2013;25(10):1939-48.
93. Ota H, Akishita M, Eto M, Iijima K, Kaneki M, Ouchi Y. Sirt1 modulates premature senescence-like phenotype in human endothelial cells. Journal of molecular and cellular cardiology. 2007;43(5):571-9.
94. Venkatasubramanian S, Noh RM, Daga S, Langrish JP, Joshi NV, Mills NL, et al. Cardiovascular effects of a novel SIRT1 activator, SRT2104, in otherwise healthy cigarette smokers. Journal of the American Heart Association. 2013;2(3):e000042.
95. Miranda MX, Van Tits LJ, Lohmann C, Arsiwala T, Winnik S, Tailleux A, et al. The Sirt1 activator SRT3025 provides atheroprotection in Apoe−/− mice by reducing hepatic Pcsk9 secretion and enhancing Ldlr expression. European heart journal. 2014;36(1):51-9.
96. Wakeling LA, Ions LJ, Escolme SM, Cockell SJ, Su T, Dey M, et al. SIRT1 affects DNA methylation of polycomb group protein target genes, a hotspot of the epigenetic shift observed in ageing. Human genomics. 2015;9(1):14.
97. Zhou S, Chen HZ, Wan YZ, Zhang QJ, Wei YS, Huang S, et al. Repression of P66Shc expression by SIRT1 contributes to the prevention of hyperglycemia-induced endothelial dysfunction. Circ Res. 2011;109(6):639-48. doi: 10.1161/CIRCRESAHA.111.243592. Epub 2011 Jul 21.
98. Wan YZ, Gao P, Zhou S, Zhang ZQ, Hao DL, Lian LS, et al. SIRT1-mediated epigenetic downregulation of plasminogen activator inhibitor-1 prevents vascular endothelial replicative senescence. Aging Cell. 2014;13(5):890-9. doi: 10.1111/acel.12247. Epub 2014 Jul 18.
99. Maleszewska M, Gjaltema RA, Krenning G, Harmsen MC. Enhancer of zeste homolog-2 (EZH2) methyltransferase regulates transgelin/smooth muscle-22alpha expression in endothelial cells in response to interleukin-1beta and transforming growth factor-beta2. Cell Signal. 2015;27(8):1589-96. doi: 10.016/j.cellsig.2015.04.008. Epub Apr 24.

100. Byles V, Zhu L, Lovaas JD, Chmilewski LK, Wang J, Faller DV, et al. SIRT1 induces EMT by cooperating with EMT transcription factors and enhances prostate cancer cell migration and metastasis. Oncogene. 2012;31(43):4619-29. doi: 10.1038/onc.2011.612. Epub 2 Jan 16.
101. Mattagajasingh I, Kim CS, Naqvi A, Yamamori T, Hoffman TA, Jung SB, et al. SIRT1 promotes endothelium-dependent vascular relaxation by activating endothelial nitric oxide synthase. Proc Natl Acad Sci U S A. 2007;104(37):14855-60. Epub 2007 Sep 4.
102. Polidoro L, Properzi G, Marampon F, Gravina GL, Festuccia C, Di Cesare E, et al. Vitamin D protects human endothelial cells from H(2)O(2) oxidant injury through the Mek/Erk-Sirt1 axis activation. J Cardiovasc Transl Res. 2013;6(2):221-31. doi: 10.1007/s12265-012-9436-x. Epub 2012 Dec 18.
103. Burridge S. Target watch: Drugging the epigenome. Nature Reviews Drug Discovery. 2013;12(2):92-3.
104. Arrowsmith CH, Bountra C, Fish PV, Lee K, Schapira M. Epigenetic protein families: a new frontier for drug discovery. Nature reviews Drug discovery. 2012;11(5):384.
105. Morera L, Lübbert M, Jung M. Targeting histone methyltransferases and demethylases in clinical trials for cancer therapy. Clinical epigenetics. 2016;8(1):57.
106. Kim KH, Roberts CW. Targeting EZH2 in cancer. Nature medicine. 2016;22(2):128-34.
107. Berman AY, Motechin RA, Wiesenfeld MY, Holz MK. The therapeutic potential of resveratrol: a review of clinical trials. NPJ precision oncology. 2017;1(1):35.
108. Cano-Rodriguez D, Rots MG. Epigenetic editing: on the verge of reprogramming gene expression at will. Current genetic medicine reports. 2016;4(4):170-9.
109. de Groote ML, Verschure PJ, Rots MG. Epigenetic editing: targeted rewriting of epigenetic marks to modulate expression of selected target genes. Nucleic acids research. 2012;40(21):10596-613.
110. Cano-Rodriguez D, Gjaltema RAF, Jilderda LJ, Jellema P, Dokter-Fokkens J, Ruiters MHJ, et al. Writing of H3K4Me3 overcomes epigenetic silencing in a sustained but context-dependent manner. Nature communications. 2016;7.
111. Hawkins RD, Hon GC, Lee LK, Ngo Q, Lister R, Pelizzola M, et al. Distinct epigenomic landscapes of pluripotent and lineage-committed human cells. Cell stem cell. 2010;6(5):479-91.
112. Lister R, Pelizzola M, Dowen RH, Hawkins RD, Hon G, Tonti-Filippini J, et al. Human DNA methylomes at base resolution show widespread epigenomic differences. nature. 2009;462(7271):315.
113. Kamps JA, Krenning G. Micromanaging cardiac regeneration: Targeted delivery of microRNAs for cardiac repair and regeneration. World journal of cardiology. 2016;8(2):163.
114. Kowalski PS, Kuninty PR, Bijlsma KT, Stuart MC, Leus NG, Ruiters MH, et al. SAINT-liposome-polycation particles, a new carrier for improved delivery of siRNAs to inflamed endothelial cells. European Journal of Pharmaceutics and Biopharmaceutics. 2015;89:40-7.
115. Kowalski PS, Zwiers PJ, Morselt HW, Kuldo JM, Leus NG, Ruiters MH, et al. Anti-VCAM-1 SAINT-O-Somes enable endothelial-specific delivery of siRNA and downregulation of inflammatory genes in activated endothelium in vivo. Journal of Controlled Release. 2014;176:64-75.
116. Choi M, Schreiber A, Eulenberg-Gustavus C, Scheidereit C, Kamps J, Kettritz R. Endothelial NF-κB blockade abrogates ANCA-induced GN. Journal of the American Society of Nephrology. 2017;28(11):3191-204.
117. Chung J, Shim H, Kim K, Lee D, Kim WJ, Kang DH, et al. Discovery of novel peptides targeting pro-atherogenic endothelium in disturbed flow regions-Targeted siRNA delivery to pro-atherogenic endothelium in vivo. Scientific reports. 2016;6.
118. Zhang Q-j, Wang Z, Chen H-z, Zhou S, Zheng W, Liu G, et al. Endothelium-specific overexpression of class III deacetylase SIRT1 decreases atherosclerosis in apolipoprotein E-deficient mice. Cardiovascular research. 2008;80(2):191-9.

Chapter 3

MicroRNA-374b induces Endothelial-to-Mesenchymal Transition and neointima formation through the inhibition of MAPK7 Signaling

Byambasuren Vanchin[1,#], Emma Offringa[1,#], Marja G.L. Brinker[1], Bianca Kiers[2],

Alexandre C. Pereira[2], Martin C. Harmsen[1], Jan-Renier A.J. Moonen[1,3] and

Guido Krenning[1,*]

1 University of Groningen, University Medical Center Groningen, Dept. Pathology and Medical Biology, Laboratory for Cardiovascular Regenerative Medicine (CAVAREM), Hanzeplein 1 (EA11), 9713GZ Groningen, The Netherlands.
2 University of São Paulo, Heart Institute (InCor), Laboratory of Genetics and Molecular Cardiology (LIM13), Avenida Dr. Eneas C. Aguiar 44, 05403-000 São Paulo, SP, Brazil.
3 Current address: Stanford University School of Medicine, Vera Moulton Wall Center for Pulmonary Vascular Disease and the Cardiovascular Institute, 269 Campus Drive, Stanford, CA 94305, United States of America.

 # Authors contributed equally.

Under review

ABSTRACT

Endothelial-mesenchymal transition occurs during intimal hyperplasia and neointima formation via mechanisms that are incompletely understood. Endothelial MAPK7 signaling is a key mechanosensitive factor that protects against endothelial-mesenchymal transition, but its signaling activity lost in vessel areas that undergoing pathological remodeling.

At sites of vascular remodeling in mice and pigs, endothelial MAPK7 signaling was lost. The TGFβ-induced microRNA-374b targets MAPK7 and its downstream effectors in endothelial cells and its expression induces endothelial-mesenchymal transition. *Gain-of-function* experiments, where endothelial MAPK7 signaling was restored, precluded endothelial-mesenchymal transition. In human coronary artery disease, disease severity associates with decreased MAPK7 expression levels and increased miR-374b expression levels.

Endothelial-mesenchymal transition occurs in intimal hyperplasia and neointima formation and is governed in part by microRNA-374b-induced silencing of MAPK7 signaling. Restoration of MAPK7 signaling abrogated these pathological effects in endothelial cells expressing miR-374b. Thus, our data suggest that the TGFβ-miR-374b-MAPK7 axis plays a key role in the induction of endothelial-mesenchymal transition during intimal hyperplasia and neointima formation and might pose an interesting target for anti-atherosclerosis therapy.

INTRODUCTION

The development of atherosclerosis is preceded by intimal hyperplasia and neointima formation [1]. Although the commonly recognized risk factors for the development of neointimal lesions and atherosclerosis are present at the systemic level [2], neointima formation and atherosclerosis manifest focally in so-called atheroprone regions [3]. These atheroprone regions are characterized by low levels of non-uniform shear stress, typically encountered at the outer walls of vascular bifurcations and at the inner wall of vascular curvatures, whereas atheroprotected regions are characterized by high levels of uniform laminar shear stress [4].

We and others have recently described a major contribution of endothelial cells to intimal hyperplasia and atherosclerosis development [5-7]. Upon exposure to inflammatory and pro-fibrotic growth factors (*i.e.* TGFβ) and cytokines, endothelial cells lose their endothelial cell markers and functionality, start to express markers of the mesenchymal lineage and gain contractile behavior [8-10]. During neointimal lesion formation, endothelial cells that undergo this Endothelial-Mesenchymal Transition (EndMT) acquire a fibroproliferative mesenchymal phenotype and migrate from the endothelial monolayer to the underlying neointima [5,6].

TGFβ is a major inducer of EndMT and highly expressed in neointimal lesions [11], which may cause EndMT. We uncovered that high levels of uniform laminar shear stress - observed at atheroprotected regions of the arteries - activates a specific mitogen-activated kinase (MAPK), namely MAPK7 (also known as Erk5 or Big MAPK (BMK1)), which inhibits the induction of EndMT by TGFβ1 [5]. Corroboratively, knockdown of MAPK7 in endothelial cells causes EndMT, even in the absence of exogenous TGFβ1 [5], suggesting a pivotal balance between TGFβ and MAPK7 signaling in the induction of EndMT and the formation of neointimal lesions. Indeed, TGFβ1 represses endothelial MAPK7 expression through unidentified mechanisms (unpublished data) and the loss of endothelial MAPK7 signaling aggravates atherosclerosis development [12].

MicroRNAs (miRNAs) are small non-coding RNAs that cause post-translational repression of their target genes. MicroRNAs elicit translational repression by imperfect base-pairing to the 3'UTR of their gene targets [13], which allows any specific microRNA to target multiple genes simultaneously. Moreover, multiplicity of microRNA targets might also allow one microRNA to specifically target multiple genes within one signal transduction cascade [14], efficiently abolishing its activity.

TGFβ induces a shift in endothelial miRNA expression levels [15-18] that may reduce MAPK7 signaling and thus facilitate EndMT induction. Here, we hypothesized that TGFβ1 induces the expression of a specific miRNA that targets MAPK7 and its signaling intermediates, resulting in the induction of EndMT.

METHODS

CLINICAL SAMPLES

Human coronary arteries were obtained from autopsy specimens from 10 patients that died from an acute coronary episode at the Heart Institute (InCor), Sao Paulo, Brazil. During necropsy each dissected coronary artery was fixed in neutral-buffered formalin with constant perfusion at a quasi-normal perfusion pressure. The mean age of subjects contributing pathology specimens was 65 years. Hypertension was resent in 9 subjects, and diabetes in 6. Five individuals were active smokers. Next-of-kin gave informed consent and the investigation was performed according to institutional guidelines (InCor, Sao Paulo #SDC 3723/11/141 and #CAPPesq 482/11) and the Declaration of Helsinki.

ANIMALS AND SURGICAL PROCEDURES

Porcine abdominal trifurcations were obtained from healthy male slaughterhouse Yorkshire pigs (12-13 weeks of age; body weight 30-35 kg, n =3, V.O.F. van Beek, Lelystad, The Netherlands). Animals were fed a normal diet and were euthanized under anesthesia (ketamine (Nimatek) and midazolam with a bolus of pentobarbital and heparin (Actrapid)). Male C57Bl/6j wild-type mice (8–12 weeks of age, n = 8, Harlan, Horst, The Netherlands) were subjected to transverse aortic constriction under anesthesia (2% Isofluorane (Forene/ Abbott, The Netherlands) and oxygen) and analgesia (Carprofen, 5 mg/kg). Briefly, an incision was made in the second intercostal space and a small incision was made in the parietal pleura to expose the ascending loop of the aorta. The aorta was supported with a 27G needle and a suture was placed around the aorta, drawn tight after which the needle was removed. Next, the pleura, muscle layers, and skin were closed by sutures. Animals received post-operative analgesia (Carprofen, 5 mg/kg/day for 48 h). Animals were kept on a 12 h light:dark cycle with ad libitum access to standard laboratory chow and water. Eight weeks after aortic constriction, animals were sacrificed under deep anesthesia [3% Isofluorane (Forene/Abbott, The Netherlands] by exsanguination, after which the thoracic aorta was explanted. Experiments on mice were approved by the local Institutional Animal Care and Use Committee (University of Groningen, #DEC-5910).

HUMAN UMBILICAL VEIN ENDOTHELIAL CELL CULTURE

Human umbilical vein endothelial cells (HUVEC, Lonza, Walkersville, MD) were cultured in endothelial cell medium up to passage 5 as described previously [8]. EndMT was initiated by re-plating the HUVEC in RPMI1640, supplemented with 20% FCS, 1% Penicillin–Streptomycin, 2 mM L-glutamine, 5 $U \cdot mL^{-1}$ heparin, and 10 $ng \cdot mL^{-1}$ TGFβ1 (Peprotech, NJ, USA). For shear stress experiments, HUVEC were plated on 1% gelatin-coated µ-Slides (Ibidi, Martinsried, Germany) and grown to confluence prior to exposure to 20 $dynes \cdot cm^{-2}$ of unidirectional uniform laminar shear stress (LSS). LSS was generated using the Ibidi Pump System (Ibidi, Martinsried, Germany).

3'UTR REPORTER ANALYSIS

Gene specific 3' UTR fragments were isolated from a cDNA pool derived from various human tissues using oligonucleotides extended with SgfI (GCGATCGC) and NotI (GCGGCCGC) restriction sequences at the sense and antisense primer (Table S1), respectively. Amplification was performed using the DyNAzyme EXT PCR kit (Finnzymes, Vantaa, Finland) according to the manufacturer's instructions. Amplicon size was validated by gel electrophoresis on 1% agarose gels. 3'UTR fragments were cloned into the SgfI/NotI-sites of the psiCHECK-2 dual luciferase reporter vector (Promega, Madison, WI). COS-7 cells were transfected with 100 ng/ml 3'UTR reporter plasmid and 50 nM miR-374b mimic or scrambled control (Life Technologies, Carlsbad, CA) using Lipofectamine2000 (ThermoFisher, Waltham, MA). 48 h post-transfection, luciferase activity was assayed using the DualGlo Luciferase assay system (Promega, Madison, WI) and recorded for 1 s on a Luminoskan ASCENT (Thermo Scientific, Waltham, MA).

PLASMIDS AND LENTIVIRAL EXPRESSION OF MIR-374B, SHRNA AND MAPK7 SIGNALING MEMBERS

For lentiviral expression of miR-374b and small hairpin RNA (shRNA) against MAPK7 signaling members, DNA oligonucleotides containing the endogenous miR-374b hairpin or specific 21-mer targeting sequences for human MAP3K3, MAPK7, MEF2D or KLF4 (all Biolegio, Leiden, The Netherlands, Table S2) were cloned into the BamHI/EcoRI sites of the pGreenPuro shRNA expression vector (Systems Bioscience, CA, USA). Scrambled sequences were used as control.

Gene-CDS fragments were isolated from a cDNA pool derived from various human tissues using oligonucleotides extended with EcoRI (GAATTC) and BamHI (GGATCC) restriction sequences at the sense and antisense primer (Table S3), respectively. Amplification was performed using the DyNAzyme EXT PCR kit (Finnzymes, Vantaa, Finland) according to the manufacturer's instructions. Amplicon size was validated by gel electrophoresis on 1% agarose gels. Gene-CDS fragments were cloned into the EcoRI/BamHI sites of the pCDH-CMV-MCS-EF1-Puro lentiviral expression vector (Systems Biosciences, Palo Alto, CA). Empty vectors served as control.

For lentiviral transduction, HEK293 cells were transfected with pGreenPuro or pCDH-CMV-MCS-EF1-Puro shuttle vectors and second-generation lentiviral helper plasmids using Endofectin (GeneCopoeia, MD, USA). Viral supernatants were collected every 24 hours, supplemented with 6 $\mu g \cdot mL^{-1}$ polybrene and directly transferred to HUVEC cultures for two consecutive rounds. Transduced cells were selected for puromycin resistance 72 h post-transduction (4 $\mu g \cdot mL^{-1}$ puromycin) for 24 hours and reseeded into puromycin-free medium for the experiments.

MICRORNA AND GENE TRANSCRIPT ANALYSIS

Total RNA was isolated using TRIzol reagent (Invitrogen, Carlsbad, CA) according to manufacturer's instructions. For microRNA transcript analyses, 20 ng of total RNA was reversely transcribed using the Taqman MicroRNA Reverse Transcription kit (Applied Biosystems) using microRNA-specific stemloop primers (Table S4). For gene transcript analysis, 1 1 µg of total RNA was reversely transcribed using the RevertAid first Strand cDNA synthesis kit (Applied Biosystems, Carlsbad, CA) according to manufacturer's protocol. Quantitive PCR expression analysis performed on a reaction mixture containing

10ng cDNA equivalent, 0.5 μM sense primers and 0.5 μM antisense primers (for microRNA primers see Table S4 and gene transcript primers see Table S5, all Biolegio, Leiden, The Netherlands). Analyses were run on Viia7 real-time PCR system (Applied Biosystems, Carlsbad, CA)

IMMNUNOFLUORESCENCE

Heat-induced antigen retrieval was performed with 0.1 M Tris-HCl (pH 9.0, 80°C, 20 mins) on the formalin fixated, paraffin-embedded sections prior to immunohistochemistry. Sections were incubated with primary antibodies at room temperature for 2 hours, followed by incubation with secondary antibodies at room temperature for 1 hour (Table S6). Detailed description of the imaging procedures is provided in the Supplementary Methods.

IMMUNOBLOTTING

Whole cell lysates were prepared in RIPA buffer (Thermo Scientific, IL, USA) supplemented with 1% protease inhibitor cocktail (Sigma-Aldrich, Germaby) and 1% HALT-phosphatase inhibitor cocktail (ThermoFisher Scientific). Protein concentrations were determined using the detergent compatible protein assay (Bio-Rad, VA), according to manufacturer's protocol. Equal amounts of protein were loaded on a 10% denaturing SDS–polyacrylamide gel and separated by gel electrophoresis (110V). Next proteins were blotted onto nitrocellulose membranes using the Trans-Blot Turbo System (Bio-Rad, AV) according to manufacturer's instructions. Blots were blocked in Odyssey Blocking Buffer (Li-COR Biosciences, NE, USA) at room temperature for 30 mins and incubated at 4°C with primary antibodies (Table S7) in Odyssey Blocking Buffer overnight, after which membranes were incubated with secondary antibodies (Table S7) in Odyssey Blocking Buffer at room temperature for 1 hour. Protein was detected using the Odyssey Infrared Imaging System (Li-COR Biosciences). Densitometric analysis was performed using Totallab 120 (Nonlinear Dynamics, Newcastle upon Tyne, England).

ANGIOGENIC SPROUTING CAPACITY

10 μl of MatriGel (BD Biosciences, San Jose, CA) was solidified in μ-Slide Angiogenesis (Ibidi, Martinsried, Germany). 10.000 cells per well were cultured on the solidified MatriGel in endothelial growth medium and the formation of sprouts was analyzed by conventional light microscopic analysis after overnight incubation.

COLLAGEN CONTRACTION ASSAY

Cells were suspended in a solution of rat tail Collagen type I (Corning, Corning, NY) containing 3 $mg{\cdot}mL^{-1}$ $NaHCO_3$ and 0.1M Na_2HPO_4. Aliquots of 50 μL (containing 100.000 cells and 0.5 mg Collagen type I) were solidified at 37°C in a humidified incubator with 5% CO_2 for 30 mins. The collagen gels were released from the culture dishes by the addition of 2 ml endothelial growth medium and were imaged using a common Flatbed-scanner and allowed to contract for an additional 24 h.

The degree of gel contraction was determined by measuring the total gel area and dividing the areas of the contracted gels by the areas of the gels before contraction.

STATISTICAL ANALYSIS

Data are presented as means ± s.e.m. N-values relate to independent experiments/ samples. P-values were calculated using one-way analysis of variance followed by Bonferroni's post-hoc comparisons tests using Prism Graphpad (Graphpad Software, La Jolla, CA, USA). $P < 0.05$ was considered statistically significant.

RESULTS

MICRORNA-374B TARGETS MAPK7 SIGNALING

Database analysis (miRanda [19,20]) identified 12 microRNAs that putatively target MAPK7 (Suppl.fig.1). Next, we cross-checked these microRNAs against other genes in the MAPK7 signaling cascade (Suppl.fig.1) and found that the miR-374 family (miR-374a and miR-374b) target not only MAPK7, but also its upstream activators Rac1, MAP3K3 and MAP3K7. Moreover, miR-374 also putatively targets the downstream transcription factors of the myocyte enhancer factor (MEF)-2 family as well as Krüppel-like factor (KLF)-4 (Suppl.fig.2). TGFβ1 induced the expression of miR-374a, miR-374b, miR-143, miR-24 and miR-410 in endothelial cells ($p<0.05$ vs unstimulated control cells), whereas it decreased the expression of miR-488 ($p<0.05$ vs unstimulated control cells). The expression of miR-429, miR-200b, miR-200c, miR-183, miR-124 and miR-506 were unchanged (Suppl.fig.3) upon TGFβ1 treatment.

MicroRNA-374a and miR-374b collectively have 1305 putative gene targets, of which 527 and 434 are unique to miR-374a and miR-374b, respectively (Suppl.fig.2). 344 putative gene targets are shared between miR-374a and miR-374b. Analysis of genes within the MAPK7 signaling cascade indicates that MAP3K7 (TAK1), MAPK7 (ERK5), MEF2A and MEF2C are putative targets of miR-374a and miR-374b, whereas Rac1, MAP3K3 (MEKK3), MEF2D and KLF4 are targets of miR-374b only. None of the genes with in the MAPK7 signaling cascade where unique targets to miR-374a (Suppl.fig.2).

MICRORNA-374B AND MAPK7 ARE DIFFERENTIALLY EXPRESSED AT ATHEROPRONE REGIONS

EndMT contributes to the formation of intimal hyperplasia [5], which is aggravated by the loss of protective MAPK7 signaling [12]. Cells co-expressing endothelial specific molecule (ESM)-1 and the mesenchymal protein SM22α were abundantly present in the hyperplastic intima of the porcine trifurcation compared to the non-hyperplastic intima (11.5 vs 1.0%; $p<0.001$, fig.1a). In the atheroprone hyperplastic regions, endothelial MAPK7 activity was decreased 2-fold ($p=0.01$) compared endothelial cells in the atheroprotected regions within the same trifurcation (fig.1b).

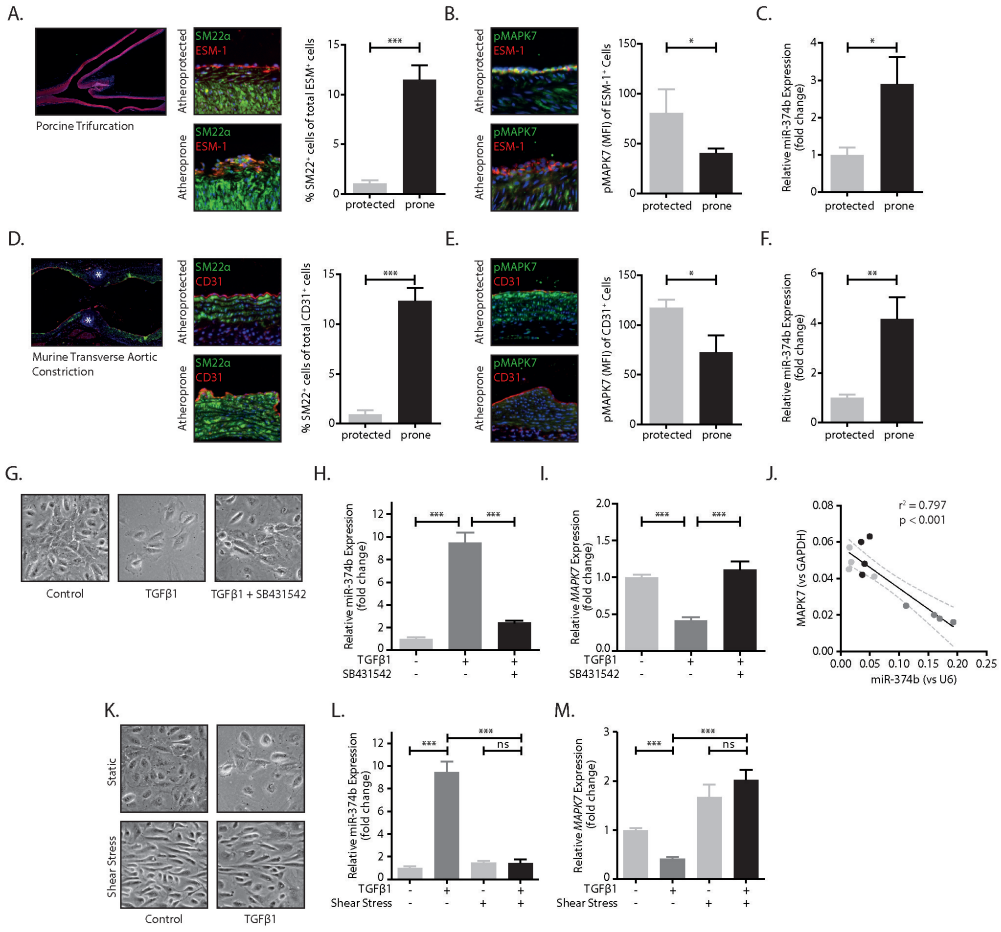

Figure 1. MicroRNA-374b and MAPK7 are differentially expressed in neointimal lesions. *Porcine intimal hyperplastic lesions contain myo-endothelial cells (myoEC) that co-express the endothelial cell marker ESM-1 (red) and mesenchymal cell marker SM22α (green). Nuclei are stained with DAPI (blue) (A). The activity of MAPK7 (pMAPK7, green) was is reduced in endothelial cells (ESM-1, red) in the atheroprone regions of the porcine trifurcation (B, n=5), whereas the expression of miR-374b was increased in the atheroprone areas compared to atheroprotected areas of the same porcine trifurcation (C, n=5). Mice were subjected to transverse aortic constriction (TAC). Eight weeks after TAC, myoEC that co-express the endothelial cell marker CD31 (red) and the mesenchymal cell marker SM22α (green) were detected at the areas exposed to disturbed flow (D, n=5, *=ligation). The activity of MAPK7 (pMAPK7, green) was is reduced in endothelial cells (CD31, red) in the areas exposed to disturbed flow compared to areas exposed to laminar flow (E, n=5), which coincides with an increase in the expression of miR-374b (F, n=5). In vitro, endothelial cells treated with TGFβ1 were hyperplastic, which was inhibited by the ALK5-inhibitor SB431542 (G) and increased their expression of miR-374b (H, n=6). The expression of MAPK7 was reduced in TGFβ1-stimulated endothelial cells, compared to untreated control cells or endothelial cells treated with TGFβ1 and the ALK5-inhibitro SB431542 (I, n=6). The expression levels of miR-374b inversely associated with MAPK7 expression levels (J, n=6). Laminar fluid shear stress (20 dyne·cm²) antagonized the cellular hypertrophy induced by TGFβ1 (K) in endothelial cells and inhibited the increase in miR-374b expression (L, n=5). Concurrently, when exposed to fluid shear stress, MAPK7 expression was unaltered in TGFβ1-treated endothelial cells compared to unstimulated control cells (M, n=5). T-test for comparison between two groups; One-way ANOVA for analyses between multiple groups. *p<0.05, **p<0.01, ***p<0.001.*

We dissected the atheroprone and atheroprotected areas of the porcine trifurcation and found increased expression levels of miR-374b in the atheroprone regions (~3-fold, p=0.04, fig.1c). Concurrently, in mice with transverse aortic banding, atheroprone regions characterized by disturbed fluid shear stress were characterized by the accumulation of cells expressing both the endothelial marker CD31 and the mesenchymal protein SM22α (12.3%, fig.1d), indicative of EndMT. At these atheroprone sites, endothelial MAPK7 activity was decreased (1.6-fold, p=0.04, fig.1e), whereas the expression of miR-374b was elevated (4-fold, p=0.01, fig.1f).

In vitro, endothelial cells treated with TGFβ1 displayed apoptosis and hypertrophy (fig.1g) and increased their expression of miR-374b (~9-fold compared to non-stimulated cells, p<0.001), which was completely abolished by the addition of a small molecule inhibitor of ALK5 (SB431542)(fig.1h). The increase in miR-374b expression associated with decreased expression of MAPK7 (r^2=0.797, p<0.001, fig.1i,j) and intermediates of MAPK7 signaling, *i.e.* Rac1 (r^2=0.595, p<0.01), MAP3K7 (r^2=0.688, p<0.01), MAPK7 (r^2=0.797, p<0.01), MEF2D (r^2=0.682, p<0.001) and KLF4 (r^2=0.555, p<0.01, Suppl. fig.4a), as well as a decreased expression of endothelial markers VE-Cadherin (r^2=0.678, p<0.001) and eNOS (r^2=0.546, p<0.01, Suppl.fig.4b) and increased expression of mesenchymal markers SM22α (r^2=0.872, p<0.001) and CNN1 (r^2=0.814, p<0.001, Suppl.fig.4c).

Under LSS, endothelial cells aligned in the direction of flow, indicating mechanosensory behavior (fig.1k). In contrast to the static cell cultures, endothelial cells exposed to LSS did not became hypertrophic and did not increase their expression of miR-374b, even when exogenous TGFβ1 was applied (fig.1l). Corroboratively, MAPK7 expression, which is diminished by TGFβ1 in static cultures, remained high under LSS even in the presence of TGFβ1 (fig.1m).

MIR-374B TARGETS MULTIPLE MEMBERS OF THE MAPK7 SIGNALING CASCADE

Computational analysis of putative miR-374b targets identified multiple members of the MAPK7 signaling cascade (fig.2a). Reporter assays, wherein the 3'UTR regions of miR-374b gene targets are coupled to the Luciferase gene, revealed that the MAPK7 Signaling members Rac1, MAP3K3, MAP3K7, MAPK7, MEF2d and KLF4 are genuine miR-374b target genes (fig.2b) as co-transfection of these reporter plasmids with miR-374b mimics reduced luciferase activity (all p<0.01). In contrast, co-transfection of reporter plasmids with a scrambled miR-374b sequence did not alter luciferase activity (fig.2b). MEF2a and MEF2c were identified as putative gene targets of miR-374b by *in silico* analyses, however, co-transfection of their respective reporter constructs with miR-374b mimics, did not result in decreased luciferase activity (fig.2b) implicating that MEF2a and MEF2c are not genuine targets of miR-374b. To establish if MAPK7 signaling members are factual endogenous miR-374b targets in mature endothelial cells, we lentivirally overexpressed miR-374b or its scrambled sequence. Unstimulated control cells readily expressed MAPK7 and its signaling members (fig.2c). Stimulation of mature endothelial cells with TGFβ1 drastically reduced expression of these molecules (fig.2c) to approx. 50% of control endothelial cells (all p<0.01). Endothelial cells that expressed miR-374b had reduced expression of MAP3K3 (~33%, p<0.01), MAPK7 (~47%, p<0.01), MEF2d (~37%, p<0.01) and KLF4 (~42%, p<0.001) compared to endothelial cells treated with scrambled controls (fig.2c) indicating that miR-374b decreases endogenous MAPK7 signaling.

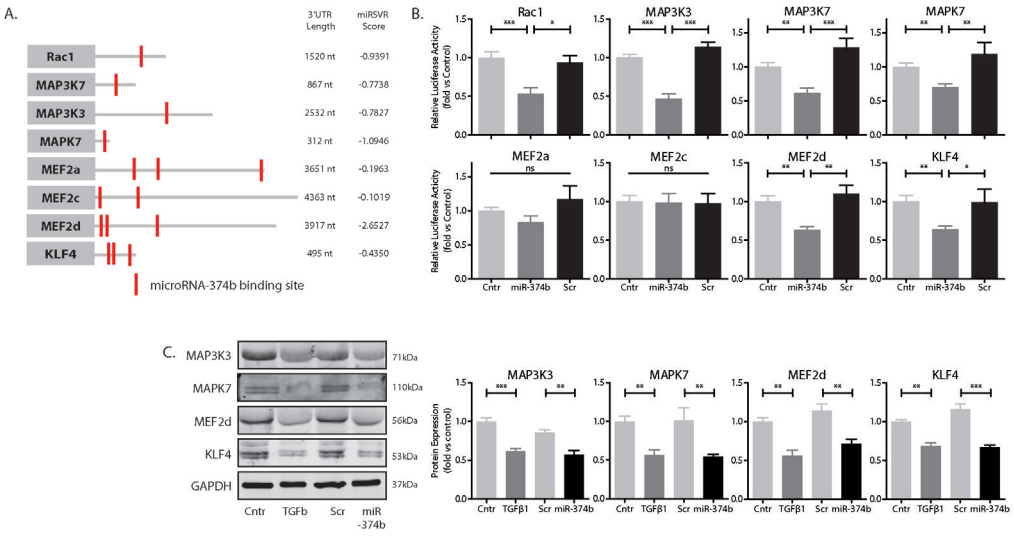

Figure 2. MicroRNA-374b interferes with MAPK7 signaling at multiple levels. *In silico analysis (Tarbase [39]) reveals that miR-374b putatively targets multiple genes within the MAPK7 signaling cascade with different efficacies (miRSVR-scores indicate the predicted target site efficacy [20])(A). Co-transfection of 3'UTR reporter constructs with miR-374b mimics or scrambled control sequences in COS7 cells suggests that Rac1, MAP3K3, MAP3K7, MAPK7, MEF2D and KLF4 are genuine miR-374b target genes (B, n=5). Transfection of miR-374b mimics in endothelial cells mimics the TGFβ1-induced decrease in expression of MAPK7 signaling members (C,D; n=3). One-way ANOVA, *p<0.05, **p<0.01, ***p<0.001.*

TGFβ-1 SUPPRESSES MAPK7 EXPRESSION THROUGH INDUCTION OF MIR-374B AND CAUSES ENDOTHELIAL-MESENCHYMAL TRANSITION

We next questioned if ectopic expression of miR-374b in endothelial cells would facilitate EndMT. Lentiviral expression caused a ~4-fold increase of miR-374b in endothelial cells (fig.3a). Consequently, endothelial cells lost their typical cobblestone morphology and started to show signs of hypertrophy (fig.3b). Consistent with EndMT, the expression of typical endothelial cell markers, *i.e.* VE-Cadherin and eNOS, was lost (fig. 3b,c) whereas expression of mesenchymal cell markers, *i.e.* SM22α and Calponin 1 (CNN1), was induced (fig. 3b,c). Additionally, miR-374b *gain-of-function* in endothelial cells, reduced the ability to form capillary-like sprouts on Matrigel (fig.3d) and fostered the gain of contractile behavior (fig.3e), all consistent with mesenchymal transition.

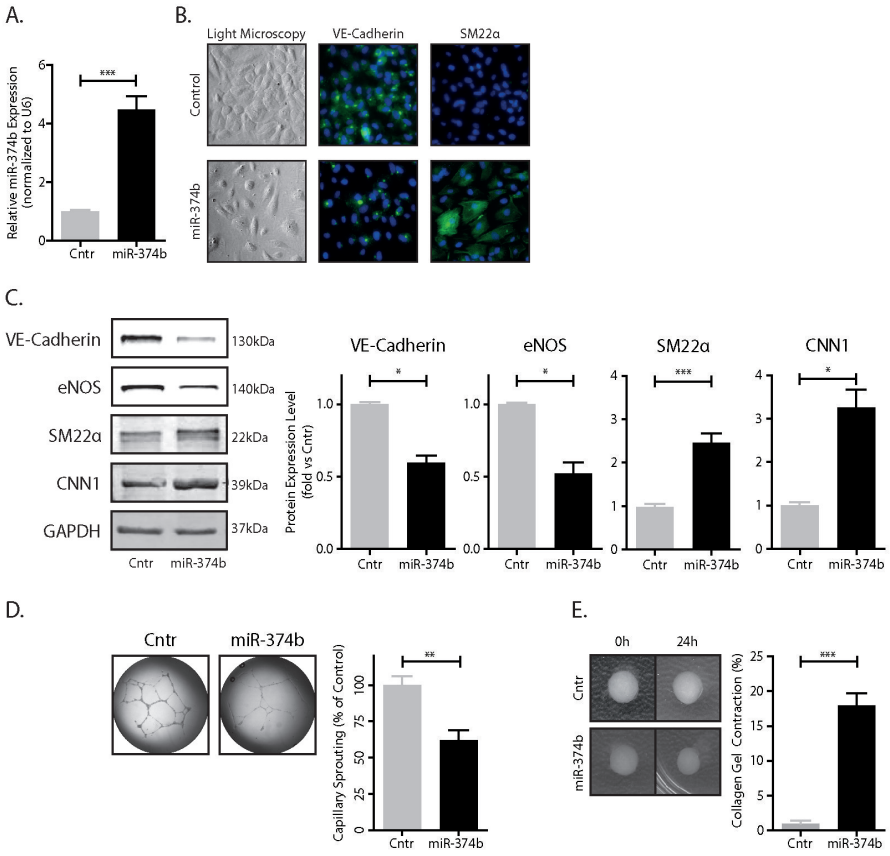

Figure 3. MicroRNA-374b gain-of-function induces EndMT. *Transformation of endothelial cells with a lentivirus encoding the stemloop sequence of miR-374b increased its expression ~4-fold (A). MiR-374b expressing endothelial cells where hypertrophic and decreased their expression of the endothelial cell marker VE-cadherin and increased expression of the mesenchymal cell marker SM22α, compared to endothelial cells that expressed a scrambled control sequence (B). VE-Cadherin and eNOS expression were decreased in endothelial cells expressing miR-374b, whereas the expression of SM22α and CNN1 was increased (C). Endothelial cells expressing miR-374b had a reduced angiogenic sprouting capacity (D) and increased contractile capacity (E) compared to endothelial cells that expressed a scrambled control sequence. All n=5, T-test for comparison between two groups, *p<0.05, **p<0.01, ***p<0.001.*

LOSS OF SPECIFIC MIR-374B TARGETS INDUCES ENDOTHELIAL-MESENCHYMAL TRANSITION

We questioned if the *loss-of-function* of specific miR-374b targets would suffice for EndMT induction and used a shRNA approach to specifically decrease MAP3K3, MAPK7, MEF2d or KLF4 expression in endothelial cells (Supl.fig.5). Decreased expression of MAPK7 signaling members caused the dissociation of endothelial cell-cell contacts and decreased the expression of VE-cadherin. Concurrently, the expression of SM22α was increased upon loss of MAPK7 signaling (fig.4a). The expression of endothelial markers VE-Cadherin and eNOS was abrogated and the expression of mesenchymal markers SM22α and Calponin was induced (fig.4b,c). Moreover, angiogenic sprouting ability decreased (fig.4d) and In contrast to the EndMT induction by the loss of downstream MAPK7 signaling members,

MAP3K3 deficiency did not alter the expression of endothelial, nor mesenchymal marker proteins (fig.4b,c). Yet, angiogenic sprouting ability was lost (fig.4d) and contractile behavior acquired (fig.4e) by endothelial cells deficient in MAP3K3.

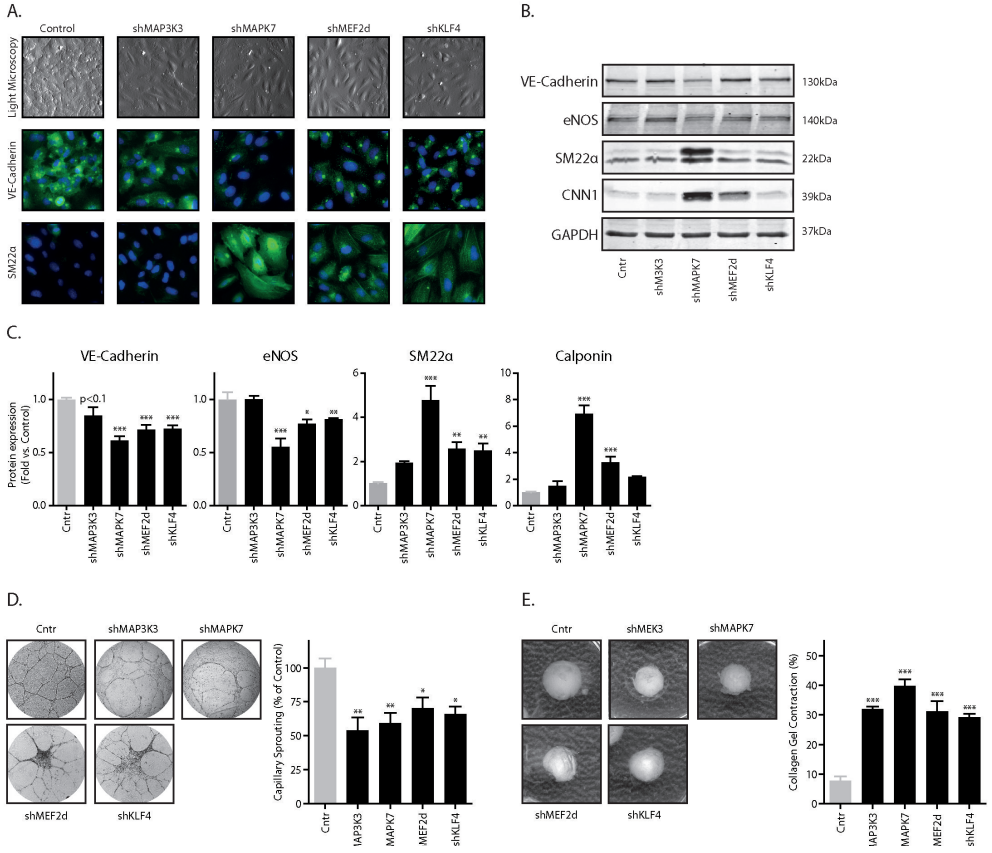

Figure 4. Knockdown of specific microRNA-374b gene targets induces EndMT. *Transformation of endothelial cells with lentiviruses encoding shRNA sequences to MAP3K3, MAPK7, MEF2D and KLF4 induced cellular hypertrophy, decreased the expression of the endothelial cell marker VE-cadherin, and increased expression of the mesenchymal cell marker SM22α, compared to endothelial cells that expressed scrambled control sequences (A). VE-Cadherin and eNOS expression were decreased in endothelial cells expressing shMAPK7, shMEF2D and shKLF4, whereas their expression was unaltered in endothelial cells expressing shMAP3K3. The expression of SM22α and CNN1 was increased in endothelial cells expressing shMAPK7, shMEF2D and shKLF4 (B,C). Endothelial cells expressing shRNA sequences to MAP3K3, MAPK7, MEF2D and KLF4 had a reduced angiogenic sprouting capacity (D) and increased contractile capacity (E) compared to endothelial cells that expressed a scrambled control sequence. All n=6, One-way ANOVA, *p<0.05, **p<0.01, ***p<0.001.*

MAINTENANCE OF ENDOTHELIAL MAPK7 SIGNALING ABROGATES MIR-374B-INDUCED ENDOTHELIAL-MESENCHYMAL TRANSITION

To investigate if restoration of MAPK7 signaling members could block miR-374b-induced EndMT, we lentivirally expressed miR-374b together with the protein-coding sequences of MAP3K3, MAPK7, MEF2D and KLF4 (fig.5a). VE-cadherin expression was reduced in endothelial cells that express miR-374b, whereas the expression of SM22α was induced.

In contrast, cells that co-expressed MAP3K3 or MAPK7 together with miR-374b maintained their expression of VE-cadherin and eNOS and were refractory to the induction of SM22a and Calponin by miR-374b (fig.5b-d), whereas cells co-expressing KLF4 and miR-374b maintained only the expression of eNOS (fig.5c,d). Restoration of MEF2D in endothelial cells expressing miR-374b, inhibited the expression of the mesenchymal proteins SM22α and Calponin, but failed to maintain the expression of endothelial marker proteins VE-Cadherin and eNOS (fig.5b-d). Restoration of all MAPK7 signaling members in endothelial cells expressing miR-374b maintained the angiogenic ability (fig.5e) and precluded the contractile behavior induced by miR-374b expression (fig.5f).

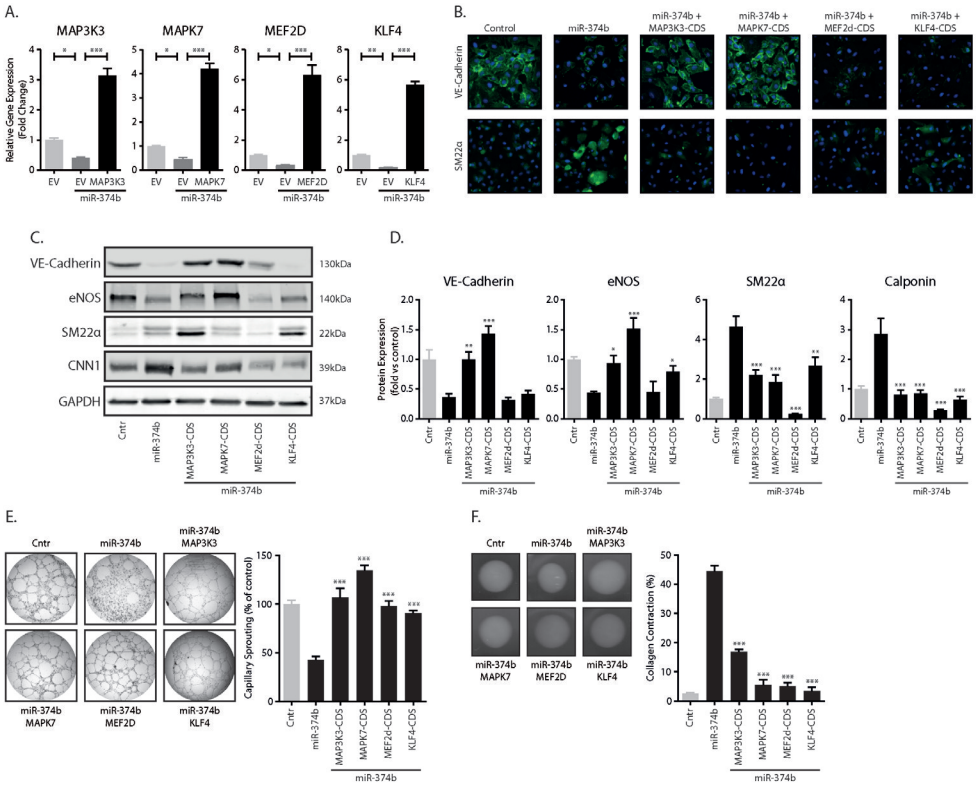

Figure 5. Re-expression of microRNA-374b target genes inhibits EndMT. *The expression of miR-374b target genes was restored by lentiviral transformation using plasmids encoding the coding sequences (CDS) of MAP3K3, MAPK7, MEF2D and KLF4 in endothelial cells that overexpress miR-374b. The (re-)expression of these genes was confirmed by qPCR (A). Endothelial cells that express miR-374b decreased their expression of VE-Cadherin and increased their expression of SM22α. These effects were counteracted by the expression of MAPK7 signaling members (B-D). Endothelial cells that expressed MAP3K3, MAPK7, MEF2D or KLF4 have an enhanced angiogenic sprouting capacity (E) and decreased contractile capacity (F) compared to endothelial cell that express miR-374b. The levels of angiogenic sprouting and contractile behavior were similar to that of endothelial cells transformed using scrambled control sequences. All n=5, One-way ANOVA, *p<0.05, **p<0.01, ***p<0.001.*

MICRORNA-374B IS INCREASED IN HUMAN CORONARY ARTERY STENOSIS

Lastly, we assessed the expression levels of miR-374b and MAPK7 in samples from progressive human coronary artery stenosis. Increasing intima-media thickness (IMT) associates with the severity of coronary stenosis (fig.6a,b) and increased miR-374b expression (fig.6c). Moreover, miR-374b levels associated with IMT (r^2=0.5874, p<0.01, fig.6d). Conversely, MAPK7 expression levels progressively decrease with increasing stenosis (fig.6e). In human coronary artery stenosis, the levels of miR-374b are associated with the expression levels of MAPK7 (r^2=0.3341,p<0.01, fig.6f), suggesting that the miR-374b-induced loss of MAPK7 signaling might contribute to stenosis development and progression.

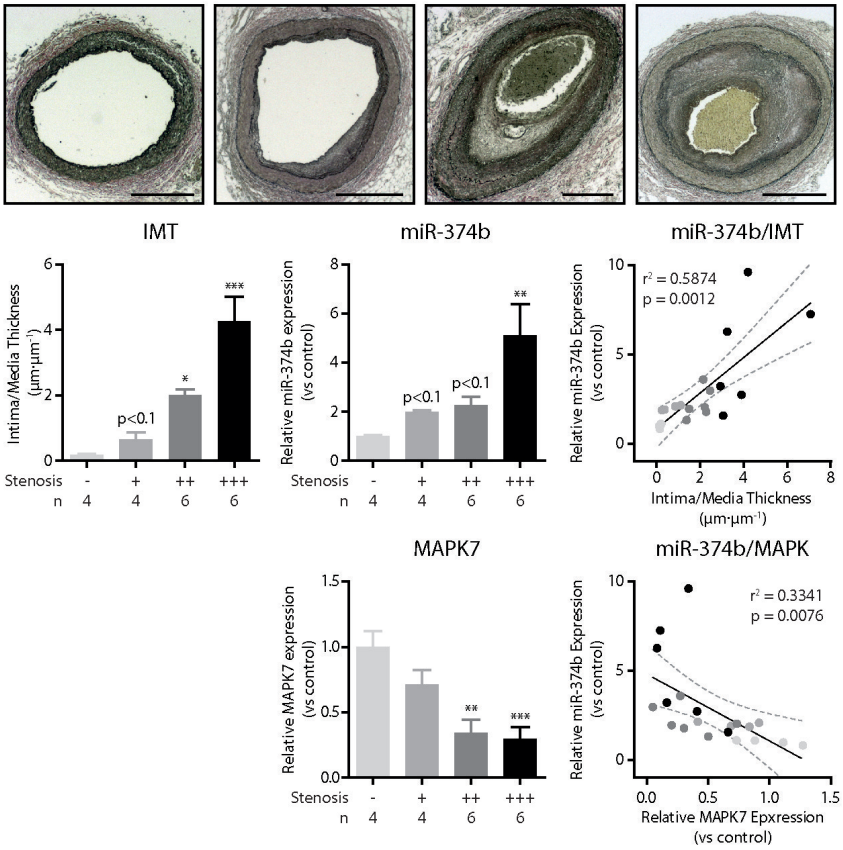

Figure 6. MicroRNA-374b is increased in human coronary artery stenosis. *Verhoeff stain of progressive coronary artery stenosis characterized by an increasing intima/media ratio (A). MiR-374b expression is elevated in human coronary artery stenosis and correlated to the degree of stenosis (B). Conversely, the expression levels of MAPK7 decrease with progressive stenosis and are inversely associated to the expression level of miR-374b (C). One-way ANOVA for comparison between groups, Pearson correlations, two-tailed. **p<0.01, ***p<0.001.*

DISCUSSION

Here, we show that EndMT occurs in intimal hyperplasia and neointima formation and is governed in part by microRNA-374b. We have previously identified the inhibitory effects of MAPK7 signaling on EndMT [5] and questioned if MAPK7 signaling is silenced at atheroprone areas in the vasculature. We uncovered that the TGFβ-induced microRNA-374b silences MAPK7 signaling and induces EndMT in the absence of exogenous TGFβ. Moreover, restoration of MAPK7 signaling abrogated these pathological effects in endothelial cells expressing miR-374b. Interestingly, we uncovered that miR-374b levels are elevated in human coronary artery disease and inversely related with MAPK7 expression. These data suggest that the TGFβ-miR-374b-MAPK7 axis plays a detrimental role in the induction of EndMT during intimal hyperplasia and neointima formation and might pose an interesting target for antiatherosclerosis therapy.

Atherosclerosis is characterized by systemic risk factors, and anti-atherosclerosis therapies are focused on maintaining these systemic contributors within clinically acceptable ranges (e.g. anti-hypertensives, anti-inflammatory agents and lipid-lowering drugs) [21-23]. Yet, it is becoming increasingly clear that focal risk factors, such as fluid shear stress levels, play a major role in the pathogenesis of atherosclerosis. Indeed, endothelial MAPK7 signaling has been identified as a major contributor to the initiation and severity of atherosclerosis [5,12]. The atheroprotective effects of MAPK7 include anti-inflammatory effects, the reduction of oxidative stress and the increased biosynthesis of Nitric Oxide [24-26], which decrease smooth muscle cell proliferation and inflammatory cell infiltration into the atherosclerotic neointima. We recently uncovered that endothelial MAPK7 signaling additionally confers atheroprotective effects through the inhibition of EndMT [5], a process increasingly recognized in the initial phases of intimal hyperplasia and neointima formation [5,7,27,28]. Indeed, the inhibition of MAPK7 activity by SUMOylation increases atherosclerosis [29,30] and endothelial specific deletion of MAPK7 aggravates atherosclerosis development and progression [12].

MicroRNAs are involved in atherosclerosis development and progression [31], and microRNA-based therapies that target endothelial dysfunction reduce atherosclerosis development in mice [32-34]. MicroRNAs regulate gene expression by imperfect base-pairing with the 3' UTR region of their gene target, causing translational repression [35]. This imperfect base-pairing allows for gene target multiplicity, wherein one microRNA targets multiple genes with a specific signaling cascade [36]. Hence, we questioned if MAPK7 signaling would be regulated by a specific microRNAs and if such microRNA would be differentially expressed at atheroprone and atheroprotected sites. We found that miR-374b expression is elevated at atheroprone areas in the vessel wall and is associated with decreased MAPK7 activity.

A role for miR-374b in atherosclerosis has not been described before, yet elevated levels of miR-374b have been reported in the plasma of acute coronary syndrome patients [37] and in stenosis of the arteriovenous fistulae of dialysis patients [38], however its relevance in these pathologies remains elusive. Here, we show that miR-374b is a shear stress-sensitive microRNA that targets MAPK7 signaling at multiple levels ranging from its upstream activating kinase (*i.e.* MAP3K3) to its downstream transcription factor (*i.e.* KLF4). The loss of MAPK7 signaling culminates in the induction of EndMT in the absence of exogenous triggers, which contributes to intimal hyperplasia and neointima formation.

Moreover, we show that restoration of MAPK7 signaling in endothelial cell that express miR-374b abolishes EndMT. From a clinical perspective, our data imply that targeting miR-374b in atherosclerosis might restore endothelial MAPK7 activity and limit neointima formation through the inhibition of EndMT.

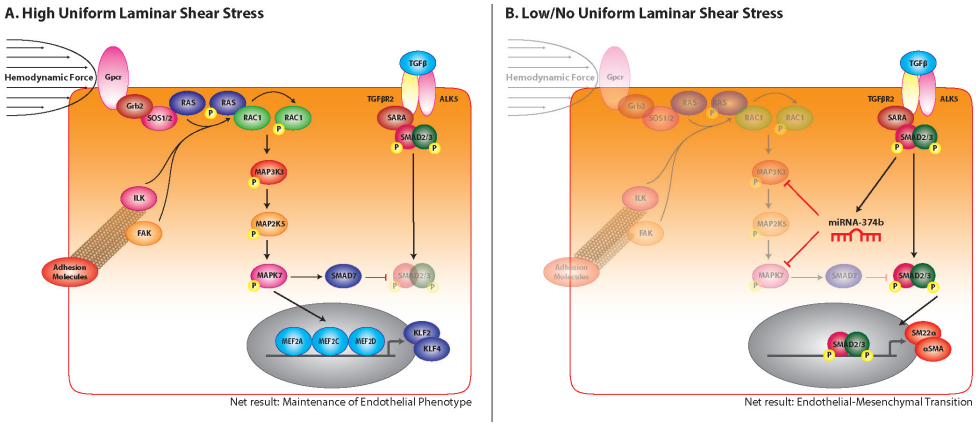

Figure 7. Schematic representation of miR-374/MAPK7 signaling in atheroprone and atheroprotected areas. *High laminar fluid shear stress induces the expression and activation of atheroprotective MAPK7 signaling, which maintains endothelial homeostasis and inhibits the proatherogenic TGFβ signaling (A). At areas of low, or non-uniform disturbed shear stress, MAPK7 activity is low and its expression is decreased by the TGFβ1-induced miR-374b, resulting in enhanced TGFβ signaling in endothelial cells, culminating in EndMT (B).*

In conclusion, here we show that miR-374b expression is elevated in coronary artery stenosis and neointima formation and abolishes endothelial MAPK7 activity, culminating in EndMT. The restoration of endothelial MAPK7 activity surmounts the induction of EndMT by miR-374b.

EXTENDED METHODS

CLINICAL SAMPLES

Human coronary arteries were obtained from autopsy specimens from 10 patients that died from an acute coronary episode at the Heart Institute (InCor), Sao Paulo, Brazil. Coronary arteries were fixed in neutral buffered formalin prior to paraffin embedding. During necropsy each dissected coronary artery was fixed in neutral-buffered formalin with constant perfusion at a quasi-normal perfusion pressure. The mean age of subjects contributing pathology specimens was 65 years. Hypertension was recent in 9 subjects, and diabetes in 6. Five individuals were active smokers. Next-of-kin gave informed consent and the investigation was performed according to institutional guidelines (InCor, Sao Paulo #SDC 3723/11/141 and #CAPPesq 482/11) and the Declaration of Helsinki.

Human coronary artery samples were deparaffinized using 100% Xylol for 10 mins and rehydrated using a series of EtOH solution of decreasing concentration (100%; 75%; 50%; 0%, all 10 mins). Samples were stained in Verhoeff's solution (92 mM hematoxylin, 137 mM $FeCl_3$, 27 mM KI, 4 mM I_2 in 55% EtOH) at room temperature for 1 hour. Samples were rinsed in tap water and differentiated in $FeCl_3$ (123 mM in dH_2O) for 1 minute and treated with Sodium Thiosulphate (316 mM in dH2O) at room temperature for 1 min. Samples were dehydrated using increasing concentrations of EtOH (50%; 75%; 100%, all 1 min) and cleared in 100% xylene. Samples were mounted in Permount resinous mounting medium.

ANIMALS AND SURGICAL PROCEDURES

Porcine abdominal trifurcations were obtained from healthy male slaughterhouse Yorkshire pigs (12-13 weeks of age; body weight 30-35 kg, n =3, V.O.F. van Beek, Lelystad, The Netherlands). Animals were fed a normal diet and were euthanized under anesthesia (ketamine (Nimatek) and midazolam with a bolus of pentobarbital and heparin (Actrapid)). Male C57Bl/6j wild-type mice (8-12 weeks of age, n=8, Harlan, Horst, The Netherlands) were subjected to transverse aortic constriction under anesthesia (2% Isofluorane (Forene/Abbott, The Netherlands) and oxygen) and analgesia (Carprofen, 5 $mg \cdot kg^{-1}$). Briefly, an incision was made in the second intercostal space and a small incision was made in the parietal pleura to expose the ascending loop of the aorta. The aorta was supported with a 27G needle and a suture was placed around the aorta, drawn tight after which the needle was removed. Next, the pleura, muscle layers, and skin were closed by sutures. Animals received post-operative analgesia (Carprofen, 5 $mg \cdot kg^{-1} \cdot day^{-1}$ for 48 h). Animals were kept on a 12 h light:dark cycle with ad libitum access to standard laboratory chow and water. Eight weeks after aortic constriction, animals were sacrificed under deep anesthesia [3% Isofluorane (Forene/Abbott, The Netherlands] by exsanguination, after which the thoracic aorta was explanted. Experiments on mice were approved by the local Institutional Animal Care and Use Committee (University of Groningen, #DEC-5910).

HUMAN UMBILICAL VEIN ENDOTHELIAL CELL CULTURE

Human umbilical vein endothelial cells (HUVEC, Lonza, Walkersville, MD) were cultured on 1% gelatin (#G9391 Sigma-Aldrich, St. Louis, MO) coated tissue culture plastics in endothelial cell medium up to passage 5 in RPMI1640 (#BE12-702F, Lonza, Verviers, Belgium) supplemented with 20% fetal bovine serum (#SH30071, HyClone Laboratories, Logan, UT), 50 µg·ml^{1} ECGF (own isolation according to Burgess et al 1985)[39], 2 mM L-glutamine (#G7513, Sigma-Aldrich, St. Louis, MO), 1% Penicillin/Streptomycin (#P4333, Sigma-Aldrich, St. Louis, MO) and 5 U·ml^{-1} heparin (Leo Pharma, Ballerup, Denmark). EndMT was initiated by re-plating the HUVEC in RPMI1640, supplemented with 20% FCS, 1% Penicillin–Streptomycin, 2 mM L-glutamine, 5 U·mL^{-1} heparin, and 10 ng·mL^{-1} TGFβ1 (Peprotech, NJ, USA) for 96 hours. For shear stress experiments, HUVEC were plated on 1% gelatin-coated µ-Slides (Ibidi, Martinsried, Germany) and grown to confluence prior to exposure to 20 dynes·cm^{-2} of unidirectional uniform laminar shear stress (LSS). LSS was generated using the Ibidi Pump System (Ibidi, Martinsried, Germany) according to manufacturer's instructions.

3'UTR REPORTER ANALYSIS

Gene specific 3'UTR fragments were isolated from a cDNA pool derived from various human tissues using oligonucleotides extended with SgfI (GCGATCGC) and NotI (GCGGCCGC) restriction sequences at the sense and antisense primer (Table S1), respectively. Amplification was performed using the DyNAzyme EXT PCR kit (Finnzymes, Vantaa, Finland) according to the manufacturer's instructions. 10 ng of cDNA was amplified in a 50 µl reaction volume containing 50 mM Tris-HCl (pH 9.0), 1.5 mM $MgCl_2$, 15 mM $(NH_4)_2SO_3$, 0.1% Triton X-100, 200 µM dNTPs, 0.6 µM 3'UTR primers and 2U DyNAzyme EXT DNA Polymerase (all Finnzymes, Vantaa, Finland) in a Biometra TProfessional thermocycler (Biometra, Göttingen, Germany) using an initial denaturation step of 94°C for 5 mins and 30 cycles of 94°C for 30 sec, 58-72°C for 2 mins, and 72°C for 2 mins, followed by a final extension step of 72°C for 10 mins. The reaction was halted at 82°C for 5 mins.

Amplicon sizes were validated by gel electrophoresis on 1% agarose gels and amplicons were dissected from the gels. 3'UTR fragments were purified using the QIAquick PCR Purification Kit (#28104, Qiagen, Venlo, The Netherlands) according to manufacturer's protocol. Purity and concentration of 3'UTR fragments was determines spectrophotometrically on a Nanodrop 1000 (ThermoFisher, Waltham, MA). 3'UTR fragments were inserted into the SgfI/NotI (both Fermentas, Vilnius, Lithuania)-linearized psiCHECK-2 dual luciferase reporter vector (Promega, Madison, WI) using T4 DNA Ligase (Sigma-Aldrich, St. Louis, MO). 3'UTR-containing plasmids were amplified in competent TOP10 E.coli (Invitrogen, Carlsbad, CA) and plasmids were isolated using the QIAprep Spin Miniprep Kit (Qiagen, Venlo, The Netherlands) according to manufacturer's instructions. COS-7 cells were transfected with 100 ng/ml 3'UTR reporter plasmid and 50 nM miR-374b mimic or scrambled control (Life Technologies, Carlsbad, CA) using Lipofectamine2000 (ThermoFisher, Waltham, MA). 48 h post-transfection, luciferase activity was assayed using the DualGlo Luciferase assay system (Promega, Madison, WI) and recorded for 1 s on a Luminoskan ASCENT (Thermo Scientific, Waltham, MA).

PLASMIDS AND LENTIVIRAL EXPRESSION OF MIR-374B, SHRNA AND MAPK7 SIGNALING MEMBERS

For lentiviral expression of miR-374b and small hairpin RNA (shRNA) against MAPK7 signaling members, equimolar amounts of DNA oligonucleotides containing the endogenous miR-374b hairpin or specific 21-mer targeting sequences for human MAP3K3, MAPK7, MEF2D or KLF4 (all Biolegio, Leiden, The Netherlands, Table S2) were annealed in a 100 µl reaction volume, containing 100 µM sense and antisense oligonucleotides, 10 mM Tris-HCl (pH 8.0), 50 mM NaCl and 1 mM EDTA. Annealing was performed by heating the reaction mixture to 98°C for 5 mins and cooling the reaction mixture at 1.5°C·min^{-1} to 20°C in a Biometra TProfessional thermocycler. Duplexed oligonucleotides were cloned into the BamHI/EcoRI (both Fermentas, Vilnius, Lithuania)-linearized pGreenPuro shRNA expression vector (Systems Bioscience, CA, USA) using T4 DNA Ligase (Sigma-Aldrich, St. Louis, MO). Scrambled sequences were used as control.

Gene-CDS fragments were isolated from a cDNA pool derived from various human tissues using oligonucleotides extended with EcoRI (GAATTC) and BamHI (GGATCC) restriction sequences at the sense and antisense primer (Table S3), respectively. Amplification was performed using the DyNAzyme EXT PCR kit (Finnzymes, Vantaa, Finland) according to the manufacturer's instructions. 10 ng of cDNA was amplified in a 50 µl reaction volume containing 50 mM Tris-HCl (pH 9.0), 1.5 mM $MgCl_2$, 15 mM $(NH_4)_2SO_3$, 0.1% Triton X-100, 200 µM dNTPs, 0.6 µM 3'UTR primers and 2U DyNAzyme EXT DNA Polymerase (all Finnzymes, Vantaa, Finland) in a Biometra TProfessional thermocycler using an initial denaturation step of 94°C for 5 mins and 30 cycles of 94°C for 30 sec, 58-72°C for 2 mins, and 72°C for 2 mins, followed by a final extension step of 72°C for 10 mins. The reaction was halted at 82°C for 5 mins. Amplicon size was validated by gel electrophoresis on 1% agarose gels and amplicons were dissected from the gels. 3'UTR fragments were purified using the QIAquick PCR Purification Kit (#28104, Qiagen, Venlo, The Netherlands) according to manufacturer's protocol. Purity and concentration of 3'UTR fragments was determines spectrophotometrically on a Nanodrop 1000 (ThermoFisher, Waltham, MA). Gene-CDS fragments were cloned into the EcoRI/BamHI sites of the pCDH-CMV-MCS-EF1-Puro lentiviral expression vector (Systems Biosciences, Palo Alto, CA) using T4 DNA Ligase (Sigma-Aldrich, St. Louis, MO). Empty vectors served as control.

ShRNA and Gene-CDS-containing plasmids were amplified in competent TOP10 E.coli (Invitrogen, Carlsbad, CA) and plasmids were isolated using the QIAprep Spin Miniprep Kit (Qiagen, Venlo, The Netherlands) according to manufacturer's instructions. For lentiviral transduction, $1.0{\cdot}10^6$ HEK293 cells were transfected with 1 µg pGreenPuro or pCDH-CMV-MCS-EF1-Puro shuttle vectors and 1 µg second-generation lentiviral helper plasmids using Endofectin (GeneCopoeia, MD, USA). Viral supernatants were collected every 24 hours, supplemented with 6 µg·mL^{-1} polybrene and directly transferred to HUVEC cultures for two consecutive rounds. Transduced cells were selected for puromycin resistance 72 h post-transduction (4 µg·mL^{-1} puromycin) for 24 hours and reseeded into puromycin-free medium for the experiments.

MICRORNA AND GENE TRANSCRIPT ANALYSIS

Total RNA was isolated using TRIzol reagent (Invitrogen, Carlsbad, CA) according to manufacturer's instructions. In brief, $1{\cdot}10^6$ cells or 10 mg of tissue was homogenized in 1

ml TRIzol reagent and supplemented 0.2 ml Chloroform. After centrifugation (12.000xg for 15 min) the aqueous phase was supplemented with 0.5 ml 2-propanol and the RNA pelleted by centrifugation (12.000xg for 10 min). RNA was further purified using two consecutive washes with 75% EtOH. RNA integrity was validated on 2% agarose gels and RNA purity and concentration were determined spectrophotometrically on a Nanodrop 1000 (ThermoFisher, Waltham, MA). For microRNA transcript analyses, 20 ng of total RNA was reversely transcribed using the Taqman MicroRNA Reverse Transcription kit (Applied Biosystems) in a 10 µl reaction volume containing 1 µl 10x RT reaction buffer, 1.6 µM microRNA-specific stemloop primers (Table S4), 1 mM dNTPs, and 3U RT enzyme (all Taqman, ThermoFisher, Waltham, MA) in a Biometra TProfessional thermocycler at 16°C for 30 mins, 42°C for 60 mins, and the reaction was stopped at 85°C for 5 mins. For gene transcript analysis, 1 µg of total RNA was reversely transcribed using the RevertAid First Strand cDNA Synthesis Kit (Applied Biosystems, Carlsbad, CA) in a in a 20 µl reaction volume containing 4 µl 5x RT reaction buffer, 5 µM random hexamer primers, 20U RiboLock RNase Inhibitor, 1 mM dNTP, and 200U RT enzyme (all Fermentas/ThermoFisher, Waltham, MA) in a Biometra TProfessional thermocycler at 25°C for 5 mins, 42°C for 60 mins, and the reaction was stopped at 70°C for 5 mins. Quantitative PCR expression analysis was performed on a reaction mixture containing 1-10 ng cDNA equivalent, 0.5 µM sense primers and 0.5 µM antisense primers (for microRNA primers see Table S4 and gene transcript primers see Table S5, all Biolegio, Leiden, The Netherlands) and FastStart SYBR Green (Roche, Almere, The Netherlands). Analyses were run on a Viia7 real-time PCR system (Applied Biosystems, Carlsbad, CA) using an initial denaturation step of 94°C for 5 mins and 40 cycles of 94°C for 30 sec, 60°C for 1 min. Cycle thresholds (Ct) values were determined at the middle of the linear phase. MicroRNA expression was normalized against the expression of RNU6B and mRNA expression levels were normalized against the expression of GAPDH prior to normalization against control samples.

IMMNUNOFLUORESCENCE

Heat-induced antigen retrieval was performed with 0.1 M Tris-HCl (pH 9.0, 80°C, 20 mins) on the formalin fixated, paraffin-embedded sections prior to immunohistochemistry. Sections were allowed to cool to room temperature for 45 mins, and incubated with 2%BSA/2% normal donkey serum in PBS for 20 mins. Sections were incubated with primary antibodies (Table S6) at room temperature for 2 hours, followed by extensive washing in TBS-Tween (0.05%). Subsequently, samples were incubated with secondary antibodies in DAPI/PBS at room temperature for 1 hour (Table S6) and mounted in CitiFluor AP1 (Electron Microscopy Sciences, Hatfield, PA). Overview images of porcine aortic trifurcation tissue and murine TAC tissue were obtained through ×10 (Plan-Neofluar 0.4 NA, dry, Ph2) and ×20 (Plan-Neofluar, 1.30 NA, dry, DIC) objectives of an upright epifluorescence microscope (Zeiss AxioObserver Z1), controlled by TissueFAXS (TissueGnostics GmbH, Vienna, Austria) and analyzed using TissueQuest software (TissueGnostics GmbH, Vienna, Austria). Confocal images were obtained using a Leica SP8 spectral confocal microscope through a ×63 (HCX PL APO 1.40 NA, oil) objective. 555 and 647 channels were scanned sequentially. Images were analyzed using Imaris 7.2.1 (Bitplane AG, Zürich, Switzerland), z-stacks were created using ImageJ version 1.43u (NIH, USA).

IMMUNOBLOTTING

Whole cell lysates were prepared in RIPA buffer (Thermo Scientific, IL, USA) supplemented with 1% protease inhibitor cocktail (Sigma-Aldrich, Germaby) and 1% HALT-phosphatase inhibitor cocktail (ThermoFisher Scientific). Protein concentrations were determined using the detergent compatible protein assay (Bio-Rad, VA), according to manufacturer's protocol. Equal amounts of protein were loaded on a 10% denaturing SDS–polyacrylamide gel and separated by gel electrophoresis (110V). Next proteins were blotted onto nitrocellulose membranes using the Trans-Blot Turbo System (Bio-Rad, AV) at 2.5A for 7 mins, according to manufacturer's instructions. Blots were incubated in Odyssey Blocking Buffer (Li-COR Biosciences, NE, USA) in TBS at room temperature for 30 mins and incubated at 4°C with primary antibodies (Table S7) in Odyssey Blocking Buffer overnight. After extensive washes with TBST, membranes were incubated with secondary antibodies (Table S7) in Odyssey Blocking Buffer at room temperature for 1 hour. Protein was detected using the Odyssey Infrared Imaging System (Li-COR Biosciences). Densitometric analysis was performed using Totallab 120 (Nonlinear Dynamics, Newcastle upon Tyne, England) set for automatic lane detection, Rolling ball background subtraction (20 pixel radius) and automatic lane detection (minimum slope=100; Noise reduction = 5%, % Max peak=1). Lane intensities were corrected for protein-loading using the intensities of GAPDH and normalized to the average intensity of control samples.

ANGIOGENIC SPROUTING CAPACITY

10 µl of MatriGel (BD Biosciences, San Jose, CA) was solidified in µ-Slide Angiogenesis (Ibidi, Martinsried, Germany). 15,000 cells per well were cultured on the solidified MatriGel in endothelial growth medium and the formation of sprouts was analyzed by conventional light microscopic analysis after overnight incubation. The number of hexagonal shapes per well was quantified manually.

COLLAGEN CONTRACTION ASSAY

Cells were suspended in a solution of rat tail Collagen type I (Corning, Corning, NY) containing 3 $mg{\cdot}mL^{-1}$ $NaHCO_3$ and 0.1M Na_2HPO_4. Aliquots of 50 µL (containing 100.000 cells and 0.5 mg Collagen type I) were solidified at 37°C in a humidified incubator with 5% CO_2 for 30 mins. The collagen gels were released from the culture dishes by the addition of 2 ml endothelial growth medium and were imaged using a common Flatbed-scanner and allowed to contract for an additional 24 h. The degree of gel contraction was determined by measuring the total gel area and dividing the areas of the contracted gels by the areas of the gels before contraction.

STATISTICAL ANALYSIS

Data are presented as means ± s.e.m. N-values relate to independent experiments/ samples. P-values were calculated using one-way analysis of variance followed by Bonferroni's post-hoc comparisons tests using Prism Graphpad (Graphpad Software, La Jolla, CA, USA). $P < 0.05$ was considered statistically significant.

SUPPLEMENTARY FIGURES

A.

Pathway	Gene
MAPK7	RAC1
	MAP3K7
	MAP3K3
	MAP2K5
	MAPK7
	MEF2A
	MEF2C
	MEF2D
	KLF4

B.

Gene	microRNA	SVR-Score
MAPK7	miR-374b	-1.095
	miR-374a	-1.090
	miR-429	-1.311
	miR-200b	-1.311
	miR-200c	-1.311
	miR-143	-0.751
	miR-24	-0.453
	miR-488	-0.353
	miR-410	-0.220
	miR-183	-0.164
	miR-124	-0.126
	miR-506	-0.122

C.

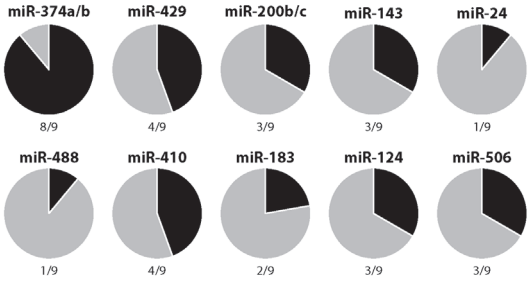

Supplementary figure 1. In silico analysis identifies miR-374 as putative regulator of MAPK7 signaling. *(A) Overview of the MAPK7 signaling pathway containing the upstream activators Rac1, MAP3K7 (TAK1), MAP3K3 (MEKK3), MAP2K5 (MEK5), MAPK7 (ERK5), and the downstream transcription factors MEF2A-D and KLF4. (B) In silico analysis (miRanda(40, 41)) identifies 12 microRNAs that target MAPK7. SVR-scores indicate the predicted target site efficacy.(41) (C) In silico analysis of genes within MAPK7 signaling targeted by microRNA-374, -429, -200b/c, -143, -24, -488, -410, -183, -124 and miR-506. The miR-374 family targets 8/9 genes in the MAPK7 signaling pathway.*

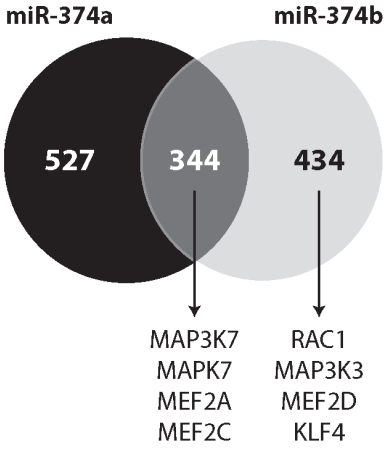

Supplemental figure 2. MicroRNA-374b targets MAPK7 signaling. *In silico analysis (TarBase(42)) reveals that miR-374a and miR-374b collectively have 1305 putative gene targets, of which 527 and 434 are unique to miR-374a and miR-374b, respectively. 344 putative gene targets are shared between miR-374a and miR-374b. Analysis of genes within the MAPK7 signaling cascade indicates that MAP3K7 (TAK1), MAPK7 (ERK5), MEF2A and MEF2C are putative targets of miR-374a and miR-374b, whereas Rac1, MAP3K3 (MEKK3), MEF2D and KLF4 are targets of miR-374b only.*

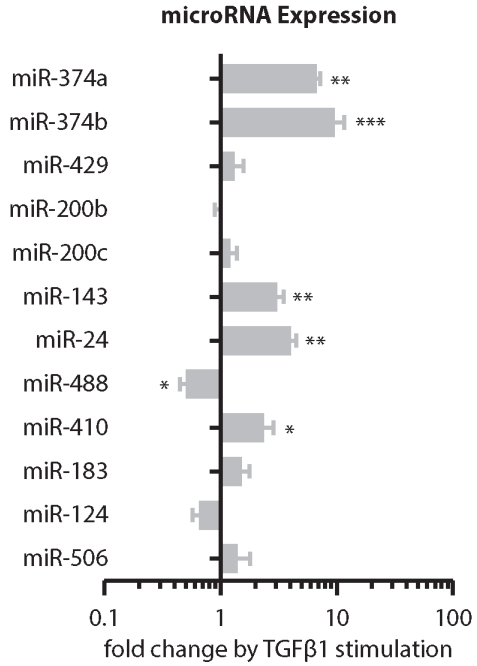

Supplemental figure 3. TGFβ1-induced microRNA expression. *TGFβ1 induced the expression of miR-374a, miR-374b, miR-143, miR-24 and miR-410 in endothelial cells (p<0.05 vs unstimulated control cells), whereas it decreased the expression of miR-488 (p<0.05 vs unstimulated control cells). The expression of miR-429, miR-200b, miR-200c, miR-183, miR-124 and miR-506 were unchanged (Suppl.fig.2) upon TGFβ1 treatment. *** p<0.001, ** p<0.01, * p<0.05, n=5, one-sample t-test.*

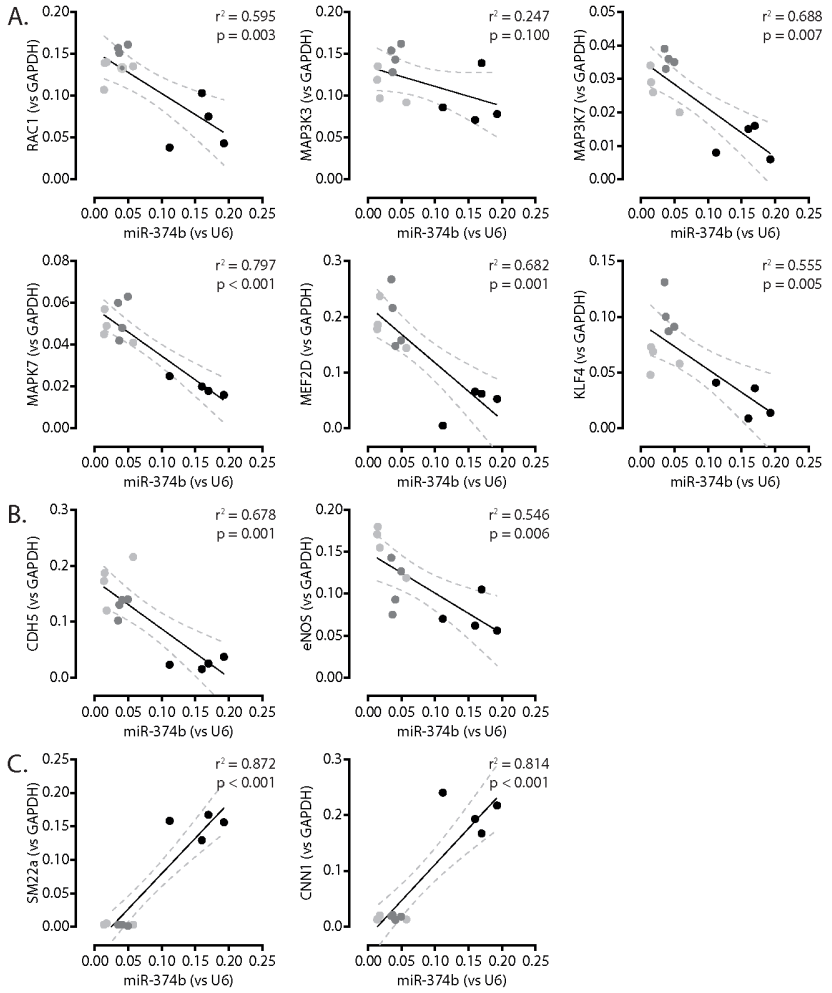

Supplemental figure 4. miR-374b expression levels associate with decreased expression of MAPK7 signaling members and EndMT. *The increased expression of miR-374b in endothelial cells treated with TGFβ1 (black) compared to TGFβ1 and SB431542-treated endothelial cells (dark grey) or non-stimulated endothelial cells (light grey) were associate with decreased expression of MAPK7 signaling members RAC1, MAP3K3, MAPK7, MEF2D and KLF4 (A), and associated with decreased expression of endothelial cell markers (VE-Cadherin and eNOS; B) and increased expression of mesenchymal cell markers (SM22a and CNN1; C). n=4, Pearson correlation, two-tailed.*

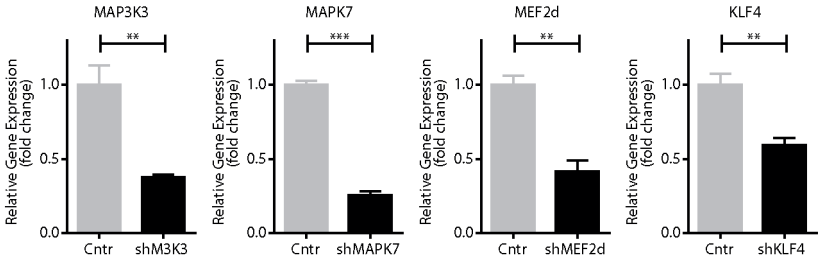

Supplemental figure 5. RNAi-mediated repression of MAPK7 Signaling members. *Lentiviral expression of shRNA oligonucleotides against MAPK7 signaling members reduced their expression >2-fold compared to endothelial cells that were transformed using scrambled-constructs. *** p<0.001, ** p<0.01, n=3, one-sample t-test.*

SUPPLEMENTARY TABLES

Table S1. Primers used for 3'-UTR-reporter construct preparations.

3'-UTR	Reference Sequence	Sense Primer (5' → 3')	Antisense Primer (5' → 3')
KLF4	NM_004235	ATCCCAGACAGTGGATATG	CAGATAAAATATTATAGGTT
MAP3K3	NM_203351	GCTCTCACGGCCACACAGCT	CTGATATAAATGATCCCTTTTATTG
MAP3K7	NM_003188	TTCTCTGGGACCGTTACATT	CAAATACATGAGAAAACAATC
MAPK7	NM_139032	GGCCCCCAGCCTGTGCCTTG	CAGGTGCAGAAGGGAACCTT
MEF2A	NM_001319206	GGCTTCCAAGCTGATGTTTG	AGCATTGTCTTCACCATTTG
MEF2C	NM_001193347	TCAGATTATTACTTACTAGT	TCACTAAGAAAGCCAGTAAC
MEF2D	NM_005920	CGATTCCCACTCCCCTCCTC	ATCAGAAACGTGTATTCTTT
RAC1	NM_018890	ATGTCTCAGCCCCTCGTTCT	ATGATTCAAGGATTTATTAA

All primers were obtained from Sigma-Aldrich, MO.

Table S2. Oligos used for lentiviral miR-374b and shRNA expression.

Construct	Reference Sequence	Sense Oligo (5' → 3')
miR-374b	NR_030620	ACTCGGATGGATATAATACAACCTGCTAAGTGTCCTAGCACTTA GCAGGTTGTATTATCATTGTCCGTGTCTTTTTTT
shKLF4	NM_004235	GCCACCCACACTTGTGATTACTTCAAGAGAGTAATCACAAGTG TGGGTGGCTTTTTTTT
shMAP3K3	NM_203351	GGTCCTACACCAGCATCAACATTCAAGAGATGTTGATGCTGGT GTAGGACCTTTTTTTT
shMAPK7	NM_139032	AAGCACTTTAAACACGACAACTTCAAGAGAGTTGTCGTGTTTA AAGTGCTTTTTTTT
shMEF2D	NM_005920	GCTTGATACCTGGACATTAAATTCAAGAGATTTAATGTCCAGGT ATCAAGCTTTTTTTT

All primers were obtained from Sigma-Aldrich, MO.

Table S3. Primers used for the cloning of MAPK7 signaling members.

Gene	Reference Sequence	Sense Primer (5' → 3')	Antisense Primer (5' → 3')
KLF4-CDS	NM_004235	ATGGCTGTCAGCGACGCGCTGCTCC	AAAATGCCTCTTCATGT
MAP3K3-CDS	NM_203351	ATGGACGAACAGGAGGCATTGAAC	GTACATGAGCTGTGCAAAGTGGTG
MAPK7-CDS	NM_139032	ATGGCCGAGCCTCTGAAGGAGGAAGA	GGGGTCCTGGAGGTCAGGCAGGT
MEF2D-CDS	NM_005920	ATGGGGAGGAAAAAGATTCAGATCC	CTTTAATGTCCAGGTATC

All primers were obtained from Sigma-Aldrich, MO.

Table S4. Primers used for microRNA transcript analysis.

microRNA	Stemloop Primer (5' - 3')	**Sense Primer (5' - 3')**
hsa-miR-24	GTCGTATCCAGTGCAGGGTCCGAGGTATTCGCACTGGATAC GACCTGTTCCT	TGCGGTGGCTCAGTTCAGC
hsa-miR-124	GTCGTATCCAGTGCAGGGTCCGAGGTATTCGCAC TGGATACGACGGCATTCA	TGCGGTTAAGGCACGCGG
hsa-miR-143	GTCGTATCCAGTGCAGGGTCCGAGGTATTCGCAC TGGATACGACGAGCTACA	TGCGGTGAGATGAAGCACT
hsa-miR-183	GTCGTATCCAGTGCAGGGTCCGAGGTATTCGCAC TGGATACGACAGTGAATT	TGCGGTTATGGCACTGGTAG
hsa-miR-200b	GTCGTATCCAGTGCAGGGTCCGAGGTATTCGCAC TGGATACGACTCATCATTAC	TGCGGTAATACTGCCTG
hsa-miR-200c	GTCGTATCCAGTGCAGGGTCCGAGGTATTCGCAC TGGATACGACTCCATCAT	TGCGGTAATACTGCCGGGTA
hsa-miR-374a	GTCGTATCCAGTGCAGGGTCCGAGGTATTCGCAC TGGATACGACCACTTATC	TGCGGTTTATAATACAACCT
hsa-miR-374b	GTCGTATCCAGTGCAGGGTCCGAGGTATTCGCAC TGGATACGACCACTTAGC	TGCGGTATATAATACAACCT
hsa-miR-410	GTCGTATCCAGTGCAGGGTCCGAGGTATTCGCAC TGGATACGACACAGGCCA	TGCGGTAATATAACACAGA
hsa-miR-429	GTCGTATCCAGTGCAGGGTCCGAGGTATTCGCAC TGGATACGACACGGTTTT	TGCGGTAATACTGTCTGGT
hsa-miR-488	GTCGTATCCAGTGCAGGGTCCGAGGTATTCGCAC TGGATACGACGACCAAGA	TGCGGTTTGAAAGGCTATT
hsa-miR-506	GTCGTATCCAGTGCAGGGTCCGAGGTATTCGCAC TGGATACGACTCTACTCA	TGCGGTTAAGGCACCCTTC
RNU6B	GTCGTATCCAGTGCAGGGTCCGAGGTATTCGCACTGGATAC GACAAAAATATGG	TGCGGCTGCGCAAGGATGA

Amplification reactions for mature microRNAs used the same antisense primer (5'-CCAGTGCAGGGTCCGAGGTCCG-3'). All primers were obtained from Sigma-Aldrich, MO.

Table S5. Primers used for mRNA transcript analysis.

Gene Name	**Reference Sequence**	**Sense Primer (5' → 3')**	**Antisense Primer (5' → 3')**
CDH5	NM_001795	GTTCACCTTCTGCGAGGATA	GTAGCTGGTGGTGTCCATCT
CNN1	NM_001308341	CCAACCATACACAGGTGCAG	TCACCTTGTTTCCTTTCGTCTT
GAPDH	NM_002046	AGCCACATCGCTCAGACAC	GCCCAATACGACCAAATCC
KLF4	NM_004235	GGGAGAAGACACTGCGTCA	GGAAGCACTGGGGGAAGT
MAP3K3	NM_203351	ACGGTGGTTTCTCTGTCAGC	AAGGAAAGCAGACGTGTGGA
MAP3K7	NM_003188	AACTCCATCCCAATGGCTTA	TTGGGCACGGTGCTAGAG
MAPK7	NM_139032	CCTGATGTCAACCTTGTGACC	CCTTTGGTGTGCCTGAGAAC
MEF2D	NM_005920	AACGCCGACATCATCGAG	GGCTCTGTTCCAGCGAGT
NOS3	NM_000603	CACATGGCCTTGGACTGAA	CAGAGCCCTGGCCTTTTC
RAC1	NM_018890	CTGATGCAGGCCATCAAGT	CAGGAAATGCATTGGTTGTG
TAGLN	NM_003186	CTGAGGACTATGGGGTCATC	TAGTGCCCATCATTCTTGGT

All primers were obtained from Sigma-Aldrich, MO.

Table S6. Antibodies used for immunofluorescence.

Antigen	Supplier	Catalogue #	Dilution
Primary Antibodies			
CD31	Santa Cruz Biotechnology, CA	sc-1506	1:200
ESM-1 (Endocan)	Lunginnov, France	lia-0901	1:200
MAPK7 (Erk5/BMK1)	Bioss, MA	bs-5486r	1:100
SM22α	Abcam, UK	ab14106	1:250
VE-Cadherin	Cell Signaling, CA	2500	1:100
Secondary Antibodies			
anti-Mouse IgG Alexa 594	Life Technologies, The Netherlands	A21203	1:500
anti-Goat IgG Alexa 594	Life Technologies, The Netherlands	A11058	1:500
anti-Rabbit IgG Alexa 647	Life Technologies, The Netherlands	A31573	1:500

Table S7. Antibodies used for immunoblotting.

Antigen	Supplier	Catalogue #	Dilution
Primary Antibodies			
Calponin (CNN1)	Abcam, UK	ab46794	1:1000
eNOS (NOS3)	BD Pharmingen	610299	1:500
GAPDH	Abcam, UK	ab9484	1:5000
MAP3K3 (MEKKK3)	Abcam, UK		
MAPK7 (Erk5/BMK1)	MerckMillipore, MA	07-039	1:1000
SM22α (Transgelin)	Abcam, UK	ab14106	1:1000
MEF2D	Bethyl Laboratories, TX	A303-522A	1:100
KLF4	Abcam, UK		
VE-Cadherin	Cell Signaling, CA	2500	1:1000
Secondary Antibodies			
anti-Ms IRDye 800	LI-COR Biosciences, Germany	926-32212	1:10.000
anti-Rb IRDye 680	LI-COR Biosciences, Germany	926-68073	1:10.000

REFERENCES

1. Ikari Y, McManus BM, Kenyon J, Schwartz SM. Neonatal intima formation in the human coronary artery. Arterioscler Thromb Vasc Biol. 1999;19(9):2036-40.
2. Vogel RA. Coronary risk factors, endothelial function, and atherosclerosis: A review. Clin Cardiol. 1997;20(5):426-32.
3. Hahn C, Schwartz MA. Mechanotransduction in vascular physiology and atherogenesis. Nat Rev Mol Cell Biol. 2009;10(1):53-62.
4. Traub O, Berk BC. Laminar Shear Stress: Mechanisms by Which Endothelial Cells Transduce an Atheroprotective Force. Arteriosclerosis, thrombosis, and vascular biology. 1998;18(5):677-85.
5. Moonen JA, Lee ES, Schmidt M, Maleszewska M, Koerts JA, Brouwer LA, et al. Endothelial-to-mesenchymal transition contributes to fibro-proliferative vascular disease and is modulated by fluid shear stress. Cardiovasc Res. 2015;108(3):377-86.
6. Chen P-Y, Qin L, Baeyens N, Li G, Afolabi T, Budatha M, et al. Endothelial-to-mesenchymal transition drives atherosclerosis progression. The Journal of clinical investigation. 2015;125(12):4514-28.
7. Evrard SM, Lecce L, Michelis KC, Nomura-Kitabayashi A, Pandey G, Purushothaman KR, et al. Endothelial to mesenchymal transition is common in atherosclerotic lesions and is associated with plaque instability. Nat Commun. 2016;7:11853.
8. Krenning G, Moonen JR, van Luyn MJ, Harmsen MC. Vascular smooth muscle cells for use in vascular tissue engineering obtained by endothelial-to-mesenchymal transdifferentiation (EnMT) on collagen matrices. Biomaterials. 2008;29(27):3703-11.
9. Moonen JR, Krenning G, Brinker MG, Koerts JA, van Luyn MJ, Harmsen MC. Endothelial progenitor cells give rise to pro-angiogenic smooth muscle-like progeny. Cardiovasc Res. 2010;86(3):506-15.
10. Maleszewska M, Moonen JR, Huijkman N, van de Sluis B, Krenning G, Harmsen MC. IL-1beta and TGFbeta2 synergistically induce endothelial to mesenchymal transition in an NFkappaB-dependent manner. Immunobiology. 2013;218(4):443-54.
11. Sinha S, Heagerty AM, Shuttleworth CA, Kielty CM. Expression of latent TGF-beta binding proteins and association with TGF-beta 1 and fibrillin-1 following arterial injury. Cardiovasc Res. 2002;53(4):971-83.
12. Le NT, Heo KS, Takei Y, Lee H, Woo CH, Chang E, et al. A crucial role for p90RSK-mediated reduction of ERK5 transcriptional activity in endothelial dysfunction and atherosclerosis. Circulation. 2013;127(4):486-99.
13. Brennecke J, Stark A, Russell RB, Cohen SM. Principles of microRNA-target recognition. PLoS biology. 2005;3(3):e85.
14. Small EM, Olson EN. Pervasive roles of microRNAs in cardiovascular biology. Nature. 2011;469(7330):336-42.
15. Ghosh AK, Nagpal V, Covington JW, Michaels MA, Vaughan DE. Molecular basis of cardiac endothelial-to-mesenchymal transition (EndMT): Differential expression of microRNAs during EndMT. Cellular signalling. 2012;24(5):1031-6.
16. Kumarswamy R, Volkmann I, Jazbutyte V, Dangwal S, Park D-H, Thum T. Transforming Growth Factor-β–Induced Endothelial-to-Mesenchymal Transition Is Partly Mediated by MicroRNA-21. Arteriosclerosis, thrombosis, and vascular biology. 2012;32(2):361-9.
17. Correia AC, Moonen J-RA, Brinker MG, Krenning G. FGF-2 inhibits endothelial-mesenchymal transition through microRNA-20a-mediated repression of canonical TGF-β signaling. Journal of cell science. 2016;129(3):569-79.
18. Chen P-Y, Qin L, Barnes C, Charisse K, Yi T, Zhang X, et al. FGF Regulates TGF-β Signaling and Endothelial-to-Mesenchymal Transition via Control of let-7 miRNA Expression. Cell reports. 2012;2(6):1684-96.

19. Betel D, Wilson M, Gabow A, Marks DS, Sander C. The microRNA.org resource: targets and expression. Nucl Acids Res. 2008;36(suppl 1):D149-D53.
20. Betel D, Koppal A, Agius P, Sander C, Leslie C. Comprehensive modeling of microRNA targets predicts functional non-conserved and non-canonical sites. Genome Biol. 2010;11(8):R90.
21. Back M, Hansson GK. Anti-inflammatory therapies for atherosclerosis. Nature reviews Cardiology. 2015;12(4):199-211.
22. Stone NJ, Robinson JG, Lichtenstein AH, et al. Treatment of blood cholesterol to reduce atherosclerotic cardiovascular disease risk in adults: Synopsis of the 2013 american college of cardiology/american heart association cholesterol guideline. Ann Intern Med. 2014;160(5):339-43.
23. Rosendorff C, Lackland DT, Allison M, Aronow WS, Black HR, Blumenthal RS, et al. Treatment of Hypertension in Patients With Coronary Artery Disease. Hypertension. 2015;65(6):1372-407.
24. Kim M, Kim S, Lim JH, Lee C, Choi HC, Woo CH. Laminar flow activation of ERK5 protein in vascular endothelium leads to atheroprotective effect via NF-E2-related factor 2 (Nrf2) activation. The Journal of biological chemistry. 2012;287(48):40722-31.
25. Clark PR, Jensen TJ, Kluger MS, Morelock M, Hanidu A, Qi Z, et al. MEK5 is activated by shear stress, activates ERK5 and induces KLF4 to modulate TNF responses in human dermal microvascular endothelial cells. Microcirculation. 2011;18(2):102-17.
26. Ohnesorge N, Viemann D, Schmidt N, Czymai T, Spiering D, Schmolke M, et al. Erk5 activation elicits a vasoprotective endothelial phenotype via induction of Kruppel-like factor 4 (KLF4). The Journal of biological chemistry. 2010;285(34):26199-210.
27. Mahmoud MM, Serbanovic-Canic J, Feng S, Souilhol C, Xing R, Hsiao S, et al. Shear stress induces endothelial-to-mesenchymal transition via the transcription factor Snail. Scientific reports. 2017;7(1):3375.
28. Chen PY, Qin L, Baeyens N, Li G, Afolabi T, Budatha M, et al. Endothelial-to-mesenchymal transition drives atherosclerosis progression. The Journal of clinical investigation. 2015;125(12):4514-28.
29. Woo CH, Shishido T, McClain C, Lim JH, Li JD, Yang J, et al. Extracellular signal-regulated kinase 5 SUMOylation antagonizes shear stress-induced antiinflammatory response and endothelial nitric oxide synthase expression in endothelial cells. Circulation research. 2008;102(5):538-45.
30. Heo KS, Chang E, Le NT, Cushman H, Yeh ET, Fujiwara K, et al. De-SUMOylation enzyme of sentrin/SUMO-specific protease 2 regulates disturbed flow-induced SUMOylation of ERK5 and p53 that leads to endothelial dysfunction and atherosclerosis. Circulation research. 2013;112(6):911-23.
31. Feinberg MW, Moore KJ. MicroRNA Regulation of Atherosclerosis. Circulation research. 2016;118(4):703-20.
32. Sun X, He S, Wara AK, Icli B, Shvartz E, Tesmenitsky Y, et al. Systemic Delivery of MicroRNA-181b Inhibits NF-κB Activation, Vascular Inflammation, and Atherosclerosis in Apoe-/- Mice. Circulation research. 2013.
33. Loyer X, Potteaux S, Vion A-C, Guerin CL, Boulkroun S, Rautou P-E, et al. Inhibition of microRNA-92a Prevents Endothelial Dysfunction and Atherosclerosis in Mice. Circulation research. 2013.
34. Schober A, Nazari-Jahantigh M, Wei Y, Bidzhekov K, Gremse F, Grommes J, et al. MicroRNA-126-5p promotes endothelial proliferation and limits atherosclerosis by suppressing Dlk1. Nat Med. 2014;20(4):368-76.
35. Bartel DP. MicroRNAs: target recognition and regulatory functions. Cell. 2009;136.
36. Small EM, Olson EN. Pervasive roles of microRNAs in cardiovascular biology. Nature. 2011;469(7330):336-42.

37. Ward JA, Esa N, Pidikiti R, Freedman JE, Keaney JF, Tanriverdi K, et al. Circulating Cell and Plasma microRNA Profiles Differ between Non-ST-Segment and ST-Segment-Elevation Myocardial Infarction. Fam Med Med Sci Res. 2013;2(2):108.
38. Lv L, Huang W, Zhang J, Shi Y, Zhang L. Altered microRNA expression in stenoses of native arteriovenous fistulas in hemodialysis patients. J Vasc Surg. 2016;63(4):1034-43.e3.
39. Burgess WH, Mehlman T, Friesel R, Johnson WV, Maciag T. Multiple forms of endothelial cell growth factor. Rapid isolation and biological and chemical characterization. Journal of Biological Chemistry. 1985;260(21):11389-
40. Betel D, Wilson M, Gabow A, et al. The microRNA.org resource: targets and expression. Nucl Acids Res 2008; 36: D149-153.
41. Betel D, Koppal A, Agius P, et al. Comprehensive modeling of microRNA targets predicts functional non-conserved and non-canonical sites. Genome Biol 2010; 11: R90.
42. Vlachos IS, Paraskevopoulou MD, Karagkouni D, et al. DIANA-TarBase v7.0: indexing more than half a million experimentally supported miRNA:mRNA interactions. Nucl Acids Res 2015; 43: D153-159.

Chapter 4

The decrease in histone methyltransferase EZH2 in response to fluid shear stress alters endothelial gene expression and promotes quiescence

Monika Maleszewska, Byambasuren Vanchin, Martin C. Harmsen[#], Guido Krenning[#]

Cardiovascular Regenerative Medicine Research Group, Department of Pathology and Medical Biology, University of Groningen, University Medical Center Groningen, Groningen, The Netherlands

[#]Equal contribution

Angiogenesis 2015, Volume 19, pp 9-24

ABSTRACT

High uniform fluid shear stress (FSS) is atheroprotective and preserves the endothelial phenotype and function through activation of downstream mediators such as MAPK7 (Erk5). Endothelial cells respond to FSS thanks to mechanotransduction. However, how the resulting signaling is integrated and resolved at the epigenetic level, remains elusive. We hypothesized that Polycomb methyltransferase EZH2 is involved in the effects of FSS in human endothelial cells.

We showed that FSS decreases the expression of the Polycomb methyltransferase EZH2. Despite simultaneous activation of MAPK7, MAPK7 pathway does not directly influence the transcription of EZH2. Interestingly though, the knock down of EZH2 activates the protective MAPK7 signaling in endothelial cells, even in the absence of FSS. To understand the influence of the FSS-decreased expression of EZH2 on endothelial transcriptome, we performed RNA-seq and differential gene expression analysis. We identified candidate groups of genes dependent on both EZH2 and FSS. Among those, Gene Ontology overrepresentation analysis revealed highly significant enrichment of the cell cycle-related genes, suggesting changes in proliferation. Indeed, the depletion of EZH2 strongly inhibited endothelial proliferation, indicating cell cycle arrest. The concomitant decrease in CCNA expression suggests the transition of endothelial cells into a quiescent phenotype. Further bioinformatical analysis suggested TXNIP as a possible mediator between EZH2 and cell cycle-related gene network.

Our data show that EZH2 is a FSS-responsive gene. Decreased EZH2 levels enhance the activation of the atheroprotective MAPK7 signaling. Decrease in EZH2 under FSS mediates the decrease in the expression of the network of cell cycle-related genes, which allows the cells to enter quiescence. EZH2 is therefore important for the protective effects of FSS in endothelium.

INTRODUCTION

Endothelial cells constitute the lining of all blood vessels and are therefore exposed to the fluid shear stress (FSS) – the frictional force exerted on the vessel wall by the flow of blood (1, 2). Geometrical features of the arterial tree, such as the aortic curve and branches, cause alterations in the patterns of blood flow. At these so-called atheroprone sites, FSS is low or even absent, which correlates with the increased susceptibility of these sites to endothelial dysfunction and atherosclerosis (3-5). Endothelial cells sense FSS through mechanotransduction. The FSS-induced activation of the MAP2K5-MAPK7 (MEK5-Erk5) signaling pathway, which is sustained under prolonged exposure to FSS (6), exerts protective effects on the endothelium (7-9). MEK5 activates MAPK7 through phosphorylation (8, 10), which results in expression of Kruppel-like factor-2 and -4 (KLF2 and KLF4), transcription factors that drive the expression of atheroprotective genes (8, 11).

Gene expression is regulated at the chromatin level through the deposition or removal of epigenetic modifications by specialized enzymes. These modifications, to histone proteins or to the DNA itself, shape the accessibility of gene promoters to the transcriptional machinery. In particular, Polycomb repressive complexes are crucial regulators of gene expression, with well-established roles during development and carcinogenesis (12). Enhancer of zeste homolog-2 (EZH2) is the main methyltransferase in the Polycomb repressive complex-2 (PRC2). EZH2 methylates histone-3 at lysine-27 (H3K27me3 mark), which maintains the repression of gene expression (13).

The epigenetic events that mediate cellular responses to mechanical forces, such as the endothelial response to FSS, are still poorly understood. EZH2 regulates the differentiation of mechanosensing Merkel cells in the skin (14). EZH2 was also shown to regulate endothelial gene expression and function (15-17). However, the link between EZH2 and endothelial mechanotransduction in response to FSS has not been reported.

We hypothesized that EZH2, through epigenetic regulation of gene expression, mediates the response of endothelial cells to the mechanical force of FSS.

MATERIALS AND METHODS

CELL CULTURE AND FLUID SHEAR STRESS EXPERIMENTS

Human Umbilical Vein Endothelial Cells (HUVEC; Lonza, Basel, Switzerland) were used between passages 5 and 8, cultured in endothelial cell medium (ECM) as described before (18), but with 5.5mM glucose and 10% heat-inactivated fetal calf serum (FCS; Lonza, Basel, Switzerland) in gelatin-coated dishes. For the FSS experiments, µ-Slides I 0.4 Luer (Ibidi, Planegg/Martinsried, Germany) were coated with gelatin, HUVEC were seeded at full confluency (approximately 60 000 cells/cm^2) and incubated overnight under standard static cell culture conditions. Slides with confluent cell monolayers were attached to a fluidic unit (Ibidi, Planegg/Martinsried, Germany), connected to the pump (Ibidi, Planegg/Martinsried, Germany), and incubated under standard cell culture conditions. Inverted pressure was used to ensure the gas exchange in the

culture medium. Fluid shear stress (FSS) of 20 dyne/cm^2 was applied to the monolayers in the slides, for 72h. Static controls were cultured in the same incubator and the same medium, refreshed daily. In the stop-flow experiments, after FSS was ceased, cells were incubated for an additional 1h in static conditions before they were lysed. MAP2K5-MAPK7 (MEK5-Erk5) pathway inhibitor BIX02189 was used at the concentration of 5μM. Simvastatin (Sigma-Aldrich, St. Louis, MO, USA) was used at the concentration of 1μM, for 24h. Appropriate volumes of DMSO were used in controls.

Human Embryonic Kidney (HEK) cells and Phoenix-Ampho cells were cultured in 10% FCS DMEM (Lonza, Basel, Switzerland), 2mM L-glutamine (Lonza, Basel, Switzerland), 1% penicillin/streptomycin (Gibco/Thermo Fisher Scientific, Wiltham, MA, USA).

VIRAL TRANSDUCTION

In MEK5D expression experiments, Phoenix-Ampho cell line stably expressing and producing retroviral particles with empty vector (pBABE-puro-EV) or constitutively active MEK5 (MAP2K5; pBABE-puro-MEK5D) was used. Cells were cultured at subconfluent densities. The collection of the viral particles was done in 10% FCS ECM medium, starting 24h after the last preceding passage. The supernatants were collected 2 times at 24h intervals, filtered through 0.45 μm filters and applied to 30%-confluent HUVEC cultures. 24h after the last transduction medium was refreshed and cells were cultured until confluent. Upon selection with 2 μg/ml of puromycin (Invitrogen, Carlsbad, CA, USA) cells were allowed to proliferate, and then were lysed for further analysis.

For lentiviral transductions to obtain the EZH2 knock down, HEK cells were transfected using Endofectin™-Lenti (Gene Copoeia, Rockville, MD, USA , EFL-1001-01) with the following plasmids: pLKO.1-shEZH2 or pLKO.1-SCR, pVSV-G (envelope plasmid) and pCMVΔR8.91 (*gag-pol* 2nd generation packaging plasmid). Virus collection was started the day after, in 10% FCS ECM medium. 30%-confluent HUVEC were transduced twice at 24h intervals. Every first transduction was done with 4μg/ml polybrene. After the last transduction cells were allowed to proliferate for another 3 days and were then selected with 2μg/ml of puromycin. Surviving cells were allowed to proliferate for another 24h. At this point, 7 days post-first transduction, cells were used for downstream experiments or analyses. The whole procedure was repeated for each replicate. A complete knock-out of EZH2 (no protein present in Western blotting analyzes) was confirmed in all EZH2 knock-down cells used in the experiments in this study.

SIRNA TRANSFECTION

HUVEC were seeded subconfluent and transfected at 80-90% confluency, in 12-well plates. Cells were washed with PBS and pre-incubated with 400μl of OptiMEM (Invitrogen, Carlsbad, CA, USA) per well at 37°C. Transfection mixes were prepared with Lipofectamine (Invitrogen, Carlsbad, CA, USA) and siRNA against EZH2 (Hs_EZH2_4 FlexiTube siRNA, cat. no. SI00063973) or AllStars Negative Control siRNA (cat. no. 1027280, QIAGEN, Venlo, The Netherlands) and a 100μl of an appropriate mix containing 30 pmol of siRNA were added per a well. Cells were incubated at 37°C for 6h, then washed 2 times with PBS and cultured further in regular culture medium. Medium was refreshed once more 48h post-transfection. Cells were lysed 72h post-transfection.

RNA ISOLATION AND REAL-TIME PCR

Cells were lysed with either RNA-Bee (TEL-TEST, Inc., Friendswood, TX, USA) or TriZOL (Invitrogen, Carlsbad, CA, USA). To isolate RNA, standard phenol/chloroform extraction was performed in accordance with the manufacturer's guidelines, followed by isopropanol precipitation. RNA pellets were washed twice with ice-cold 75% ethanol, dried and resuspended in RNAse-free water. Concentrations were measured by spectrophotometry (NanoDrop /Thermo Fisher Scientific, Waltham, MA, USA). cDNA was synthetized with the RevertAid™ First Strand cDNA Synthesis Kit (Thermo Fisher Scientific, Wiltham, MA, USA). Real-time PCR (ViiA7 Real Time PCR system, Applied Biosystems, Foster City, CA, USA) was performed with 150nmol of primers and 10ng of cDNA input per reaction, using SYBR-Green chemistry (BioRad, Hercules, CA, USA, or Roche, Basel, Switzerland). Data were analysed with the ViiA7 software (Applied Biosystems, Foster City, CA, USA) and further processed in Excel. Geometrical mean of *ACTB* and *GAPDH* Ct values, or only *GAPDH* Ct values (consistent within an experimental set) were used for the ΔCt normalization as follows: $\Delta Ct = Ct_{\text{Gene of interest}} - Ct_{\text{Housekeeping genes}}$. Fold change over control samples was calculated using ΔΔCt method, as $2^{\wedge - \Delta\Delta Ct}$, where $\Delta\Delta Ct = \Delta Ct_{\text{control}} - \Delta Ct_{\text{treatment}}$.

Primers used in this study are shown in Table 1.

Gene symbol	Forward primers	Reverse primers
ACTB	CCAACCGCGAGAAGATGA	CCAGAGGCGTACAGGGATAG
CCNA1	GGGGCTCCCAGATTTCGTCT	CAGCACAACTCCACTCTTGG
CCNA2	GAGGCCGAAGACGAGACG	CTTTCCAAGGAGGAACGGTGA
CCNB1	CGGCCTCTACCTTTGCACTT	GGCCAAAGTATGTTGCTCGAC
CCNB2	TGCGTTGGCATTATGGATCG	AAGCCAAGAGCAGAGCAGTA
CDC20	ATTCGCATCTGGAATGTGTGC	TGTAATGGGGAGACCAGAGGA
DSCC1	CCGGACCAGTTGAAGAAGGAA	GGGTCTACGTCTTCTTAATTCCC
KIF20A	ACTGCTCTGTCGTCTCTACCT	GGTAACAAGGGCCTAACCCTC
NCAPG	CACCAGAACCAGGCGAAG	GAAAAACTGTCTTATCATCCATCG
NOS3	CACATGGCCTTGGACTGAA	CAGAGCCCTGGCCTTTTC
MAPK7	CCTGATGTCAACCTTGTGACC	CCTTTGGTGTGCCTGAGAAC
EZH2	GCGAAGGATACAGCCTGTGCACA	AATCCAAGTCACTGGTCACCGAAC
GAPDH	AGCCACATCGCTCAGACAC	GCCCAATACGACCAAATCC
KLF2	CATCTGAAGGCGCATCTG	CGTGTGCTTTCGGTAGTGG
KLF4	GGGAGAAGACACTGCGTCA	GGAAGCACTGGGGGAAGT

WESTERN BLOTTING

Cells were lysed with RIPA buffer (Thermo Fisher Scientific, Wiltham, MA, USA), freshly supplemented with proteinase inhibitor cocktail and phosphatase inhibitor cocktails-2 and -3 (all from Sigma-Aldrich, St. Louis, MO, USA). Electrophoresis was performed in 10% polyacrylamide gels, followed by electrotransfer onto nitrocellulose membranes. Membranes were blocked with Odyssey Blocking Buffer (Li-COR Biosciences, Lincoln, NE, USA) 1:1 in Tris-Buffered Saline (TBS) for 1h at room temperature (RT). Blots were then incubated with primary antibodies at 4˚C, overnight, and afterwards with secondary antibodies for 1h at RT. The membranes were washed 3 times with TBS with 0.1% Tween in between incubations, and additionally with TBS before the scanning. Odyssey scanner (Li-COR Biosciences, Lincoln, NE, USA) was used to retrieve the digital images of the membranes. These were analysed with Odyssey software (Li-COR Biosciences, Lincoln, NE, USA) and densitometry was performed with TotalLab 120 software (Nonlinear Dynamics, Newcastle, UK). Images depicted in figures were processed in Adobe Photoshop and Illustrator, and if necessary brightness of a whole image was adjusted in linear fashion.

The following antibodies were used: NOS3/eNOS (1:1000, BD Biosciences, San Jose, CA, USA, 610299), MAPK7/Erk5 (1:500, Upstate/Merck Millipore, Billerica, MA, USA, 07-039), EZH2 (1:1000, Cell Signaling, Danvers, MA, USA, 5246), GAPDH (1:1000, Abcam, Cambridge, UK, ab9485 or ab9484), KLF2 (1:250, Santa Cruz Biotechnology, Dallas, TX, USA, sc-28675), KLF4 (1:250, Santa Cruz Biotechnology, Dallas, TX, USA, sc-20691), Cyclin A (1:500, Santa Cruz Biotechnology, Dallas, TX, USA, sc-751), Cyclin B1 (1:500, Santa Cruz Biotechnology, Dallas, TX, USA, sc-s45) and Cyclin E (1:500, Santa Cruz Biotechnology, Dallas, TX, USA, sc-247), anti-rabbit IgG IRDye-680LT (1:10 000, Li-COR Biosciences, Lincoln, NE, USA, 926-68021), anti-mouse IgG IRDye-800CW (1:10 000, Li-COR Biosciences, Lincoln, NE, USA, 926-32210).

RNA-SEQ

Puromycin-selected HUVEC cells, expressing either scrambled control (SCR) or anti-EZH2 short-hairpin (shEZH2) constructs (at total 7 days after the first viral transduction), were used in FSS experiments (72h of control static culture or FSS exposure). Each replicate experiment consisted of viral transductions (described above) and selection of a separate HUVEC batch, followed by the FSS experiment. Two FSS experimental sets of the same HUVEC batch were run every time in parallel and lysed at the same end time point, one in RNAse-free conditions with RNA-Easy Mini Plus kit RLT Plus lysis buffer (QIAGEN, Venlo, The Netherlands), and one with RIPA buffer. The RIPA-lysates were analyzed with Western blotting and confirmed the complete (no protein present) knock-down of EZH2.

From the RNA-lysates, RNA was isolated using the RNA-Easy Mini Plus kit (QIAGEN, Venlo, The Netherlands). High quality RNA samples (pre-assessed by Nanodrop measurements) were (19) further processed in the Genome Analysis Facility of the University Medical Center Groningen. The RNA quality and integrity were verified using PerkinElmer Labchip GX with a cut-off value of 9 (scale 1 to 10, where 9 is very high quality RNA). RNA library was created in accordance with the TruSeqTM RNA Sample

Preparation v2 Guide (Illumina, San Diego, CA, USA), using the PerkinElmer Sciclone liquid handler, resulting in 330bp cDNA fragments. The paired-end sequencing (100bp reads) was performed using the Illumina HiSeqTM 2500.

Sequencing data were analysed using the Tuxedo pipeline(19), with TopHat2 (v.0.6), Cufflinks (v.0.0.6), Cuffmerge (v.0.0.6), CuffDiff (v. 0.0.7), as available at the public Galaxy platform usegalaxy.org as of August 2014 (20-22). Prior to the alignment, FASTQ Groomer (v. 1.0.4) was used to groom the .fq files, and FastQC (v. 0.52) was used to assess the quality of the reads. Trim sequences tool (v. 1.0.0) was used to trim the reads. Picard Insertion size metrics tool (v. 1.56.0) was used to estimate the distance between mate pairs (paired-end reads). Reads were aligned to the hg_19, and iGenomes hg_19 (v. 1.1.3) was used for annotation.

Differential expression analysis was performed with CuffDiff, with FPKM (Fragments Per Kilobase of exon per Million fragments mapped) normalization method and false discovery rate (FDR) correction, where corrected p-values (q-values) <0.05 were considered to indicate significant changes.

The CuffDiff output was explored using CummeRbund (v. 0.1.3) in R-Studio 0.98. For the comparisons of interest, the gene sets of significantly differentially expressed genes were extracted at alpha=0.05.

For a scheme of the subsequent analysis flow please refer to the Online Figure 5. Gene Ontology (GO) (23) enrichment analysis was performed using the PANTHER database, at the www.PANTHERdb.org website (PANTHER 9.0), as of August 2014 (24). Gene lists were analysed with the Overrepresentation tool. The Bonferroni correction for multiple testing was applied, and the corrected p-value (q-value) of 0.05 was considered the cut-off for significantly overrepresented terms.

The intersection of the lists of genes was performed with the BioVenn tool (25). The Venn diagrams were plotted using the R package VennDiagram. Pathway enrichment analysis was performed using KEGG database using the Enrichr tools available at the Enrichr website (with the combined ranking method)(26). REVIGO online tool was used to organize and visualize the enriched GO terms obtained from the PANTHER 9.0; q-values obtained in PANTHER GO enrichment analysis were used as the rating parameter in REVIGO (only the terms with q<0.05 were used)(27). STRING 9.1 tool was used to explore the mutual relationships between the products of the genes(28, 29). Additional information on the genes of interest, that can be found in the Online Tables, was retrieved from Ensembl (30), using the BioMart tool (31). The data discussed in this publication have been deposited in NCBI's Gene Expression Omnibus (32) and are accessible through GEO Series accession number GSE71164 (http://www.ncbi.nlm.nih.gov/geo/query/acc.cgi?acc=GSE71164).

KI67 IMMUNOFLUORESCENT STAINING

HUVEC expressing either scrambled control (SCR) or SH-EZH2 constructs were seeded at density of 25 000 cells per a well in 24-well plates in 2% FCS ECM and incubated for 24h. After that cells were washed with PBS, fixed with 2% paraformaldehyde for 30 min, washed with PBS, permeabilized with 0.5% Triton-X in PBS for 10 min, washed with PBS and blocked with 10% donkey serum in PBS. Cells were then incubated with primary antibodies, rabbit-anti-human Ki67 (1:500, Monosan, PSX1028) in 10% donkey

serum in PBS, while negative controls were incubated with the 10% donkey serum in PBS, at 4˚C overnight. Cells were then washed with PBS with 0.05% Tween-20 and incubated with secondary antibodies, donkey-anti-rabbit IgG Alexa Fluor-555 (1:500, Life Technologies, Carlsbad, CA, USA, A31572) in 10% human serum in PBS with DAPI (1:5000), for 40 min at RT. Cells were next washed with PBS with 0.05% Tween and with PBS, and the plates were scanned and images were taken in an automated manner with the Tissue FAXS microscope (TissueGnostics, Vienna, Austria). Exposure of the images was optimized and regulated by the software, and unprocessed images were used in the quantitative analysis, performed with the Tissue Quest 4.0.1.0127 software (TissueGnostics, Vienna, Austria), which counts the positive cells and measures the fluorescence intensity. The data were normalized by dividing the Ki67-positive cell numbers by all DAPI-positive cell numbers. The brightness of the representative images depicted in Figure 7 was adjusted in a linear manner and to the same extent in each image, to better visualize the stained cells.

STATISTICAL ANALYSIS

Statistical analysis was performed in GraphPad Prism 4 or 5 (La Jolla, CA, USA), with t-test, or 1-way ANOVA followed by *post-hoc* tests with corrections specified in figure legends. Graphs depict mean and standard deviation or standard error of the mean (specified in figure legends), the number of independent experiments is indicated in the dot-plots and in figure legends. P-values < 0.05 were considered to indicate a significant difference between means.

RESULTS

FLUID SHEAR STRESS REGULATES EZH2 EXPRESSION IN ENDOTHELIAL CELLS

FSS of 20 dyne/cm^2 decreased the expression of EZH2 in HUVEC (Fig. 1 A – C). As expected, it also activated MAPK7 signaling (Fig. 1A) and increased expression of KLF2, KLF4 and endothelial nitric oxide synthase (NOS3/eNOS) (Online Fig. 1 A – F).

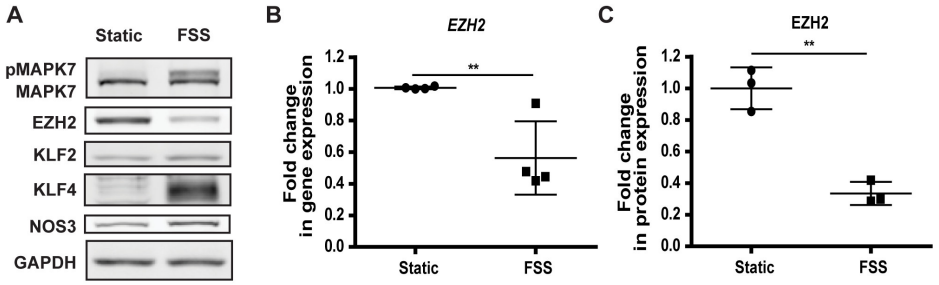

Figure 1. FSS causes a decrease in EZH2 gene and protein expression. *HUVEC were cultured for 72h under 20 dyne/cm^2 FSS.* ***A*** *– Representative Western blotting images.* ***B –*** *Gene expression of EZH2 under FSS, n=4, **p<0.01, t-test.* ***C –*** *Protein expression of EZH2 under FSS, obtained through the densitometry of the Western blotting data, n=3, **p<0.01, t-test.*

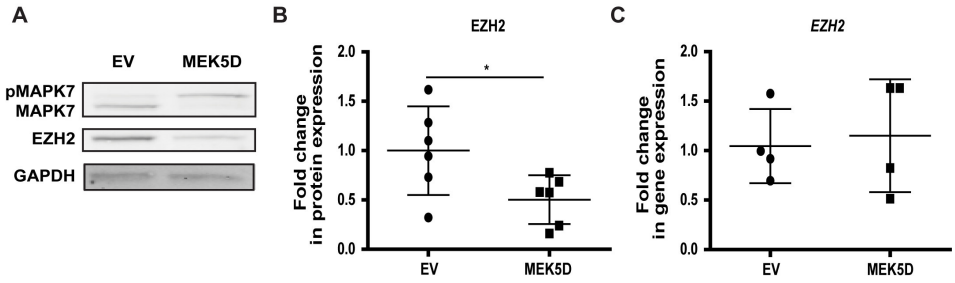

Figure 2. The protein expression of EZH2 is decreased along MAPK7 activation. *The constitutively active MEK5 mutein (MEK5D) was expressed in HUVEC.* ***A –*** *Representative Western blotting images.* ***B –*** *Protein expression of EZH2 in cells expressing MEK5D, obtained through the densitometry of the Western blotting data, n=6, *p<0.05, t-test.* ***C –*** *Gene expression of EZH2 in cells expressing MEK5D, n=4.*

To evaluate whether the decrease in EZH2 expression under FSS is a result of MAPK7 activation, we expressed MEK5D, a constitutively active mutant of MEK5/MAP2K5(8), in endothelial cells. MEK5D expression resulted in activation of MAPK7 (Fig. 2A) and increased the expression of *KLF2* and *KLF4* (Online Fig. 2A and B), confirming that the model worked properly. MAPK7 activation coincided with decreased expression of EZH2 at the protein level, but not at the mRNA level (Fig. 2A – C). Pharmacological inhibition of MAPK7 activation by the small molecule inhibitor BIX02189 did not rescue the expression of EZH2 decreased by FSS (Online Fig. 3A) or by treatment with simvastatin (Online Fig. 3B). These data suggested that while FSS decreases the expression of EZH2 in HUVEC, MAPK7 is not involved in mediating this effect.

DEPLETION OF EZH2 ENHANCES MAPK7 ACTIVATION

Although it did not directly regulate the expression of EZH2, MAPK7 is an important mediator of FSS in endothelial cells. We therefore investigated how, on the other hand, the FSS-induced decrease in EZH2 affects the expression and activity of MAPK7. Knock-down of EZH2 by either shRNA or siRNA did not alter the gene expression levels of *MAPK7* in endothelial cells (Fig. 3A and Online Fig.4A and B). However, knock-down of EZH2 did increase the basal phosphorylation levels of MAPK7 under static conditions (Fig. 3B and C) as well as enhanced the activation of MAPK7 in the cells exposed to FSS (Fig. 3D – G). These data imply that the levels of EZH2 determine the activation capacity of MAPK7 in endothelial cells. As MAPK7 activation is maintained upon prolonged exposure to FSS (6), we checked if the decrease in EZH2 expression under FSS would modulate the deactivation (dephosphorylation) of MAPK7 after FSS was stopped. The decrease in EZH2 under FSS (Fig. 3H and I) did not affect the dephosphorylation of MAPK7 within 1h after the FSS-exposure was stopped, as the MAPK7 phosphorylation levels were diminished to a level comparable with static control samples. These data suggest that MAPK7 activation, rather than deactivation, is affected by the decrease in EZH2 (Fig. 3H and J, "1h stop FSS"/"stop").

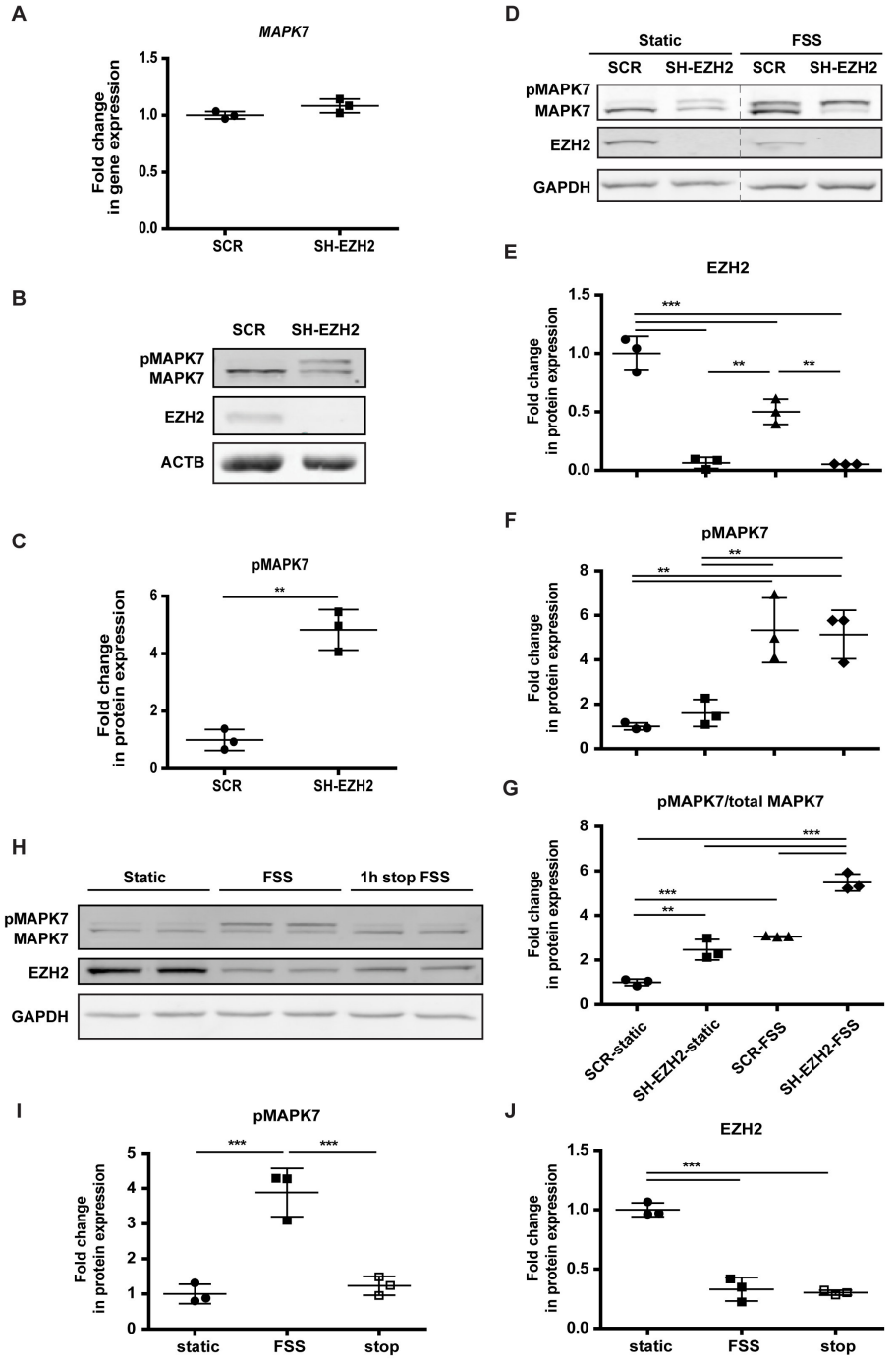

Figure 3. EZH2 levels determine the activation capacity of MAPK7. A – *Gene expression of MAPK7 in cells depleted of EZH2. Anti-EZH2 shRNA was expressed in HUVEC for 7 days by means of lentiviral delivery. Scrambled shRNA was used as control, n=3.* ***B –*** *Representative images of Western blotting showing the enhanced activation*

of MAPK7 in static conditions upon 7-day knock-down of EZH2 in HUVEC. ***C –*** *Densitometry results showing the enhanced activation of MAPK7 in static conditions upon the knock-down of EZH2, derived from the Western blotting data, normalized to b-actin (ACTB), n=3, **p<0.01, t-test.* ***D –*** *Representative Western blotting images, showing enhanced activation of MAPK7 in EZH2-depleted cells compared to control, both in static and in FSS-exposed cultures. Dashed line indicates where the images were artificially connected: they are parts of the same membrane (one image), and were only moved to depict the lanes in the order which is easier for interpretation. Control and EZH2-depleted HUVEC were cultured under FSS for 3 days.* ***E –*** *Densitometry results of the Western blotting data showing the protein expression levels of EZH2, n=3, **p<0.01, ***p<0.001, 1-way ANOVA with Tukey post-hoc comparisons between all pairs of means.* ***F and G –*** *Densitometry results of the Western blotting data showing the total phosphorylation levels of MAPK7 (normalized to GAPDH) and the ratio of phosphorylated MAPK7 to total expressed MAPK7 (both normalized to GAPDH), respectively, n=3, **p<0.01, ***p<0.001, 1-way ANOVA with Tukey post-hoc comparisons between all pairs of means.* ***H*** *– Representative Western blotting images showing rapid dephosphorylation of MAPK7 upon the cessation of the flow. Cells were cultured for 72h in static conditions or under FSS; afterwards 1 group was kept for an additional 1h in static conditions before cells lysis ("1h stop FSS").* ***I and J –*** *Densitometry results showing the levels of MAPK7 phosphorylation and EZH2 protein expression, respectively, normalized to GAPDH. The "stop" caption refers to the 1h stop FSS condition (see* ***H****), n=3, ***p<0.001, 1-way ANOVA with Tukey post-hoc comparisons between all pairs of means.*

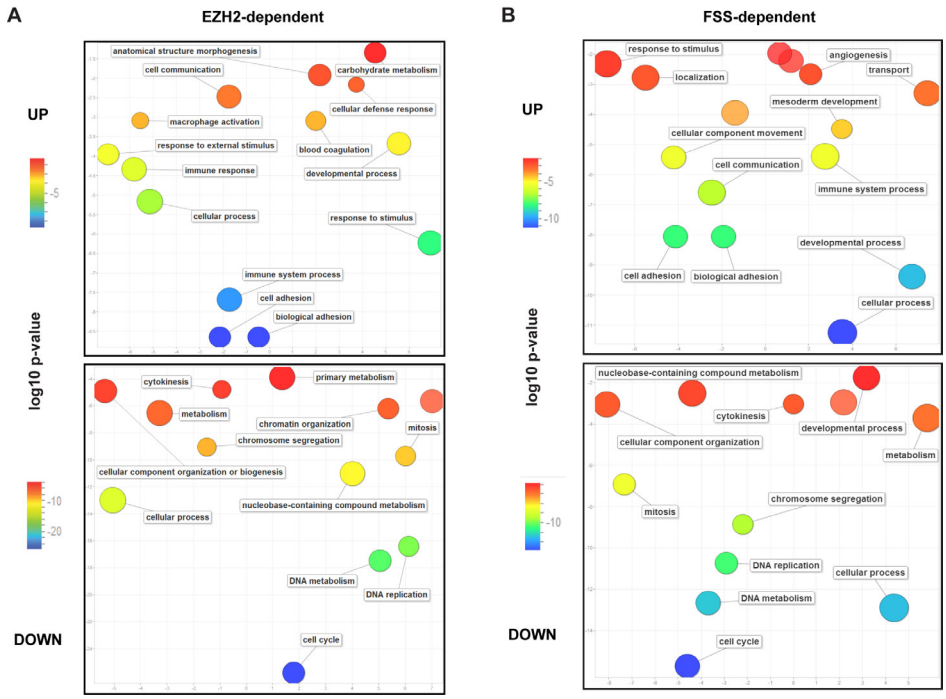

Figure 4. Biological Process Gene Ontology terms which were significantly overrepresented among genes regulated by EZH2 (panel A) or by FSS (panel B). *The figure shows the REVIGO representation of GO BP terms enriched in the lists of genes regulated 2-fold or more upon EZH2-depletion* ***(A)*** *or FSS-exposure* ***(B)****. The lists of GO significantly enriched terms (cut-off q<0.05) were obtained through the overrepresentation analysis using PANTHER 9.0. The size of a bubble corresponds to the size of the group of genes in the analysis, belonging to the specific GO term. UP – upregulated genes, DOWN – downregulated genes. For the exact (corrected) p-values, please compare Supplementary Tables 2, 3, 5 and 6.*

EZH2 REGULATES GENES INVOLVED IN CELL ADHESION AND CELL CYCLE IN ENDOTHELIAL CELLS

To understand the role of EZH2 in the regulation of transcription in endothelial cells in response to FSS we employed a transcriptomic approach (Online Fig. 5). First, the genes regulated by the knock-down of EZH2 or by FSS were explored separately, to gain insight into the groups of genes affected by either condition. Then, the groups of genes regulated by both EZH2-depletion and FSS-exposure were identified. In both cases, Gene Ontology overrepresentation analysis was performed to classify the differentially expressed genes and to identify the most significantly enriched groups of genes (which are likely to be highly biologically relevant in the conditions tested). Overview of the analysis is presented in Online Fig. 5.

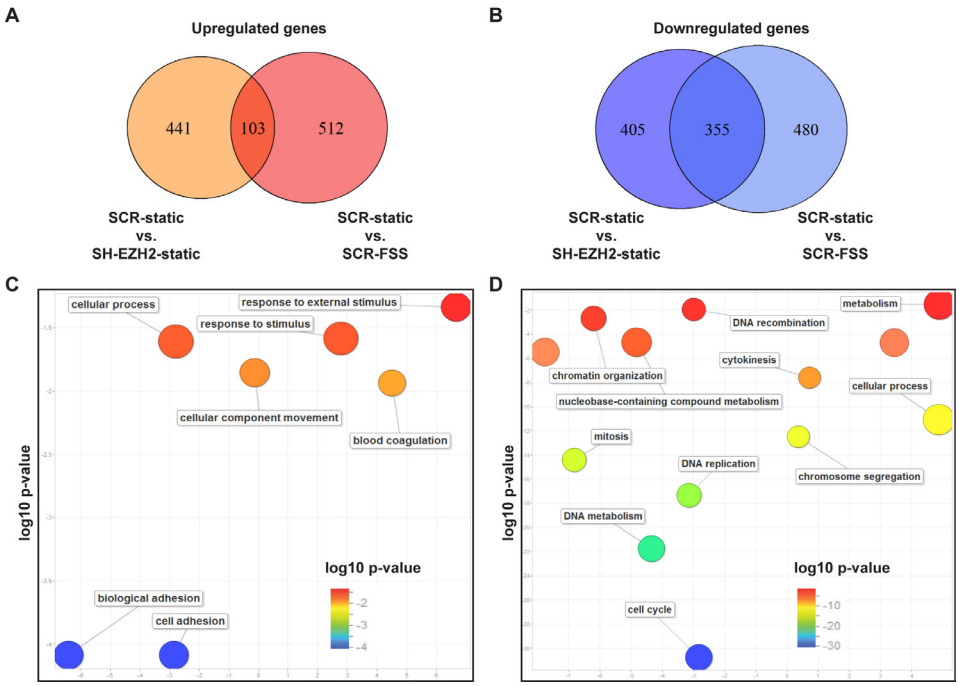

Figure 5. The genes regulated by both EZH2 and FSS are the most significantly enriched within GO terms Cell adhesion and Cell cycle. A – *Area-proportional Venn diagram, depicting the intersection of the lists of genes upregulated by EZH2-depletion (SCR-static vs. SH-EZH2-static) and genes upregulated by exposure to FSS (SCR-static vs. SCR-FSS).* ***B –*** *Area-proportional Venn diagram, depicting the intersection of the lists of genes downregulated by EZH2-depletion (SCR-static vs. SH-EZH2-static) and genes downregulated by exposure to FSS (SCR-static vs. SCR-FSS).* ***C –*** *REVIGO-derived representation of the most significantly overrepresented GO BP terms in the list of 103 genes upregulated by both EZH2-depletion and FSS-exposure.* ***D –*** *REVIGO-derived representation of the most significantly overrepresented GO BP terms in the list of 355 genes downregulated by both EZH2-depletion and FSS-exposure. The significantly enriched GO terms (q<0.05) were derived from the PANTHER 9.0 overrepresentation analysis. The GO-enrichment q-values are available in Supplementary Tables 9 and 10.*

RNA-seq analysis of control (SCR) and EZH2-depleted (SH-EZH2) cells, showed that the depletion of EZH2 in endothelial cells increased the expression of 2042 genes

(q<0.05), of which 550 were increased ≥2-fold (Online Table 1). Overrepresentation analysis of these genes using PANTHER database revealed that the most significantly overrepresented Biological Process (BP) Gene Ontology (GO) term was Cell adhesion (Fig. 4A upper panel and Online Table 2), with 58 genes (Online Fig. 6A). Of 2654 genes whose expression was decreased in cells depleted of EZH2 (q<0.05), 760 genes were ≥2-fold decreased (Online Table 1). The most overrepresented group within these 760 genes were the genes associated with the BP GO term Cell cycle (Fig. 4A lower panel, and Online Table 3), including 136 genes (Online Fig. 6B).

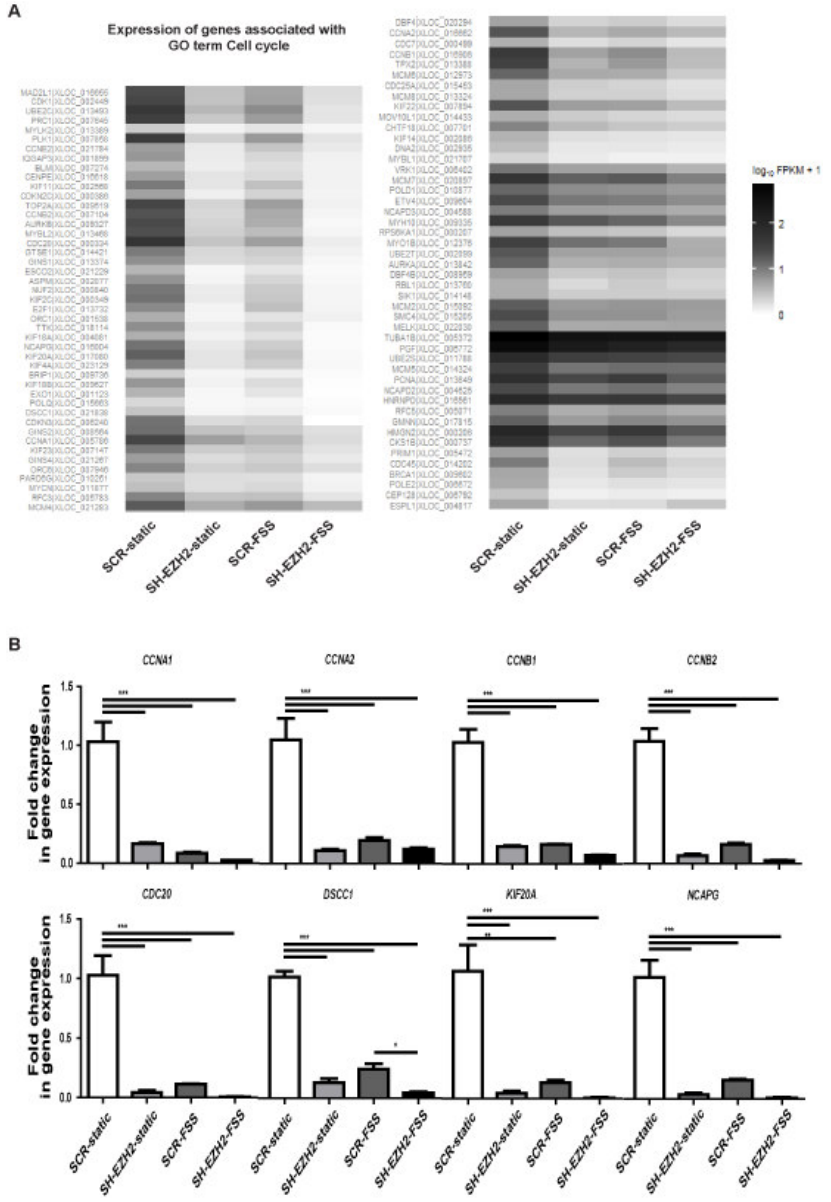

Figure 6. Cell cycle-associated genes are a candidate group of genes regulated by the decrease in EZH2 upon FSS. A – *Heatmap representation of relative expression levels of genes associated with the BP GO term Cell cycle, which were regulated by both EZH2-depletion and FSS-exposure.* ***B –*** *Real-time PCR validation of the RNA-seq results for a sub-group of the cell cycle-associated genes, n=3, error bars depict standard error of the mean, **p<0.01, ***p<0.001 1-way ANOVA with Tukey post-hoc comparisons between all pairs of means.*

FSS-REGULATED GENES IN ENDOTHELIAL CELLS

Next, we analyzed the transcriptomic effects of FSS in endothelial cells. Exposure of endothelial cells to FSS increased the expression of 2142 genes (q<0.05) of which 615 genes were increased ≥2-fold (Online Table 4), with the most significantly overrepresented groups within the BP GO terms Cellular process, Developmental process and Cell adhesion (Fig. 4B upper panel, Online Fig. 7A and Online Table 5). FSS decreased the expression of 3035 genes (q<0.05), of which 835 genes were ≥2-fold decreased (Online Table 4). The most enriched group was associated with the BP GO term Cell cycle (Fig. 4B lower panel, Online Fig. 7B and Online Table 6).

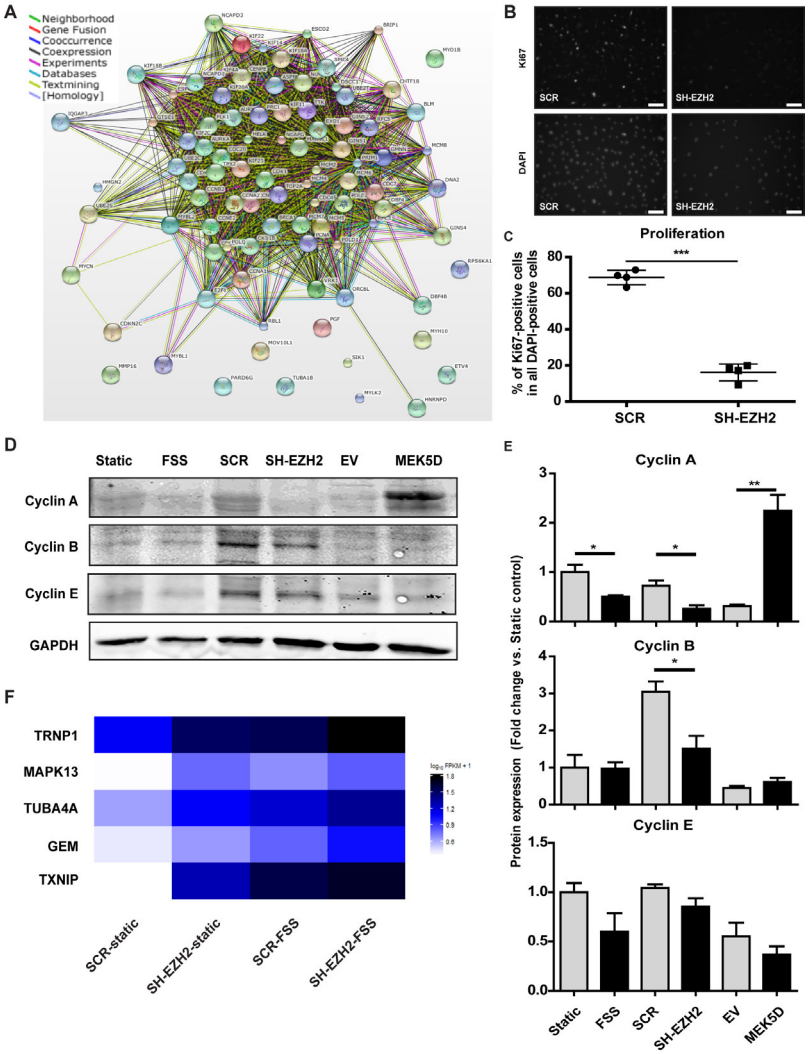

Figure 7. The downregulation of the network of cell cycle-associated genes leads to the decrease in proliferation of endothelial cells. A – *Products of the genes associated with the GO term cell cycle, which are regulated by both EZH2 and FSS, form a network of interdependencies. The list of genes regulated by both EZH2 and FSS belonging to the GO term Cell cycle (most significantly enriched group) was analyzed using String 9.1. Depicted is the evidence view of interactions between the gene products.* ***B –*** *Representative images of the immunofluorescent staining detecting the Ki67 protein expression in scrambled control (SCR) and EZH-depleted (SH-EZH2) endothelial cells (upper panel). Lower panel depicts DAPI signal, indicating nuclear staining. The white bars indicate 100μm.* ***C –****The average percentage of proliferating cells, derived as the percentage of Ki67-positive cells among all the DAPI-positive cells (i.e. Ki67-positive cell numbers are normalized to the number of all cells (DAPI) in the quantified region), showing the decrease in proliferation capacity of the EZH2-depleted cells. These results were obtained through the analysis with the TissueFAXS TissueQuest software, n=4, ***p<0.001, t-test. D – Representative Western blotting results of protein expression of Cyclins A, B and E. E – Densitometric quantification of the protein expression of Cyclins A, B and E, normalized to GAPDH. n=4, *p<0.05, **p<0.01, Student t-test, error bars depict standard error of the mean. F – Heatmap representation of the relative expression of MAPK13, TRNP1, TUBA4A, GEM and TXNIP, the cell cycle-related genes whose expression was increased by both EZH2-depletion and FSS-exposure in HUVEC.*

IDENTIFICATION OF CANDIDATE GENES REGULATED BY EZH2 IN RESPONSE TO FSS IN ENDOTHELIAL CELLS

We next set out to identify the genes that are affected by both EZH2 and FSS, which are the candidate genes regulated by the decrease of EZH2 under FSS. The expression of 103 genes increased, and the expression of 355 genes decreased upon both the depletion of EZH2 and the exposure to FSS (Fig. 5A and B, and Online Table 7 and 8).

The group of 103 genes with increased expression was the most significantly enriched in genes belonging to the BP GO term Cell adhesion (Fig. 5C and Online Table 9). The group of 355 genes with decreased expression was the most significantly enriched in genes associated with the BP GO term Cell cycle (Fig. 5D, right panel and Online Table 10). Additional pathway enrichment analysis with Enrichr using KEGG database showed significant enrichment of terms Cell adhesion molecules (genes with increased expression, Online Fig. 8A) and Cell cycle (genes with decreased expression, Online Fig. 8B)

THE FSS-EXERTED DECREASE IN EZH2 INHIBITS ENDOTHELIAL PROLIFERATION THROUGH DOWNREGU-

LATION OF CELL CYCLE-ASSOCIATED NETWORK OF GENES

The expression of genes associated with the term Cell adhesion, increased by the depletion of EZH2 and exposure to FSS, was in most cases also increased in the EZH2-depleted cells under FSS (Online Fig. 9A). However, most of these genes have not been reported to interact with each other (Online Fig. 9B), as they did not seem to form a functional network based on String 9.1 analysis. We therefore continued with the analysis of the Cell cycle-associated genes.

The expression of genes associated with the GO term Cell cycle was decreased / suppressed by EZH2-depletion, FSS-exposure, and in EZH2-depleted cells under FSS (Fig. 6A). Real-time PCR validation of a subset of these genes confirmed this expression pattern (Fig. 6B). It further confirmed that the expression of master regulators of cell cycle progression such as *CCNA2*, *CCNB1* or *CCNB2(33)* was decreased by both FSS and the depletion of EZH2 in endothelial cells (Fig. 6B).

Most of the products of the cell cycle-related genes we identified (Fig. 6A) were interconnected by mutual relationships (Fig. 7A). These results suggested that

the decrease in expression of these cell cycle-related genes could be a part of an orchestrated response, regulated by FSS through the decrease in EZH2, and aimed at the inhibition of cell cycle progression and proliferation.

To confirm that low levels of EZH2 functionally inhibit the cell cycle, we demonstrated that the depletion of EZH2 indeed decreased the proliferation rates of endothelial cells (Fig. 7B and C). These data suggested that the decrease in EZH2 (under FSS) could lead to the cell cycle arrest.

To further validate this notion, we analyzed the protein expression of chosen Cyclins whose expression was decreased in our transcriptomic data. While Cyclin B (CCNB) and Cyclin E (CCNE) did not show consistent changes in protein expression, Cyclin A (CCNA) protein levels were decreased both by the depletion of EZH2 and by the exposure to FSS (Fig. 7D and E). These patterns of expression, in particular the decrease in Cyclin A levels, seemed to be specifically dependent on EZH2, and independent from the MEK5/MAPK7 pathway, as they were not observed in MEK5D-expressing cells (Fig. 7D and E).

As EZH2 is an epigenetic repressor, there could be other gene products, likely repressors, which are upregulated and mediate between the decrease in EZH2 availability and the decrease in cell cycle-related gene expression. To explore this possibility, we performed an additional GO-overrepresentation analysis of all the genes regulated by EZH2-depletion and FSS-exposure (up- and downregulated genes together). As could be expected, the GO term Cell cycle was once more the most significantly overrepresented. In addition to the downregulated genes identified before (Fig. 6A), this analysis revealed 5 cell cycle-related genes, MAPK13, TRNP1, TUBA4A, GEM and TXNIP, whose expression was increased in EZH2-depleted and in FSS-exposed cells (Fig. 7F). This small group of genes provides a set of potential mediators between EZH2 and the downregulated cell cycle-regulating genes.

DISCUSSION

We demonstrated that EZH2 is a fluid shear stress (FSS)-responsive gene. EZH2 levels influence the activation levels of MAPK7. EZH2 regulates the expression of multiple groups of genes in endothelial cells. In particular, it regulates the genes associated with cell adhesion and cell cycle. The FSS-induced decrease in EZH2 levels elicits an orchestrated response of cell cycle-regulating genes, which leads to inhibition of endothelial cell proliferation and likely to quiescence.

Our data altogether suggest that high FSS might keep the EZH2 expression levels low, which preserves the protected, quiescent state of endothelium. On the other hand, in case of low or absent FSS, e.g. in atheroprone arterial regions, high expression of EZH2 could contribute to endothelial dysfunction, e.g. by releasing endothelial cells from quiescence and promoting their (excessive) proliferation.

We demonstrated that high FSS is able to decrease the expression of the global epigenetic regulator, EZH2, at both mRNA and protein level. This decrease in expression of EZH2 seems to mediate some of the beneficial effects of FSS. Our RNA-seq analysis identified groups of genes dependent both on the EZH2 levels and on the presence of FSS. It is not surprising that there are several groups of genes (as classified by Gene

Ontology terms) that are affected: on one hand FSS is an important factor regulating many aspects of endothelial cell biology, on the other hand EZH2 is a global epigenetic regulator, acting on multiple genomic *loci*. In the current study, we focused on the most significantly enriched group of cell cycle-related genes. However, exploration of the other groups of genes identified in this study could provide further examples of singular pathways regulated by FSS through decrease in EZH2.

The mechanism of the regulation of EZH2 expression by FSS remains to be fully elucidated. However, we succeeded in demonstrating that the major known FSS-induced pathway, MEK5/MAPK7 pathway, is of minor importance for regulation of EZH2 expression. Other pathways should be assessed in future studies. Furthermore, we established an exciting novel feedback link between EZH2 and MAPK7 pathway, by showing that MAPK7 activation capacity is increased when EZH2 levels decrease. This means that the protective, long-term activation of MAPK7 by high FSS could be mediated by the FSS-induced decrease in EZH2 levels.

A few other studies that so far reported on the role of EZH2 in endothelial cells confirm that EZH2 is involved in the regulation of endothelial gene expression and endothelial function (15, 16). In particular, EZH2 regulates angiogenesis in the tumor microenvironment, where it is itself regulated by VEGF-miRNA-101 axis(16, 17, 34). One study has so far addressed the role of EZH2 in endothelial cells with a global approach, similar to ours, but in static conditions only. Dreger *et al*. studied the short-term effects of a transient (siRNA-mediated) knock-down of EZH2 in HUVEC (15). They reported enrichment of Cell communication and Cell adhesion related genes among the genes regulated by EZH2, which corroborates our finding that the Cell adhesion genes are the most enriched group among the genes upregulated by the knock-down of EZH2. The main difference between the studies is that we used a stable and long-term knock-down of EZH2 (total knock-down time of 10 days). Our approach allowed us to study more downstream (and secondary) effects of EZH2-depletion, which correspond well to the effects of the continuously low EZH2 levels under prolonged exposure to FSS. These long-standing effects are more similar, and likely more relevant, to the conditions of continuous blood flow and FSS in the blood vessels.

Therefore, our results extend the current knowledge on the role of EZH2 in endothelial cells, investigated so far only in static conditions, by providing insights into the role of EZH2 under mechanical force of FSS.

FSS also affects some of the other epigenetic regulators, such as histone deacetylases (HDACs)(35-37) and miRNAs (37, 38). Moreover, recent studies demonstrated the role of DNA-methylation in mediating the effects of FSS in endothelium, further substantiating the importance of epigenetic mechanisms in mediating the mechanosignaling (39, 40). Our study is the first to add Polycomb and the histone methyltransferase EZH2 to the group of epigenetic-level regulators of endothelial response to FSS.

The genes related to GO term Cell cycle were the most significantly enriched group regulated by the decrease in EZH2 and by FSS in our study. These genes form a dense network of interactions, suggesting that their products function together to regulate cell cycle progression. Indeed, for example CDK1 is a major cell cycle regulator, which at different stages binds CCNA1 (41), CCNA2 (42), CCNB1 (43), and CCNB2(44), and all of these genes were downregulated by EZH2-depletion and by FSS in our experiments. CDK1 also links directly to EZH2, as it can bind and phosphorylate

EZH2 to change its epigenetic activity (45, 46). The presence of these and many other concomitant interactions between the members of this group suggests that it is indeed a functional network, whose orchestrated downregulation serves to inhibit the cell cycle progression in endothelial cells. Indeed, our results show that depletion of EZH2 caused decrease in proliferation of endothelial cell, while others observed that high expression of EZH2 promotes the proliferation of many types of cancer cells(47-50). These data imply that the decrease in EZH2 under FSS likely serves as the mechanism to downregulate the network of cell cycle regulators, therefore inhibiting the proliferation of endothelial cells.

EZH2 is an epigenetic repressor, which suggests that the decrease in EZH2 expression is more likely to induce expression of genes, rather than to decrease it. However, other groups investigating the transcriptomic effects of EZH2 also found that its inhibition or knock-down results in both increase and decrease in expression of genes, which is consistent with our findings(51, 52). Nevertheless, we attempted to identify a possible link between the Cell cycle-related genes and EZH2 in our study, by looking for an upregulated EZH2-dependent and cell cycle-related gene. The additional GO overrepresentation analysis revealed 5 cell cycle-related genes, MAPK13, TRNP1, TUBA4A, GEM and TXNIP, that were upregulated by both EZH2-depletion and FSS-exposure.

Of those candidate genes, TXNIP is the only one so far reported to be affected by EZH2. In the study by Zhou *et al*., TXNIP expression was increased by EZH2 inhibition, which resulted in suppression of cell growth (51). These data are therefore consistent with our findings of TXNIP expression being upregulated and endothelial proliferation being inhibited in EZH2-depleted cells.

TXNIP (thioredoxin interacting protein, also known as VDUP1) is primarily related to oxidative stress regulation. However, it has been recognized as a tumour suppressor gene whose upregulation inhibits the growth of cancer cells (51, 53, 54). This inhibitory effect of TXNIP has been linked to the cell cycle arrest in G1/G0 phase (53, 55). Therefore, TXNIP is a likely mediator of the cell cycle arrest occuring after the decrease of EZH2 under FSS.

This could happen through the known TXNIP-dependent stabilization of p27 (CDKN1B) protein, which is a negative regulator of cell cycle (53, 54). CDKN1B expression was indeed shown to be reversely correlated with EZH2 levels (56, 57). Our results reproduced such increase in CDKN1B levels upon EZH2-depletion (Online Table 1). However, the CDKN1B expression was not affected by FSS in our dataset, suggesting that CDKN1B is not involved in FSS-induced inhibition of cell cycle.

Another potential target gene downstream of TXNIP is CCNA (Cyclin A). The study by Han *et al.* showed that TXNIP can act as a transcriptional repressor, and is able to repress the promoter activity of CCNA2(55). CCNA expression was decreased in our experiments both at gene and protein level. Therefore, the EZH2-TXNIP-CCNA2 axis provides an interesting example of a link between EZH2 and cell cycle regulation. Nevertheless, it might be one of multiple connections feeding into the reported network of genes, while the whole network is important for the net effect of cell cycle inhibition.

The decrease in expression of EZH2 under FSS, along with the decrease in expression of cell cycle regulating machinery, results in the decrease of proliferation, suggesting

that the endothelial cells enter quiescence – the arrest of the cell cycle in G1/G0 phase. Endothelial cells are known to acquire a quiescent phenotype under high FSS(1, 11, 58). Quiescence was also observed upon inhibition of EZH2 in multiple cell lines (59, 60). In B lymphocytes, the decrease in EZH2 levels was necessary for entering the quiescent state(61). Interestingly, both the increase in TXNIP and the decrease in Cyclin A levels, consistently with our findings, have also been associated with G1/G0 arrest, and hence the quiescent phenotype (53, 55, 60, 62).

The quiescent state of endothelium under high FSS is deemed beneficial and protective for endothelium. Endothelial cells in the regions of disturbed flow proliferate intensively, which might result in their early senescence and contribute to the susceptibility of such vascular *foci* to atherosclerotic remodeling (1, 58). We showed that the decrease in EZH2 levels also enhances the activation of MAPK7, a major FSS-responsive MAP-kinase, which promotes atheroprotection through increased expression of KLF2, KLF4 and NOS3(7-9, 63, 64). Altogether, our results indicate that the suppression of EZH2 expression by high FSS is one of the mechanisms mediating the beneficial effects of high FSS in endothelial cells.

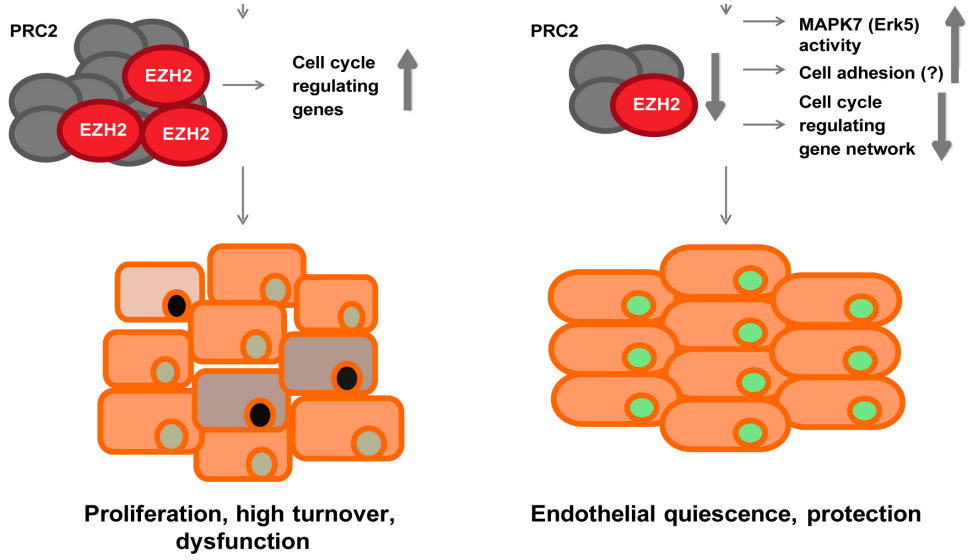

Figure 8. Graphical abstract showing the proposed mechanism of action of EZH2 under

Our data establish EZH2 as a regulator of endothelial gene expression, involved in the endothelial response to FSS. In particular, we propose that the suppression of EZH2 expression by high FSS restricts the expression of a whole network of cell cycle-regulating genes, which results in the protected quiescent endothelial phenotype (Fig. 8). Given the atheroprotective role of high FSS and the availability of several EZH2 inhibitors, our results further suggest that EZH2 might become a promising pharmacological target to treat or prevent vascular disease.

SUPPLEMENTARY FIGURES

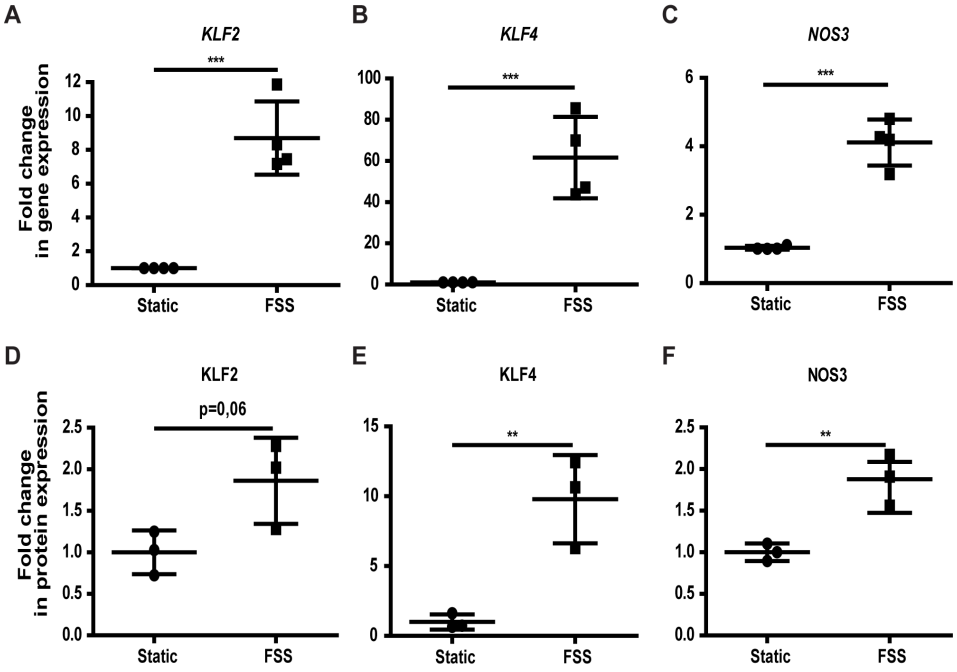

Online Figure 1. FSS upregulates gene and protein expression of KLF2, KLF4 and NOS3. *Cells were exposed to laminar flow with FSS of 20 dyne/cm2 for 72h. A – C Gene expression of KLF2, KLF4 and NOS3, respectively, n=4, ***p<0.001, t-test. D – F Protein expression of KLF2, KLF4 and NOS3, respectively, n=3, **p<0.01, t-test.*

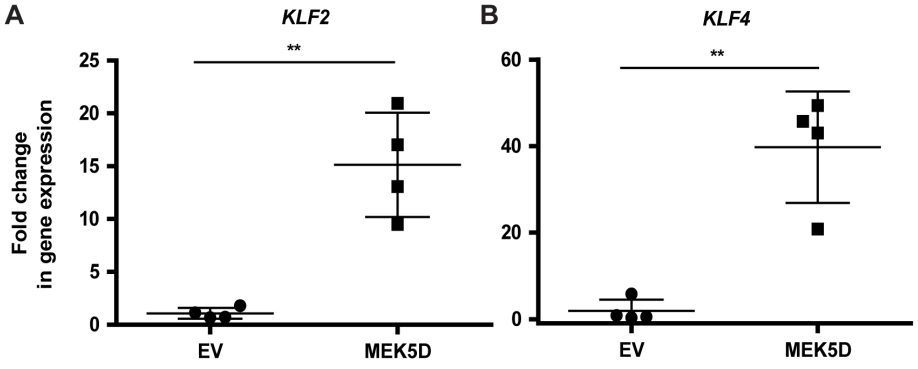

Online Figure 2. Expression of the constitutively active MAP2K5 (MAP2K5D/MEK5D) leads to upregulation of MAPK7 target genes, confirming the increase in MAPK7 activity. *A and B – Gene expression of KLF2 and KLF4, respectively, n=4, **p<0.01, t-test.*

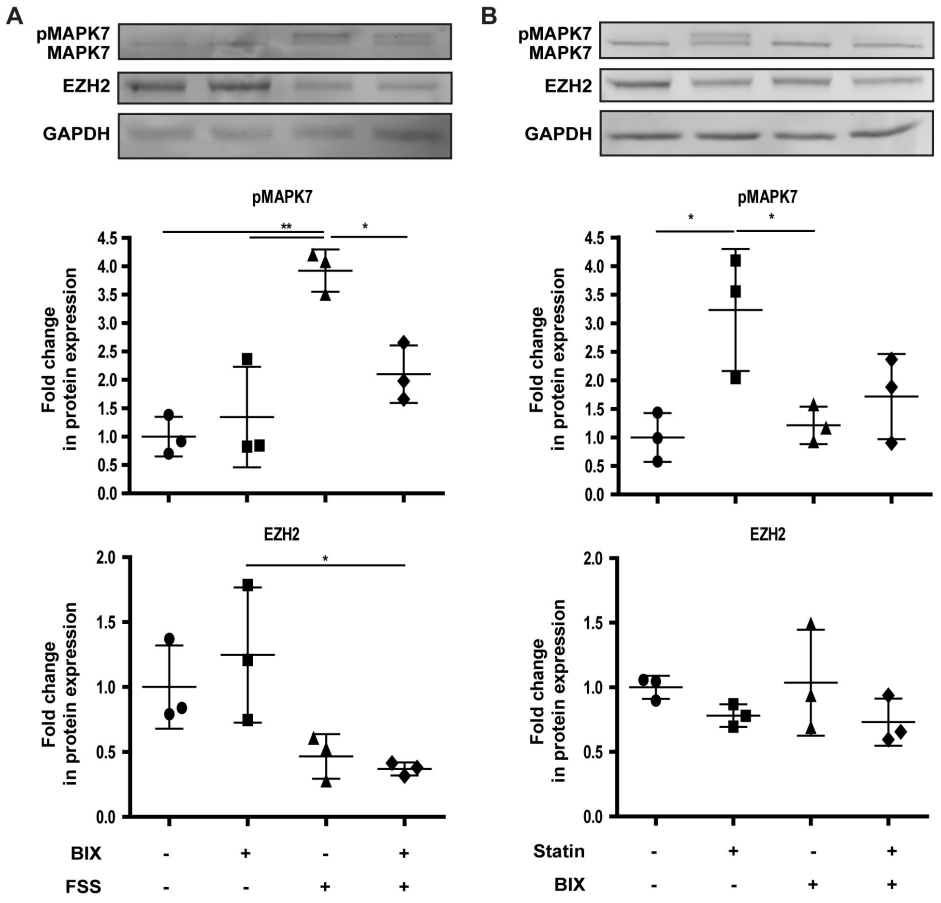

Online Figure 3. Inhibition of MAP2K5-MAPK7 (MEK5-Erk5) with BIX02189 does not rescue the decrease in EZH2 expression. *A – Representative Western blotting images (upper panel). Phosphorylated-MAPK7 (pMAPK7) and EZH2 protein expression derived through densitometry and normalized to GAPDH (lower panel). Cells were cultured under FSS for 72h, with or without 5 μM BIX02189 (BIX), n=3, *p<0.05, **p<0.001, 1-way ANOVA with Tukey post hoc comparisons between all pairs of means. B – Representative Western blotting images (upper panel). Phosphorylated-MAPK7 (pMAPK7) and EZH2 protein expression derived through densitometry and normalized to GAPDH (lower panel). Cells were treated for 24h with 1 μM simvastatin (statin) and/or 5 μM MAP2K5-MAPK7 inhibitor BIX02189 (BIX). *p<0.05, 1-way ANOVA with Tukey post hoc comparisons between all pairs of means.*

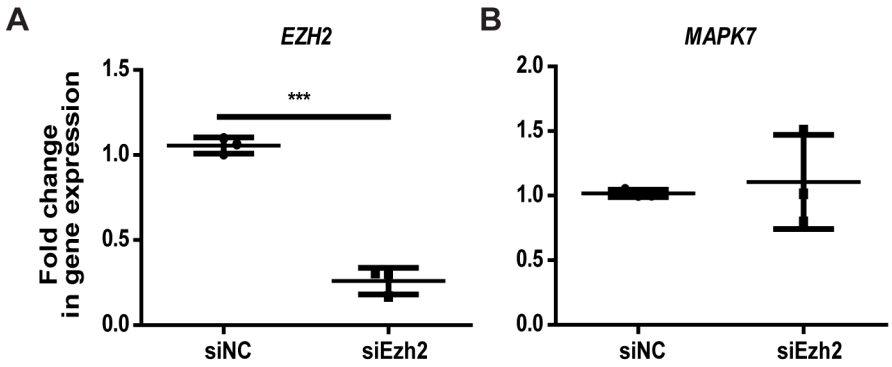

Online Figure 4. The gene expression of MAPK7 is preserved upon knock-down of EZH2. *Cells were transfected with siRNA against EZH2 and analysed after 72h post-transfection. A and B – Gene expression of EZH2 and MAPK7, respectively, n=3, ***p<0.001, t-test.*

Online Figure 9. Exploration of the cell adhesion-related genes upregulated by both EZH2 and FSS, identified based on the GO enrichment analysis. A – A heatmap representation of the relative expression of the cell adhesion-related genes upregulated by both EZH2-depletion and FSS-exposure. B – Network representation of the mutual relationships of the products of the genes associated with the GO term cell adhesion, String 9.1, evidence view.

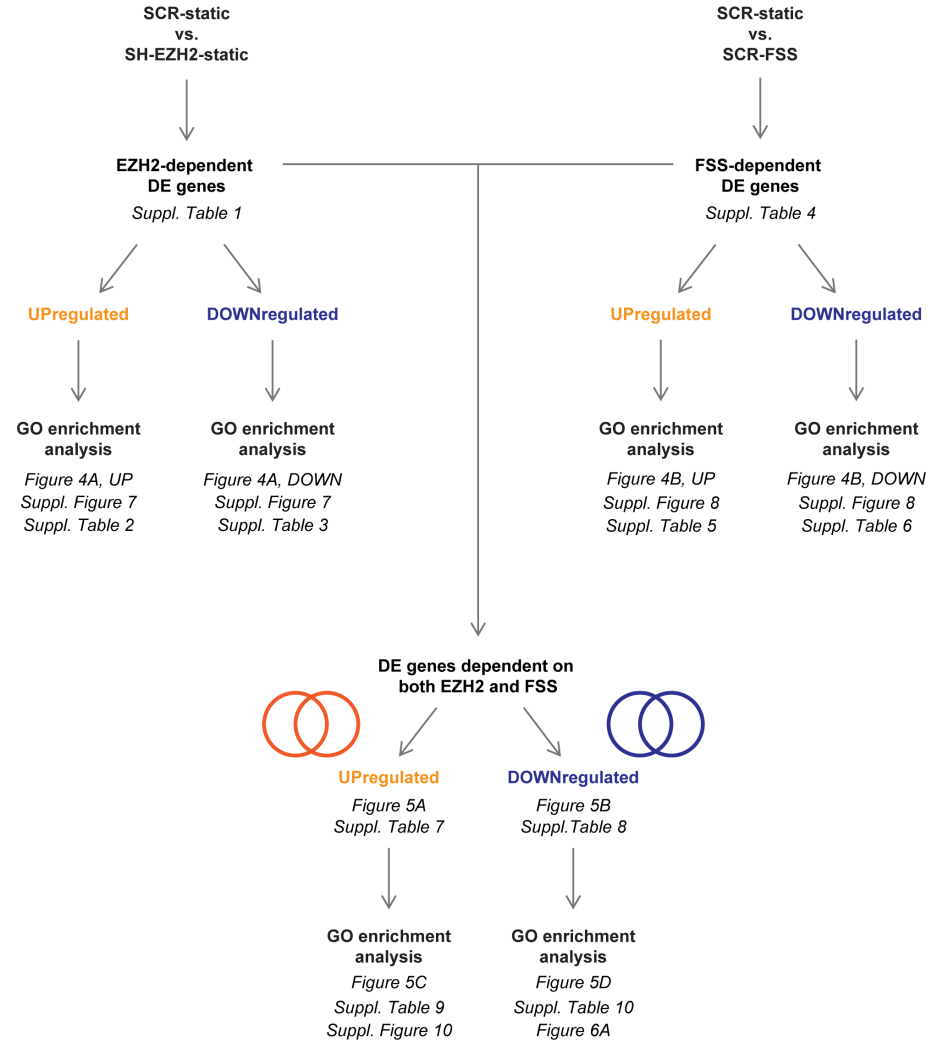

Online Figure 5. Schematic representation of data analysis. DE – differential expression, GO – Gene Ontology.

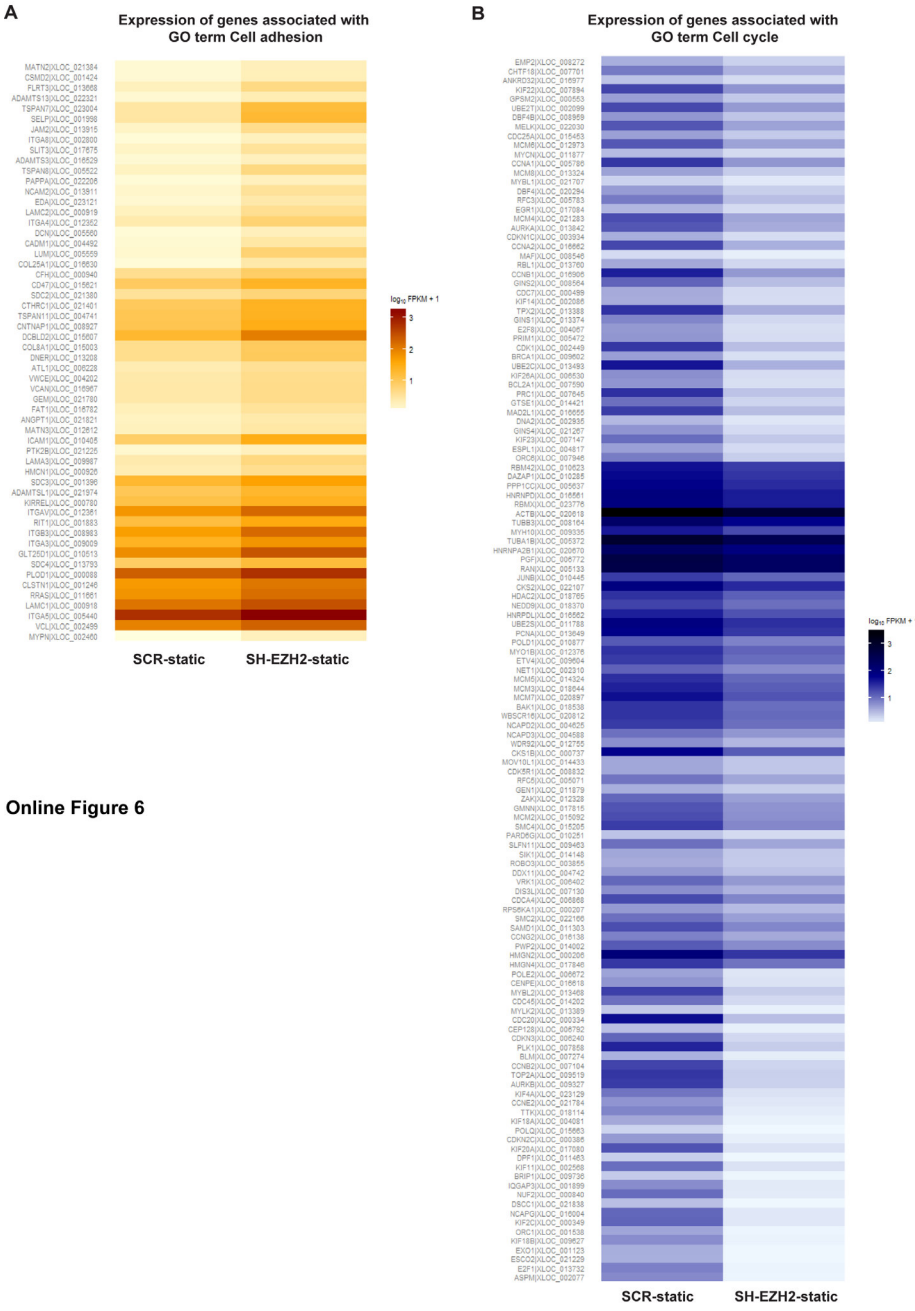

Online Figure 6

Online Figure 6. Relative expression of genes regulated by EZH2, belonging to the most significantly enriched GO terms. *A – Heatmap representation of the relative expression of the genes upregulated by the EZH2-depletion that belong to the BP GO term Cell adhesion. B – Heatmap representation of the relative expression of the genes downregulated by the EZH2-depletion that belong to the BP GO term Cell cycle.*

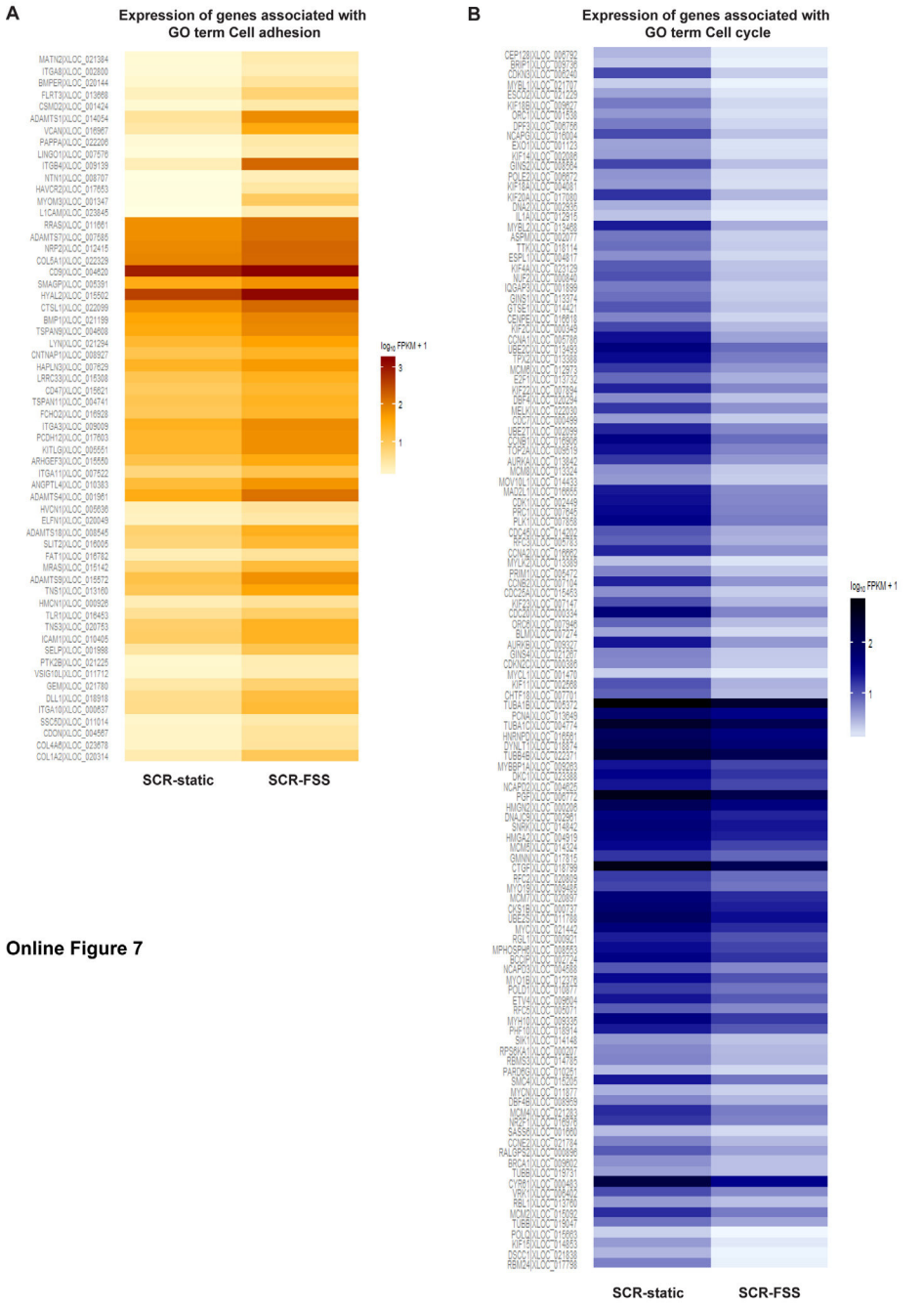

Online Figure 7

Online Figure 7. Relative expression of genes regulated by FSS, belonging to the most significantly enriched GO terms. *A – Heatmap representation of the relative expression of the genes upregulated by the exposure to FSS, that belong to the BP GO term Cell adhesion. B – Heatmap representation of the relative expression of the genes downregulated by the exposure to FSS, that belong to the BP GO term Cell cycle.*

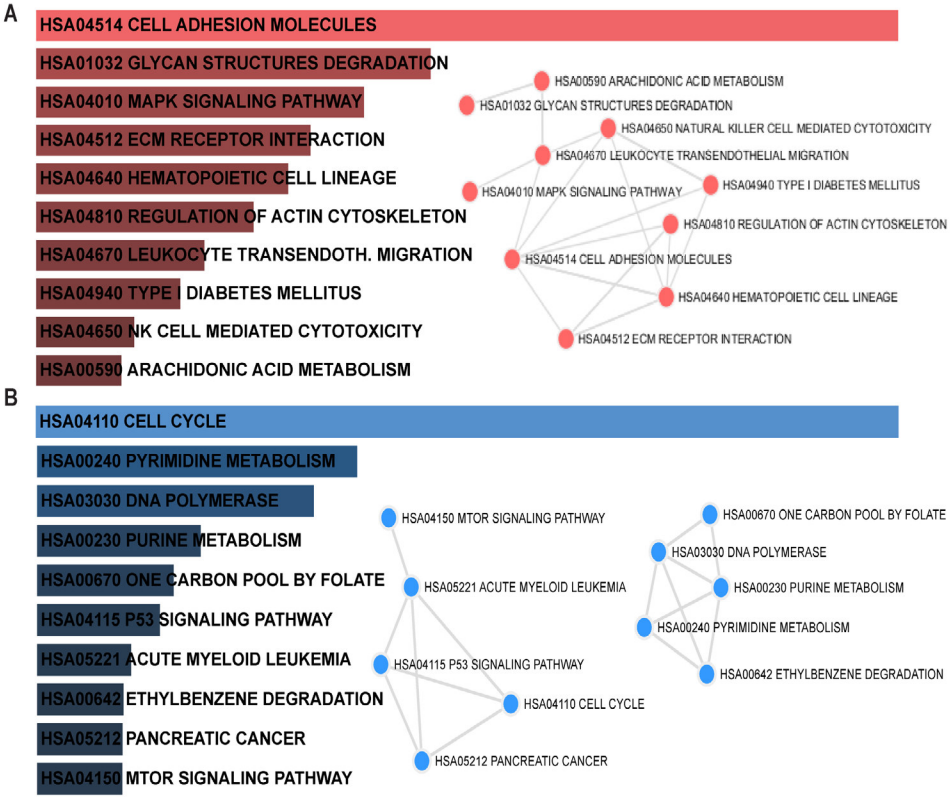

Online Figure 8. Pathway enrichment analysis of the genes upregulated or downregulated by both EZH2-depletion and FSS-exposure. *A – Pathway enrichment analysis of the 103 genes upregulated by both EZH2-depletion and FSS-exposure. B – Pathway enrichment analysis of the list of the 355 genes downregulated by both EZH2-depletion and FSS-exposure. The lists of genes were analysed using Enrichr and KEGG database, using the combined score ranking. The brighter the colour, the more significantly enriched the term is. The inserts represent the network of dependencies between the enriched terms (the force field has been neglected).*

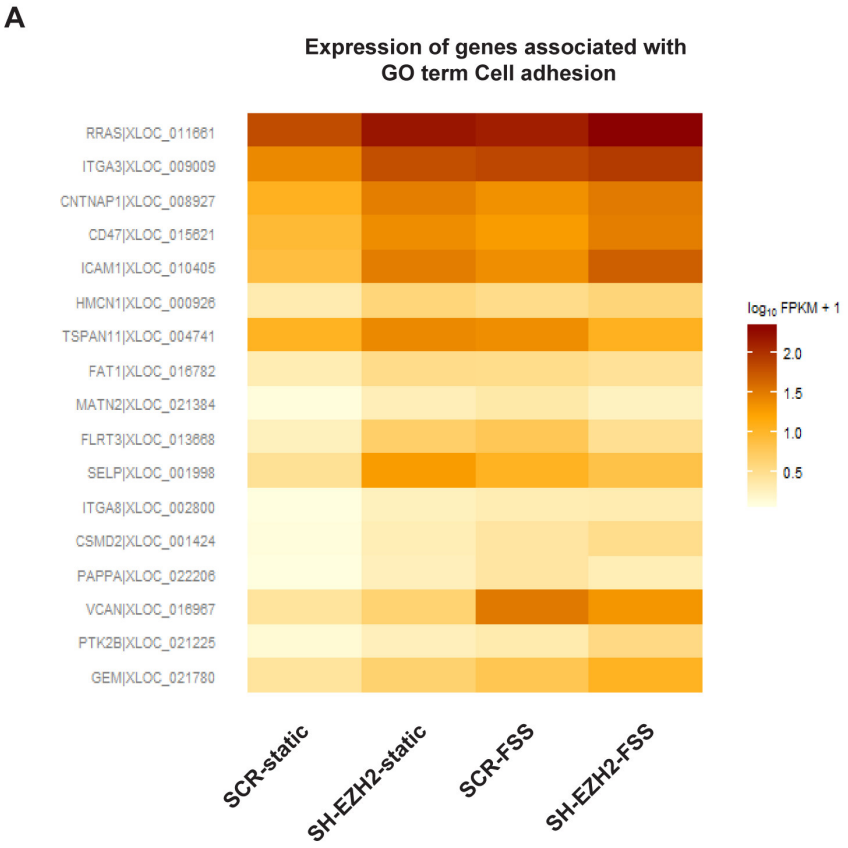

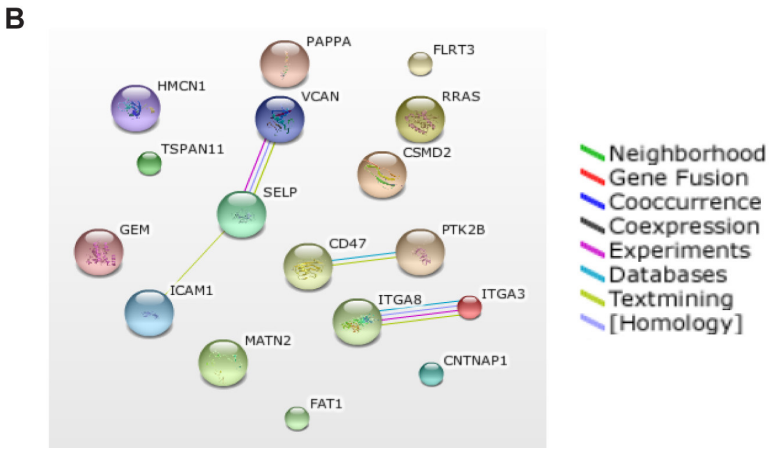

Online Figure 9. Exploration of the cell adhesion-related genes upregulated by both EZH2 and FSS, identified based on the GO enrichment analysis. *A – A heatmap representation of the relative expression of the cell adhesion-related genes upregulated by both EZH2-depletion and FSS-exposure. B – Network*

representation of the mutual relationships of the products of the genes associated with the GO term cell adhesion, String 9.1, evidence view.

SUPPLEMENTARY TABLES

Supplementary table 1-10 can be found via following link
https://static-content.springer.com/esm/art%3A10.1007%2Fs10456-015-9485-2/MediaObjects/10456_2015_9485_MOESM1_ESM.pdf

Supplementary Table 1. Genes up- or down-regulated 2 times or more by the depletion of EZH2 in HUVEC.
Supplementary Table 2. Biological Process Gene Ontology terms that were significantly overrepresented in the analysis of the list of genes upregulated 2 times or more by EZH-depletion.
Supplementary Table 3. Biological Process Gene Ontology terms that were significantly overrepresented in the analysis of the list of genes downregulated 2 times or more by EZH-depletion.
Supplementary Table 4. Genes up- or down-regulated 2 times or more by the exposure of HUVEC to FSS.
Supplementary Table 5. Biological Process Gene Ontology terms that were significantly overrepresented in the analysis of the list of genes upregulated 2 times or more by the exposure to FSS.
Supplementary Table 6. Biological Process Gene Ontology terms that were significantly overrepresented in the analysis of the list of genes downregulated 2 times or more by the exposure to FSS.
Supplementary Table 7. The 103 genes that were upregulated 2 times or more by both EZH2-depletion and the exposure to FSS.
Supplementary Table 8. The 355 genes that were downregulated 2 times or more by both EZH2-depletion and the exposure to FSS.
Supplementary Table 9. Biological Process Gene Ontology terms that were significantly overrepresented in the analysis of the list of the 103 genes upregulated 2 times or more by both EZH2-depletion and the exposure to FSS.
Supplementary Table 10. Biological Process Gene Ontology terms that were significantly overrepresented in the analysis of the list of the 355 genes upregulated 2 times or more by both EZH2-depletion and the exposure to FSS.

REFERENCES

1. Chiu J-J, Chien S. Effects of disturbed flow on vascular endothelium: pathophysiological basis and clinical perspectives. Physiological reviews. 2011;91(1):327-87.
2. Hahn C, Schwartz MA. Mechanotransduction in vascular physiology and atherogenesis. Nature reviews Molecular cell biology. 2009;10(1):53.
3. Zarins CK, Giddens DP, Bharadvaj B, Sottiurai VS, Mabon RF, Glagov S. Carotid bifurcation atherosclerosis. Quantitative correlation of plaque localization with flow velocity profiles and wall shear stress. Circulation research. 1983;53(4):502-14.
4. Asakura T, Karino T. Flow patterns and spatial distribution of atherosclerotic lesions in human coronary arteries. Circulation research. 1990;66(4):1045-66.
5. Gibson CM, Diaz L, Kandarpa K, Sacks FM, Pasternak RC, Sandor T, et al. Relation of vessel wall shear stress to atherosclerosis progression in human coronary arteries. Arteriosclerosis, Thrombosis, and Vascular Biology. 1993;13(2):310-5.
6. Slater SC, Ramnath RD, Uttridge K, Saleem MA, Cahill PA, Mathieson PW, et al. Chronic exposure to laminar shear stress induces Kruppel-like factor 2 in glomerular endothelial cells and modulates interactions with co-cultured podocytes. The international journal of biochemistry & cell biology. 2012;44(9):1482-90.
7. Clark PR, Jensen TJ, Kluger MS, Morelock M, Hanidu A, Qi Z, et al. MEK5 is activated by shear stress, activates ERK5 and induces KLF4 to modulate TNF responses in human dermal microvascular endothelial cells. Microcirculation. 2011;18(2):102-17.
8. Ohnesorge N, Viemann D, Schmidt N, Czymai T, Spiering D, Schmolke M, et al. Erk5 activation elicits a vasoprotective endothelial phenotype via induction of Krüppel-like factor 4 (KLF4). Journal of Biological Chemistry. 2010;285(34):26199-210.
9. Pi X, Yan C, Berk BC. Big mitogen-activated protein kinase (BMK1)/ERK5 protects endothelial cells from apoptosis. Circulation research. 2004;94(3):362-9.
10. Nakamura K, Uhlik MT, Johnson NL, Hahn KM, Johnson GL. PB1 domain-dependent signaling complex is required for extracellular signal-regulated kinase 5 activation. Molecular and cellular biology. 2006;26(6):2065-79.
11. Dekker RJ, Boon RA, Rondaij MG, Kragt A, Volger OL, Elderkamp YW, et al. KLF2 provokes a gene expression pattern that establishes functional quiescent differentiation of the endothelium. Blood. 2006;107(11):4354-63.
12. Bracken AP, Helin K. Polycomb group proteins: navigators of lineage pathways led astray in cancer. Nature Reviews Cancer. 2009;9(11):773.
13. Riising EM, Comet I, Leblanc B, Wu X, Johansen JV, Helin K. Gene silencing triggers polycomb repressive complex 2 recruitment to CpG islands genome wide. Molecular cell. 2014;55(3):347-60.
14. Bardot ES, Valdes VJ, Zhang J, Perdigoto CN, Nicolis S, Hearn SA, et al. Polycomb subunits Ezh1 and Ezh2 regulate the Merkel cell differentiation program in skin stem cells. The EMBO journal. 2013;32(14):1990-2000.
15. Dreger H, Ludwig A, Weller A, Stangl V, Baumann G, Meiners S, et al. Epigenetic regulation of cell adhesion and communication by enhancer of zeste homolog 2 in human endothelial cells. Hypertension. 2012:HYPERTENSIONAHA. 112.191098.
16. Smits M, Mir SE, Nilsson RJA, van der Stoop PM, Niers JM, Marquez VE, et al. Down-regulation of miR-101 in endothelial cells promotes blood vessel formation through reduced repression of EZH2. PloS one. 2011;6(1):e16282.
17. Lu C, Han HD, Mangala LS, Ali-Fehmi R, Newton CS, Ozbun L, et al. Regulation of tumor angiogenesis by EZH2. Cancer cell. 2010;18(2):185-97.

18. Maleszewska M, Moonen J-RA, Huijkman N, van de Sluis B, Krenning G, Harmsen MC. IL-1β and TGFβ2 synergistically induce endothelial to mesenchymal transition in an NFκB-dependent manner. Immunobiology. 2013;218(4):443-54.
19. Trapnell C, Roberts A, Goff L, Pertea G, Kim D, Kelley DR, et al. Differential gene and transcript expression analysis of RNA-seq experiments with TopHat and Cufflinks. Nature protocols. 2012;7(3):562.
20. Blankenberg D, Kuster GV, Coraor N, Ananda G, Lazarus R, Mangan M, et al. Galaxy: a web-based genome analysis tool for experimentalists. Current protocols in molecular biology. 2010:19.0. 1-.0. 21.
21. Goecks J, Nekrutenko A, Taylor J. Galaxy: a comprehensive approach for supporting accessible, reproducible, and transparent computational research in the life sciences. Genome biology. 2010;11(8):R86.
22. Giardine B, Riemer C, Hardison RC, Burhans R, Elnitski L, Shah P, et al. Galaxy: a platform for interactive large-scale genome analysis. Genome research. 2005;15(10):1451-5.
23. Ashburner M, Ball CA, Blake JA, Botstein D, Butler H, Cherry JM, et al. Gene Ontology: tool for the unification of biology. Nature genetics. 2000;25(1):25.
24. Mi H, Muruganujan A, Casagrande JT, Thomas PD. Large-scale gene function analysis with the PANTHER classification system. Nature protocols. 2013;8(8):1551.
25. Hulsen T, de Vlieg J, Alkema W. BioVenn–a web application for the comparison and visualization of biological lists using area-proportional Venn diagrams. BMC genomics. 2008;9(1):488.
26. Chen EY, Tan CM, Kou Y, Duan Q, Wang Z, Meirelles GV, et al. Enrichr: interactive and collaborative HTML5 gene list enrichment analysis tool. BMC bioinformatics. 2013;14(1):128.
27. Supek F, Bošnjak M, Škunca N, Šmuc T. REVIGO summarizes and visualizes long lists of gene ontology terms. PloS one. 2011;6(7):e21800.
28. Franceschini A, Szklarczyk D, Frankild S, Kuhn M, Simonovic M, Roth A, et al. STRING v9. 1: protein-protein interaction networks, with increased coverage and integration. Nucleic acids research. 2012;41(D1):D808-D15.
29. Jensen LJ, Kuhn M, Stark M, Chaffron S, Creevey C, Muller J, et al. STRING 8—a global view on proteins and their functional interactions in 630 organisms. Nucleic acids research. 2008;37(suppl_1):D412-D6.
30. Flicek P, Amode MR, Barrell D, Beal K, Billis K, Brent S, et al. Ensembl 2014. Nucleic acids research. 2013;42(D1):D749-D55.
31. Kinsella RJ, Kähäri A, Haider S, Zamora J, Proctor G, Spudich G, et al. Ensembl BioMarts: a hub for data retrieval across taxonomic space. Database. 2011;2011.
32. Edgar R, Domrachev M, Lash AE. Gene Expression Omnibus: NCBI gene expression and hybridization array data repository. Nucleic acids research. 2002;30(1):207-10.
33. Gong D, Ferrell JE. The roles of cyclin A2, B1, and B2 in early and late mitotic events. Molecular biology of the cell. 2010;21(18):3149-61.
34. Smits M, Nilsson J, Mir SE, van der Stoop PM, Hulleman E, Niers JM, et al. miR-101 is down-regulated in glioblastoma resulting in EZH2-induced proliferation, migration, and angiogenesis. Oncotarget. 2010;1(8):710.
35. Rössig L, Urbich C, Brühl T, Dernbach E, Heeschen C, Chavakis E, et al. Histone deacetylase activity is essential for the expression of HoxA9 and for endothelial commitment of progenitor cells. Journal of Experimental Medicine. 2005;201(11):1825-35.

36. Lee D-Y, Lee C-I, Lin T-E, Lim SH, Zhou J, Tseng Y-C, et al. Role of histone deacetylases in transcription factor regulation and cell cycle modulation in endothelial cells in response to disturbed flow. Proceedings of the National Academy of Sciences. 2012;109(6):1967-72.
37. Chen LJ, Wei SY, Chiu JJ. Mechanical regulation of epigenetics in vascular biology and pathobiology. Journal of cellular and molecular medicine. 2013;17(4):437-48.
38. Marin T, Gongol B, Chen Z, Woo B, Subramaniam S, Chien S, et al. Mechanosensitive microRNAs—role in endothelial responses to shear stress and redox state. Free Radical Biology and Medicine. 2013;64:61-8.
39. Dunn J, Qiu H, Kim S, Jjingo D, Hoffman R, Kim CW, et al. Flow-dependent epigenetic DNA methylation regulates endothelial gene expression and atherosclerosis. The Journal of clinical investigation. 2014;124(7):3187-99.
40. Jiang Y-Z, Jiménez JM, Ou K, McCormick ME, Zhang L-D, Davies PF. Hemodynamic disturbed flow induces differential DNA methylation of endothelial Kruppel-like Factor 4 (KLF4) promoter in vitro and in vivo. Circulation research. 2014:CIRCRESAHA. 114.303883.
41. Sweeney C, Murphy M, Kubelka M, Ravnik SE, Hawkins CF, Wolgemuth DJ, et al. A distinct cyclin A is expressed in germ cells in the mouse. Development. 1996;122(1):53-64.
42. Horton LE, Templeton DJ. The cyclin box and C-terminus of cyclins A and E specify CDK activation and substrate specificity. Oncogene. 1997;14(4):491.
43. Hagting A, Karlsson C, Clute P, Jackman M, Pines J. MPF localization is controlled by nuclear export. The EMBO journal. 1998;17(14):4127-38.
44. Bellanger S, De Gramont A, Sobczak-Thepot J. Cyclin B2 suppresses mitotic failure and DNA re-replication in human somatic cells knocked down for both cyclins B1 and B2. Oncogene. 2007;26(51):7175.
45. Chen S, Bohrer LR, Rai AN, Pan Y, Gan L, Zhou X, et al. Cyclin-dependent kinases regulate epigenetic gene silencing through phosphorylation of EZH2. Nature cell biology. 2010;12(11):1108.
46. Wei Y, Chen Y-H, Li L-Y, Lang J, Yeh S-P, Shi B, et al. CDK1-dependent phosphorylation of EZH2 suppresses methylation of H3K27 and promotes osteogenic differentiation of human mesenchymal stem cells. Nature cell biology. 2011;13(1):87.
47. Jia N, Li Q, Tao X, Wang J, Hua K, Feng W. Enhancer of zeste homolog 2 is involved in the proliferation of endometrial carcinoma. Oncology letters. 2014;8(5):2049-54.
48. Shi M, Shahsafaei A, Liu C, Yu H, Dorfman DM. Enhancer of zeste homolog 2 is widely expressed in T-cell neoplasms, is associated with high proliferation rate and correlates with MYC and pSTAT3 expression in a subset of cases. Leukemia & lymphoma. 2015;56(7):2087-91.
49. Nakagawa S, Okabe H, Sakamoto Y, Hayashi H, Hashimoto D, Yokoyama N, et al. Enhancer of zeste homolog 2 (EZH2) promotes progression of cholangiocarcinoma cells by regulating cell cycle and apoptosis. Annals of surgical oncology. 2013;20(3):667-75.
50. Chang LC, Lin HY, Tsai MT, Chou RH, Lee FY, Teng CM, et al. YC-1 inhibits proliferation of breast cancer cells by down-regulating EZH2 expression via activation of c-Cbl and ERK. British journal of pharmacology. 2014;171(17):4010-25.
51. Zhou J, Bi C, Cheong L-L, Mahara S, Liu S-C, Tay K-G, et al. The histone methyltransferase inhibitor, DZNep, up-regulates TXNIP, increases ROS production, and targets leukemia cells in AML. Blood. 2011;118(10):2830-9.
52. Bracken AP, Dietrich N, Pasini D, Hansen KH, Helin K. Genome-wide mapping of Polycomb target genes unravels their roles in cell fate transitions. Genes & development. 2006;20(9):1123-36.

53. Yamaguchi F, Takata M, Kamitori K, Nonaka M, Dong Y, Sui L, et al. Rare sugar D-allose induces specific up-regulation of TXNIP and subsequent G1 cell cycle arrest in hepatocellular carcinoma cells by stabilization of p27kip1. International journal of oncology. 2008;32(2):377-85.
54. Jeon J-H, Lee K-N, Hwang CY, Kwon K-S, You K-H, Choi I. Tumor suppressor VDUP1 increases p27kip1 stability by inhibiting JAB1. Cancer research. 2005;65(11):4485-9.
55. Han SH, Jeon JH, Ju HR, Jung U, Kim KY, Yoo HS, et al. VDUP1 upregulated by TGF-β1 and 1, 25-dihydorxyvitamin D 3 inhibits tumor cell growth by blocking cell-cycle progression. Oncogene. 2003;22(26):4035.
56. Wolters T, Vissers KJ, Bangma CH, Schröder FH, Van Leenders GJ. The value of EZH2, p27kip1, BMI-1 and MIB-1 on biopsy specimens with low-risk prostate cancer in selecting men with significant prostate cancer at prostatectomy. BJU international. 2010;106(2):280-6.
57. Kuroki H, Hayashi H, Okabe H, Hashimoto D, Takamori H, Nakahara O, et al. EZH2 is associated with malignant behavior in pancreatic IPMN via p27Kip1 downregulation. PloS one. 2014;9(8):e100904.
58. Wasserman SM, Topper JN. Adaptation of the endothelium to fluid flow: in vitro analyses of gene expression and in vivo implications. Vascular Medicine. 2004;9(1):35-45.
59. Nakagawa S, Sakamoto Y, Okabe H, Hayashi H, Hashimoto D, Yokoyama N, et al. Epigenetic therapy with the histone methyltransferase EZH2 inhibitor 3-deazaneplanocin A inhibits the growth of cholangiocarcinoma cells. Oncology reports. 2014;31(2):983-8.
60. Kikuchi J, Takashina T, Kinoshita I, Kikuchi E, Shimizu Y, Sakakibara-Konishi J, et al. Epigenetic therapy with 3-deazaneplanocin A, an inhibitor of the histone methyltransferase EZH2, inhibits growth of non-small cell lung cancer cells. Lung cancer. 2012;78(2):138-43.
61. Baxter J, Sauer S, Peters A, John R, Williams R, Caparros ML, et al. Histone hypomethylation is an indicator of epigenetic plasticity in quiescent lymphocytes. The EMBO journal. 2004;23(22):4462-72.
62. Makarević J, Rutz J, Juengel E, Kaulfuss S, Reiter M, Tsaur I, et al. Amygdalin blocks bladder cancer cell growth in vitro by diminishing cyclin A and cdk2. PloS one. 2014;9(8):e105590.
63. Dekker RJ, van Soest S, Fontijn RD, Salamanca S, de Groot PG, VanBavel E, et al. Prolonged fluid shear stress induces a distinct set of endothelial cell genes, most specifically lung Krüppel-like factor (KLF2). Blood. 2002;100(5):1689-98.
64. Villarreal G, Zhang Y, Larman HB, Gracia-Sancho J, Koo A, García-Cardeña G. Defining the regulation of KLF4 expression and its downstream transcriptional targets in vascular endothelial cells. Biochemical and biophysical research communications. 2010;391(1):984-9.

Chapter 5

Reciprocal regulation of Endothelial-Mesenchymal Transition by MAPK7 and EZH2 activity in Intimal Hyperplasia and Coronary Artery Disease

Byambasuren Vanchin[1,#], Marloes Sol[1,#], Gjaltema RAF [2], Marja Brinker[1], Bianca Kiers[3],

Alexandre C. Pereira[3], Martin C. Harmsen[1], Jan-Renier A.J. Moonen[1,4], Guido Krenning[1]

[1] Laboratory of Cardiovascular Regenerative Medicine, Dept. Pathology and Medical Biology, University of Groningen, University Medical Center Groningen, Hanzeplein 1 (EA11), 9713GZ Groningen, The Netherlands
[2] Epigenetic Editing Research Group, Dept. Pathology and Medical Biology, University of Groningen, University Medical Center Groningen, Hanzeplein 1 (EA11), 9713GZ Groningen, The Netherlands
[3] Laboratory of Genetics and Molecular Cardiology (LIM13), Heart Institute (InCor), University of São Paulo, Avenida Dr. Eneas C. Aguiar 44, 05403-000 São Paulo, SP, Brazil.
[4] Center for Congenital Heart Diseases, Dept. Pediatric Cardiology, Beatrix Children's Hospital, University of Groningen, University Medical Center Groningen, Hanzeplein 1 (CA40), 9713GZ Groningen, The Netherlands.
[#]Authors contributed equally.

Submitted

ABSTRACT

Endothelial-Mesenchymal Transition (EndMT) is a specific form of endothelial dysfunction wherein endothelial cells acquire a mesenchymal phenotype and lose their endothelial functions. We, and others, recently described that EndMT contributes to intimal hyperplasia and atherosclerosis.

The mitogen activated protein kinase 7 (MAPK7, also known as Erk5) inhibits EndMT. MAPK7 activation decreases the expression of the histone methyltransferase Enhancer-of-Zeste homologue 2 (Ezh2) thereby maintaining endothelial quiescence. This decrease in Ezh2 expression may therefore be responsible for the protective effects of MAPK7 activation. Ezh2 is the catalytic subunit of the Polycomb Repressive Complex 2 that methylates lysine 27 on histone 3 (H3K27me3). it is elusive how the crosstalk between MAPK7 and Ezh2 is regulated in the endothelium and if the balance between MAPK7 and EZH2 is disturbed during intimal hyperplasia.

In this study, we showed that in endothelial cells there is reciprocity between MAPK7 signaling and EZH2 expression and that disturbances in this reciprocal signaling circuit associate with the induction of EndMT and severity of human coronary artery stenosis. The reciprocity between MAPK7 and EZH2 is governed by a complex mechanism involving microRNAs and the phosphatases DUSP-1 and DUSP-6.

INTRODUCTION

Neointimal hyperplasia is characterized by an increasing amount of fibroproliferative cells and extracellular matrix in the neointimal lesion, resulting in vascular lumen narrowing and eventually obstruction of the vessel. Endothelial cells play a pivotal role in the formation of neointimal lesions by the acquisition of a fibro-proliferative phenotype through endothelial-to-mesenchymal transition (EndMT)(1-5). EndMT is characterized by a change from an endothelial phenotype into a phenotype comprising of mesenchymal-like properties, in which the expression of endothelial cells markers, such as eNOS, PECAM-1 and VE-cadherin is lost, and the expression of mesenchymal genes, including SM22α, αSMA and vimentin is gained. Moreover, EndMT-derived fibroproliferative cells secrete extracellular matrix components, which might contribute to the buildup of the neointima(6).

EndMT was originally identified during embryogenesis, where it plays a pivotal role in cardiac valve, septum and endocardial cushion formation(7). In adults, EndMT contributes to fibroproliferative diseases, including atherosclerosis(1-5), cerebral cavernous malformation(8), pulmonary fibrosis(9), kidney fibrosis(10) and cardiac fibrosis(11). Uniform laminar shear stress (LSS) conveys atheroprotective effects to the endothelium, while endothelial cells exposed to disturbed or low oscillatory shear stress are prone to EndMT(12, 13). Uniform LSS activates the mitogen-activated protein kinase 7 (MAPK7) - also known as extracellular signal-related kinase 5 (Erk5) and big-mitogen kinase-1 (BMK-1) - which suppresses EndMT(5, 14, 15). Concurrently, the loss of MAPK7 signaling facilitates EndMT(5, 16). Currently, it is elusive how MAPK7 activity is regulated in fibroproliferative disease.

The histone methyltransferase Enhancer of Zeste Homolog 2 (EZH2), which is the catalytic subunit of the Polycomb Repressive Complex 2, plays a pivotal role in endothelial dysfunction(17-19). EZH2 is responsible for the trimethylation of lysine 27 on histone 3, which silences gene expression and is elevated in endothelial cells in atherosclerotic lesions(20). Serendipically, we uncovered that uniform LSS reduces the expression of EZH2, whereas the RNAi-mediated repression of EZH2 reciprocally activates MAPK7 signaling in endothelial cells even in the absence of LSS(18). Currently, it is elusive how the crosstalk between MAPK7 and EZH2 is regulated in the endothelium and whether the balance between MAPK7 and EZH2 is disturbed during intimal hyperplasia and coronary artery stenosis.

Here, we describe the reciprocity that exists between MAPK7 and EZH2 in the regulation of EndMT and in human coronary artery stenosis. In uniform LSS-stimulated endothelial cells, activation of MAPK7 increases the expression of microRNA (miR)-101, which represses the expression of EZH2. Reciprocally, the loss of EZH2 coincides with a decreased expression of the Dual Specificity Phosphatase (DUSP)-1 and DUSP-6 – the phosphatases responsible for the dephosphorylation of MAPK7(21) - which facilitates the activation of MAPK7. Disbalances in this reciprocal signaling circuit culminate in the induction of EndMT and associate to the severity of human coronary artery stenosis.

MATERIALS AND METHODS

HUMAN CORONARY ARTERY SAMPLES

Human coronary arteries were obtained from autopsy specimens from 10 patients (age 59.1±2.6 years, range 39-69) that died from an acute coronary episode at the Heart Institute (InCor), Sao Paulo, Brazil. Hypertension was resent in 9 subjects, and diabetes in 6. Five individuals were active smokers. Next-of-kin gave informed consent and the investigation was performed according to institutional guidelines (InCor, Sao Paulo #SDC 3723/11/141 and #CAPPesq 482/11) and the Declaration of Helsinki. During necropsy each dissected coronary artery was fixed in neutral-buffered formalin with constant perfusion at a quasi-normal perfusion pressure before paraffin embedding.

DETERMINATION OF INTIMA-MEDIA THICKNESS

Four micron-tick sections were prepared from human coronary artery samples and deparaffinized using Xylol and rehydrated using a series of EtOH solutions of decreasing concentration. Samples were stained in Verhoeff's solution (92 mM hematoxylin, 137 mM $FeCl_3$, 27 mM KI, 4 mM I_2 in 55% EtOH) at room temperature for 1 hour. Samples were differentiated in $FeCl_3$ (123 mM in dH_2O) for 1 minute and treated with Sodium Thiosulphate (316 mM in dH_2O) at room temperature for 1 min. Samples were dehydrated using increasing concentrations of EtOH and cleared in 100% xylene. Samples were mounted in Permount resinous mounting medium. The intimal thickness was determined as the distance between the inner elastic lamina and the lumen and the medial thickness was determined by measuring the distance between the inner elastic lamina and the outer elastic lamina at 10 spots within 1 samples. Intimal/Medial thickness was calculated by dividing the average intimal thickness by the average medial thickness.

HUMAN UMBILICAL VEIN ENDOTHELIAL CELL CULTURE AND SHEAR STRESS EXPERIMENTS

Human umbilical vein endothelial cells (HUVEC, Lonza #C2519) were cultured in endothelial cell culture medium (ECM) as described previously(5, 22). EndMT was the addition of 10 ng/ml TGFβ1 to the culture medium as described before(5, 23). For shear stress experiments, HUVEC (60 000 cells/cm^2) were seeded on 0.1% gelatin-coated µ-Slides I 0.4 Luer (Ibidi GmbH, Martinsried, Germany) and allowed to adhere under standard culture conditions overnight. Slides with a confluent endothelial cell monolayer were exposed to uniform laminar shear stress (20 dyne/cm^2) for 24hours. Where indicated 5µM of the small molecule inhibitor to DUSP-1/6 (BCI, Axon Medchem, Groningen, The Netherlands) was applied.

VIRAL TRANSDUCTION OF ENDOTHELIAL CELLS

pLKO.1-shEZH2 and pLKO.1-SCR were kindly provided by Prof.dr. J.J. Schuringa (dept. Hematology, UMCG). HEK293 cells were co-transfected with pLKO.1-shEZH2 or pLKO.1-SCR, pVSVG (envelope plasmid) and pCMV-R8.91 (gag-pol 2nd generation packaging

plasmid) using Endofectin-Lenti (Gene Copoeia, Rockville, MD, USA). At 48 and 72 hours post-transfection, viral supernatants were collected.

A retroviral construct encoding the constitutively active rat MEK5-α1 (pBabePuro-MEK5D) and empty vector controls were kindly provided by Prof.dr. M. Schmidt (Dept. Dermatology, University Würzburg, Germany). Retroviral transduction of HUVEC was performed as detailed before(24). In brief, virus-producing Phoenix cells were cultured until 70% confluency, after which basal medium was replaced by ECM after which viral supernatants were collected twice at 24 hours intervals.

Viral supernatants were supplemented with polybrene (6µg/ml; Sigma, St.Louis, MO) and applied to 30% confluent HUVEC for two consecutive rounds of 24h exposure. Transduced HUVECs were passaged twice and transduced cells were selected by puromycin (4µg/ml; Invitrogen, Carlsbad, CA, USA).

MICRORNA TRANSFECTIONS IN ENDOTHELIAL CELLS

HUVEC or COS7 cells were seeded in antibiotic free medium at a density of 20 000/ cm^2. Cells were transfected with 50 pmol of microRNA mimics (miR-101 (#PM11414), miR-200a (#PM10991), miR-200b (#PM10492), miR-200c (#PM11714), miR-141 (#PM10860), miR-429 (#PM10221) or scrambled control (#AM17110, all Ambion/Life Technologies, Carlsbad, CA) using the siRNA reagent system (Santa Cruz, #sc-45064, Santa Cruz, CA) according to manufacturer's instructions.

IMMUNOFLUORESCENCE

Cells were fixed using 2% paraformaldehyde in PBS at room temperature for 30 minutes. For the analysis of intracellular proteins, cells were permeabilized by 0.05% Triton X-100 solution for 10 minutes. Blocking of non-specific antibody binding was performed using 5% donkey serum in PBS for 10 minutes. Samples were incubated with antibodies to VE-Cadherin (1:200, R&D #9381, Minnepolis, MN) or SM22α (1:200, Abcam #14106, Cambridge, UK) in PBS containing 2% donkey serum at 4°C overnight. Samples were washed extensively with 0,05% Tween-20 in PBS and incubated with Alexa Fluor® 594-conjugated antibodies to Rabbit IgG (Life Technologies, Carlsbad, CA, #A21207) in DAPI/PBS with 2% human serum at RT for 1 hour. Image analysis was performed on TissueFAXS (TissueGnostics, Vienna, Austria) in fluorescence mode, in combination with Zeiss AxioObserver Z1 microscope. Data analysis was performed using TissueQuest fluorescence (TissueGnostics, Vienna, Austria) software.

IMMUNOBLOTTING

Cells were harvested in RIPA buffer (Thermo Fisher Scientific, Wiltham, MA) supplemented with 1% v/v protease inhibitor cocktail (Sigma Aldrich, St Louis, MO) and 1% v/v phosphatase inhibitor cocktail (Sigma Aldrich, St Louis, MO). Samples were sonicated and protein concentration was determined with a DC protein assay (BioRad, Hercules, CA). Equal amount of protein were separated by electrophoresis on 10% polyacrylamide gels after which proteins were blotted onto nitrocellulose membranes using the semi dry Transblot Turbo system (Bio-rad, Hercules, CA). Membranes were blocked with Odyssey

Blocking buffer (Li-COR Biosciences, Lincolin, NE) at RT for 1 hour, and incubated with antibodies against β-actin (1:2000, Cell Signaling, Danvers, MA, USA), EZH2 (1:1000, Cell Signaling, Danvers, MA, USA), MAPK7 (1:1000, Merck Millipore, Billerica, MA, USA), MKP-1(DUSP-1, 1:1000, Abcam #195261) or MKP-3 (DUSP-6, 1:500, Santa cruz, #sc377070) at 4^0C overnight. Membranes were washed in TBS Tween (0.1%) and developed using IrDye-conjugated antibodies to rabbit IgG (1:10,000, #926-68021), mouse IgG (1:10,000, # 926-32210, both Li-COR Biosciences) or AP-conjugated antibodies to rabbit IgG (1:2000, #7054S, Cell Signaling) at RT for 1hour. Protein detection was done using the Odyssey Infrared Imaging System (Li-COR Biosciences). The development of AP-conjugated antibodies, membranes were incubated with AP-detection buffer (100nM NaCl, 100mM Tris, 50mM $MgCl_2$, pH 9.5) supplemented with nitro-blue tetrazolium chloride (NBT) (330µg/mL) and 5-bromo-4-chloro-3'-indolyphosphate p-toluidine salt (BCIP) (165µg/mL). Densitometry analysis was performed using Totallab 120 (Nonlinear Dynamics, Newcastle upon Tyne, England).

RNA ISOLATION AND GENE EXPRESSION ANALYSIS

RNA was isolated using the TRIzol reagent (Invitrogen Corp, CA, USA) according to the manufacturer's protocol. RNA concentration and purity were assessed using UV spectrometry (Nanodrop 1000, Thermo Scientific MA, USA) and RNA integrity validated on 1% agarose gels. For gene expression analysis, cDNA synthesis was performed using RevertAid™ First Strand cDNA Synthesis Kit (Thermo Scientific, MA, USA), according to the manufacturer's protocol. For microRNA transcript analysis, 10ng of total RNA was reversely transcribed using the ABI Taqman microRNA reverse transcription kit (#4366597, ThermoFisher Scientific) according to manufactures instructions using 1.0 µM microRNA-specific stemloop primers (table 1). For all transcript analyses, the cDNA was amplified on a VIIA7 thermal cycling system (Applied Biosystems, Carlsbad, CA) in a reaction containing 0.6 µM primers (table 2) using SYBR Green chemistry (Bio-Rad, VA, USA). Cycle threshold (C_T) values for individual reactions were determined and normalized against GAPDH/ACTB (gene transcript analysis) or RNU6 (microRNA transcript analysis). All cDNA samples were amplified in triplicate. Relative expression was calculated using the ΔC_T method. Data are presented as fold change compared with control.

Gene	Sequence
miR-101	*Stem loop:* GTCGTATCCAGTGCAGGGTCCGAGGTATTCGCACTGGATACGACTTCAGTTA *Sense:* TGCGGTACAGTACTGTGAT
miR-141	*Stem loop:* GTCGTATCCAGTGCAGGGTCCGAGGTATTCGCACTGGATACGACCCATCTTTAC *Sense:* TGCGGTAACACTGTCTG
miR-200a	*Stem loop:* GTCGTATCCAGTGCAGGGTCCGAGGTATTCGCACTGGATACGACACATCGTT *Sense:* TGCGGTAACACTGTCTGGT
miR-200b	*Stem loop:* GTCGTATCCAGTGCAGGGTCCGAGGTATTCGCACTGGATACGACTCATCATTAC *Sense:* TGCGGTAATACTGCCTG
miR-200c	*Stem loop:* GTCGTATCCAGTGCAGGGTCCGAGGTATTCGCACTGGATACGACCCAAACACTG *Sense:* TGCGGCGTCTTACCCAG
miR-429	*Stem loop:* GTCGTATCCAGTGCAGGGTCCGAGGTATTCGCACTGGATACGACACGGTTTTAC *Sense:* TGCGGTAATACTGTCTG

U6	*Stem loop:* GTCGTATCCAGTGCAGGGTCCGAGGTATTCGCACTGGATACGACAAAAATATGG *Sense:* TGCGGCTGCGCAAGGATGA
U24	*Stem loop:* GTCGTATCCAGTGCAGGGTCCGAGGTATTCGCACTGGATACGACTGCATCAGCG *Sense:* TGCGGTGCAGATGATGTAA
	Antisense: GTGCAGGGTCCGAGGT

Table 1. Primer sequences for microRNA expression analysis

Gene Name	Forward Primer	Reverse Primer
DUSP1	TGGGTACATCAAGTCCATCTGA	GCAAAAAGAAACCGGATCAC
DUSP6	GACGCTCGCTGTTTGTATCC	GACTCAGCCTCGCACACC
EZH2	GCGAAGGATACAGCCTGTGCAC	AATCCAAGTCACTGGTCACCGAA
GAPDH	AGCCACATCGCTCAGACAC	GCCCAATACGACCAAATCC
MAPK7	CCTGATGTCAACCTTGTGACC	CCTTTGGTGTGCCTGAGAAC

Table 2. Primer sequences for gene expression analysis

3'UTR BINDING ASSAYS

3'UTR fragments were isolated from a cDNA pool of various human tissues using specific primers for *EZH2*-3'UTR (sense 5'-CATCTGCTACCTCCTCCCCC-3', antisense 5'-GACAAGTTCAAGTATTCTTT-3'), *DUSP-1*-3'UTR (sense 5'-AAGGCCACGGGAGGTGAGGC-3', antisense 5'-CAATAGAAATGCCATAATTT-3'), and *DUSP-6*-3'UTR (sense 5'-AAGACCCCACACCCCTCCTT-3', antisense 5'-CAATAGCCAAAATAGTTATT-3', all 0.6 µM, Biologio, Leiden, The Netherlands). Sense and antisense primers were extended with SgfI (GCGATCGC) and NotI (GCGGCCGC) restriction sequences, respectively. Amplification was performed using the DyNAzyme EXT PCR kit (Finnzymes, Vantaa, Finland) according to manufacturers' instructions. Amplicon size was validated by gel electrophoresis on 1% agarose gels prior to purification using the QIAquick PCR Purification kit (Qiagen, Venlo, The Netherlands) and cloning into the dual luciferase reporter vector psiCHECK-2 (Promega, Madison, WI) using T4 DNA Ligase (Fermentas/Thermo Fisher Sci., Waltham, MA) according to standard protocols.

COS7 cells were transfected with 100 ng UTR reporter plasmid and 50 pmol microRNA mimics as detailed above. 48 hours post-transfection, luciferase activity was assayed using the DualGlo Luciferase assay system (Promega, Madison, WI) and recorded for 500 ms on a Luminoskan ASCENT (Thermo Scientific, Waltham, MA) according to manufacturer's instructions. Relative luciferase activity was calculated by dividing the luminescence from *Renilla* luciferase activity by the luminescence from firefly luciferase activity and normalized to control samples.

HISTONE CHROMATIN-IMMUNOPRECIPITATION (CHIP)

Cells were harvested using accutase, pelleted and the chromatin crosslinked using 1% formaldehyde (37% F1268 Sigma-Aldrich) for 8 minutes. Crosslinking activity was quenched using 125mM glycine (104201 Merck). Cell pellets were lysed on ice with SDS

Genomic Region	Chr.	Sense Sequence	Antisense Sequence
miR-200b/a/429			
-2.5kb	1	GGAGGAGCTGGTGTGTTCTC	CAAAGCCGCCATTTCACC
-2.0kb	1	GCGGTGATGATTAACCCAAC	GTGGCCACAGGTCAAGAAAT
-1.5kb	1	GGTGAGAACGCAATGACTGA	CTCCCACTGCCAGGTTCA
-1.0kb	1	TTGGAGGAGGAGACTGGAAC	AGTTTTCTGGCACCTTCCAC
-0.5kb	1	GACCAGCAGACACACAAACC	GACCCCTCTCCCATGCTG
TSS	1	TACTGAGCTTCCCAGCGAGT	AATGCTGCCCAGTAAGATGG
+0.5kb	1	GAGCAGGACCCAACAGAGG	CAGGAGGGAAGATGGCTGT
miR-200c/141			
-2.5kb	12	CACCTCCAGGTTCCAGCTAC	AAATGCTTCCACAGGGTCAG
-2.0kb	12	ACAGGGTGGTTGTGAAAAGC	CGCCACGGTAAAATGAGAAT
-1.5kb	12	CATGTCAGGAGTGGGGTTTC	CTTTGGGACCTGTGCTGTCT
-1.0kb	12	GACTCCACTGAGGGCTGTG	TGAAGTTACCCACCGCTACC
-0.5kb	12	GCCTAGAGGAGTGGCCAAG	GGTGTGTCCTCCTGCCATAG
TSS	12	AGGGCTCACCAGGAAGTGT	AGGATCCCTGCGGAAAAG
+0.5kb	12	CCCTGTAGCAACTGGTGAGC	GGGAGCCATCTTTACCAGAC
miR-101-1			
-2.5kb	1	CCACAGGCCTGGTTGTAGAT	AATCATTGGCCTTGGTGAAG
-2.0kb	1	TGGGTAGAGCAGAGGGAAGA	ATCCTTCATTGTGCCAGTCC
-1.5kb	1	TGACCGCAGACTGAGACTCTT	GCCAGGGAGAGAAAAACCAT
-1.0kb	1	TGGAGGTTGAAGATGTGTGC	CTGGTCTTGACCTCCTGAGC
-0.5kb	1	TGACAGCAGCAGCAATAACA	
TSS	1	TTCTTCCTGGGTACGGTGAG	CCGACACAGTGACTGACAGG
+0.5kb	1	ACTGACTGTGCCTCCCTGAC	TGAGCACTTTGAAGACAGGA
DUSP-1 (MKP-1)			
-2.5kb	5	CCTCACCCCTGCTCTTTATG	ATGGCTTGCAGTGACCTTCT
-2.0kb	5	CAGCAAGGGAGGAGAGAGAA	GCCTGGTGACAGAGCAAGAC
-1.5kb	5	GCCTCGCTTAGCTTGTGTGT	CACTCCATGCCCTGAACTTT
-1.0kb	5	GCAGTGGATTCCAGGGTTT	GAAAGGGATGGAGAAGCTCA
-0.5kb	5	GCTTCCTGTGCTTTTGCATAC	CCCCAGTAGTGTGGTTCTGG
TSS	5	CGCTTTTGGACTGAGAGAGG	CTCGCTGCGAAGGACATT
+0.5kb	5	AGGGCGTACCTTTGAGGAAG	GTGGTGTTGCTGGACGAG
DUSP-6 (MKP-3)			
-2.5kb	12	AGGCCTAGGTTGCCAATTTT	AAAATGGTGCGGAGAGGAG
-2.0kb	12	ATTGGAAGCCGGATGGAG	GCAGGCTTCGGCACTTTTAT
-1.5kb	12	AATGATTTCTGGGCAAGGAG	GGTCTTGCGGGAGGACTT
-1.0kb	12	GACCCAAGTTCGCCTTAACC	ACACAGCCTCGGCTAAAAGA
-0.5kb	12	AGGCAGCTCCTCAATGGATA	TCATCAACACAACCTGTTCCA
TSS	12	GTCTTGCTGATCGCCATTTC	AGCTCGACCCCCATGATAG
+0.5kb	12	GGAAGCGAGTGGATTCTGAG	CGCGTGGATTGAAAATACCT

Table 3. Primers used for histone CHIP RT- PCR assays

lysis buffer (1% SDS, 50mM Tris HCl pH 8.0, 10mM EDTA) supplemented with freshly added 100mM protease inhibitor cocktail (Sigma Aldrich P8340) for 15 minutes. The chromatin was fragmented by Biorupter (Diagenode, Seraing, Belgium) with 5 cycles of (30' ON/OFF). The sonicated sample was centrifuged and chromatin containing supernatant was kept for further analysis. The chromatin was diluted 10 times with RIPA buffer (0.1% SDS, 0.1% Sodiumdeoxycholate, 1% Triton-X100, 1mM EDTA, 10mM Tris-HCl pH 7.5, 140mM NaCl, 0,5mM EGTA) supplemented with 100 mM protease inhibitor cocktail. Immunoprecipitation was performed by 4µg H3K27Me3 antibody (Merk Millipore 07-449) or IgG control (Abcam ab46540) added to the 40uL Dynabeads Protein-A (Life technologies, 10002D) coated tubes. Subsequently, the chromatin of $0.8*10^6$ cells was added to antibody bound beads and incubated overnight at 4^0C while rotating. The beads were washed 3 times with ice cold PBS and the remaining complexes were eluted with 100nM $NaHCO_3$ and 1% SDS in PBS. 5M NaCl and RNAse (Roche #11119915001) were added to the eluted samples and incubated at 62^0C to reversing the crosslink for 4 hours. 2µL Proteinase K (Roche #03115828001) was added and incubated at 62^0C for 1 hour to liberate the DNA from the histones. DNA fragments were purified using a QIAquick PCR purification kit (Qiagen) according to manufacturers' instructions. Precipitated DNA was analyzed by qPCR using 7 sets of primers for each promoter area. (Table 3; all 0.6µM Biolegio) Enrichment of promoter sequences in the precipitate was calculated relative to the percentage of input.

ANGIOGENIC SPROUTING ASSAY

10µL Matrigel (BD Corning, 356230) was added into the bottom compartment of µ slide Angiogenesis (81501, Ibidi GmbH, Martinsried, Germany) and incubated at 37^0C, 5% CO_2 for 1 hour. Cells were diluted to $2*10^6$ cells/ml. 50µl cell suspension was added on top compartment. After 6 hours incubation at 37^0C, 5% CO_2, light microscopy images were obtained and complete octamer niches were counted by eye.

COLLAGEN CONTRACTION ASSAY

Cells were dissociated using trypsin-EDTA, pelleted and suspended at a concentration of $22.5*10^6$ cells/ml ECM. 45µL cell suspension was added to a collagen solution (3.3mg/ml rat tail collagen type I (#354236, BD, San Jose, CA), 100mM Na_2HPO_4 and 5mg/ml $NaHCO_3$) of neutral pH. The cell/collagen mixture was immediately aliquoted into 50ul droplets and allowed to polymerize at 37^0C, 5% CO_2 for 30 min. Polymerized gels were released and 1mL of ECM was added. At time points t=0 hours and t=24 hours, gels were visualized using a regular flatbed scanner and the gel surface area quantified using with ImageJ (NIH). Gel contraction was calculated as the relative reduction in gel surface area at 24 hours.

PERMEABILITY ASSAY

Cells ($5*10^4/cm^2$) were cultured on polycarbonate cell culture inserts strips (pore size 0.4µm, porosity, $0.9*10^8/cm^2$ Fisher Scientific, #15639536) coated with 0.1% gelatin for 72 hours to establish a monolayer. Monolayer permeability was assessed by the addition of 5 µg/mL FITC dextran (Sigma) in upper compartment. Fluorescence was measured

in the bottom compartment on fluorescence reader at Ex485/Em519 30 minutes after the addition of dextran. Relative permeability levels were calculated using the fluorescence signal of a naked strip (100% permeability) or the fluorescence signal from the culture medium (0% permeable). Permeability was calculated by following formula: Permeability=(Em_{519}(sample)- Em_{519}(ECM))/ Em_{519}(Empty well)*100.

DATA REPRESENTATION OF STATISTICAL ANALYSES

Data are expressed as mean ± s.e.m. from at least five independent experiments. Where the mean of two groups were compared, p-values were calculated using student t-tests. Otherwise, p-values were calculated using the one-way analysis of variance (ANOVA) followed by Bonferroni's post-hoc comparisons tests using Prism Graphpad (Graphpad Software, La Jolla, CA, USA). $P < 0.05$ was considered statistically significant.

RESULTS

RECIPROCITY BETWEEN MAPK7 AND EZH2 IN CORONARY ARTERY STENOSIS

Human coronary artery samples were stratified into three groups based on their intima/media thickness, ranging from mild stenosis (IMT <1 $\mu m \cdot \mu m^{-1}$), medium (IMT 1-3 $\mu m \cdot \mu m^{-1}$) and severe stenosis (IMT >3 $\mu m \cdot \mu m^{-1}$; fig,1a-d). Coronary artery stenosis is characterized by progressively increasing intima-media thickness (fig.1a-d), wherein coronary artery *MAPK7* expression decreases with an increasing stenosis (r^2=0.2517, p=0.04; fig.1f). In contrast, *EZH2* expression is elevated in coronary artery stenosis (fig.1g,h) and increasing stenosis associates with increased *EZH2* expression (r2=0.4417, p=0.004, fig.1h),

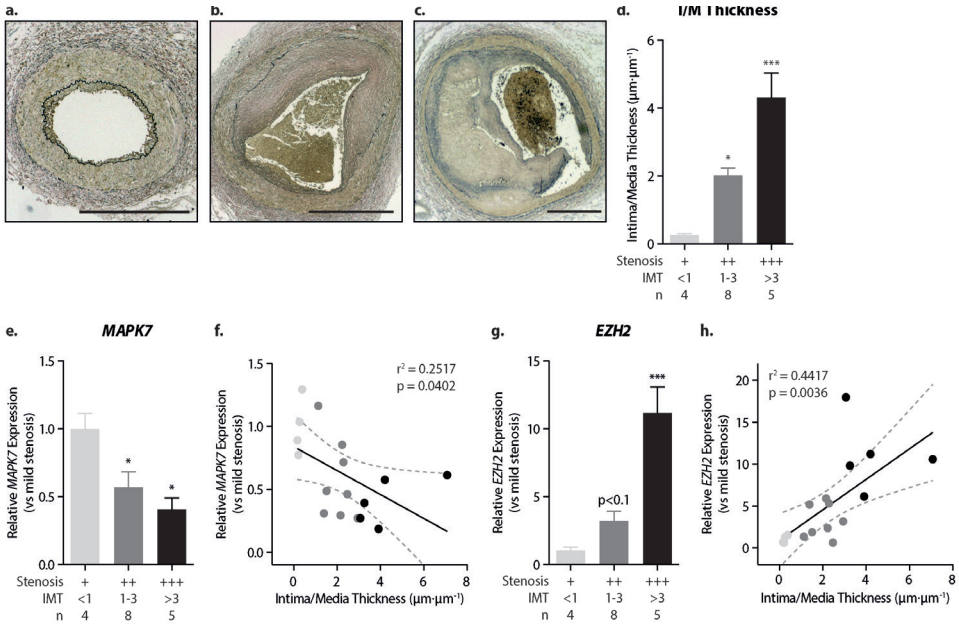

Figure 1. Reciprocity between MAPK7 and EZH2 in human coronary artery stenosis. *(a-c) Representative pictures of Verhoeff-stained human coronary artery samples with mild (IMT<1, a), medium (IMT 1-3, b) or severe (IMT >3, c) stenosis. Intima-media thickness was measured (µm/µm) and divided in groups based on their intima-media thickness (d). MAPK7 expression levels were determined by qPCR and normalized to mild stenosis (e). MAPK7 decreases with increasing stenosis (f). EZH2 expression levels were determined by qPCR and normalized to mild stenosis (g). EZH2 expression increased with stenosis severity (h). *p<0.05, ***p<0.001.*

RECIPROCAL SIGNALING BETWEEN MAPK7 AND EZH2 IN ENDOTHELIAL CELLS

We recently uncovered that disturbed fluid shear stress contributes to intima hyperplasia by the induction of endothelial-mesenchymal transition (EndMT)(5), partially mediated by EZH2(18). Atheroprotective uniform laminar shear stress (LSS) decreases EZH2 expression at both the gene (2.2-fold, p<0.001; fig.2a) and protein (1.9-fold, p=0.028; fig.2b) level. Uniform laminar shear stress does not change the expression of MAPK7, neither on transcript (fig.2c) nor on protein level, however, FSS increases the activity of MAPK7 as indicated by the increased phosphorylation (3.5-fold, p=0.036, fig.2d). Knockdown of EZH2 does not alter its expression, whereas MAPK7 activity is increased upon EZH2 reduction (1.9-fold, p=0.049; fig. 2d). Moreover, protein expression levels of EZH2 associate with MAPK7 activation (r^2=0.7723, p=0.021; fig.2e) proving evidence of the reciprocity between EZH2 expression levels and MAPK7 activity.

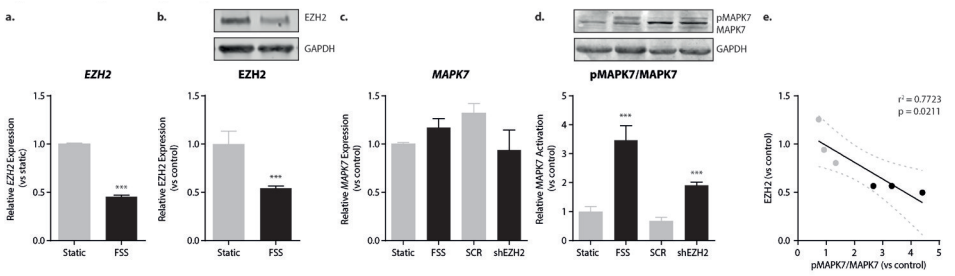

Figure 2. Reciprocal signaling between MAPK7 and EZH2 in endothelial cells. *EZH2 expression levels were determined by qPCR in HUVEC exposed to FSS (20dyne/cm²) compared to static controls (a). EZH2 protein levels were determined by western blot in HUVEC exposed to FSS and compared to static control (b). MAPK7 expression levels were determined by qPCR in HUVEC exposed to FSS, and HUVEC that are deficient in EZH2 (shEZH2)(c). MAPK7 activation (pMAPK7) levels were determined by immunoblotting and normalized to total MAPK7 protein levels (d Protein expression of EZH2 and MAPK7 activation were associated in endothelial cells (e). ***p<0.001.*

MAPK7 DECREASES EZH2 THROUGH MICRORNA-101

As MAPK7 decreases EZH2 post-transcriptionally(18), we investigated whether miRNA-101 - a known translational repressor of EZH2 in endothelial cells(25) - is regulated by MAPK7 signaling. FSS increased the expression of miR-101 in a MAPK7-dependent manner (2.3-fold, p<0.01; fig. 3a). In luciferase reporter assays, miR-101 binds to the 3'UTR of EZH2, reducing the luminescence signal (1.9-fold, p<0.001; fig.3b). In endothelial cells, ectopic expression of miR-101 decreases EZH2 expression at both the gene (2.6-fold, p=0.002; fig. 3c) and protein (2.9-fold, p=0.008; fig. 3c) level, whereas miRNA-101 has no effect on *MAPK7* gene expression (fig. 3e) or MAPK7 protein expression level (fig.3f). In human coronary artery stenosis, *miR-101* expression is decreased (p<0.01, fig.3g) and increased stenosis associates with a progressive decrease in *miR-101* (r^2=0.5109, p=0.001, fig.3h). Moreover, the expression level of miR-101 associates with MAPK7 (r^2=0.4262, p=0.005; fig.3i) and EZH2 (r^2=0.2304, p=0.051; fig.3j) in coronary artery stenosis, where a negative association between MAPK7 and EZH2 expression (r^2=0.2568, p=0.038; fig.3kj) is present. Collectively, these data suggest that in coronary artery stenosis, the reciprocity between MAPK7 activity and EZH2 expression is regulated by miR-101.

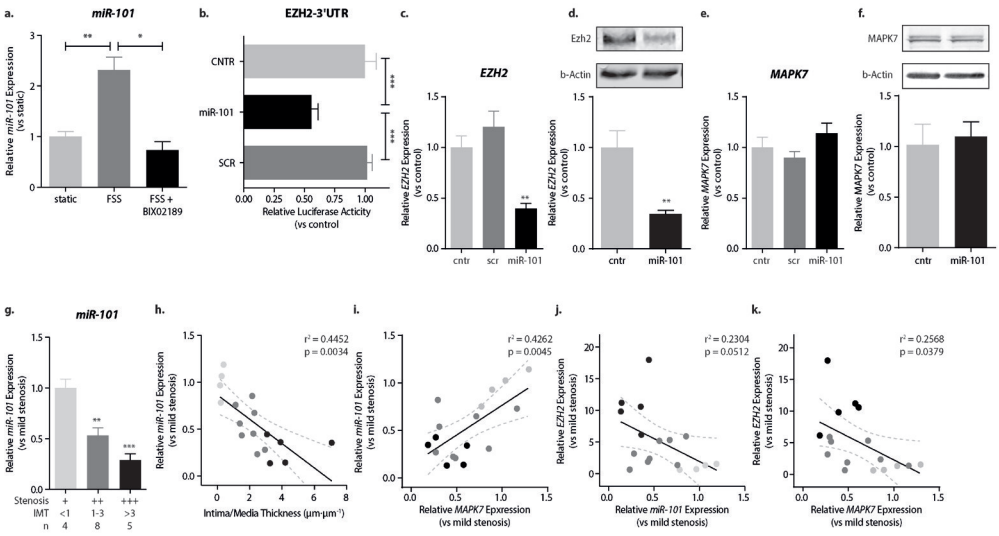

Figure 3. MAPK7 decreases EZH2 through miRNA-101. *MiR-101 expression levels were determined by qPCR in HUVEC exposed to FSS (20dyne/cm²) with or without the MAPK7 inhibitor BIX02189 and normalized to the level of static controls (a). Luciferase reporter binding assays were performed for the 3'UTR of EZH2 in HUVEC with ectopic expression of miR-101 or scrambled control sequences (scr). Luciferase activity was normalized to non-transfected cells (b). EZH2 and MAPK7 expression levels were determined by qPCR in HUVEC with ectopic expression of miR-101 or SCR and normalized to control (c, e). EZH2 and MAPK7 protein levels were determined by western blot in HUVEC with ectopic expression of miR-101 and control (d, f). MiR-101 expression levels were determined by qPCR and normalized to mild stenosis (g). MiR-101 decreases with stenosis severity (h), and associates with MAPK7 (i) and EZH2 (j) expression levels. In coronary artery stenosis, MAPK7 expression negatively correlates to EZH2 expression (k). *p<0.05, **p<0.01, ***p<0.001.*

EZH2 REGULATES DUSP-1 AND DUSP-6 EXPRESSION THROUGH MIR200A-C

However, EZH2 is a transcriptional repressor that cannot directly regulate the activity of a kinase. MAPK7 activity is regulated by the Dual Specificity Phosphatases (DUSP)-1 and DUSP-6(21), yet a reduction in EZH2 expression is associated with a decreased expression of DUSP-1 and DUSP-6(26, 27). Therefore, we investigated alternative mechanisms that might decrease DUSP expression upon the reduction of EZH2. In silico analysis, using Targetscan.org(28), putatively identifies the microRNA-200 family (miR-200a, miR-200b, miR-200c, miR-141 and miR-429) as regulators of DUSP-1 and DUSP-6. Therefore, we investigated if the expression of the miR-200b/a/429 cluster on chromosome 1 and the miR-200c/141 cluster on chromosome 12 are under control of EZH2. Uniform LSS increased the expression of miR-200b (2.5-fold, p=0.008) and miR-200c expression (2.5-fold, p=0.001; fig.4a,e). Moreover, knockdown of EZH2 increased the expression of miR-200b and miR-200c to a similar extend (fig.4a,e).

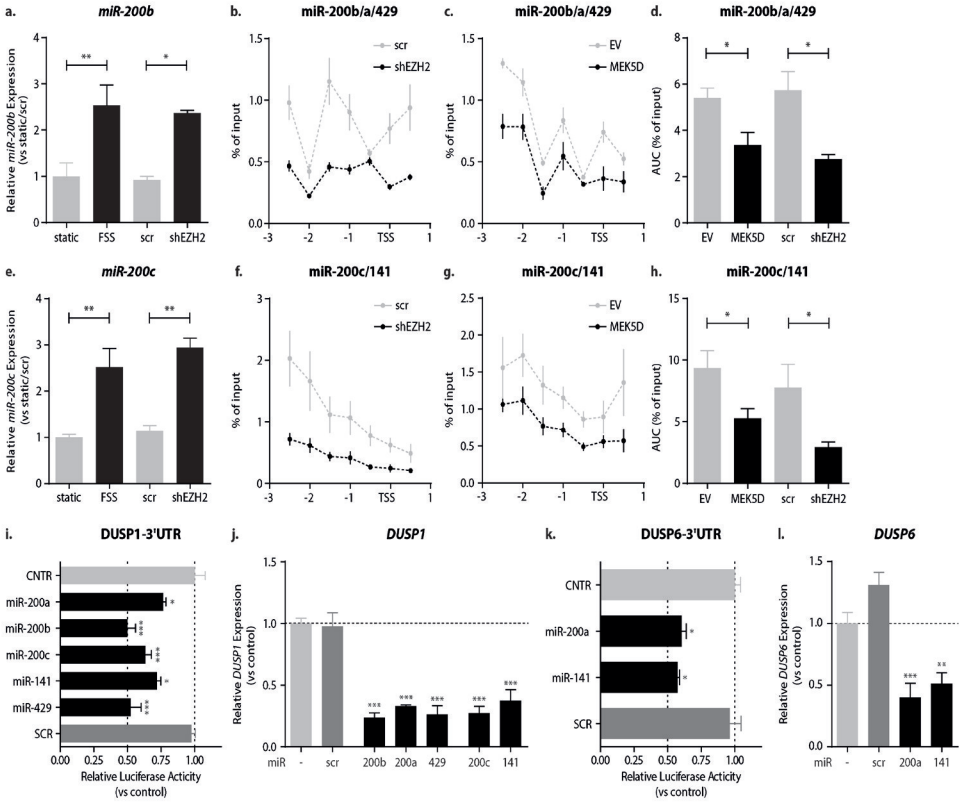

Figure 4. EZH2 regulates DUSP-1 and DUSP-6 expression through miR200a-c. *MiR-200b (a) and miR-200c (e) expression levels were determined by qPCR in HUVEC exposed to FSS (20 dyne/cm²), transduced HUVEC with scr or shEZH2 and normalized to static or scr control cells. H3K27me3 enrichment around the transcription start site (TSS) of the miR-200b/a/429 cluster was determined using ChIP in shEZH2-HUVEC and scr-HUVEC (b) and MEK5D-HUVEC and EV-HUVEC (c). H3K27me3 enrichment is shown as area under the curve (AUC) compared to input samples (d). H3K27me3 enrichment at the around the TSS of miR-200c/141 cluster was determined using ChIP in scr-HUVEC and shEZH2 (f) and in MEK5D-HUVEC and EV-HUVEC (g). H3K27me3 enrichment is shown as AUC compared to input samples (h). Luciferase reporter assays for microRNA binding were performed for the 3'UTR of DUSP-1 in HUVEC with ectopic expression of miR-200a, -200b, -200c, -141, -429 or SCR (i). DUSP-1 expression levels were determined by qPCR in HUVEC with ectopic expression of miR-200b, miR-200a, miR-429, miR-200c, miR-141 or scr, normalized to control (j). Luciferase reporter assay identified miR-200a and miR-141 to target DUSP-6 (k) and ectopic expression of miR-200a or miR-141 decreases DUSP-6 expression in endothelial cells (l). *P<0.05, **P<0.01, ***P<0.001.*

INHIBITION OF DUSP ACTIVITY INCREASES MAPK7 ACTIVITY AND DECREASES EZH2 EXPRESSION

H3K27Me3, the repressive histone mark placed by EZH2, is abundantly present in the promoter regions of the miR-200b/a/429 and miR-200c/141 gene clusters (fig.4b,f). Endothelial cells deficient in EZH2 have reduced levels of H3K27Me3 at these gene promoters (fig.4b,f), which associates with the increased expression of miR-200b and miR-200c. In endothelial cells with constitutively active MAPK7 signaling (MEK5D), the enrichment of H3K27Me3 at the promoter regions of miR-200b/a/429 (1.6-fold, p=0.034; fig.4c,d) and miR-200c/141 (1.9-fold, p=0.035; fig.4g,h) is decreased, suggesting that

MAPK7 activation results in the increased expression of miR-200 family members through the decrease in EZH2 activity.

In luciferase reporter assays, all miR-200 family members were able to bind to the 3'UTR of DUSP-1 (fig.4i), but only miR-200a and miR-141 were able to bind the 3'UTR of DUSP-6 (fig.4k). Corroboratively, exogenous expression of all miR-200 family members in endothelial cells decreased DUSP-1 expression (fig.4j), whereas only miR-200a and miR-141 decreased the expression of DUSP-6 (fig.4l). Collectively, these data imply that the activation of MAPK7 by uniform LSS decreases the expression of DUSP-1 and DUSP-6 expression via the EZH2-dependent regulation of miR-200b/a/429 and miR-200c/141 expression.

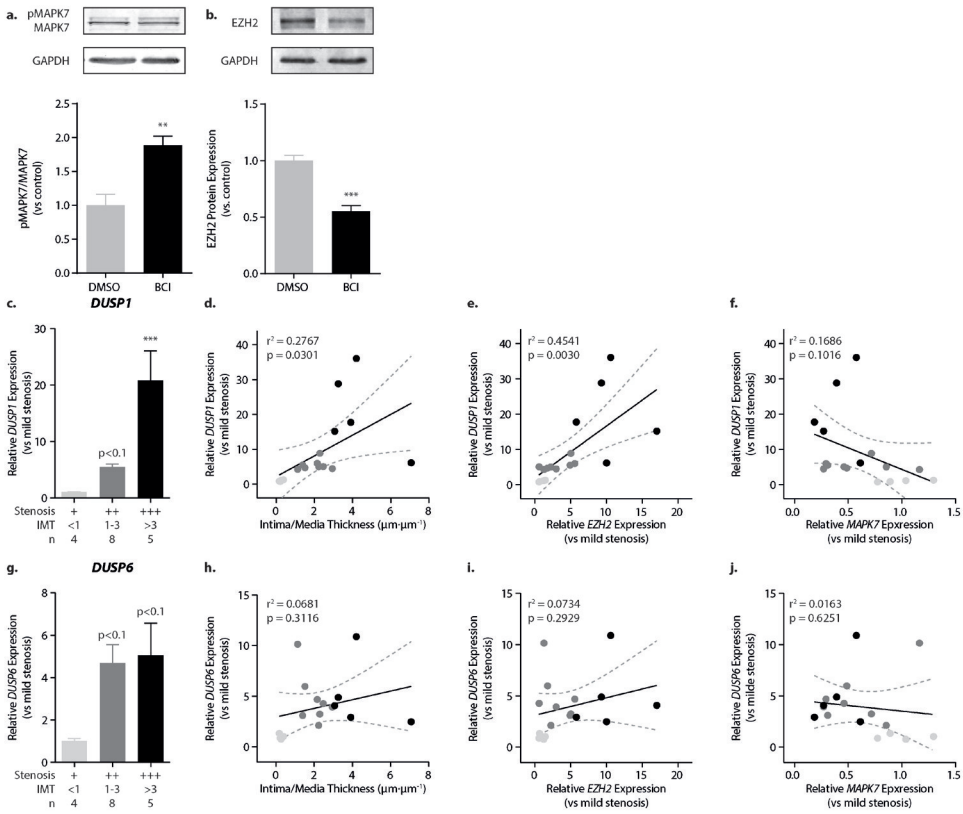

Figure 5. Inhibition of DUSP activity increases MAPK7 activity and decreases EZH2 expression. *MAPK7 (a) and EZH2 (b) protein expressions were determined using western blotting, in HUVEC treated with 5μM of the DUSP-1/6 small molecule inhibitor BCI and normalized to untreated control cells. DUSP-1 expression levels were determined in uman coronary artery stenosis samples by qPCR and normalized to mild stenosis (c). DUSP-1 expression increases with increasing stenosis severity (d) and is associated to EZH2 expression levels (e). DUSP-1 levels show a negative correlation with MAPK7 levels in stenosis (f). DUSP-6 expression levels were determined by qPCR and normalized to mild stenosis (g). DUSP-6 expression is elevated in coronary artery stenosis, but does not associate to the severity of stenosis (h), the level of EZH2 expression (i), nor the level of MAPK7 expression (j). **p<0.01, ***p<0.001.*

We investigated if the pharmacological inhibition of DUSP-1 and DUSP-6 activity in endothelial cells would activate MAPK7 signaling and decrease the expression of EZH2. BCI-treated endothelial cells increased MAPK7 phosphorylation (1.9-fold, p=0.007; fig.5a) and decreased EZH2 expression (1.8-fold, p=0.002; fig.5b). In human coronary artery stenosis, DUSP-1 is increased (p<0.001, fig. 5c) and increased stenosis associates with increased *DUSP-1* expression (r^2=0.2767, p=0.0301; fig.5d). Moreover, the increase in *DUSP-1* expression associates with increased *EZH2* expression in stenosis (r^2=0.4541, p=0.0030; fig.5e) and increase in *DUSP-1* expression seems to correlate with decreased *MAPK7* expression (r^2=0.1686, p=0.1016; fig.5f), although not significantly. Also *DUSP-6* seems to be increased in coronary artery stenosis (p<0.1, fig.5g), the increase in *DUSP-6* expression does not associate with the severity of stenosis (r^2=0.0681, p=0.3116; fig.5h), nor do the expression levels of DUSP-6 associate with *EZH2* (r^2=0.0734, p=0.2929; fig.5i) and *MAPK7* expression (r^2=0.0163, p=0.6251; fig.5j).

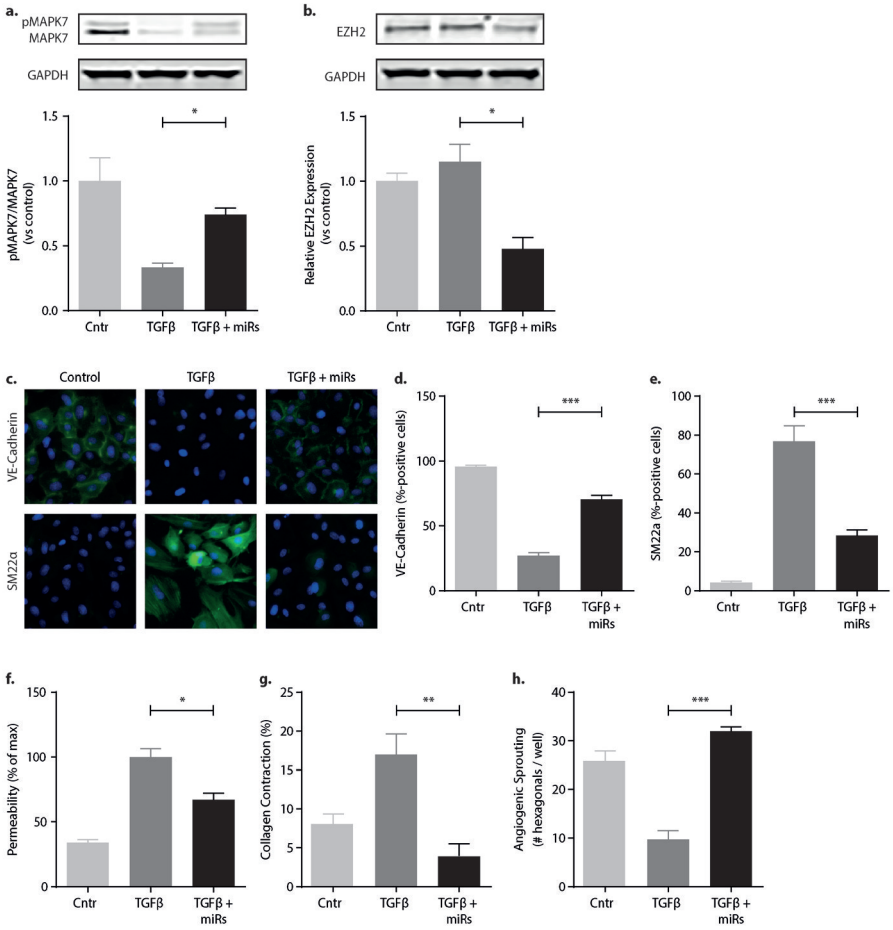

Figure 6. Ectopic expression of miRNA-101, miRNA-141 and miRNA-200a inhibits endothelial dysfunction and EndMT. *MAPK7 (a) and EZH2 (b) protein expressions were determined using western blotting, in HUVEC treated with 10ng/ml TGFb1 with ectopic expression of miRs-101, -200a and -141 and normalized to untreated control cells. The expression of VE-Cadherin (c,d) and SM22a*

*(c,e) were assessed by immunofluorescence and quantified using TissueFaxs analyses. Endothelial cell permeability was assessed using transwell FITC-dextran leakage (f) and collagen gel contraction (g) was assessed as a mesenchymal cell function. The angiogenic sprouting behavior of endothelial cells was assessed using the Matrigel assay (h). *p<0.05, **p<0.01, ***p<0.001.*

As coronary artery stenosis is associated with EndMT(1, 29), we investigated if the ectopic expression of miR-101 or miR-200 family members could preclude EndMT. Endothelial cells transfected with only a single microRNA were susceptible to TGFβ1-induced EndMT (data not shown), however, when miR-101, miR-200a and miR-141 were transfected in combination, endothelial cells increased their MAPK7 activity (fig.6a) and showed reduced expression levels of EZH2 (fig.6b). Corroborating the protective effects of MAPK7 signaling in the preclusion of EndMT(5), TGFβ1 stimulation did not decrease VE-Cadherin expression (fig.6c,d) nor induce the expression of the mesenchymal marker protein SM22α (fig.6c,e) in endothelial cells transfected with miRs-101/200a and -141. Moreover, the ectopic microRNA expression reduced the TGFβ1-induced increase in endothelial permeability by ~40% (fig.6f) and precluded the TGFβ1-induced collagen contraction (fig.6g) – two functional adaptations associated with EndMT – and maintained the endothelial angiogenic sprouting capacity (fig.6h).

DISCUSSION

In this study, we show that reciprocity exists between the atheroprotective MAPK7 activation and the expression of histone methyltransferase EZH2 in endothelial cells. The reciprocity is regulated by the MAPK7-induced silencing of EZH2 expression by miR-101 and the EZH2-mediated silencing of the miR-200 family, which increases DUSP-1 and DUSP-6 expression and inhibits MAPK7 activation. The reciprocity between MAPK7-EZH2 might reflect an autoregulatory feedback loop in endothelial cells that ensures endothelial homeostasis. As such, disturbances in this reciprocity leading to increased EZH2 expression can induce endothelial dysfunction and EndMT. In contrary artery stenosis - a condition associated with EndMT(1, 29) – the reciprocity between MAPK7 and EZH2 is disturbed, resulting in elevated expression of DUSP-1 and EZH2 and the decreased expression of MAPK7. Restoring the reciprocity by ectopic expression of miR-101/200a/141 precludes EndMT and might offer therapeutic benefit in coronary artery stenosis.

EndMT contributes to intimal hyperplasia during coronary artery stenosis(1-5), wherein MAPK7 signaling plays a protective role(5, 16). Yet, during intimal hyperplasia the signaling activity of MAPK7 is rapidly lost (Vanchin et al., J. Pathol, under revision). DUSP-1 and DUSP-6 expression levels are elevated in a number of cardiovascular diseases and DUSP-1 deficient mice are protected from atherosclerosis development (30, 31). The elevated expression of DUSPs might explain the loss in protective MAPK7 signaling activity during coronary artery stenosis, which is corroborated by our finding that pharmacological inhibition of DUSP-1/6 is sufficient to activate MAPK7 signaling.

The expression of DUSP-1 and -6 is associated with high expression of EZH2 in various oncology's(26, 27), albeit by a currently unknown mechanism. We found that EZH2 silences the expression of the microRNA-200 family, which posttranscriptionally regulate the

expression of DUSP-1 and DUSP-6 (fig.7). The loss of EZH2 expression by fluid shear stress therefore might increase the expression of miR-200 family members and decrease the expression of the DUSPs culminating in atheroprotective MAPK7 activation. Interestingly, the endothelial cell-specific overexpression of miR-200b precludes EndMT and alleviates diabetic cardiomyopathy in mice(32). In coronary artery stenosis, EZH2 expression levels are elevated and high EZH2 expression is associated with endothelial dysfunction(18, 19).

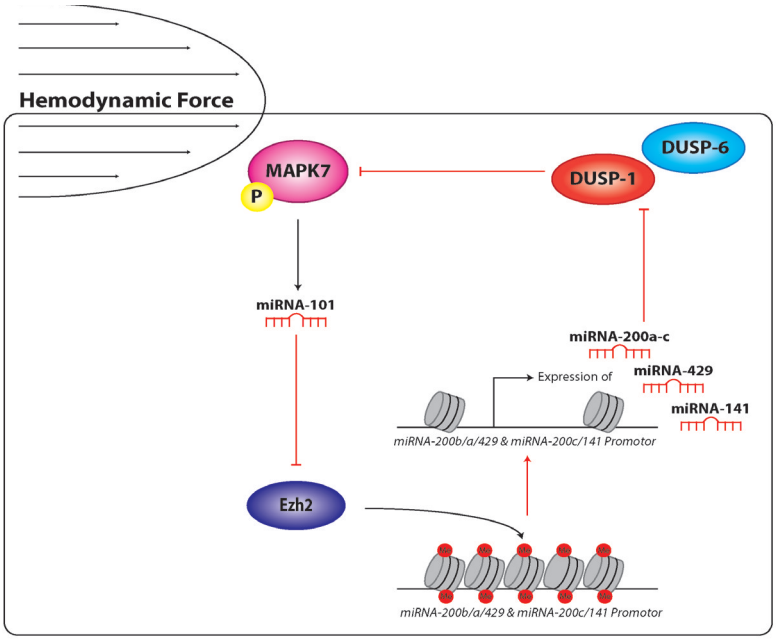

Figure 7. Schematic representation of the reciprocity between MAPK7 activity and EZH2 expression. *Hemodynamic force (laminar shear stress) induces the activation of MAPK7 signaling, resulting in the expression of microRNA-101 that posttranscriptionally silences EZH2 expression. This culminates in the hypomethylation of H3K27 at the promoters of the miR-200 family and the miR-200-mediated silencing of DUSP-1/6. In the absence of laminar shear stress – e.g. during coronary artery stenosis – EZH2 expression is increased resulting in the reduction of miR-200 expression and increase in DUSP-1/6 expression. DUSP-1/6 dephosphorylate MAPK7 culminating in a decrease in its activation.*

In combination, our current data might explain these observations and unifies them into a single mechanism, linking endothelial mechanotransduction to the epigenetic regulation of MAPK7 activity through DUSP-1/6 (fig.7). This double negative feedback loop might resemble a sensitive autoregulatory mechanism that ensures endothelial homeostasis, which when disturbed culminates in EndMT and possibly coronary artery stenosis.

In summary, we show that in endothelial cells there is reciprocity between MAPK7 signaling and EZH2 expression and that disturbances in this reciprocal signaling circuit associate with the induction of EndMT and severity of human coronary artery stenosis. The reciprocity between MAPK7 and EZH2 is governed by a complex mechanism involving microRNAs and the phosphatases DUSP-1 and DUSP-6 (fig.7). Our study contributes to a better understanding of the molecular and epigenetic cascades that underlie EndMT during coronary artery stenosis and might identify novel targets for therapy.

REFERENCES

1. Chen PY, Qin L, Baeyens N, Li G, Afolabi T, Budatha M, et al. Endothelial-to-mesenchymal transition drives atherosclerosis progression. J Clin Invest. 2015;125(12):4514-28. doi: 10.1172/JCI82719.
2. Evrard SM, Lecce L, Michelis KC, Nomura-Kitabayashi A, Pandey G, Purushothaman KR, et al. Endothelial to mesenchymal transition is common in atherosclerotic lesions and is associated with plaque instability. Nat Commun. 2016;7:11853.
3. Mahmoud MM, Kim HR, Xing R, Hsiao S, Mammoto A, Chen J, et al. TWIST1 Integrates Endothelial Responses to Flow in Vascular Dysfunction and Atherosclerosis. Circulation research. 2016;119(3):450-62.
4. Mahmoud MM, Serbanovic-Canic J, Feng S, Souilhol C, Xing R, Hsiao S, et al. Shear stress induces endothelial-to-mesenchymal transition via the transcription factor Snail. Scientific reports. 2017;7(1):3375.
5. Moonen JA, Lee ES, Schmidt M, Maleszewska M, Koerts JA, Brouwer LA, et al. Endothelial-to-mesenchymal transition contributes to fibro-proliferative vascular disease and is modulated by fluid shear stress. Cardiovasc Res. 2015;108(3):377-86.
6. Souilhol C, Harmsen MC, Evans PC, Krenning G. Endothelial-mesenchymal transition in atherosclerosis. Cardiovasc Res. 2018;114(4):565-77.
7. Markwald RR, Fitzharris TP, Manasek FJ. Structural development of endocardial cushions. Am J Anat. 1977;148(1):85-119.
8. Maddaluno L, Rudini N, Cuttano R, Bravi L, Giampietro C, Corada M, et al. EndMT contributes to the onset and progression of cerebral cavernous malformations. Nature. 2013;498(7455):492-6. doi: 10.1038/nature12207. Epub 2013 Jun 9.
9. Hashimoto N, Phan SH, Imaizumi K, Matsuo M, Nakashima H, Kawabe T, et al. Endothelial-mesenchymal transition in bleomycin-induced pulmonary fibrosis. Am J Respir Cell Mol Biol. 2010;43(2):161-72. doi: 10.1165/rcmb.2009-0031OC. Epub 2009 Sep 18.
10. Zeisberg EM, Potenta SE, Sugimoto H, Zeisberg M, Kalluri R. Fibroblasts in kidney fibrosis emerge via endothelial-to-mesenchymal transition. J Am Soc Nephrol. 2008;19(12):2282-7. doi: 10.1681/ASN.2008050513. Epub 2008 Nov 5.
11. Zeisberg EM, Tarnavski O, Zeisberg M, Dorfman AL, McMullen JR, Gustafsson E, et al. Endothelial-to-mesenchymal transition contributes to cardiac fibrosis. Nat Med. 2007;13(8):952-61. Epub 2007 Jul 29.
12. Wentzel JJ, Chatzizisis YS, Gijsen FJ, Giannoglou GD, Feldman CL, Stone PH. Endothelial shear stress in the evolution of coronary atherosclerotic plaque and vascular remodelling: current understanding and remaining questions. Cardiovasc Res. 2012;96(2):234-43. doi: 10.1093/cvr/cvs217. Epub 2012 Jun 29.
13. Texon M. A hemodynamic concept of atherosclerosis, with particular reference to coronary occlusion. AMA Arch Intern Med. 1957;99(3):418-27.
14. Kim M, Kim S, Lim JH, Lee C, Choi HC, Woo CH. Laminar flow activation of ERK5 protein in vascular endothelium leads to atheroprotective effect via NF-E2-related factor 2 (Nrf2) activation. The Journal of biological chemistry. 2012;287(48):40722-31.
15. Le NT, Takei Y, Izawa-Ishizawa Y, Heo KS, Lee H, Smrcka AV, et al. Identification of activators of ERK5 transcriptional activity by high-throughput screening and the role of endothelial ERK5 in vasoprotective effects induced by statins and antimalarial agents. Journal of immunology. 2014;193(7):3803-15.
16. Le NT, Heo KS, Takei Y, Lee H, Woo CH, Chang E, et al. A crucial role for p90RSK-mediated reduction of ERK5 transcriptional activity in endothelial dysfunction and atherosclerosis. Circulation. 2013;127(4):486-99. doi: 10.1161/CIRCULATIONAHA.112.116988. Epub 2012 Dec 14.

17. Kumar A, Kumar S, Vikram A, Hoffman TA, Naqvi A, Lewarchik CM, et al. Histone and DNA methylation-mediated epigenetic downregulation of endothelial Kruppel-like factor 2 by low-density lipoprotein cholesterol. Arterioscler Thromb Vasc Biol. 2013;33(8):1936-42.
18. Maleszewska M, Vanchin B, Harmsen MC, Krenning G. The decrease in histone methyltransferase EZH2 in response to fluid shear stress alters endothelial gene expression and promotes quiescence. Angiogenesis. 2016;19(1):9-24.
19. Dreger H, Ludwig A, Weller A, Stangl V, Baumann G, Meiners S, et al. Epigenetic regulation of cell adhesion and communication by enhancer of zeste homolog 2 in human endothelial cells. Hypertension. 2012;60(5):1176-83.
20. Greissel A, Culmes M, Burgkart R, Zimmermann A, Eckstein HH, Zernecke A, et al. Histone acetylation and methylation significantly change with severity of atherosclerosis in human carotid plaques. Cardiovasc Pathol. 2016;25(2):79-86. doi: 10.1016/j.carpath.2015.11.001. Epub Nov 9.
21. Kondoh K, Nishida E. Regulation of MAP kinases by MAP kinase phosphatases. Biochimica et Biophysica Acta (BBA) - Molecular Cell Research. 2007;1773(8):1227-37.
22. Krenning G, Moonen JR, van Luyn MJ, Harmsen MC. Vascular smooth muscle cells for use in vascular tissue engineering obtained by endothelial-to-mesenchymal transdifferentiation (EnMT) on collagen matrices. Biomaterials. 2008;29(27):3703-11.
23. Correia AC, Moonen JR, Brinker MG, Krenning G. FGF2 inhibits endothelial-mesenchymal transition through microRNA-20a-mediated repression of canonical TGF-beta signaling. Journal of cell science. 2016;129(3):569-79.
24. Ohnesorge N, Viemann D, Schmidt N, Czymai T, Spiering D, Schmolke M, et al. Erk5 activation elicits a vasoprotective endothelial phenotype via induction of Kruppel-like factor 4 (KLF4). J Biol Chem. 2010;285(34):26199-210. doi: 10.1074/jbc.M110.103127. Epub 2010 Jun 15.
25. Smits M, Mir SE, Nilsson RJA, van der Stoop PM, Niers JM, Marquez VE, et al. Down-Regulation of miR-101 in Endothelial Cells Promotes Blood Vessel Formation through Reduced Repression of EZH2. PloS one. 2011;6(1):e16282.
26. Pawlyn C, Bright MD, Buros AF, Stein CK, Walters Z, Aronson LI, et al. Overexpression of EZH2 in multiple myeloma is associated with poor prognosis and dysregulation of cell cycle control. Blood Cancer Journal. 2017;7(3):e549.
27. Zhang H, Qi J, Reyes JM, Li L, Rao PK, Li F, et al. Oncogenic deregulation of EZH2 as an opportunity for targeted therapy in lung cancer. Cancer discovery. 2016;6(9):1006-21.
28. Agarwal V, Bell GW, Nam J-W, Bartel DP. Predicting effective microRNA target sites in mammalian mRNAs. eLife. 2015;4:e05005.
29. Chen PY, Qin L, Barnes C, Charisse K, Yi T, Zhang X, et al. FGF regulates TGF-beta signaling and endothelial-to-mesenchymal transition via control of let-7 miRNA expression. Cell reports. 2012;2(6):1684-96.
30. Reddy ST, Nguyen JT, Grijalva V, Hough G, Hama S, Navab M, et al. Potential Role for Mitogen-Activated Protein Kinase Phosphatase-1 in the Development of Atherosclerotic Lesions in Mouse Models. Arterioscler Thromb Vasc Biol. 2004;24(9):1676-81.
31. Shen J, Chandrasekharan UM, Ashraf MZ, Long E, Morton RE, Liu Y, et al. Lack of MAP Kinase Phosphatase-1 Protects ApoE-null Mice against Atherosclerosis. Circulation research. 2010;106(5):902-10.
32. Feng B, Cao Y, Chen S, Chu X, Chu Y, Chakrabarti S. miR-200b Mediates Endothelial-to-Mesenchymal Transition in Diabetic Cardiomyopathy. Diabetes. 2016;65(3):768-79.

Chapter 6

INTRACELLULAR GALECTIN-3 FACILITATES TGFβ-INDUCED ENDOTHELIAL-MESENCHYMAL TRANSITION

Byambasuren Vanchin, Ruud Wichers Schreur, Linda A Brouwer, Guido Krenning

Cardiovascular Regenerative Medicine Research Group Department of Pathology and Medical Biology, University Medical Center Groningen, University of Groningen, Groningen, The Netherlands

Manuscript in preparation

ABSTRACT

Endothelial cells give rise to a population of myofibroblasts in cardiac fibrosis through a mechanism called endothelial-mesenchymal transition (EndMT). The process by which EndMT takes place in cardiac fibrosis is incompletely understood. Galectin-3 (Gal-3) has been identified as a novel biomarker for heart failure and its pharmacological inhibition reduced cardiac fibrosis. Here, we investigated if inhibition of Gal-3 is able to attenuate EndMT in vitro. The expression and function of Gal-3 in TGFβ1-induced EndMT was studied in Human Umbilical Vein Endothelial cells (HUVECs). TGFβ1-induced EndMT leads to increased Gal-3 transcription and expression. siRNA-mediated knockdown of Gal-3 attenuates TGFβ1-induced EndMT whereas recombinant GAL-3 did not induce, not aggravate TGFβ-induced mesenchymal transition. Our findings indicate that intracellular Gal-3 facilitates EndMT, suggesting a role for Gal-3 as transcriptional coactivator in EndMT.

INTRODUCTION

Heart failure (HF) is a clinical syndrome in which the heart is unable to pump a sufficient amount of blood to meet the body's needs. Based on the ejection fraction, the heart failure is classified into the heart failure with preserved, mid-range and reduced ejection fraction (1). Heart failure with preserved ejection fraction (HFpEF) or diastolic dysfunction is more common in older individuals, with risk factors such as hypertension, obesity or coronary artery diseases (2). The pathologic basis of HFpEF is left ventricular remodeling, especially abnormal left ventricular relaxation and an increased left ventricular myocardial stiffness (3). The pathologic basis of the myocardial stiffness in the heart is explained by cardiac fibrosis, which encompasses hyperproliferation of myofibroblasts and excessive deposition of extracellular matrix in the cardiac muscle.

Cardiac fibroblasts are responsible for the production of extracellular matrix (ECM). The ECM serves as a structural scaffold for cardiomyocytes, distributing mechanical forces throughout the cardiac tissue and mediating electronic conduction. The production of ECM is a continuous process where older collagen is broken down and new collagen is deposited (4, 5). However, in response to injuries (e.g. ischemia, hypertension, degeneration etc), fibroblasts undergo a phenotypic transition into myofibroblast (6). Myofibroblasts secrete excessive amounts of collagen and produce alpha smooth muscle actin (αSMA), a protein encoded by the ACTA2 gene. Together with myosin, αSMA forms a contractile complex involved in wound closure (7, 8). The excessive deposition of ECM culminates in several pathologies, such as reduced cardiac contractility, diastolic dysfunction, impaired coronary blood flow and malignant arrhythmias. Altogether, these processes lead to a decrease in tissue compliance and impairs cardiac function, ultimately accelerating the progression of heart failure (9).

The myofibroblasts in cardiac tissue displays a large heterogeneity that can partially be explained by the different origins of the myofibroblasts. Next to resident fibroblasts (10), also bone marrow-derived myofibroblasts (11), circulating monocyte-derived myofibroblasts (12) and endothelium-derived myofibroblasts (13) have been identified. The process by which endothelial cells progressively lose their endothelial functionality and gain myofibroblast-like properties is called endothelial-to-mesenchymal transition (EndMT). A protein associated with heart failure, as well as fibrosis is Galectin-3 (Gal-3), which is encoded by the LGALS3 gene. Increased levels of circulating Gal-3 were measured in heart failure patients (14, 15), and the infusion of Gal-3 into the pericardial sac of rats resulted in increased myocardial fibrosis and cardiac dysfunction(16). Furthermore, the genetic and pharmacological inhibition of Gal-3 in murine models for HFpEF attenuated fibrosis and αSMA expression in fibroblasts compared to the controls(17). Hence, we hypothesized that GAL-3 might be involved in EndMT as an underlying pathological process in cardiac fibrosis. In this study, we investigated effects of Gal-3 on EndMT and identified intracellular Gal3 as a coactivator in TGFb-induced EndMT.

MATERIALS AND METHODS

CELL CULTURE AND STIMULATION

Human umbilical vein endothelial cells (HUVEC, Lonza, Walkersville, MD) were cultured on 1% gelatin-coated (Sigma, #G9391, St. Louis, MO) flasks or wells. Cells were detached using Trypsin EDTA in PBS (TEP, GIBCO #15400054) solution. Experiments were performed between passage 5 to 7. Cells were cultured in endothelial cell medium (ECM) consisting of RPMI 1640 basal medium (Lonza, #BE12-702F, Verviers, Belgium) with heat inactivated Fetal Bovine Serum (Lonza, 20% v/v), Heparin (LEO, #BE013587 5U/ml), Endothelial Cell Growth Factor (ECGF; own preparation 50 µg/ml), penicillin / streptomycin (Gibco, #15140-122, (1%v/v)) and L-Glutamine (Lonza, #BE17-605E 2nM) at 37°C, 5% CO_2.

Unless stated otherwise, TGFβ1 stimulation was performed by culturing cells for 96h in ECM without ECGF, with 10ng mL^{-1} TGFβ1 (R&D systems, #240b, batch 15072). Control conditions were cultured in regular ECM. For recombinant human Gal-3 (rh-Gal-3) stimulation, cells were stimulated with TGFβ1 as described, of which the final 18h of stimulation 20µg/mL rh-Gal-3 (Acro Biosystems, GA3-H5129) was added. During TGFβ1 stimulation, medium was refreshed daily.

SIRNA TRANSFECTION

HUVEC were transfected at 60-80% confluency. Prior to transfection, cells were pre-incubated with Opti-MeM (ThermoFischer, #31985062) at 37°C. siRNA transfection mixes (315.6nM siRNA and 315.7 nM Lipofactamine 2000 (Invitrogen, #19155578)) prepared with either siRNA against Gal-3 (LGAL3 silencer select siRNA, Ambion, #4392421) or the control siRNA (All-star negative control siRNA, Qiagen, #1027281). Transfections were performed by adding 26.3 uL Lipofectamine / siRNA transfection mix per cm^2 culture area. Cells were incubated with transfection mix for 8h at 37°C and 5% CO_2, after which transfection medium was replaced by ECM. After a recovery period of 18h cells were stimulated with TGFβ1 as described earlier.

GENE EXPRESSION ANALYSIS

Cells were lysed in TriZOL (Ambion, #15596-018). RNA was isolated by phenol/chloroform (Emparta) extraction in accordance with the TriZOL manufacturers' guidelines. RNA was precipitated using 75% Ethanol, air-dried and resuspended in RNAse-free water. RNA concentration and purity were determined via Nanodrop 1000 spectrophotometer (Thermo Scientific) and checked the integrity by gel electrophoresis. cDNA was synthesized using the Revert Aid First strand cDNA synthesis kit (Thermo scientific, #K1622) according to the manufacturers guidelines using 500ng RNA as input material. Real-time PCR (ViiA7 Real Time PCR System, Thermo Fischer) was performed by combining cDNA (1ng/µl) with primer master mix (1.2 µm forward and reverse primers, 2x SYBR Green, (Roche, FastStart Universal SYBR Green Master, #04913914001)) in a 1:1 ratio in a total volume of 10µl per well. Data was analyzed using the ViiA7 software (Thermo Scientific) and fold change was calculated using the $2^{-\Delta\Delta C_t}$ method. Primer sequences are shown in table 1.

Gene	Sequence Forward	Sequence Reverse
GAPDH	AGCCACATCGCTCAGACAC	GCCCAATACGACCAAATCC
ACTA2	CTGTTCCAGCCATCCTTCAT	TCATGATGCTGTTGTAGGTGGT
COL3A1	CTGGACCCCAGGGTCTTC	CATCTGATCCAGGGTTTCCA
SNAI1	GCTGCAGGACTCTAATCCAGA	ATCTCCGGAGGTGGGATG
SNAI2	TGGTTGCTTCAAGGACACAT	GTTGCAGTGAGGGCAAGAA
TWIST1	AAGGCATCACTATGGACTTTCTCT	GCCAGTTTGATCCCAGTATTTT
S100A4	CGCTTCTTCTTTCTTGGTTTGA	CGAGTACTTGTGGAAGGTGGA

IMMUNOBLOTTING

Cells were lysed in RIPA buffer (Thermo Scientific, #89901) supplemented with protease inhibitor cocktail (Sigma-Aldrich #P8340, 1:100v/v) and phosphatase inhibitor cocktail (Thermo Fisher Scientific, #78420 (1:250 v/v)). Samples were loaded on 4-20% precast gradient gel (Bio-Rad, #4561083). SDS-PAGE gels were blotted onto nitrocellulose membranes (Bio-Rad, #1704270) using the transblot turbo system (Bio-Rad) according to the guidelines of the manufacturer. Membranes were blocked for 1h in odyssey blocking buffer (Li-Cor #92740000). Membranes were incubated overnight at 4°C with primary antibodies for either Gal-3 (Cell Signaling #87985, 1:500v/v) or β-Actin (Cell signaling 4967L, 1:2000). Membranes were washed three times in TBS with 0.1% tween (Sigma, #p2287) (TBST) and incubated with secondary antibody (goat anti-rabbit IgG [Li-Cor #926-68021] 1:10000 v/v in blocking buffer) for 1h at room temperature. Membranes were washed 2 times with TBST, 1 time with TBS and scanned with the Odyssey® CLx (Li-Cor), using the 700 nm channel. Scans were analyzed using Image Studio lite edition (Odyssey, V5.2).

IMMUNOFLUORESCENCE

12 Hours prior to immunofluorescence analysis, transfected and stimulated HUVEC were re-seeded at 80% confluency in NUNC LAB-TEK 8 well chamber slides (Sigma-Aldrich, C7182-1CS). After overnight incubation, cells were fixed with 2% paraformaldehyde for 20 min and permeabilized with 0.5% Triton X in PBS for 5 min. Samples were blocked in 3% Bovine Serum Albumin (Sanquin, #800228065) in PBS for 20 min, and incubated with primary antibodies against Collagen 3 (Cell Signaling, #ab7778 1:50 v/v), or eNOS (BD Pharmingen, #610299 1:100v/v) diluted in PBS containing 2% BSA for 1 hour at room temperature. Cells were washed with PBS and incubated with Goat anti-Rabbit IgG (H+L) Alexa Fluor 594 secondary antibody (Invitrogen, #A11037 1:500 v/v) and DAPI (Sigma-Aldrich #D9542 1:5000v/v) in PBS containing 2% BSA for 20 minutes at RT. Image was taken via Leica DM2000 immunofluorescence microscopy.

FLOW CYTOMETRY

Cells were harvested by trypsinization and incubated with CD31-PE (IQ Products, #IQP-552R50 1:10 v/v) and matching isotype controls (IQ Products, #IQP-191 1:20 v/v) in FACS Buffer (2mM EDTA (Sigma, #ED-100G) and 0.5% FBS in PBS) at 4°C for 30 min. Cells were washed in FACS buffer, fixed in 2% PFA (w/v) in PBS for 20 min, washed in FACS buffer, permeabilized in (0.1% Saponin (Sigma, 47036-50G-F), 0.5% FBS in PBS) for 10 min, incubated for 30 min at 4°C with αSMA (Abcam, #Ab7817 (1:50v/v)) and FSP1 (Biorbyt, #ORB88159(1:250 v/v)) conjugated to FITC using the FITC conjugation kit (Abcam, #188285) prior to the staining. Samples were analyzed on a BD FACSCALIBUR flow cytometer. Analysis was performed using Kaluza analysis software (Beckman)

ANGIOGENIC SPROUTING CAPACITY

µ-Slides (Ibidi, #81506) were coated with 10 µl Matrigel (Corning, #354248)) and allowed to solidify for 1 hour. Cells were harvested by trypsinization and seeded at a density of 15.000 cells per well. Images were recorded 24h post-seeding. Sprouting capability was quantified by counting complete hexagonal shapes.

STATISTICAL ANALYSIS

Data are presented as means± s.e.m. Multiple comparison one-way ANOVA was performed to evaluate the difference between groups and p-values < 0.05 were considered to statistically significant.

RESULTS

TGFβ1 INDUCES GAL-3 EXPRESSION IN ENDOTHELIAL CELLS

In order to study the effect of a Gal-3 on EndMT, we induced siRNA mediated knockdown of *LGALS3*. Silencing of Gal-3 in endothelial cells reduced *LGALS3* gene expression to an almost undetectable level (fig. 1a) and a 5-fold ($p=0.549$) decrease at the protein level was observed. These findings indicate that siRNA mediated intracellular Gal-3 silencing was effective. The TGFβ is main inducer of EndMT, hence we questioned whether TGFβ modulates Gal-3 expression. TGFβ1 stimulation increased the expression of LGALS3 (~3-fold,$p<0.05$) and protein expression of Gal-3 ($p<0.01$) compared to unstimulated controls (fig. 1a and fig.1b). These results indicate that TGFβ1 induce Gal-3 gene and protein expression in endothelial cells.

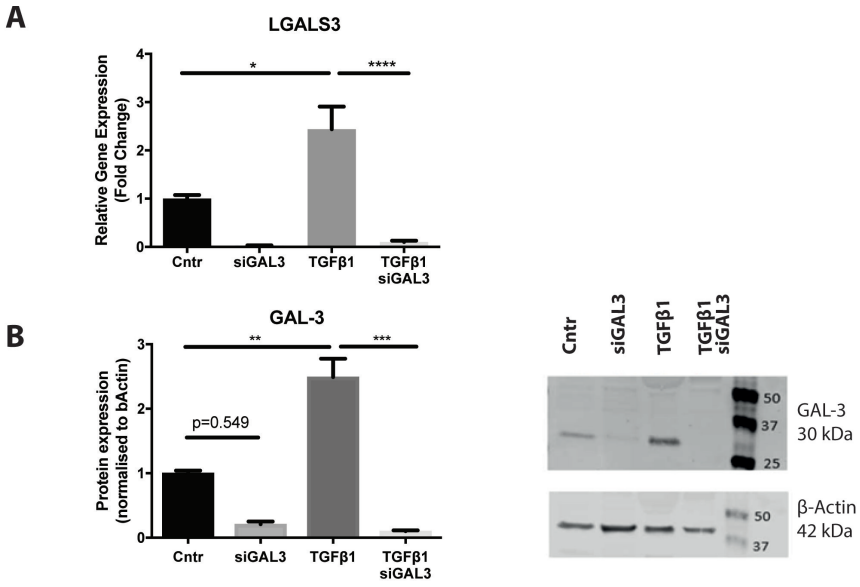

Figure 1. GAL-3 expression is induced by TGFβ1 and successfully inhibited by siGAL3. ***a)*** *LGALS3 expression levels were determined by quantitative RT-PCR. Under TGFβ1 stimulation, GAL3 is upregulated, whereas siGAL transfection successfully decreased GAL3 expression.* ***B)*** *Representative western blots of Gal-3 expression. Quantified GAL-3 protein expression normalized against β-actin. Statistical analysis in this picture: one-way ANOVA test *p<0.05, **p<0.01, ***p<0.001 and ****p<0.0001*

6

siGAL-3 INDUCED KNOCKDOWN OF GAL-3 ATTENUATES ENDMT PROGRESSION

Since Gal-3 expression increased upon TGFβ1 stimulation, we studied its effect on EndMT. TGFβ1-induces EndMT in HUVEC via the canonical and non-canonical pathway. HUVECs deficient in GAL-3 had lower expression levels ACTA2 ($p< 0.05$), S100A4 ($p< 0.01$), and COL3A1 ($p< 0.01$), as compared to TGFβ1-treated cells (fig. 2a). At the protein level, αSMA ($p< 0.0001$) and FSP1 ($p< 0.001$) expression was increased in endothelial cells treated with TGFβ1 compared to control HUVECs. Knockdown of GAL-3 reduced the TGFb-induced expression of αSMA ($p< 0.01$), FSP1 ($p< 0.05$) (fig. 2b) and Collagen III (fig. 2c).

EndMT is not only characterized by the increased mesenchymal gene expression but also by the loss of endothelial specific gene expression and functions. eNOS expression was higher in Gal-3 decifient cells compared to their control HUVECs. TGFβ1-treatment abrogated eNOS expression and siRNA against Gal-3 mildly rescued the TGFβ1-induced eNOS decline. (fig. 2d)

Moreover, TGFβ1-stimulation lead to less angiogenic sprouting capacity of endothelial cells compared to unstimulated controls. A knockdown of Gal-3 slightly improved the angiogenic sprouting capability after 24h (fig. 2e, fig. 2f). Combined, these data indicate that Gal-3 inhibition attenuates EndMT.

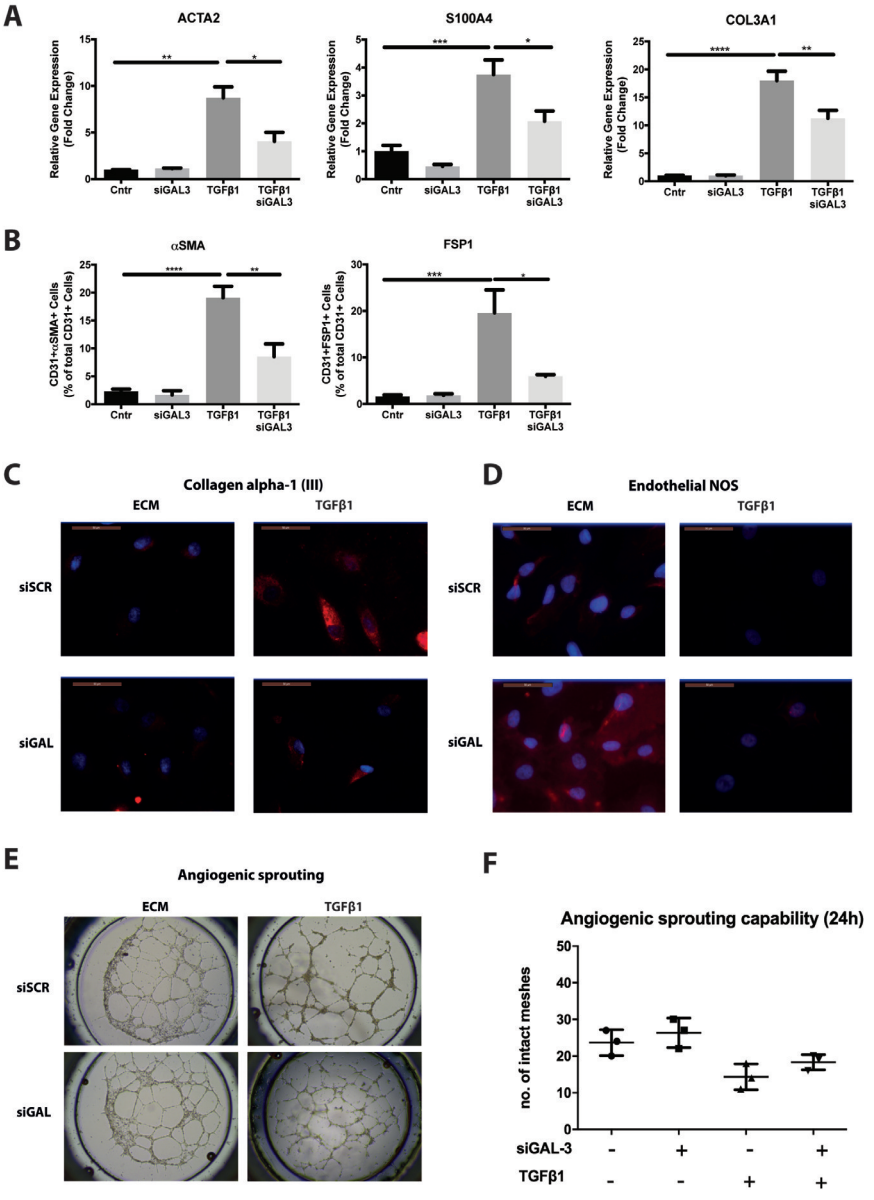

Figure 2. siGAL3 mediated knockdown of Gal-3 attenuates EndMT progression. a) *ACTA2, S100A4 and COL3A1 transcription levels were determined by quantitative RT-PCR and normalized against its control conditions. siGAL3 attenuates TGFβ1 induced ACTA2, S100A4 and COL3A1 transcriptional increment.* ***b)*** *Gal-3 deficient endothelial cells have significantly lower expression of αSMA and FSP1 upon TGFβ1 stimulation compared to TGFβ1 stimulated negative controls* ***c)*** *Collagen III level was evaluated by the immunofluorescence staining and DAPI (blue) and COL3A1 (red) are shown. Upon TGFβ1 stimulation Collagen III protein expression increases, whereas this increment is attenuated by the siRNA against GAL-3.* ***d)****. Representative immunofluorescence images of DAPI (blue) and eNOS (red). TGFβ1 stimulation reduces eNOS expression, whereas a knockdown of Gal-3 directly increases eNOS expression compared to ECM control conditions.* ***e)*** *Representative bright field images of sprouting capabili-*

ties of HUVECs. Although it is not statistically significant, the TGFβ1 treated cells lose their endothelial functionality compared to their controls. There has tendency that siGAL3 attenuates the loss of endothelial functionality. ***f)*** *Quantification of angiogenic sprouting capability by scoring intact meshes after 24h. Statistical analysis in this figure: one-way ANOVA test *p<0.05, **p<0.01, ***p<0.001 and ****p<0.000*

EXTRACELLULAR GAL-3 DOES NOT MODULATE TGFB1-INDUCED ENDMT

Galectin-3 facilitates EndMT, albeit through an unknown mechanism. We investigated if Gal-3 signaling through its receptors might induce or aggravate of EndMT by treating HUVEC with recombinant Gal3. rhGAL3 did not induce the expression of αSMA and FSP1 in control endothelial cells, nor did the addition of rhGal3 aggravate the TGFβ1-induced expression of αSMA and FSP1. These findings suggest that extracellular GAL3 does not influence EndMT, but rather intracellular levels of GAL3 modulate EndMT in vitro (fig. 3).

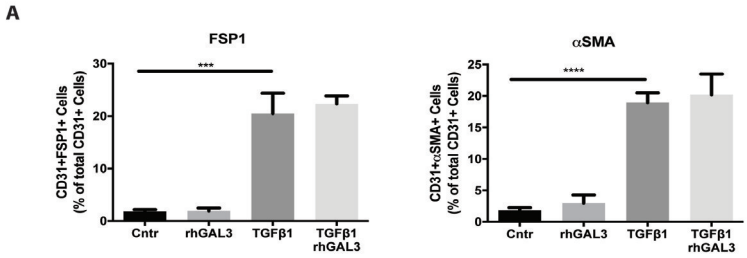

Figure 3. Extracellular Gal-3 doesn't modulate EndMT. *Population of cells undergoing EndMT were analyzed via flow cytometry by double staining for endothelial marker CD31 and mesenchymal marker aSMA or FSP1. TGFβ1-induced aSMA and FSP1 expressions is unaltered by rh-Gal-3. *p<0.05, **p<0.01, ***p<0.001 and ****p<0.0001*

ENDMT TRANSCRIPTION FACTOR SNAI1, SNAI2 AND TWIST1 ARE MODULATED VIA INTRACELLULAR GAL-3

GAL3 knockdown had no direct effect on the expression of the EndMT transcription factors Snai1, Snai2 and Twist1, whereas TGFβ1 stimulation increased their expression. TGFβ1 -stimulated endothelial cells that were deficient in GAL3 had reduced expression levels of SNAI1 (p< 0.01), SNAI2 (p< 0.05) and TWIST1 (p=0.512), indicating that GAL3 is involved in the transmission of TGFβ1 -induced signaling. (fig. 4) These findings suggest that intracellular Gal-3 might be a transcriptional coactivator to TGFβ during EndMT.

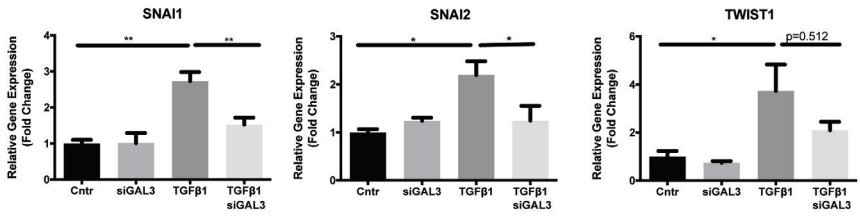

Figure 4. Gal-3 modulate EndMT transcription factors expression in endothelial cells. *SNAI1, SNAI2 and TWIST1 gene expression levels were determined by quantitative RT-PCR and data is normalized to GAPDH. TGFβ1 increased expression of SNAI1, SNAI2 and TWIST1 gene expression and siGAL-3 normalized the expression. *p<0.05, **p<0.01, ***p<0.001*

DISCUSSION

In this study we found that Gal-3 facilitates TGFβ-induced EndMT. In the absence of TGFβ, Gal-3 does not induce or aggravate EndMT, however in the presence of TGFβ the loss of GAL3 expression inhibits EndMT. In contrast, rhGAL3 didn't show any effect on both control and TGFβ - stimulated condition, suggesting that this modulation is happening through intracellular Gal-3. Moreover, our data suggests the GAL3 is not an independent modifier of EndMT, but rather acts as an intracellular modulator of TGFβ signaling.

In this study, gene expression and immunoblotting analysis clearly showed that Gal-3 expression was induced by TGFβ1. We also showed that a knockdown of Gal-3 is able to attenuate the expression of EndMT-related transcription factors SNAI1, SNAI2 and TWIST1. However, it remains elusive how GAL-3 modulates this gene expressions. Transcriptional control of fibrosis encompasses a highly interactive multi-protein signaling system including TGFβ, WNT, YAP/TAZ and other signaling mechanism (18). (19). Herein, Gal-3 can bind to the β-catenin/Tcf complex and facilitate its nuclear translocation (20). β-catenin is an important part of the WNT signaling cascade and this finding may explain the merge between TGFβ and WNT signaling in cardiac fibrosis. During idiopathic pulmonary fibrosis, Gal-3 inhibition prevented TGFβ and bleomycin-induced fibrosis via β-catenin phosphorylation and nuclear translocation(21). Combined, these data suggest that during EndMT, GAL3 might act as a transcriptional coactivator for TGFβ signaling. Further research will be needed to identify its signaling partners.

In conclusion, we show here that intracellular Gal-3 facilitates TGFβ-induced endothelial-mesenchymal transition in endothelial cells, possibly via the potentiation of TGFβ signaling.

REFERENCES

1. Ponikowski P, Voors AA, Anker SD, Bueno H, Cleland JG, Coats AJ, et al. 2016 ESC Guidelines for the diagnosis and treatment of acute and chronic heart failure: The Task Force for the diagnosis and treatment of acute and chronic heart failure of the European Society of Cardiology (ESC) Developed with the special contribution of the Heart Failure Association (HFA) of the ESC. European heart journal. 2016;37(27):2129-200.
2. Dunlay SM, Roger VL, Redfield MM. Epidemiology of heart failure with preserved ejection fraction. Nature Reviews Cardiology. 2017;14(10):591.
3. Zile MR, Baicu CF, Gaasch WH. Diastolic heart failure—abnormalities in active relaxation and passive stiffness of the left ventricle. New England Journal of Medicine. 2004;350(19):1953-9.
4. Travers JG, Kamal FA, Robbins J, Yutzey KE, Blaxall BC. Cardiac fibrosis. Circulation research. 2016;118(6):1021-40.
5. Vasquez C, Benamer N, Morley GE. The cardiac fibroblast: functional and electrophysiological considerations in healthy and diseased hearts. Journal of cardiovascular pharmacology. 2011;57(4):380.
6. Leask A. Getting to the Heart of the Matter. Circulation research. 2015;116(7):1269-76.
7. Desmoulière A, Geinoz A, Gabbiani F, Gabbiani G. Transforming growth factor-beta 1 induces alpha-smooth muscle actin expression in granulation tissue myofibroblasts and in quiescent and growing cultured fibroblasts. The Journal of cell biology. 1993;122(1):103-11.
8. Santiago JJ, Dangerfield AL, Rattan SG, Bathe KL, Cunnington RH, Raizman JE, et al. Cardiac fibroblast to myofibroblast differentiation in vivo and in vitro: expression of focal adhesion components in neonatal and adult rat ventricular myofibroblasts. Developmental dynamics. 2010;239(6):1573-84.
9. Krenning G, Zeisberg EM, Kalluri R. The origin of fibroblasts and mechanism of cardiac fibrosis. Journal of cellular physiology. 2010;225(3):631-7.
10. Fredj S, Bescond J, Louault C, Potreau D. Interactions between cardiac cells enhance cardiomyocyte hypertrophy and increase fibroblast proliferation. Journal of cellular physiology. 2005;202(3):891-9.
11. Van Amerongen M, Bou-Gharios G, Popa E, Van Ark J, Petersen A, Van Dam G, et al. Bone marrow-derived myofibroblasts contribute functionally to scar formation after myocardial infarction. The Journal of pathology. 2008;214(3):377-86.
12. van Amerongen MJ, Harmsen MC, van Rooijen N, Petersen AH, van Luyn MJ. Macrophage depletion impairs wound healing and increases left ventricular remodeling after myocardial injury in mice. The American journal of pathology. 2007;170(3):818-29.
13. Zeisberg EM, Tarnavski O, Zeisberg M, Dorfman AL, McMullen JR, Gustafsson E, et al. Endothelial-to-mesenchymal transition contributes to cardiac fibrosis. Nature medicine. 2007;13(8):952.
14. Lok DJ, Lok SI, Badings E, Lipsic E, van Wijngaarden J, de Boer RA, et al. Galectin-3 is an independent marker for ventricular remodeling and mortality in patients with chronic heart failure. Clinical Research in Cardiology. 2013;102(2):103-10.
15. van Kimmenade RR, Januzzi JL, Ellinor PT, Sharma UC, Bakker JA, Low AF, et al. Utility of amino-terminal pro-brain natriuretic peptide, galectin-3, and apelin for the evaluation of patients with acute heart failure. Journal of the American College of Cardiology. 2006;48(6):1217-24.
16. Liu Y-H, D'Ambrosio M, Liao T-d, Peng H, Rhaleb N-E, Sharma U, et al. N-acetyl-seryl-aspartyl-lysyl-proline prevents cardiac remodeling and dysfunction induced by galectin-3, a mammalian adhesion/growth-regulatory lectin. American Journal of Physiology-Heart and Circulatory Physiology. 2009;296(2):H404-H12.

17. Yu L, Ruifrok WP, Meissner M, Bos EM, van Goor H, Sanjabi B, et al. Genetic and pharmacological inhibition of galectin-3 prevents cardiac remodeling by interfering with myocardial fibrogenesis. Circulation: Heart Failure. 2012:CIRCHEARTFAILURE. 112.971168.
18. Piersma B, Bank RA, Boersema M. Signaling in fibrosis: TGF-β, WNT, and YAP/TAZ converge. Frontiers in medicine. 2015;2:59.
19. Kovacic JC, Mercader N, Torres M, Boehm M, Fuster V. Epithelial-to-mesenchymal and endothelial-to-mesenchymal transition: from cardiovascular development to disease. Circulation. 2012;125(14):1795-808.
20. Shimura T, Takenaka Y, Tsutsumi S, Hogan V, Kikuchi A, Raz A. Galectin-3, a novel binding partner of β-catenin. Cancer research. 2004;64(18):6363-7.
21. MacKinnon AC, Gibbons MA, Farnworth SL, Leffler H, Nilsson UJ, Delaine T, et al. Regulation of transforming growth factor-β1–driven lung fibrosis by galectin-3. American journal of respiratory and critical care medicine. 2012;185(5):537-46.

Chapter 7

Research summary

RESEARCH SUMMARY

The ultimate goal of cardiovascular medicine is to reduce the global burden of cardiovascular disease and to improve the patients' quality-of-life. Fundamental to the development of successful medical treatments for cardiovascular diseases is an in-depth knowledge of the disease process, i.e. knowledge on the molecular signaling cascades in healthy cells and an in-depth understanding of how these molecular pathways get disturbed during disease. Endothelial homeostasis plays crucial role in vascular health by preventing unwarranted thrombosis, inflammation and regulating vascular tone. Endothelial dysfunction is a culprit in the development of many cardiovascular pathologies (1-3). Hence, insight into the molecular mechanisms that underlie endothelial dysfunction might allow for the discovery of innovative drugable targets to reduce the cardiovascular disease burden.

Adverse endothelial plasticity and its specialized form Endothelial-mesenchymal transition (EndMT) contributes to the development of multiple cardiovascular diseases including atherosclerosis (4, 5) and cardiac fibrosis (6). The pleiotropic cytokine TGFβ(7), inflammation (8) and oxidative stress (9) are established inducers of EndMT through the activation of canonical and non-canonical TGFβ signaling and the concurrent induction of mesenchymal gene expression by the transcription factors SNAIL, SLUG, TWIST1 and GATA4 (10, 11). The induction of gene expression is not only regulated by changes in transcription factor binding to the DNA, but also by the accessibility of the DNA to these transcription factors, which is tightly regulated by epigenetics. (**Chapter 1 and Chapter 2**) Epigenetic modifications, through changes in histone tail modifications and DNA methylation, facilitate the compaction and decompaction of the DNA, thereby orchestrating its accessibility to transcription factors. Furthermore, transcribed genes are not always translated into proteins, as non-coding RNAs might induce posttranscriptional inhibition. In **Chapter 2**, we proposed to therapeutically target epigenetic enzymes in the pro-atherogenic endothelium to ameliorate atherosclerosis development. We used the histone methyltransferase EZH2 and the histone deacetylase SIRT1 to exemplify how their pleiotropic functions can preclude atherosclerosis pathways and safeguard endothelial homeostasis.

In following chapters, we investigated the molecular mechanisms that drive EndMT with a focus on the multi-layered regulatory system consisting of epigenetic and post-transcriptional modifications. Furthermore, we investigated how these mechanisms contribute to the development of intimal hyperplasia and cardiac fibrosis.

ADVERSE ENDOTHELIAL PLASTICITY CONTRIBUTES TO THE DEVELOPMENT OF INTIMAL HYPERPLASIA

Intimal hyperplasia is an initiating event of atherosclerosis development and yet the molecular epigenetic mechanism is still elusive. Intimal hyperplasia is the consequence of migration and proliferation of fibro-proliferative cells in the tunica intima and which thickens the vascular wall (12). The origin of these fibro-proliferative cells is extensively investigated, and at least four types of cells are shown to give rise myofibroblast-like cells in the hyperplastic intima, i.e. resident fibroblasts, smooth muscle cells, endothelial cells and circulating progenitor cells. Vein grafting in an arterial environment by the

coronary artery bypass surgery (CABG) can trigger intimal hyperplasia and occlude the grafted vein (13), suggesting the importance of the EndMT in development of intimal hyperplasia. Also, endothelium-derived fibroproliferative cells accumulate in vascular areas exposed to low oscillatory shear stress where intimal hyperplasia is eminent (5) (14). Vice versa, vascular areas exposed to high laminar shear stress contain quiescent endothelial cells that are refractory to EndMT (14). Collectively, these data imply that fluid shear stress is a pivotal determinant of EndMT.

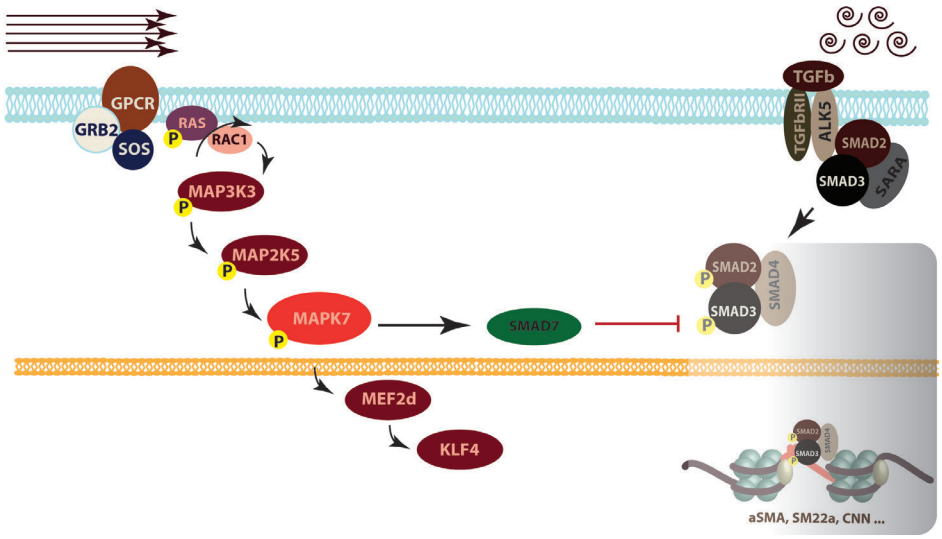

Figure 1. High laminar shear stress-induced MAPK7 activation precludes TGFβ-induced Endothelial-Mesenchymal transition. *Upon high laminar shear stress, endothelial MAPK7 signaling is activated. The downstream transcription factors of MAPK7, such as KLF4, are known to induce production of nitric oxide. The activation of MAPK7 signaling further results in the inhibition of TGFβ signaling by SMAD2/SMAD3, thereby inhibiting EndMT (14)*

In **Chapter 3**, we uncovered that at sites of intimal hyperplasia, MAPK7 expression and activity is silenced by microRNA-374b. MicroRNA-374b expression is induced by TGFβ and silences 4 target genes in the MAPK7 signaling cascade, i.e. MAP3K3, MAPK7, MEF2D and KLF4. Ectopic expression of microRNA-374b in endothelial cells, induces EndMT in the absence of exogenous TGFβ, suggesting that the microRNA-374b-dependent silencing of MAPK7 signaling is pivotal to intimal hyperplasia. Indeed, the expression of microRNA-374b is increased in experimental models of intimal hyperplasia where MAPK7 signaling is lost. (Figure 2). Moreover, in patients suffering from coronary artery disease, the expression of microRNA-374b associates with disease severity and with a decreased expression of MAPK7.

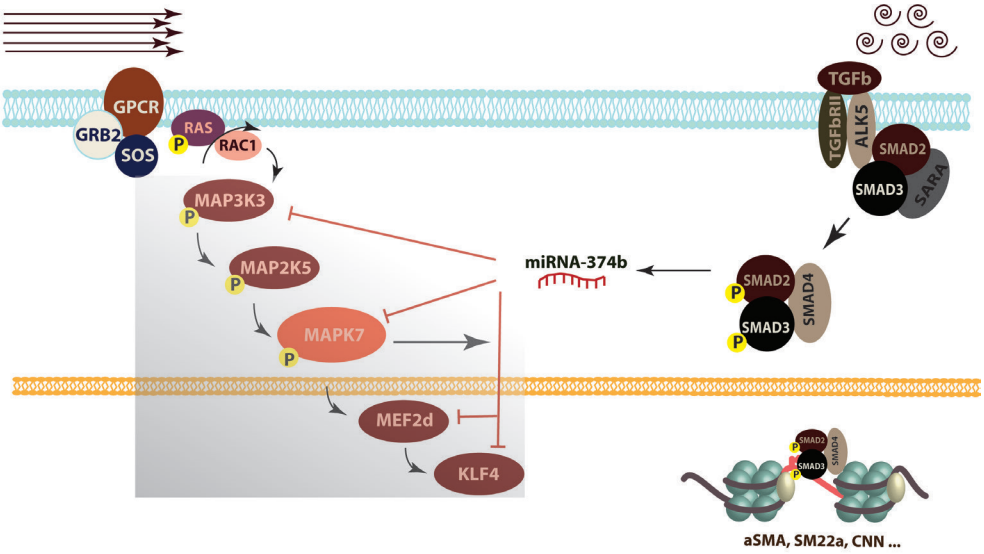

Figure 2. MicroRNA - 374b inhibits MAPK7 signaling and induces EndMT. *MicroRNA-374b is induced upon TGFβ1 stimulation and silences 4 members of the MAPK7 signaling cascade. This silencing mechanism explains how the MAPK7 signaling cascade is silenced by TGFβ in endothelial cells.*

Intimal hyperplasia is progressive process, which narrows the vascular lumen by the accumulation of fibroproliferative cells. How endothelium-derived fibroproliferative cells lose their quiescence and acquire this hyper-proliferative behavior is still elusive.

In **Chapter 4**, we uncovered that under atheroprotective - high laminar shear stress, the expression of the histone methyltransferase EZH2 is decreased. EZH2 is an epigenetic enzyme that tri-methylates lysine 27 on histone 3 (H3K27me3), which results in transcriptional repression (15). The increase in EZH2 is associated with elevated expression of cell cycle genes and increased proliferation of endothelial cells. It is still elusive how the reduction in EZH2 can result in a reduced cell cycling ability of endothelial cells, we conclude that the high laminar shear stress-dependent decrease in EZH2 expression facilitates endothelial quiescence (16). (Figure 3)

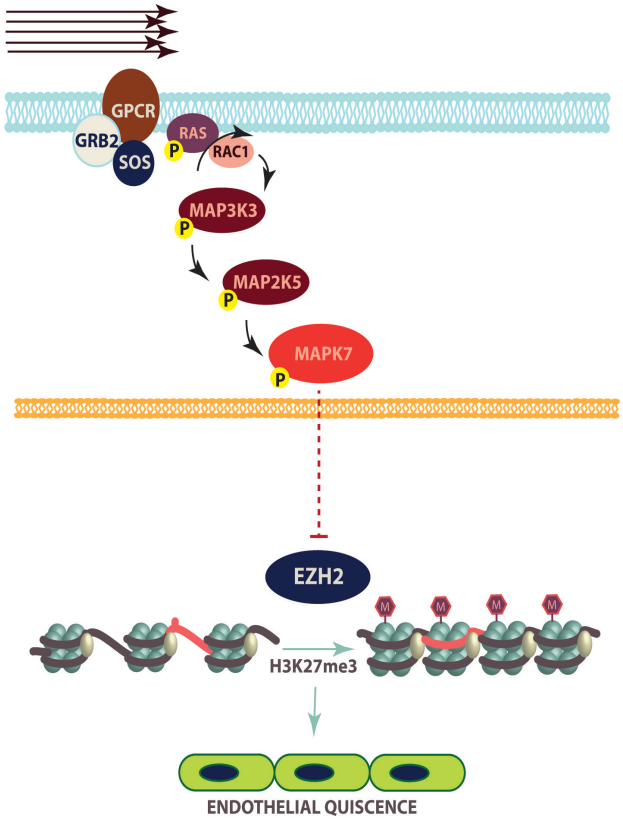

Figure 3. Uniform laminar shear stress mediated endothelial quiescence is mediated by the EZH2 decline. *Under the shear stress MAPK7 get phosphorylated and activated. This activation led to the decline in histone methyltransferase EZH2 protein level. RNA sequencing result revealed that both EZH2 decline and high laminar shear stress can inhibit cell cycle genes, which may explain to a certain extend how endothelial cells acquire endothelial quiescence.*

In Chapter 4, we noted that there was reciprocity between MAPK7 signaling and EZH2 expression, which cannot be explained by a direct interaction. Therefore, in **Chapter 5**, we investigated the reciprocity between MAPK7 and EZH2. Uniform laminar shear stress induces the MAPK7-dependent expression of microRNA-101 that silences EZH2 expression. Reciprocally, the loss of EZH2 expression results in the expression of microRNAs that target *DUSP1* and *6*, which inactivate MAPK7. In human coronary artery stenosis, *EZH2*, *DUSP1* and *DUSP6* level are increased whereas *MAPK7* expression is reduced. Moreover microRNA-101 expression is decreased which is associated with an increase in *EZH2* and the severity of the stenosis. These data might explain the difference in the development of intimal hyperplasia at sites exposed of high laminar shear stress and low oscillatory shear stress (Figure 4).

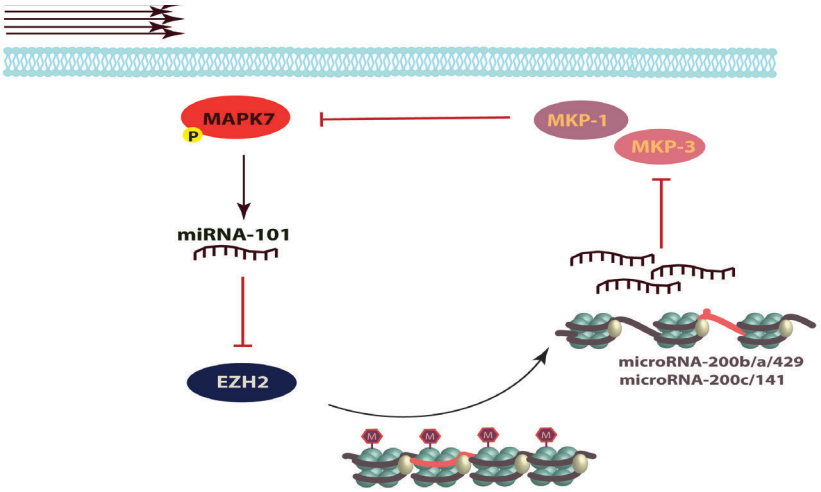

Figure 4. Reciprocal crosstalk between pMAPK7 and EZH2. Upon high laminar shear stress MAPK7 gets activated which induces the expression of miR-101. *Consequentially, the expression of EZH2 is silenced. On the other hand, EZH2 modulates the expression of miRNAs through H3k27me3 – a repressive chromatin mark. The decline of EZH2 leads to open chromatin, which elevates the expression level of these microRNAs. The microRNAs further silence the DUSP1 and DUSP6. This leads less protein expression of MKP-1 and MKP-3 which removes MAPK7 phosphorylation mark, thereby MAPK7 phosphorylation kept high.*

ADVERSE ENDOTHELIAL PLASTICITY IN CARDIAC FIBROSIS

Cardiac fibrosis is the fundamental pathology underlying heart failure for which no effective treatment is currently available. Plasma Galectin-3 levels are associated with all-cause mortality rate and recognized as a prognostic biomarker of cardiac fibrosis(17). GAL-3 knockdown attenuates cardiac fibrosis, indicating that Gal3 is not only a biomarker, but also a key molecule in the initiation of cardiac fibrosis (18). It has been reported that during cardiac fibrosis myofibroblast are derived from the endothelial lineage through EndMT(6). Hence, in **Chapter 6**, we investigated if Gal-3 could induce of EndMT. Although Gal-3 is generally believed to signal through a number of receptors, the addition of recombinant human Gal-3 did not induce or aggravate EndMT. In contrast, the loss of endogenous Gal-3 precluded TGFβ-induced EndMT via unknown mechanism. These data suggest that Gal-3 might act as a transcriptional co-activation during TGFβ-induced EndMT (19, 20), which is currently under investigation

CONCLUSIONS

Endothelial-mesenchymal transition is a crucial component of atherosclerosis and cardiac fibrosis development and shown to be modulated by fluid shear stress. In this thesis, we show that endothelial-mesenchymal transition is regulated on multiple

levels by MAPK7, EZH2 and microRNAs and found dysregulation of these factors in experimental models of intimal hyperplasia and in human coronary artery disease. We uncovered a number of pivotal regulators of EndMT that might have therapeutic potential to ameliorate intimal hyperplasia and cardiac fibrosis.

REFERENCES

1. Gimbrone MA, Topper JN, Nagel T, Anderson KR, GARCIA-CARDEÑA G. Endothelial dysfunction, hemodynamic forces, and atherogenesis. Annals of the New York Academy of Sciences. 2000;902(1):230-40.
2. Sena CM, Pereira AM, Seiça R. Endothelial dysfunction—a major mediator of diabetic vascular disease. Biochimica et Biophysica Acta (BBA)-Molecular Basis of Disease. 2013;1832(12):2216-31.
3. Vanhoutte P, Shimokawa H, Feletou M, Tang E. Endothelial dysfunction and vascular disease–a 30th anniversary update. Acta Physiologica. 2017;219(1):22-96.
4. Chen P-Y, Qin L, Baeyens N, Li G, Afolabi T, Budatha M, et al. Endothelial-to-mesenchymal transition drives atherosclerosis progression. The Journal of clinical investigation. 2015;125(12):4514.
5. Evrard SM, Lecce L, Michelis KC, Nomura-Kitabayashi A, Pandey G, Purushothaman K-R, et al. Endothelial to mesenchymal transition is common in atherosclerotic lesions and is associated with plaque instability. Nature communications. 2016;7.
6. Zeisberg EM, Tarnavski O, Zeisberg M, Dorfman AL, McMullen JR, Gustafsson E, et al. Endothelial-to-mesenchymal transition contributes to cardiac fibrosis. Nature medicine. 2007;13(8):952.
7. Arciniegas E, Sutton AB, Allen TD, Schor AM. Transforming growth factor beta 1 promotes the differentiation of endothelial cells into smooth muscle-like cells in vitro. Journal of cell science. 1992;103(2):521-9.
8. Maleszewska M, Moonen J-RA, Huijkman N, van de Sluis B, Krenning G, Harmsen MC. IL-1β and TGFβ2 synergistically induce endothelial to mesenchymal transition in an NFκB-dependent manner. Immunobiology. 2013;218(4):443-54.
9. Lee ES, Boldo LS, Fernandez BO, Feelisch M, Harmsen MC. Suppression of TAK1 pathway by shear stress counteracts the inflammatory endothelial cell phenotype induced by oxidative stress and TGF-β1. Scientific Reports. 2017;7:42487.
10. Souihol CE, Harmsen MC, Evans PC, Krenning G. Endothelial-Mesenchymal Transition in Atherosclerosis. Cardiovascular research. 2018.
11. Medici D, Potenta S, Kalluri R. Transforming growth factor-β2 promotes Snail-mediated endothelial–mesenchymal transition through convergence of Smad-dependent and Smad-independent signalling. Biochemical Journal. 2011;437(3):515-20.
12. Ross R, Glomset JA. Atherosclerosis and the arterial smooth muscle cell. Science. 1973;180(4093):1332-9.
13. Cooley BC, Nevado J, Mellad J, Yang D, Hilaire CS, Negro A, et al. TGF-β signaling mediates endothelial-to-mesenchymal transition (EndMT) during vein graft remodeling. Science translational medicine. 2014;6(227):227ra34-ra34.
14. Moonen J-RA, Lee ES, Schmidt M, Maleszewska M, Koerts JA, Brouwer LA, et al. Endothelial-to-mesenchymal transition contributes to fibro-proliferative vascular disease and is modulated by fluid shear stress. Cardiovascular research. 2015;108(3):377-86.
15. Di Croce L, Helin K. Transcriptional regulation by Polycomb group proteins. Nature structural & molecular biology. 2013;20(10):1147-55.
16. Maleszewska M, Vanchin B, Harmsen MC, Krenning G. The decrease in histone methyltransferase EZH2 in response to fluid shear stress alters endothelial gene expression and promotes quiescence. Angiogenesis. 2016;19(1):9-24.
17. Ho JE, Liu C, Lyass A, Courchesne P, Pencina MJ, Vasan RS, et al. Galectin-3, a marker of cardiac fibrosis, predicts incident heart failure in the community. Journal of the American College of Cardiology. 2012;60(14):1249-56.

18. Yu L, Ruifrok WP, Meissner M, Bos EM, van Goor H, Sanjabi B, et al. Genetic and pharmacological inhibition of galectin-3 prevents cardiac remodeling by interfering with myocardial fibrogenesis. Circulation: Heart Failure. 2012:CIRCHEARTFAILURE. 112.971168.
19. MacKinnon AC, Gibbons MA, Farnworth SL, Leffler H, Nilsson UJ, Delaine T, et al. Regulation of transforming growth factor-β1–driven lung fibrosis by galectin-3. American journal of respiratory and critical care medicine. 2012;185(5):537-46.
20. Shimura T, Takenaka Y, Tsutsumi S, Hogan V, Kikuchi A, Raz A. Galectin-3, a novel binding partner of β-catenin. Cancer research. 2004;64(18):6363-7.

Chapter 8

EPILOGUE

OUTCOME OF THIS THESIS

In this thesis, we studied the mechanisms that safeguard endothelial homeostasis with a focus on the signaling induced by laminar shear stress. We uncovered an intrinsic multi-layered mechanism that encompasses classical signal transduction and converges with regulatory mechanisms depending on epigenetics and posttranscriptional repression. Dysregulation of these mechanisms culminate in endothelial to mesenchymal transition (EndMT) and might contribute to the development of intimal hyperplasia and cardiac fibrosis. The in-depth knowledge on the factors that induce, facilitate or aggravate EndMT may contributes to the development of novel therapeutic approaches to treat intimal hyperplasia and cardiac fibrosis in the future.

MOLECULAR INSIGHTS ON ADVERSE ENDOTHELIAL PLASTICITY – POSSIBLE TARGET?

Despite the fact that endothelial cells throughout the body have the same origin – the hemangioblast (1) - there are distinct functional and structural differences between endothelial cells originating from their function in specific organs or the microenvironment the endothelial cells are in (2). This cellular heterogeneity is a reflection of the physiological endothelial plasticity and enables the optimal functioning of the residing organ(3). For instance, the endothelium in the blood-brain barrier forms a non-fenestrated endothelial layer which is impermeable to toxic substances thereby safeguarding the proper functioning of the brain(4), whereas a highly fenestrated endothelial layer is present in the liver sinusoid that enables the fast uptake of metabolites, plasma proteins and even drug molecules by the hepatocytes and hepatic satellite cells(5).

In the medium and large sized arteries, non-fenestrated endothelial cells reside on the basement membrane and align to the direction of blood flow. The biomechanical signal originating from the laminar shear stress sensed by the endothelium, is a key driving force of signaling pathways by which the endothelium safeguards the vascular integrity (e.g. endothelial cell-cell junctions and anti-inflammatory signaling) and maintains the blood flow (e.g. vasodilatory and anti-thrombogenic pathways). It is well established that at sites of vascular curvatures and bifurcation, endothelial cells are exposed to low and oscillatory shear stress(LOSS)(6, 7) and might undergo endothelial-mesenchymal transition(8), an adverse form of plasticity. Endothelial cells exposed to LOSS induce the expression of proinflammatory genes while reducing antioxidant gene expression (9-11). This distinct change in gene expression profile can partly be explained by the activities of the LOSS-induced transcription factors SMAD2/3 (12), SNAI1 (8), TWIST (13) and others. We uncovered that EZH2-dependent (Chapter 4 and 5) H3K27me3 bears important role in modulating the expression of protein coding genes as well as the microRNAs in response to the loss of laminar shear stress, thereby modulate endothelial quiescence (14).

EndMT contributes to the development of several pathologies including intimal hyperplasia, atherosclerosis, cardiac fibrosis and other fibroproliferative diseases. The intrinsic EndMT inhibitors therefore bear a therapeutic potential, which needs to be

further characterized in atherosclerosis and cardiac fibrosis models. The future looks bright because we and other researchers recognized intrinsic protectives signaling molecules such as pMAPK7(15), BMP7(16) and FGFRI (17) are capable of inhibiting EndMT. In this thesis, we uncovered that a combination of microRNA miR-101, miR-200a and miR-141 can preclude EndMT in endothelial cell models. Moreover, we uncovered that the antimir-374b inhibits the induction of EndMT in endothelial cell. These data suggest that microRNA mimetics or antimiRs might have anti-atherosclerosis potential through the maintenance of endothelial homeostasis. MicroRNAs "fine-tune" key signaling cascades and their therapeutic potential is exemplified in preclinical atherosclerosis models (18). For instance, miR-92a is a flow responsive microRNA that targets the mRNA of transcription factors KLF2 and KLF4, which are essential to endothelial homeostasis. The specific inhibition of miR-92a ameliorates endothelial activation and reduces plaque size in LDLR-/- mice (19). In humans, synthetic antisense oligonucleotides similar in chemistry to miR mimics or antimiRs have been therapeutically used. Mipomersen, a second-generation anti-sense oligonucleotide molecule targeting the messenger RNA encoding for ApoB, effectively reduces the LDL-C level among patients suffering from familiarly hypercholesterolemia and coronary heart disease patients non-responding to the maximum tolerated dose of other LDL-C lowering medications (20, 21), providing support for , future RNA-based treatment possibilities.

Likewise, small molecule drugs that alter the activity of specific epigenetic enzymes might have an anti-atherosclerosis potential and are starting to enter the clinics. Although data on cardiovascular endpoints are scarce in the initial clinical studies, these drugs have proven safe in oncology trials, which warrant their transition for treatment of cardiovascular disease. This transition allows to test the hypothesis that treating epigenetic dysregulations in endothelial cells (e.g. SIRT1 deactivation or EZH2 innervation in atherosclerosis), precludes the development of atherosclerosis and potentially reduces the disease burden. The review only addressed to the early stage of atherosclerosis and the effect may differ late stages of atherosclerosis, especially in vulnerable plaques.

Also, we found that inhibition of intracellular Gal-3 attenuated EndMT. This finding can be linked with study which showed Gal-3 knockdown in mice lead to less cardiac fibrosis and improved cardiac function (22). Since reduction of GAL-3 reduces nuclear accumulation of β-catenin/TCF4 in colorectal cells (23) and induces gene expression of SNAI1, SNAI2 and TWIST1 in endothelial cells, the beneficial effect may explained via occurring through modulation of EndMT transcription factors.

TARGETING ADVERSE ENDOTHELIAL PLASTICITY IN ATHEROSCLEROSIS AND CARDIAC FIBROSIS

There is ample experimental and clinical evidence that high laminar shear stress benefits endothelial function and homeostasis and suppresses adverse endothelial plasticity and dysfunction. The easiest, reliable and risk-free way to physically induce shear stress magnitude is doing optimal regular physical exercise, which results in favorable effects in heart and vessel (24, 25). Thereby supporting physical activity among general population is important for endothelial health.

Although, vascular bifurcations and curvatures remain at risk due to their geometry – and these areas are atheroprone areas. In order to tackling this issue, we stated our prospect of ameliorating atherosclerosis via targeting pro-atherogenic endothelium using pre-exemplifying epigenetic enzymes namely SIRT1 activation and EZH2 inhibition in Chapter 2. Treatment against adverse endothelial plasticity is also inquired after successful coronary artery bypass graft (CABG) or percutaneous coronary intervention (PCI) to prevent from vein graft failure or restenosis, since the underlying pathology of these complications are due to the EndMT-derived intimal hyperplasia (30). Targeted delivery to endothelium such as with immunoliposomes (26) is obligatory to deliver intrinsic EndMT inhibiting molecules in vivo. Because we need to take into account that targets of miRNAs and functions of epigenetic enzymes vary in different cell types, systemic administration of these molecules may result in adverse off-target effects. The promising targeting delivery method is immune-liposome based technology which can selectively deliver siRNAs to the activated endothelial cells using surface markers such as E-selectin (27, 28).

Regarding cardiac fibrosis, targeting endMT during cardiac fibrosis may be a novel therapeutic strategy, because 30% of the myofibroblasts are derived via EndMT (16). Successful inhibition of EndMT in heart may ameliorate fibrosis in certain extend. The net result may be not only happening through the inhibition of EndMT-derived myofibroblast differentiation but also reducing hypoxia via maintaining endothelial phenotype. As hypoxia is well established to promote myofibroblast differentiation.

CONCLUDING REMARKS

Adverse endothelial plasticity is fundamental basis of multiple adult pathologies including atherosclerosis, intimal hyperplasia and cardiac fibrosis. We uncovered a number of signaling mechanisms, including signaling intermediates, epigenetics and post-transcriptional silencing that might preclude the development or progression of atherosclerosis and cardiac fibrosis. These mechanisms need to be investigated in future research by interventional studies in diseased animal models. Advances in the field of targeted drug delivery are essential to deliver therapeutic molecules in the cells they need treatment and enable to avoid undesirable side effects.

REFERENCE

1. Bautch VL. Stem cells and the vasculature. Nature medicine. 2011;17(11):1437.
2. Dyer LA, Patterson C, editors. Development of the endothelium: an emphasis on heterogeneity. Seminars in thrombosis and hemostasis; 2010: NIH Public Access.
3. Aird WC. Endothelial cell heterogeneity. Cold Spring Harbor perspectives in medicine. 2012;2(1):a006429.
4. Ballabh P, Braun A, Nedergaard M. The blood–brain barrier: an overview: structure, regulation, and clinical implications. Neurobiology of disease. 2004;16(1):1-13.
5. Poisson J, Lemoinne S, Boulanger C, Durand F, Moreau R, Valla D, et al. Liver sinusoidal endothelial cells: physiology and role in liver diseases. Journal of hepatology. 2017;66(1):212-27.
6. Davies PF. Flow-mediated endothelial mechanotransduction. Physiological reviews. 1995;75(3):519-60.
7. Conway DE, Schwartz MA. Flow-dependent cellular mechanotransduction in atherosclerosis. J Cell Sci. 2013;126(22):5101-9.
8. Mahmoud MM, Serbanovic-Canic J, Feng S, Souilhol C, Xing R, Hsiao S, et al. Shear stress induces endothelial-To-mesenchymal transition via the transcription factor Snail. Scientific Reports. 2017;7(1):3375.
9. Brooks AR, Lelkes PI, Rubanyi GM. Gene expression profiling of human aortic endothelial cells exposed to disturbed flow and steady laminar flow. Physiological genomics. 2002;9(1):27-41.
10. Passerini AG, Polacek DC, Shi C, Francesco NM, Manduchi E, Grant GR, et al. Coexisting proinflammatory and antioxidative endothelial transcription profiles in a disturbed flow region of the adult porcine aorta. Proceedings of the National Academy of Sciences of the United States of America. 2004;101(8):2482-7.
11. Malek AM, Alper SL, Izumo S. Hemodynamic shear stress and its role in atherosclerosis. Jama. 1999;282(21):2035-42.
12. Goumans M-J, Liu Z, Ten Dijke P. TGF-β signaling in vascular biology and dysfunction. Cell research. 2009;19(1):116.
13. Mahmoud M, Kim HR, Xing R, Hsiao S, Mammmoto A, Chen J, et al. TWIST1 integrates endothelial responses to flow in vascular dysfunction and atherosclerosis. Circulation research. 2016:CIRCRESAHA. 116.308870.
14. Maleszewska M, Vanchin B, Harmsen MC, Krenning G. The decrease in histone methyltransferase EZH2 in response to fluid shear stress alters endothelial gene expression and promotes quiescence. Angiogenesis. 2016;19(1):9-24.
15. Moonen J-RA, Lee ES, Schmidt M, Maleszewska M, Koerts JA, Brouwer LA, et al. Endothelial-to-mesenchymal transition contributes to fibro-proliferative vascular disease and is modulated by fluid shear stress. Cardiovascular research. 2015;108(3):377-86.
16. Zeisberg EM, Tarnavski O, Zeisberg M, Dorfman AL, McMullen JR, Gustafsson E, et al. Endothelial-to-mesenchymal transition contributes to cardiac fibrosis. Nature medicine. 2007;13(8):952.
17. Chen P-Y, Qin L, Tellides G, Simons M. Fibroblast growth factor receptor 1 is a key inhibitor of TGFb signaling in the endothelium. 2014.
18. Feinberg MW, Moore KJ. MicroRNA regulation of atherosclerosis. Circulation research. 2016;118(4):703-20.
19. Loyer X, Potteaux S, Vion A-C, Guérin CL, Boulkroun S, Rautou P-E, et al. Inhibition of microRNA-92a prevents endothelial dysfunction and atherosclerosis in mice. Circulation research. 2013:CIRCRESAHA. 113.302213.

20. Raal FJ, Santos RD, Blom DJ, Marais AD, Charng M-J, Cromwell WC, et al. Mipomersen, an apolipoprotein B synthesis inhibitor, for lowering of LDL cholesterol concentrations in patients with homozygous familial hypercholesterolaemia: a randomised, double-blind, placebo-controlled trial. The Lancet. 2010;375(9719):998-1006.
21. Thomas GS, Cromwell WC, Ali S, Chin W, Flaim JD, Davidson M. Mipomersen, an apolipoprotein B synthesis inhibitor, reduces atherogenic lipoproteins in patients with severe hypercholesterolemia at high cardiovascular risk: a randomized, double-blind, placebo-controlled trial. Journal of the American College of Cardiology. 2013;62(23):2178-84.
22. Yu L, Ruifrok WP, Meissner M, Bos EM, van Goor H, Sanjabi B, et al. Genetic and pharmacological inhibition of galectin-3 prevents cardiac remodeling by interfering with myocardial fibrogenesis. Circulation: Heart Failure. 2012:CIRCHEARTFAILURE. 112.971168.
23. Song S, Mazurek N, Liu C, Sun Y, Ding QQ, Liu K, et al. Galectin-3 mediates nuclear β-catenin accumulation and Wnt signaling in human colon cancer cells by regulation of glycogen synthase kinase-3β activity. Cancer research. 2009;69(4):1343-9.
24. Niebauer J, Cooke JP. Cardiovascular effects of exercise: role of endothelial shear stress. Journal of the American College of Cardiology. 1996;28(7):1652-60.
25. Hambrecht R, Fiehn E, Weigl C, Gielen S, Hamann C, Kaiser R, et al. Regular physical exercise corrects endothelial dysfunction and improves exercise capacity in patients with chronic heart failure. Circulation. 1998;98(24):2709-15.
26. Kamps JA, Krenning G. Micromanaging cardiac regeneration: Targeted delivery of microRNAs for cardiac repair and regeneration. World journal of cardiology. 2016;8(2):163.
27. Kowalski PS, Kuninty PR, Bijlsma KT, Stuart MC, Leus NG, Ruiters MH, et al. SAINT-liposome-polycation particles, a new carrier for improved delivery of siRNAs to inflamed endothelial cells. European Journal of Pharmaceutics and Biopharmaceutics. 2015;89:40-7.
28. Gholizadeh S, Visweswaran GRR, Storm G, Hennink WE, Kamps JA, Kok RJ. E-selectin targeted immunoliposomes for rapamycin delivery to activated endothelial cells. International journal of pharmaceutics. 2017.

Chapter 9

Nederlandse Samenvatting

NEDERLANDSE SAMENVATTING

Het ultieme doel van cardiovasculaire geneeskunde is het voorkomen en genezen van ziektes aan het hart en vaatstelsel en zo de kwaliteit-van-leven te verbeteren voor patiënten met een cardiovasculaire ziekte. Fundamenteel in de ontwikkeling van nieuwe therapieën gericht tegen cardiovasculaire ziekten, is een gedegen begrip van het onderliggende ziekteproces, i.e. de moleculaire processen die ten grondslag liggen aan gezondheid en welke gedereguleerd worden tijdens ziekte. Homeostase van het endotheel – de binnenste cellaag in alle bloedvaten – speelt een belangrijke rol in het voorkomen van trombose, ontsteking en bij de regulatie van de vasculaire tonus. Dysfunctie van het endotheel is veelvoorkomend tijdens cardiovasculaire ziekten (1-3). Het is daarom belangrijk om meer inzicht te krijgen in de moleculaire mechanismen die leiden tot endotheelceldysfunctie, zodat mogelijk nieuwe aangrijpingspunten gevonden kunnen worden voor de ontwikkeling van innovatieve therapieën tegen cardiovasculaire ziekten.

Averse plasticiteit van het endotheel, en de transitie van endotheel naar mesenchym (EndMT) speelt een belangrijke rol in het ontstaan van atherosclerose (4, 5) en de verlidtekening van het hart (cardiale fibrose) (6). Hierbij wordt de inductie van genexpressie van mesenchymale genen niet alleen gereguleerd door de binding van transcriptiefactoren aan het DNA, maar ook door de bereikbaarheid van het DNA voor deze transcriptiefactoren, welke bepaald wordt door epigenetica. Epigenetische modificaties, door alteraties aan histon eiwitten of DNA methylatie, bepalen de toegankelijkheid van het DNA voor transcriptiefactoren. Een tweede regulatoir mechanisme wordt gevonden in microRNAs, die de translatie van messenger RNA naar eiwit posttranscriptioneel kan inhiberen.

ADVERSE ENDOTHEELCELPLASTICITEIT IN HET ONTSTAAN VAN INTIMALE HYPERPLASIE

Het ontstaan van intimale hyperplasie is een van de initiële processen van atherogenese. Het moleculaire mechanisme hiervan is niet geheel bekend. Intimale hyperplasie is het gevolg van de migratie en deling van fibroproliferatieve cellen in de vaatwand die hierdoor verdikt (12). De oorsprong van deze fibroproliferatieve cellen wordt veelvuldig onderzocht, en tenminste 4 celtypen kunnen differentiëren in deze zogenaamde myofibroblast-achtige cellen in de hyperplastische intima; fibroblasten, gladde spiercellen, endotheelcellen en circulerende voorlopercellen. De transplantatie van een vene naar een arteriële omgeving tijden bypass chirurgie leidt tot EndMT en kan de vorming van intimale hyperplasie veroorzaken, waarbij de getransplanteerde vene verstopt raakt (13), suggestief voor een rol van EndMT in het ontstaan van intimale hyperplasie. Daarnaast worden endotheelcel-afkomstige fibroproliferatieve cellen vaak gevonden in vaatgebieden waarbinnen atherosclerose ontwikkeld, *i.e.* vaatgebieden die blootgesteld worden aan zogenaamde 'low oscilatory shear stress' (5)(14). Andersom, in vaatgebieden die beschermd lijken tegen de ontwikkeling van atherosclerose, i.e. vaatgebieden die blootgesteld worden aan zogenaamde 'high laminar shear stress', is het endotheel quiescent en ongevoelig voor stimuli die EndMT

induceren (14), hetgeen impliceert dat het patroon waarmee het bloed door de vaten stroomt een bepalende factor is in de inductie van EndMT.

In hoofdstuk 3, hebben wij gevonden dat in vaatgebieden waar intimale hyperplasie plaatsvindt, de expressie van MAPK7 wordt voorkomen door microRNA-374b. De expressie van microRNA-374b wordt geïnduceerd door TGFβ en microRNA-374b voorkomt de eiwitexpressie van 4 genen in de MAPK7 signaaltransductiecascade, *i.e.* MAP3K3, MAPK7, MEF2D en KLF4. De ectopische expressie van microRNA-374b in het endotheel leidt tot EndMT in de afwezigheid van TGFβ stimulatie, hetgeen suggereert dat de inhibitie van MAPK7 signalering door microRNA-374b een essentiële voorwaarde is voor de ontwikkeling van intimale hyperplasie. In experimentele modellen voor intimale hyperplasie komt microRNA-374b verhoogt tot expressie en is de expressie van MAPK7 verlaagt. Daarnaast is het expressieniveau van microRNA-374b geassocieerd met het expressieniveau van MAPK7 en de ernst van intimale hyperplasie in de coronair arteriën van patiënten die zijn overleden aan coronaire hartziekte.

Intimale hyperplasie is een progressieve aandoening die leidt tot de vernauwing van der arteriën. Hierin speelt hyperproliferatie van fibroproliferative cellen een rol. Echter, het mechanisme waardoor endotheelcel-afkomstige fibroproliferatieve cellen hun quiescence verliezen en een hyperproliferatief fenotype aannemen is onbekend. In hoofdstuk 4 laten wij zien dat het epigenetisch enzym EZH2 een belangrijke rol speelt in deze transitie. EZH2 is een epignetisch enzym dat verantwoordelijk is voor de tri-methylatie van lysine 27 op histon 3 (H3K27Me3), hetgeen leidt tot repressie van genexpressie (15). Onder atheroprotectieve condities is de expressie van EZH2 laag. De toename in EZH2 expressie in vaatgebieden die gevoelig zijn voor de ontwikkeling van intimale hyperplasie, gaat gepaard met een toename in de expressie van celcyclus genen. Hoewel wij het precieze mechanisme achter de regulatie van celcyclus door EZH2 niet hebben kunnen bepalen, hebben we aangetoond dat EZH2, en dus epigenetische mechanismen, een belangrijke rol spelen in de regulatie van endotheliale quiescence en hyperproliferatie (16)(Figuur 3).

In ons onderzoek naar de regulatie van de celcyclus door EZH2, viel ons op dat er reciprociteit bestaan tussen de expressie van EZH2 en de activatie status van MAPK7. Deze interactie kan niet verklaart worden door een directe interactie tussen EZH2 en MAPK7. In hoofdstuk 5 hebben we onderzocht hoe de activiteit van MAPK7 wordt beïnvloedt door EZH2 en waarom de expressie van EZH2 afhankelijk is van de mate van activatie van MAPK7. Atheroprotectieve laminaire shear stress zorgt voor de activatie van MAPK7, hetgeen leidt tot de expressie van microRNA-101. De expressie van microRNA-101 leidt tot een verlaagde expressie van EZH2. Visa versa leidt een verhoogde expressie van EZH2 tot een verlaagde expressie van microRNA-200a, -b, -c en microRNA-141. Deze microRNAs reguleren de activiteit van MAPK7 door de inhibitoren van MAPK7 activiteit, *i.e.* de Dual-specificity phosphatase (DUSP)-1 en DUSP-6, te verlagen. Een toename in EZH2 leidt dus tot een hogere inhibitie van MAPK7 activiteit in het endotheel. Deze interactie hebben we niet alleen kunnen vinden in "gezonde" endotheelcellen *in vitro*, maar is ook aanwezig in vaatweefsel van patiënten die leiden aan coronaire hartziekte (figuur 4).

ADVERSE ENDOTHEELCELPLASTICITEIT IN HET ONTSTAAN VAN CARDIALE FIBROSE

Cardiale fibrose, oftewel verlittekening van het hart, is het pathologische proces dat ten grondslag ligt aan het ontstaan van hartfalen, waarvoor geen effectieve therapie beschikbaar is. Het niveau van galectin-3 in het bloedplasma van patiënten die leiden aan hartfalen is geassocieerd met hun overleving, en een prognostische biomarker in de kliniek (17). Een verminderde expressie van galectin-3 reduceert de ontwikkeling van hartfalen, hetgeen duidt op een op mechanistische functie voor galectin-3 in cardiale fibrose (18). Cardiale fibrose wordt gekenmerkt door de accumulatie van fibroproliferatieve cellen in het hart, waarvan een deel afkomstig zijn vanuit het endotheel (6). Om deze reden hebben wij in hoofdstuk 6 onderzocht of de expressie van galectin-3 geassocieerd is met de inductie van EndMT. Het is algemeen geaccepteerd dat galectine-3 zijn functie uitoefent via binding aan zijn receptor in het celmembraan, echter leidt de additie van galectin-3 aan endotheelcellen niet tot EndMT of tot een verhoogde effectiviteit van TGFβ-geïnduceerde EndMT. Wel leidt de inhibitie van endogene galectin-3 productie tot een verlaging van TGFβ-geïnduceerde EndMT. Tezamen duiden deze data op een intracellulaire rol voor galectin-3 in de regulatie van EndMT, mogelijk als transcriptionele coactivator (19, 20). Deze hypothese wordt momenteel onderzocht.

CONCLUSIE

De transitie van endotheel naar mesenchym is een belangrijke component in de ontwikkeling van atherosclerose (intimale hyperplasie) en hartfalen (cardiale fibrose) en wordt gereguleerd door biomechanische krachten, zoals het patroon van de bloedstroom. In dit proefschrift hebben wij laten zien dat EndMT gereguleerd wordt door MAPK7, EZH2 en microRNAs en gevonden dat de expressie van deze moleculen gedereguleerd is in experimentele modellen voor intimale hyperplasie en in humane coronaire hartziekte. We hebben een aantal belangrijke regulatoren van EndMT geïdentificeerd die mogelijk een therapeutische effect kunnen hebben om de ontwikkeling van intimale hyperplasie of het ontstaan van hartfalen tegen te gaan. Toekomstig onderzoek moet zich op deze mogelijkheid richten.

REFERENTIES

1. Gimbrone MA, Topper JN, Nagel T, Anderson KR, GARCIA-CARDEÑA G. Endothelial dysfunction, hemodynamic forces, and atherogenesis. Annals of the New York Academy of Sciences. 2000;902(1):230-40.
2. Sena CM, Pereira AM, Seiça R. Endothelial dysfunction—a major mediator of diabetic vascular disease. Biochimica et Biophysica Acta (BBA)-Molecular Basis of Disease. 2013;1832(12):2216-31.
3. Vanhoutte P, Shimokawa H, Feletou M, Tang E. Endothelial dysfunction and vascular disease–a 30th anniversary update. Acta Physiologica. 2017;219(1):22-96.
4. Chen P-Y, Qin L, Baeyens N, Li G, Afolabi T, Budatha M, et al. Endothelial-to-mesenchymal transition drives atherosclerosis progression. The Journal of clinical investigation. 2015;125(12):4514.
5. Evrard SM, Lecce L, Michelis KC, Nomura-Kitabayashi A, Pandey G, Purushothaman K-R, et al. Endothelial to mesenchymal transition is common in atherosclerotic lesions and is associated with plaque instability. Nature communications. 2016;7.
6. Zeisberg EM, Tarnavski O, Zeisberg M, Dorfman AL, McMullen JR, Gustafsson E, et al. Endothelial-to-mesenchymal transition contributes to cardiac fibrosis. Nature medicine. 2007;13(8):952.
7. Arciniegas E, Sutton AB, Allen TD, Schor AM. Transforming growth factor beta 1 promotes the differentiation of endothelial cells into smooth muscle-like cells in vitro. Journal of cell science. 1992;103(2):521-9.
8. Maleszewska M, Moonen J-RA, Huijkman N, van de Sluis B, Krenning G, Harmsen MC. IL-1β and TGFβ2 synergistically induce endothelial to mesenchymal transition in an NFκB-dependent manner. Immunobiology. 2013;218(4):443-54.
9. Lee ES, Boldo LS, Fernandez BO, Feelisch M, Harmsen MC. Suppression of TAK1 pathway by shear stress counteracts the inflammatory endothelial cell phenotype induced by oxidative stress and TGF-β1. Scientific Reports. 2017;7:42487.
10. Souihol CE, Harmsen MC, Evans PC, Krenning G. Endothelial-Mesenchymal Transition in Atherosclerosis. Cardiovascular research. 2018.
11. Medici D, Potenta S, Kalluri R. Transforming growth factor-β2 promotes Snail-mediated endothelial–mesenchymal transition through convergence of Smad-dependent and Smad-independent signalling. Biochemical Journal. 2011;437(3):515-20.
12. Ross R, Glomset JA. Atherosclerosis and the arterial smooth muscle cell. Science. 1973;180(4093):1332-9.
13. Cooley BC, Nevado J, Mellad J, Yang D, Hilaire CS, Negro A, et al. TGF-β signaling mediates endothelial-to-mesenchymal transition (EndMT) during vein graft remodeling. Science translational medicine. 2014;6(227):227ra34-ra34.
14. Moonen J-RA, Lee ES, Schmidt M, Maleszewska M, Koerts JA, Brouwer LA, et al. Endothelial-to-mesenchymal transition contributes to fibro-proliferative vascular disease and is modulated by fluid shear stress. Cardiovascular research. 2015;108(3):377-86.
15. Di Croce L, Helin K. Transcriptional regulation by Polycomb group proteins. Nature structural & molecular biology. 2013;20(10):1147-55.
16. Maleszewska M, Vanchin B, Harmsen MC, Krenning G. The decrease in histone methyltransferase EZH2 in response to fluid shear stress alters endothelial gene expression and promotes quiescence. Angiogenesis. 2016;19(1):9-24.

17. Ho JE, Liu C, Lyass A, Courchesne P, Pencina MJ, Vasan RS, et al. Galectin-3, a marker of cardiac fibrosis, predicts incident heart failure in the community. Journal of the American College of Cardiology. 2012;60(14):1249-56.
18. Yu L, Ruifrok WP, Meissner M, Bos EM, van Goor H, Sanjabi B, et al. Genetic and pharmacological inhibition of galectin-3 prevents cardiac remodeling by interfering with myocardial fibrogenesis. Circulation: Heart Failure. 2012:CIRCHEARTFAILURE. 112.971168.
19. MacKinnon AC, Gibbons MA, Farnworth SL, Leffler H, Nilsson UJ, Delaine T, et al. Regulation of transforming growth factor-β1–driven lung fibrosis by galectin-3. American journal of respiratory and critical care medicine. 2012;185(5):537-46.
20. Shimura T, Takenaka Y, Tsutsumi S, Hogan V, Kikuchi A, Raz A. Galectin-3, a novel binding partner of β-catenin. Cancer research. 2004;64(18):6363-7.

Ap

Ab
C
Ap

ABBREVIATIONS

αSMA	alpha smooth muscle actin
ACTB	actin beta
APOE-/-	apolipoprotein-E knockout mice
BMK-1	big mitogen activated protein kinase 1
BMP7	bone morphogenic protein 7
BSA	bovine serum albumin
CABG	coronary Artery Bypass Graft
CD31	cluster of Differentiation 31
CD144	cluster of Differentiation 144, CDH5
CNN1	calponin 1
CpG	cytosine followed immediately by guanine base
CVD	cardiovascular Diseases
DMSO	dimethyl sulfoxide
DNMT1	DNA methyltransferase 1
DNMT3a	DNA methyltransferase 3 alpha
DNMT3b	DNA methyltransferase 3 beta
DNA	deoxyribonucleic acid
DUSP1	dual specificity Phosphatase 1
DUSP6	dual specificity Phosphatase 6
EC	endothelial cells
ECM	endothelial cell medium
ECGF	endothelial cell growth factor
EDCF	endothelial-derived contracting factor
EDRF	Endothelial-derived relaxing factor
EDTA	ethylenediaminetetraacetic acid
EED	embryonic ectorderm development
EMT	epithelial-mesenchymal transition
EndMT	endothelial-eesenchymal transition
eNOS	endothelial nitric oxide synthase, NOS3
ERK5	extracellular signal-regulated kinase 5
EZH1	enhancer of zeste homologue 1
EZH2	enhancer of zeste homologue 2
FBS	fetal bovine serum
FGF2	fibroblast Growth Factor 2
FSP1	fibroblast specific protein
FSS	fluid shear stress
Gal-3	galectin 3
GAPDH	glyceraldehyde 3-phosphate dehydrogenase
H202	hydrogen peroxide
H2A	histone 2A
H2B	histone 2B
H3	histone 3
H3K9	histone 3 lysine 9
H3k27me3	histone 3 lysine 27 trimethylation

H4	histone 4
HF	heart failure
HFpEF	heart failure with preserved ejection fraction
HUVEC	human umbilical vein endothelial cells
IL-6	interleukin 6
IL1β	interleukin 1β
IMT	intima-Media thickness
KLF2	kruppel like factor 2
KLF4	kruppel like factor 4
LDL-C	low density lipoprotein cholesterol
LSS	laminar shear stress
MAP3k3	mitogen activated protein kinase kinase kinase 3
MAPK7	mitogen activated protein kinase 7
MCP1	monocyte chemoattractant protein 1
MEF2D	myocyte enhancer factor 2D
MEF2C	myocyte enhancer factor 2C
MEK	extracellular signal-regulated kinase kinase
MEK5D	constitutive active MEK5
miRNA	micro RNA
NADH	nicotinamide adenine dinucleotide
NADPH	nicotinamide adenine dinucleotide phosphate
NFkB	nucleic factor kappa B
NO	nitric oxide
Ox-LDL	oxidized low density lipoprotein
PAR-1	protease activated receptor
PCI	percutaneous coronary intervention
PCSK9	proprotein convertase subtilisin/kexin type 9
PFA	paraformaldehyde
pMAPK7	phosphorylated MAPK7
PRC 1	polycomb repressive complex 1
PRC 2	polycomb repressive complex 2
RbAP48	retinoblastoma binding protein 48
RISC complex	RNA-induced silencing complex
RNA	ribonucleic acid
ROS	reactive oxygen species
SEM	standard error of the mean
sm22α	smooth muscle 22 alpha
SUZ12	suppressor of zeste 12
TAGLN	transgelin (sm22α)
TGFβ1	transforming growth factor beta 1
TGFβR	transforming growth factor beta receptor
TNFα	tumor necrosis factor alpha
VCAM1	vascular cell adhesion protein 1
VE-cad	vascular endothelial cadherin
VEGF	vascular endothelial growth factor
vWF	von Willebrand factor

BIOGRAPHY

The author of this thesis Byambasuren Vanchin was born on 13th of December, 1986 in Ulaanbaatar, Mongolia. After finishing high school #5 with "cum laude" in Ulaanbaatar, she started medical school at the Mongolian National University of Medical Sciences (MNUMS) in 2004.

In 2010, she graduated as a Medical Doctor and started her master study in Prof.dr. Munkhzol Malchinkhuu's team. Her master thesis focused traditional CVD risk factors' influence on vascular stiffness among healthy young people. In 2011, she started her internal medicine residency program and worked at the First Central Hospital, Shastin Central hospital and MNUMS university hospital. After completing the internal medicine residency, she enrolled to the Cardiology residency training program under supervision of Dr. Burmaa Badrakh at the MNUMS.

During her master studies, she realized the importance of endothelial dysfunction in development of cardiovascular diseases and raised interest in this topic. Upon the collaboration between Mongolian State Training Fund, Mongolian National University of Medical Sciences and University of Groningen, she joined the Cardiovascular Regenerative Medicine Group (CAVAREM) under the supervision of Dr. Guido Krenning and Prof. dr. Marco Harmsen. She investigated molecular epigenetic and post-transcriptional mechanisms of Endothelial-Mesenchymal transition in coronary artery stenosis and cardiac fibrosis.

ACKNOWLEDGEMENT

The experience in Groningen taught me valuable lessons in my life. It was not solely about endothelial cells in heart diseases, it was also about finding right life-work balance and keeping yourself calm, strong and kind whatever is happening. This experience as well as this thesis would not have been possible without the generous professional and personal support of some great people around me. I am honored that this part of my thesis is dedicated to them.

Dear Guido, from the very first day you were my mentor and one who truly cared about me. I appreciate for your patient guidance, encouragement and cordial advices throughout my entire study. Your passion and discipline in research was inspiring and you shared it with the people around you generously. Besides learning a great deal about endothelial molecular biology, you taught me how to deal with challenges, how to be persistent and the importance of knowing what you want and courage to go after it. i will always make you proud. Leerkrachten als jij zijn niet makkelijk te vinden. Dank je wel ☺

Thank you very much **Marco,** you are great professor and wonderful person. Our scientific and casual conversations were really interesting. You always fascinated us by your open mindedness, casualty and kindness. Thank you very much for allowing me to work in this wonderful international environment.

Marianne, thank you very much for your kind collaboration on Chapter 2. Your expertise in epigenetics was truly inspiring. It was great opportunity to discuss ideas, manuscripts and hear lectures from one of the pioneers of the Epigenetic Editing field.

Eliane, the Scientific Writing A-Z class, was the oxygen mask during my writing. The handouts you provided during the course was guided and moved me forward when I get stuck. I am sure I will use them in the future as well ☺ Thank you very much.

I would like to express my deep gratitude to the reading committee, Professor **Jan Luuk Hillebrands**, Professor **Marie Jose Goumans** and Professor **Elizabeth M Zeisberg** for their valuable time.

Marja thank you very much for your all kind assistance during my PhD. We tackled many technical issues with your knowledge and expertise. The MOBITEC course organized by you and **Peter** gave me courage and speed to complete my projects successfully.

Linda, your calmness and discipline are admirable. Thank you for your all help during my PhD and especially your support in vivo part of GAL-3 project although we couldn't include in this booklet.

Thanks to for all former and current **CAVAREM members**; Joep, Julian, Jolien, Xenos, Vincenzo, Mojtaba, Ee Soo, Monika, Azi, Joris, Jorien, Gabriel, Tacia, Daniel, Thais and students who were part of this group. The international atmosphere was a cheerful working and learning environment. I wish you all the best!

Maroesjka, almost Doctor Spiekman ☺ You were always there for me during the most difficult times including I had surgery at the Martini hospital. We shared office, experiences, food... sometimes even shared our socks when we visit each other's home. The stamppot you cooked was the first and the best Dutch food I had so far ☺ Keep doing amazing work my dear - you are such a smart and beautiful person.

Marloes, you are cute and tiny but there is a hidden MEGA-factor within you. You can complete any tasks as long as it is written in your magic agenda. We have collaborated on

Chapter 5 for two years, and it turned out really beautiful ☺ I wish you all the best to my dear paranymph.

L sanne, we started our journey at the same time and shared our ups and downs. Do you remember we used to run untill Kardinge bridge in the rain? You always paced me and I always admired your patience and calmness. Please update me about your Africa trip adventures ☺

Ghazelah, I still remember your wisdom "If it doesn't matter in 5 years, don't worry about it for more than 5 minutes". I also enjoyed our lunch breaks next to the perycyte-like plant in the canteen, while hearing your fashion and life advices. All the best azizam!

Monica, Ana Maria and Francisco, the lab could have been quite boring if there would not have been any latin - American hot blooded spirits. The humors, new nicknames and loud laughs are rooted by you guys and it was so much fun to be around you. Thank you for the salsa nights, late night talks and AREPAs. **Tamara** and **Susana**, thank you very much for all the wonderful memories, laughters and coffee breaks. All the best ☺

Rutger thank you very much for teaching me CHIP experiment and always helped me for troubleshooting. Dank je wel Rutger!

I am grateful to the students I have worked with; **Bauke, Melanie**, **Andrea** and **Ruud**. I am proud that three of you started PhD and two of you stayed in vascular biology and cardiovascular medicine field. It was never one sided road. We learned from each other and raised together as researchers.

It is pleasure to thank all amazing technicians in Medical Biology; Henk, Pytrick, Jelleke, Peter, Theo (MATRIX), Geert, Theo, Anita, Wendy, Josee, Timara, Rianne, Anita-Meter, Marnix and Johen. Thank for your all kind professional support and nice accompany in the laboratory.

I would like to thank all former and current colleagues in the Medical Biology ; Desiree, Chengcheng, Bram, Olaf, Niha, David, Genaro, Dandan, Monique, Erna, Rui, Ranran, Julio, Rosa, Praghyi, Ditmer, Martin, Luis, Renate, Nataly, Diana, Archipold, Sophie, Kristen, Hataitip, Virinchi and Martha.

Thank you **Hans** for being such a wonderful and understanding person. You cared us-graduate students' issues with attention and compassion. Marcel, Pietra, Carolien, Anita and Susan, thank you very much for all your kind support during my study.

I am grateful to my Mongolian colleagues at the UMCG ; **Orchlon, Tugsuu, Turuu, Khosoo, Ariuka, Zulaa** and their family (Gerel, Dulguun, Saraa and Zorigoo). You made my days in Groningen more colorful and joyful. We encouraged each other when we face challenges and celebrated each others' achievements. Thank you very much for all the beautiful trips, celebrations and experiences we shared together. I wish you all the best my friends! Dear Khatnaa, Nergui, Buyanaa, Oguu, Sainaa, Jamba and Deegii, thank you very much for all your kindness and Mongolian hospitality during my stay in Groningen.

Also, I would like to thank Ellen, Mendee, Josine, Yuan, Amina, Enhrii, Liesbeth, Charu and Indranil for their kindness and friendship.

Using this opportunity, I would like to acknowledge my former professors and mentors. Dear **[Prof. Ichinkhorloo]**, you were the first one who introduced me research and flamed my curiosity. You will be dearly remembered in my heart... Dear **Prof. Munkhzol,** you always encouraged me to be braver and smarter. I still remember our discussion on the importantce of the endothelial cells in vascular stiffness and atherosclerosis. That was the turning point in my life, which further lead me to this PhD research. Special thanks to

Dr.Burmaa and colleagues at Department of Cardiology, MNUMS for helped me to make my first baby steps in the big ocean named Cardiology, I still have more to study from all of you.

I am really grateful for my friends **Sandro** and **Hisayo**. Although we have lived thousands of kms away from each other, we managed to make reunions and always rooted for each other. Thank you **Khulan**, you are simply genuine, lovely and reliable person who has such a kind heart. Your "Belgium fries – happiness" theory always worked for us ☺ my stay in Netherlands wouldn't be as happy as it is without you.

Thank you very much **Kasia** my fitness instructor – you are fantastic. Your jumping fitness and bootcamp classes gave me stamina, happiness and energy to overcome stressful times. The real high shear stress effect was delivered me through sporting.

My heartfelt gratitude to **Tjalling** and **Uulii** for your continuous support and kindness. Thank you very much for eveything you have done for me. You have been great bridge between Mongolia and Netherlands. Furthermore, I would like to extend my acknowledgement to **Prof. Han Moshage, Xuefei** and president **Poppema** for making my study at the UMCG possible. I believe this collaboration will prosper more in the future.

I would like to acknowledge **Dr. Scholten**, **Ina** and burn center nurses and caregivers for their professionalism and kindness during my two months hospitalization in your department.

Simeon, your calmness, kindness and love nurtured me every day and filled my life with joy. Thanks to Claudia and Guenter for being kind and always welcoming to me.

My deepest gratitude **to my beloved parents Vanchin and Lkhagva** for their unconditional love and support. Your love and wisdom were the driving force of my life. This thesis is dedicated to you my lovely parents. You seeded education and tenacity in my brain and kindness and honesty in my heart. I would like to express my sincere gratitude to my beautiful sister Rentsenkhand, brother-in-law Sergelenbat and cousin Tungaa for being always there for me. Love you all and thank you very much ☺ Аав, ээж, эмээ, ах, эгч, ахан дүүсдээ хамгаас их хайртай шүү, та бүхэн минь миний амьдралын утга учир гэрэл гэгээ минь билээ. Алс холоос ч эрдэм ухаан, хайр энэрэлээ түгээж байдаг Амгалан багшдаа маш их баярлалаа.

Byambasuren Vanchin
June, 2018